Republic of Iraq
Ministry of Higher Education and Scientific Research
University of Misan/College of Engineering
Civil Engineering Department

NUMERICAL ANALYSIS OF REINFORCED CONCRETE BEAMS STRENGTHENED WITH CFRP

A THESIS
SUBMITTED TO THE COLLEGE OF ENGINEERING
UNIVERSITY OF MISAN
IN PARTIAL FULFILLMENT
OF
THE REQUIREMENTS FOR THE DEGREE
OF MASTER OF SCIENCE
IN
CIVIL ENGINEERING
(STRUCTURES)
BY

AHMED KADHEM SAKBAN
(B. Sc. Civil Engineering,2011)
Supervised by
Prof.Dr.Mohammed A. Mashrei

2020 A.D 1441 A.H

بسم الله الرحمن الرحيم

﴿ الرَّحْمَٰنُ {1} عَلَّمَ الْقُرْآنَ {2} خَلَقَ الْإِنسَانَ {3} عَلَّمَهُ الْبَيَانَ {4} الشَّمْسُ وَالْقَمَرُ بِحُسْبَانٍ {5} وَالنَّجْمُ وَالشَّجَرُ يَسْجُدَانِ {6} وَالسَّمَاءَ رَفَعَهَا وَوَضَعَ الْمِيزَانَ {7} ﴾

صدق الله العلي العظيم

سورة الرحمن ﴿ الآيات 1-7 ﴾

Abstract

In reiforced concrete structures, two types of strengthening techniques by carbon fiber reinforced polymer (CFRP) meterial are used, The first one is near surface mounted (NSM) and the second one is externally bonded reinforcement (EBR).

This study concerns with flexural and shear behavior of RC beams strengthened with CFRP stirp or sheet using the finite element method- commercial software ABAQUS.

The analytical results using fnite element method by ABAQUS program compares with experimental results to check the validity and accuracy of the present FEM.

Three-dimensional eight-node element (C3D8R) was used to represent the concrete, one-dimensional wire element (T3D2) was used to represent the steel and three-dimensional shell element (S4R) was used to represent the CFRP sheet, a full bond between concrete and carbon used surface to surface contact.

The load-deflection relationship, crack pattern, concrete strain distrubution with depth of beams and mode of failure of RC beam are studied. After validation the models, a paramtric studies are presented to assess the influence of compression strength of concrete, configuration of CFRP (U shape and 2 side bond shape) and shear span to depth ratio (a/h ratio) on shear strength. Also, the effect of compression strength of concrete, sheet thickness, length laminate ratio to clear span and the effect of presence of CFRP on steel bar stresses on flexture strength of RC beams.

From the results of flexural behavior, it is obtained that the strength capacity of RC beams strengthened with CFRP increased by 6.6% to 108.8% compared with the reference beams. Also, it is found that by increasing of the compressive strength of concrete from 30 MPa to 70 MPa the maximum load increase by 25.6%. Increasing

the length ratio of CFRP laminate (L) to clear span (S) from 0.66 to 1 leads to increase the max load by 12.7%. Increasing the thickness of CFRP sheet from 0.11 mm to 0.5 mm will increase stiffness and max load by 47.9%.

From the numerical results of shear behavior, it is found that the load carrying capacity of RC beams strengthened with CFRP increased by maximum percentage of 111.7% compare to unstrengthen beam. Also, it is found that by increasing the compressive strength of concrete from 40 MPa to 65 MPa the load carrying capacity increase by 28% and the stiffness also increased while the decrease of shear span to depth ratio from 1.66 to 2.33 lead to increasing the load carrying capacity by 23%. The maximum load of beams strengthened with U shape of increased by 5.9% to 11.5% for beams strengthened with CFRP sheet A12-M and B10-M respactively when compared with the same beams strengthened with two side bond shape of CFRP. However, the gain in the strength was between 8.7% to 22.7% for beams strengthened with CFRP laminate in precense of stirrups reinforcment compared to unstrengthen beams (with stirrups).

The strengthening RC beams by CFRP laminates using NSM technique is more efficient than EBR techniques for all beams in the flexural and shear behavior.

The finite element models provide good level of accuracy in comparison with exprimental results. Also the current results compared with ACI-440, the result shows that there is a not good agreement between ACI-440 and numerical results according to maximum load because the ACI-440 uses factor of safty for the most equation and There is no relative slip between external FRP reinforcement and the concrete.

ACKNOWLEDGEMENT

In The Name of Allah, The Most Gracious The Most Merciful First great thanks are to **ALLAH HIS MAJESTY** for enabling me to complete this work.

I would like to express my sincere appreciation and deepest gratitude to Prof. Dr. Mohammad A. Mashrei, whom I had the honor of being under his supervision, for his continuous encouragement and invaluable guidance throughout this thesis.

Great thanks to the Dean of the College of Engineering Assist.Prof. Dr.Abbas Oda Dawood and to the Head and Staff of the Department of Civil Engineering Dr. Samir Mohammed Hassib in the University of Misan for their appreciable support.

I would like to thank my family, especially my mother, for their encouragement, patience, and assistance over the years.

Finally, I would like to thank all my friends and my brother haider for their help in accomplishing this study.

List of Contents

List of Figures

List of Tables

Notation

Symbol	Description
Scalars	
A_v	the cross section area of the two arms steel stirrups
A_{fv}	the area of CFRP shear reinforcement within spacing (mm)

Af	area of FRP external reinforcement (mm^2)
As	area of nonprestressed steel reinforcement (mm^2)
bc	concrete width (mm)
bf	CFRP plate width (mm)
b	width of beam (mm)
c	distance from extreme compression fiber to the neutral axis
df	effective depth of FRP flexural reinforcement (mm)
d	the effective depth (mm)
Ef	tensile modulus of elasticity of FRP (MPa)
Ec	elastic modulus (MPa)
Es	modulus of elasticity of steel (MPa)
ft	tension strength of concrete (MPa)
f_c'	compressive strength of concrete for slender (MPa)
fs	stress in nonprestressed steel reinforcement (MPa)
fy	specified yield strength of nonprestressed steel reinforcement (MPa)
ffe	effective stress in the FRP (MPa)
F_{fe}	the effective tensile stress at ultimate conditions in the FRP (MPa)
f_y	the yield stresses of steel (MPa)
f_{fe}	The effective stress in the FRP (MPa)
Gi	the shear modulus of resin (GPa)
Gc	the shear modulus of concrete (GPa)
h	the height of the beam (mm)
k_v	a bond-reduction coefficient
n	the number of layers per strip
P_{max_EXP}	maximum load of strengthened beams of experimental tests
P_{max_FE}	maximum load of strengthened beams of finite element method
P_{ser_EXP}	is the load for a deflection of L/400 of experimental tests
P_{ser_FE}	is the load for a deflection of L/400 of finite element
P_{yeild}	the load for reinforced steel yield
$q^{-\alpha}$	The instantaneous magnitude of the flux for field
S	the spacing between stirrups (mm)
s_f	the spacing of the wet lay-up strips of CFRP sheets
ti	the resin thickness (mm)
tc	is the concrete thickness
ts, *tt*	shear stresses of the interface
t_f	the thickness of a layer (mm)

V_s	the strength of steel stirrup for shear (kN)
V_c	the strength of concrete for shear (kN)
V_{ff}	the strength of CFRP for shear (kN)
w_f	the width of the strips (mm)
x	the position of the neutral axis
ϵ_t	strain in zone tension (mm/mm)
σ_t	tension stress in plastic (MPa)
ϵ_{cst}	strain tension in plastic range (mm/mm)
ϵ_{c1}	strain at peak stress in compression
σ_c	compressive strength in plastic (MPa)
σ_n	the cohesive tensile
t, n, s	the direction of the stress component
εfd	debonding strain of externally bonded FRP reinforcement (mm/mm)
εfe	effective strain level in FRP reinforcement attained at failure (mm/mm)
εfu	design rupture strain of FRP reinforcement (mm/mm)
εbi	strain level in concrete substrate at time of FRP installation (mm/mm)
εcu	ultimate axial strain of unconfined concrete (mm/mm)
εs	strain level in nonprestessed steel reinforcement (mm/mm)
α_1	multiplier on fc' to determine intensity of an equivalent rectangular stress distribution for concrete
β_1	ratio of depth of equivalent rectangular stress block to depth of the neutral axis
γ_f	a safety factor
ϕ	the strength-reduction factor required by ACI
ψ_f	an additional reduction factor
τ^{α}_{max}	The largest residual in the balance equation for field
c^{α}_{max}	The largest correction to any nodal variable of type α provided by the current Newton iteration.
ΔU^{α}_{max}	The largest change in a nodal variable of type α in the increment
	Matrices
[B]	Strain- nodal displacement matrix
[D]	Constitutive matrix
$[K^e]$	Element stiffness matrix

[K]	Overall structural stiffness matrix
[N]	Shape function matrix
	Vectors
{F}= {Fa}	Vector of applied loads (total external force vector)
$\{F_i^{nr}\}$	Vector of restoring loads corresponding to the element internal loads
{u}	Unknown nodal displacements vector (local displacements)
{U}	Body displacements vector (global displacements).
{σ}	Elements of real stress vector
{ε}	Elements of strain vector
	Abbreviations
ACI	American Concrete Institute
AFRP	Aramid Fiber Reinforced Polymer
CFRP	Carbon Fiber Reinforced Polymer
EXP	Experimental Results
FEM	Finite Element Analysis
FRP	Fiber Reinforced Polymer
RC	Reinforced Concrete
NSM	Near surface mounted
EBR	External bond reinforce

Dedication

To My mother, Mrs .Samera

My Wife, Al hussna

My beloved son Ali

And my beloved son Redah

Thanks for your ongoing supports and love .

AHMED.K

Chapter One

Introduction

1.1 General

Reinforced concrete structures usually have to face modification and improvement of their performance throughout their service life. The most contributing factors are modification in their use, construction errors, deterioration because of corrosion in the steel caused by exposure to an aggressive environment and accident events such earthquakes [1]. Fiber reinforced polymer used to improve the reinforced concrete structures.

The fiber-reinforced polymer is a composite material consisting of polymer matrix and fibers. The polymer matrix is usually a vinylester or polyester thermosetting plastic, epoxy, and phenol formaldehyde resins. The matrix is used for protecting the fiber from the environment, gathering the fibers and transferring the forces within fibers. Fig. (1.1) shows the composition of FRP.

FRP composites are used in many applications of engineering structures, such as helicopters, spacecraft, craft through to ships, offshore platforms, boats and automobiles, chemical process equipment, sports goods, and civil structures as buildings and bridges [2].

Reinforced Concrete (RC) structures strengthened with FRP in two techniques. In the first techniques, the near surface mounted (NSM) which pre-cured bar or strips inserted into pre-cut grooves and surround it on three sides with a thin layer of epoxy or some other bonding agent. In the second techniques, externally Bonded of FRP (EBR) consists of bonding the FRP reinforcement to the external surface of the material to be strengthened. Fig (1.2) shows strengthening techniques in FRP.

Table (1.1) shows The properties of the matrix. The matrix has more ability to carry a strain than fibers as shown in Fig. (1.3), and this provides a protection for the fiber

[3]. Generally, Table (1.2) shows the material properties of concrete, steel and carbon fiber.

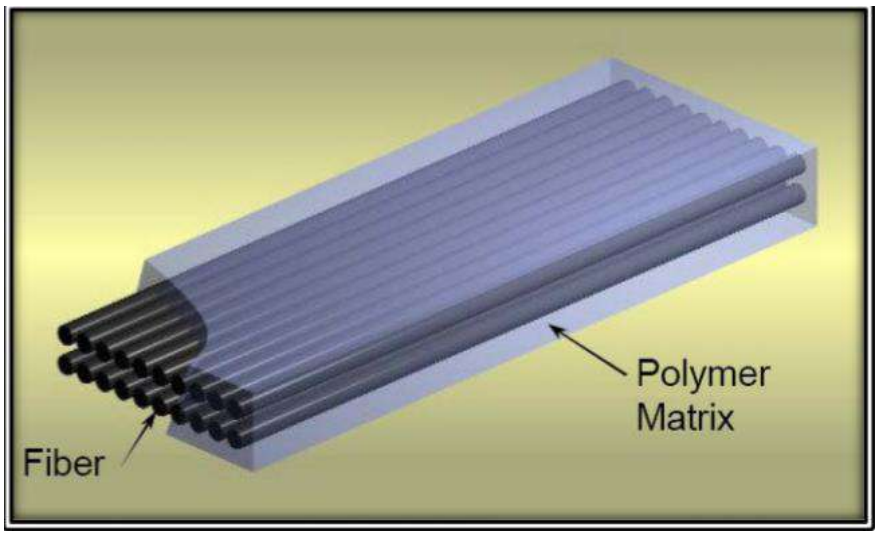

Figure (1.1) Typical compositions of FRP material [4]

a) EBR sheet in the external surface b) NSM strips in the grooves.

Figure (1.2) Typical strengthening techniques

Table (1.1) Properties of matrix materials [5]

Material	Modulus of Elasticity (Gpa)	Tensile Strength (MPa)	Failure Strain (%)	Density (kg/m3)
Polyster	2.1-4.1	20-100	1.0-6.5	1000-1450
Epoxy	2.5-4.1	55-130	1.5-9	1100-1300

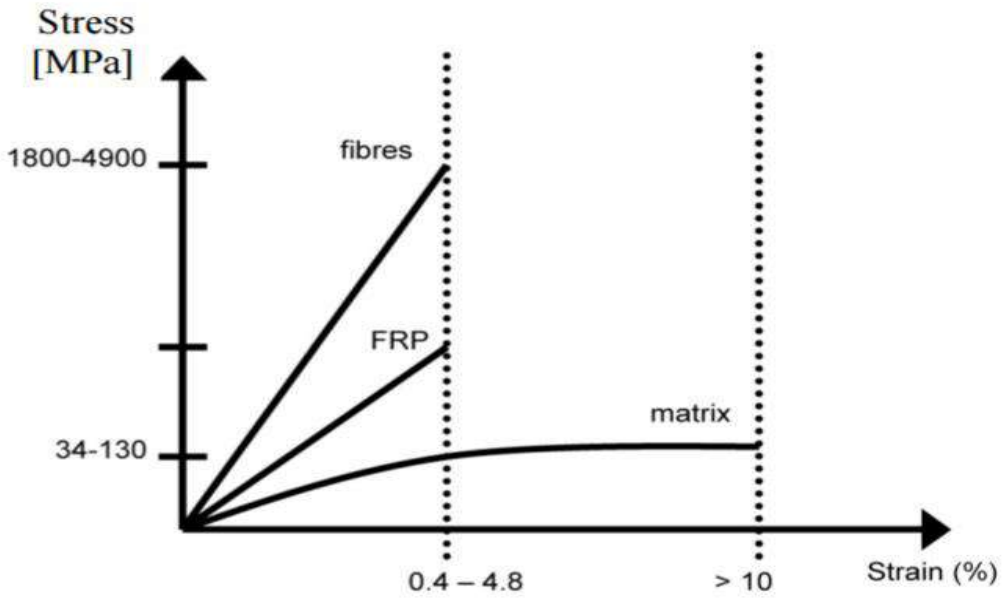

Figure (1.3) Stress-strain curves of fibers, FRP, and matrix [6]

Table (1.2) Material properties of concrete, steel, and carbon fibers [5]

Material	Modulus of Elasticity (GPa)	Compressive Strength (MPa)	Tensile Strength (MPa)	Density (kg/m3)
Concrete	20-40	5-60	1-3	2400
Steel	200-210	240-690	240-690	7800
Carbon Fiber	200-800	N/A	2100-6000	1750-1950

Many types of fibers such as carbon, glass and aramid are available. Most of civil engineering applications for strengthening purposes are accomplished by using carbon fibers [3].

FRP composites are no-corrosive, lightweight, and easily constructed which exhibit high specific stiffness and strength. FRP can also be used for satisfying performance requirements because of their advantageous characteristics.

FRP composites have been used in rehabilitation and new construction structures, and external reinforcement for seismic upgrade and strengthening [7].

Table (1.3) shows a summary of FRP advantages and disadvantages for concrete structures as compared with conventional steel reinforcement.

Table (1.3) Advantages and disadvantages of FRP reinforcement [8]

Advantages	Disadvantages
1- High tensile strength 2- High corrosion resistance 3- Non-magnetic. 4- High fatigue endurance. 5- Light weight (about 1/4 to 1/5 the density of steel). 6- Low thermal and electric conductivity for glass and aramid fibers.	1- Low transverse strength. 2- No yielding before brittle rupture. 3- Low durability of the glass fibers reinforcement in a moist environment. 4- Low durability of some aramid and glass fibers in an alkaline environment. 5- Poor resistance to fire depend on the matrix type. 6- High coefficient of the thermal expansion. perpendicular to fibers relative to concrete. 7- More expensive, more than 30 times of steel

Fiber reinforced polymer is different in mechanical properties according to type of fiber. Some responses of uniaxial loaded FRP materials and steel are shown in Fig. (1.4). In this figure, HM and HS are abbreviations of high modulus of elasticity and high strength respectively. The failure of fiber is brittle failure and the fibers have a linear elastic behavior [3].

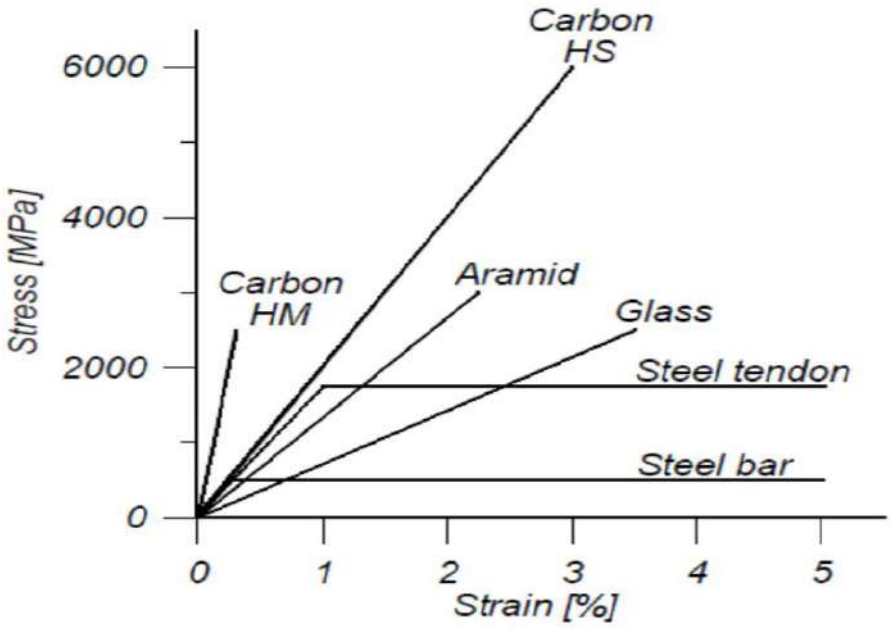

Figure (1.4) Relationship between Stress-strain of steel and fibers [9]

1.2 Applications and Use of FRP

In structural applications, FRP is available as plates, strips or sheets, and reinforcing bars. The use of FRP can be either as an alternative reinforcing instead of steel or for retrofitting to strengthening existing structures. Fiber reinforced polymer can be used to retrofit columns, slabs and beams elements. It is possible to increase these member's strength even after they had been seriously damaged due to loading conditions. In order to strengthen beams under flexural effect, FRP can be added to the tension face of a beam. This increases stiffness, deflection capacity and beam strength. In order to get higher shear resistance, the FRP strips can be put in "U" shape around the bottom and sides of a beam in critical regions [10]. Also, FRP can be warp on columns in buildings for achieving higher strength. This technique called wrapping around columns. It works by preventing the lateral expansion of columns. Strengthening of slabs can be done by pasting FRP strips at the tension face of a slab. This will give better performance, since the slab tensile resistance is supplemented by the FRP tensile strength. In the cases of both beams and slabs, the effectiveness of

FRP strengthening techniques depend on the performance of the resins chosen for bonding [11].

1.3 FRP Reinforcement Versus Steel Reinforcement

The mechanical properties of FRP is different that of steel. FRP have a low modulus of elasticity in glass and aramid fiber compared with steel bars, thus, if a direct substitution between the two materials is used, sections reinforced with FRP would have larger deflections and crack widths than sections reinforced with steel bars [12].

In steel reinforced concrete beams, the section is usually designed to be under-reinforced. The failure mode can be ensured by specifying a maximum steel reinforcement amount. However, beams reinforced with FRP do not have the same plasticity that is noticed for beams under-reinforced sections reinforced with steel bars [12].

On the other hand, concrete failure in compression-controlled sections reinforced with FRP serve as warning and reserves FRP tensile capacity. The failure mode may be ensured by specifying a minimum FRP reinforcement amount. Tension-controlled failure, in under-reinforced sections, is also permitted, but this mode is much different than that of sections reinforced with steel bars. Tension-controlled failure results in rupture of FRP bars, and this rupture may be sudden and catastrophic according to the FRP material linear failure. However, deformability is achievable (comparison to beams reinforced with steel bars and to beams reinforced with FRP). Therefore, the design of beams reinforced with FRP is usually controlled by the serviceability limit states, while the design of beams reinforced with steel bars is usually controlled by the ultimate limit states [12].

1.4 Structural Behavior and Design Philosophy

Although analysis for shear and flexural capacities of concrete elements draw on several of similar assumptions used for steel reinforcement, significant differences between the behavior of FRP and steel necessitate a shift away from a standard concrete design philosophy. In particular, the linear elastic stress-strain characteristic of most FRP composites (1–3% ultimate strain)[13] implies that FRP-reinforced concrete design procedures should account for inherently less plasticity than that exhibited by conventionally reinforced concrete[14]. Currently, FRP-reinforced concrete is designed exploitation limit states principles to ensure sufficient strength, to work out the governing failure mode, and to verify adequate bond strength. Serviceability limit states like deflections and crack dimensions, stress levels under fatigue or sustained loads, and relaxation losses of prestressed concrete are then checked. Though serviceability criteria are usually applied when strength design, relatively elastic modules lower especially for glass FRP and aramid FRP. This is means that serviceableness criteria can typically control the design [15].

1.4.1 Flexure Capacity

Flexural behavior is the best understood reinforced concrete-FRP, with basic principles applying regardless of member configuration, reinforcement geometry, or material type. Two possible flexural failure modes prevail. Sections with smaller amounts of reinforcement fail by FRP tensile rupture, whereas larger amounts of reinforcement lead to failure by crushing of concrete in the compression-zone before the attainment of ultimate tensile strain within the outermost layer of FRP reinforcement. The absence of plasticity in FRP materials implies that under reinforced flexural sections experience a sudden tensile rupture rather than a gradual yielding, as in the case of section reinforced with steel reinforcement. Thus,

the concrete crushing failure mode of an over reinforced member may be desirable [14].

Nominal flexural capacity is calculated from the constituent behaviors of concrete and FRP reinforcement using strain compatibility and internal force equilibrium principles, assuming the concrete strength for tensile is negligible. A perfect bond assumes between the FRP and concrete, and proportional the strain with distance from the neutral axis. The shape of the analytical expression can depend upon the prevailing failure mode. The Whitney rectangular stress block is appropriate for flexural capacity prediction when crushing of concrete in compression-zone occurs in over reinforced sections, provided that strain compatibility is used to determine FRP tensile forces as shown in Fig. (1.5). If FRP tensile rupture controls failure, the Whitney stress block might not be applicable, unless compression-zone concrete is at near-ultimate conditions. The moment capacity will be determined using a calculated moment arm in tension force. Presence of FRP in Compression-zone is not considered effective for increasing moment capacity, enhancing ductility, or reducing long-term deflections[14].

For steel-reinforced concrete, ductility will be defined as the ratio of the deformation at the failure to deformation at yielding. Members with ductility ratios of four were exhibiting important signs of distress prior to failure. As FRP reinforcement does not yield, alternate means that of quantifying the warning signs of impending failure should be used. A variety of indices to measure pseudo ductility are proposed, including deformability indices, defined as the ratio of ultimate deflection to service-load deflection or ultimate curvature to service-load curvature.

An approach considers the values of the net tensile strain within the outermost layer of FRP bars as the concrete compressive strain reaches the ultimate limit state. If the net tensile strain is 0.005 or larger, the section is ‘‘tension-controlled’’ and a lower resistance factor is needed to compensate for the suddenness of FRP tensile rupture[14, 16].

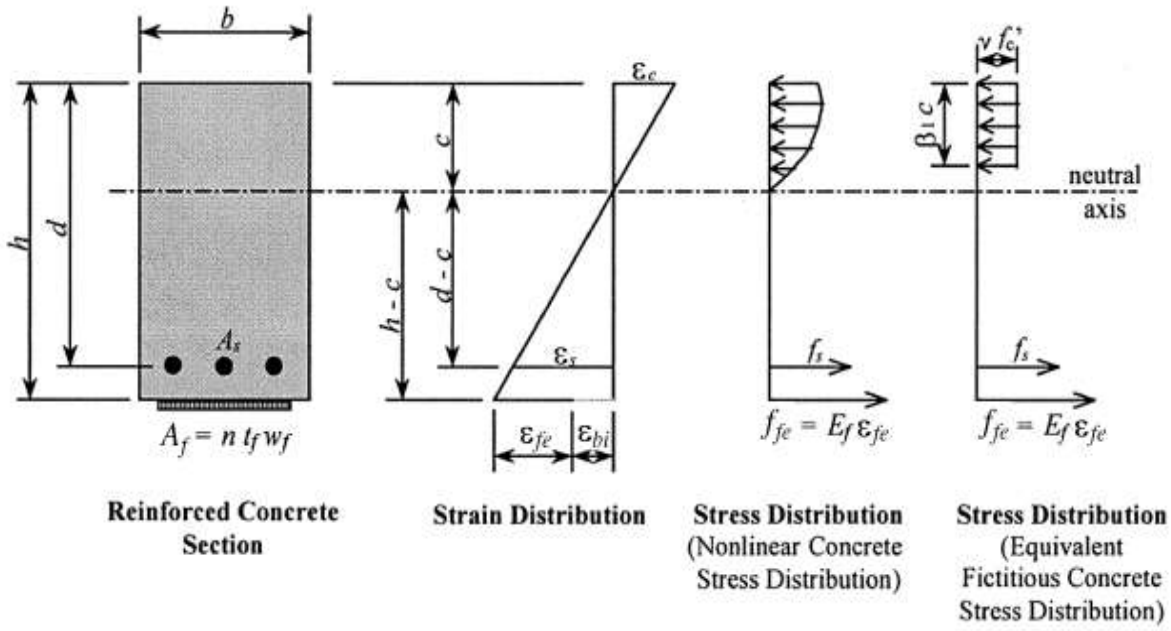

Figure (1.5) Internal strain and stress distribution for a rectangular section under flexure at ultimate stage [17].

1.4.2 Shear Capacity

The contribution of concrete strength in shear capacity is decreased in beams strengthened with FRP longitudinal bar due to smaller dowel forces, wider cracks and smaller of the concrete section in compression zones. A reduction factor proportional to the ratio of elastic modulus of FRP to the modulus of steel (E_{FRP} /E_{steel}) usually applied to concrete shear contribution equations for beams, although such an approach decreased the shear strength in flexural beams with larger magnitudes of FRP longitudinal reinforcement [18].

In beams reinforced with FRP as stirrups, the failures occur by FRP rupture or by a shear-compression failure within the shear span of the beam. Failure from stress concentrations at stirrup leads to a decrease in the effective capacity to thirty-fifth of the strength parallel to the fibers [19] . Multidirectional FRP grids. Also can be used to strengthen the concrete beams for shear resistance [20, 21].

1.4.3 Common Mode Failure in Flextural Strengthening

Flexural failure modes may be classified as:

1. yielding of major steel reinforcement and then FRP rupture failure. This failure mode usually takes place in lightly reinforced and lightly strengthened sections [22].
2. yielding of primary steel reinforcement and then concrete crushing. This failure mode usually occurs in moderately reinforced and moderately strengthened sections [23].
3. yielding of steel reinforcement and then cover delamination failure primarily occurring. This failure mode starts at the FRP curtailment because of stress concentration at the plate or sheet. Once cracking starts at an angle and then changes to a horizontal crack parallel to steel bar at the level of major steel because the steel stirrups inside the beam hold the inclined crack. The FRP and the entire concrete cover delaminates [22].
4. FRP Plate or sheet debonding along the interface plane due to the intermediate crack mechanism typically after yielding of primary steel reinforcement when the flexural cracks widen. The crack occurs along with the adhesive layer or parallel to it within the concrete cover. This failure mode is especially applicable to beams with end U-wrap anchorage[22].
5. for over-reinforced concrete beams, concrete crushing failure or cover delamination failure in beams with short FRP plates before primary steel yielding [24].

Reinforced concrete beams may also be retrofitted with (NSM) bars or laminate. This strengthening reinforcement is usually made of FRP bars or FRP laminate inserted in near-surface cut grooves and then closed with epoxy that fills the groove surrounding the bar or laminate[25].

FRP in NSM is similar to EBR sheets. However, failure modes are usually limited to

1. yielding of primary steel and then FRP rupture.
2. yielding of primary steel and then concrete crushing.

3. Concrete crushing and then yielding of primary steel.

In other words, cover spiliting and FRP debonding are less likely to occur with NSM technology.

1.4.4 Bond and Development of Reinforcement

Differences in FRP reinforcing products make bond characteristics quite variable. In some cases, the bond strength is comparable to or greater than that in steel reinforcement, while other products exhibit less bond strength [26].

Local bond-slip relations have been applied to glass FRP reinforcements of different diameters and embedment lengths (in pullout tests), and were found to match experimental results reasonably well while providing predictive capability for bars of arbitrary diameter and embedment length. Development lengths for glass FRP reinforcement bars by pullout failure are generally in the range of 26–37 times the bar diameter [16].

1.5 Strengthening Techniques

1.5.1 Externally Bonded FRP(EBR)

Externally bonded reinforcement of FRP (EBR) is the most common form of external FRP strengthening. It consists of bonding the FRP reinforcement to the external surface of the material to be strengthened. EBR typically consists of wet-lay-up sheets or a pre-cured plate. Advantages of EBR include the ease and speed of application. The disadvantages of the EBR technique include lack of bond between materials and this leads to debonding failure mechanisms.

1.5.2 Near Surface Mounted FRP (NSM)

Near surface mounted (NSM) of FRP is a technique in which pre-cured strips, bar, or rod are inserted into pre-cut grooves in the surface of the strengthened member. The grooves are usually cut large enough to contain the FRP and surround it on three sides with a thin layer of epoxy or some other bonding agent.

The advantages of this technique include the limited aesthetic impact and the potential for the development of higher strain in the FRP prior to debonding due to better confinement from the three bonded sides than comparable EBR applications which are usually not confined and are bonded only on one side.

1.6 Aim of the Study

The main objectives of this research can be summarized by the followings:

1- Investigating numerically using the finite element method to study the shear and flexural behavior of the RC beam strengthened by CFRP with different methods of strengthening (NSM and EBR) and different configurations of CFRP under four-point loading. The beams are simply supported with rectangular cross-sections.

2- Investigating the feasibility of using the ABAQUS program to evaluate failure modes and crack patterns of RC beams strengthened by CFRP.

3- Comparing the results obtained by ABAQUS with experimental results of Barros et al, 2006 and with equations proposed by ACI440-2R code.

4- After building the proper model, the effect of various parameters is study such as compression strength of concrete, sheet thickness and length ratio of CFRP laminate to clear span for the flexural. Also, the effect of strengthened U shape with two sides bond shape, shear span to depth ratio (a/h ratio) and configuration of CFRP for shear on the behavior of beams are studied.

1.7 Layout of Thesis

The thesis is organized in five chapters**.** Chapter one is a general introduction discuses behavior of concrete beams strengthened with CFRP sheet or laminate and describes the FRP and their shapes, types, applications, and properties. Chapter two presents a literature review of experimental and theoretical researches of concrete beams strengthened or repair with CFRP using NSM and EBR techniques.

Chapter three offers the principal formulation of finite elements and the derivation of the equations of governing equilibrium using the precept of virtual work. It also deals with the description of the ABAQUS/CAE/2014 software program application further to the non-linear performance of the systems and their solution method in ABAQUS/CAE/2014. Chapter four includes the modeling of concrete, steel, and CFRP in the finite element method to obtain the results of beams strengthened with CFRP in flexural and shear behavior and compared these results with experimentally (Barros et al, 2006) and ACI. Also, the various parametric study of flexural and shear behavior of RC beams. Finally, Chapter five summarizes the conclusions of the present study and points out some of suggestions for future work.

Chapter Two

Literature Review

2.1 General

The maximum strength of RC members is depending on several factors one of all them is that the type of reinforcement materials. Because of the durability and corrosion problems of steel reinforcement, different materials such as fiber reinforcement polymers (FRP), have seemed to be an alternative reinforcement material. FRP reinforced concrete members started to be used in retrofitting of the concrete beams to improve the shear behavior, bond performance and flexural behavior …etc[1].

2.2 Strengthening of RC Beams by CFRP for Flexure

Lorenzis et al. 2000, [27] carried out tests on four RC beams with a T-shaped cross-section and a total length of 4.5 m. They studied the effectiveness of NSM FRP rods as a strengthening system for RC structures. The effect of groove size on the structural behavior of FRP-beams has been investigated. An increasing groove size led to higher bond strength was observed. The max load increased by 8% and 24% as the groove size increased from 1.6 cm to 1.9 cm. Generally, they showed that an increase in capacity ranging from 25.7% to 44.3% for strengthened beams with FRP over the control beam. Also, the increase in stiffness was obtained.

Barros and Fortes, 2005, [28] showed that the near-surface mounted (NSM) strengthening technique using CFRP laminate strips were applied for increasing the strength of reinforced concrete beams failing in bending. The NSM technique has provided an increment of the load serviceability limit state, as well as, the stiffness when concrete cracking. They concluded that the proposed strengthening technique provided an average increase of 32% in the service load which represented the load corresponding to the deflection equal to L/400, 39% in the load corresponding to the yielding of steel reinforcement, 28% in the stiffness at a load level

corresponding to the service load of the retrofitted beams, and 32% in the stiffness at load equal to 90% of the maximum load of the reference beams. The maximum strain of CFRP laminates has earned values between 62% and 91% of its ultimate strain.

Obaidat et al. 2010, [29] A finite element model depended on experimental tests of eight beams were presented. All beams had the same rectangular cross-section geometry and subjected to four-point bending. The lengths of the CFRP plate were changed and have been studied. The finite element method with ABAQUS programs was used to represent the RC beams retrofitted with CFRP. Different material models were tested to explain the behavior of the beams. Linear elastic orthotropic and isotropic models were used for the CFRP. Two types of the bond had been used: a cohesive bond model and a perfect bond model to represent the CFRP-concrete interface. A plastic damage model was utilized for the concrete element. They concluded that a good agreement with the experimental results relating to crack pattern, load–displacement response, and debonding failure mode when the cohesive bond model was used. The perfect bond model did not give the exact behavior of the beams. Also, they showed that there was no significant difference between the elastic orthotropic and isotropic models in the behavior of RC beams.

Obaidat et al. 2011, [30] showed the results of an experimental investigation to study the behavior of RC beams retrofitting with CFRP laminates in flexure and shear. The length of CFRP and position of retrofitting were studied. The experimental results, generally, indicated that the beams retrofitted in shear and flexure by CFRP laminates were structurally efficient to stiffness and the carrying capacity of the beams. It had been found that the efficiency of the strengthening technique by CFRP in flexure varied depend on the length for CFRP. Also, the results showed most of the beams failed by plate debonding mode.

Attari et al. 2012, [31] presented a study to exam the efficiency of EBR for RC beams exploitation FRP material (Glass–Carbon). They dealt with different strengthening configurations thought out the research (use of separate one-way glass and carbon fibers with some U-anchorages or of two-way glass–carbon fiber hybrid fabric). A total of seven flexural strengthened concrete beams are instrumented and tested under repeated loading sequences employing a four-point bending device to study the behavior until failure occurs. The results showed that the use of a two-layer Glass–Carbon fibers composite material for strengthening RC beams is very efficient due to increase in strength capacity of 114% was obtained for the strengthened beam specimens in comparison with the reference control specimen. The U-anchorage strengthening configuration improves the flexural strength and contributes to the redistribution of the internal forces through greater deformations of the beam specimens.

Pecce et al. 2014, [32] investigated experimentally and numerically the behavior of GFRP reinforced concrete beams in bending. The samples used were three concrete beams with dimensions (3400mm span length, 500mm width, 185 mm height) reinforced with GFRP. The investigated characteristics of structural behavior were the curvature, width and crack spacing, and deflection, moreover the verifications at the serviceability and ultimate conditions were analyzed. They concluded that the simplified (i.e stress block) was acceptable to calculate the ultimate moment of beams, depending on the test values. For the evaluation of deflection, the proposed modified ACI code model obtained a good agreement for the experimental results. They observed the difference in the failure modes between the design criteria and the experimental results.

Bilotta et al. 2015, [33] presented the efficiency of FRP materials for retrofitting existing RC structures by NSM and EBR techniques. Ten RC beams with simply supported over a clear span of 2.1 m had been tested. All beams had a rectangular cross-section with a height of 160 mm and a width of 120 mm. The load

was applied into two different schemes: a) four-point bending scheme with 2 forces at a distance of 250 mm, b) eight loading points spaced 250 mm a distributed along the beam axis. The results showed the NSM technique is a better method than the EBR technique. Also, the results conducted from the numerical by approach suggested in the Italian Guidelines and experimental test of RC beams strengthened with EBR influenced by the loading pattern. The results of flexural tests under distributed load for RC beams reinforced with each NSM and EBR techniques were discussed to show the debonding phenomena for NSM strip strengthened beams were less significant than for EBR beams. Finally, the experimental results were compared with the perdition of theoretical models such as the approach suggested in the Italian Guidelines (CNRDT200/R1) and code.

Zhang et al, 2016, [34] presented a numerical model of the structural behavior of RC beams-reinforced by CFRP under four-point loading. They investigated 3 beams for flexural-shear strengthening and flexural. Two beams were retrofitted with one layer of CFRP sheets for flexural and U shape for shear and one beam without strengthening as a control beam. They employed the extended finite element method (XFEM) model was applied in ABAQUS to show the effects of localized cracks on the response of CFRP sheets strengthened RC beam. The good agreement between numerical results and experimental data at the early stage of the behavior, but this case does not found as load increased. Concrete damaged plasticity model used to represent concrete element in FE. They found that the (XFEM) can be used to simulate crack propagation in structures under simple conditions, but the constitutive relations of concrete based on the XFEM in ABAQUS still needs further development.

Khalifa, 2016, [35] showed that the NSM and EBR technique used to reinforce RC beams by FRP increasing the load-carrying capacity of RC beams. NSM technique has many advantages compared to the EBR method, such as reducing the risk of debonding, and much better protection from the external

sources of damage. The study was investigated the effectiveness and performance of the NSM and EBR techniques for the flexural retrofitting of RC beams. Beams were reinforced with different (CFRP) and examined. Beams were designed to fail in flexural mode. The results indicated the beams retrofitted with NSM laminate achieved a higher maximum load than those reinforced with EBR for a similar area of CFRP. An increase in the maximum load ratio ranged between 12% and 18%. Moreover, a design approach in the ACI 440.2R-08 for computing the moment capability of RC flexural beams reinforced with NSM CFRP laminate was presented and developed.

Garyfalia et al. 2017, [36] Seven RC beams with a width of 150 mm, a height of 300 mm and a length of 2300 mm were tested. Beam RC-N was a reference beam with no corrosion, while the remaining six beams were applied to an accelerated corrosion technique at medium and low corrosion levels. Beam R-CO1 was the control corroded beam at low corrosion level, while R-CO1S1 and R-CO1S2 were corroded beams repaired and strengthened with EBR and NSM carbon FRP systems, respectively. At medium corrosion level, the control beam was named R-CO2, while the strengthened and repaired with EBR and NSM CFRP were named R-CO2S1 and R-CO2S2, respectively. They used a 3D nonlinear finite element (FE) approach using the ABAQUS program in the study. The results showed that all repaired beams presented an increased load-carrying capacity with respect to the non-corroded beam. Both EBR and NSM techniques may be used to repair RC structures efficiently. A comparison with the experimental data has been achieved a good agreement between the experimentally and analytically results was obtained.

Raoof et al. 2017, [37] presented the comparison between reinforced with FRP and textile-reinforced mortar (TRM) of RC beams for flexural. They studied the number of FRP or TRM layers, the type of fiber material, the surface condition, (uncoated and coated) and the end-anchorage system of the external reinforcement. The experimental work was conducted on 13 RC beams subjected to four-point

bending. The first beam represented as a reference beam, five beams strengthened with FRP and seven with TRM. The results: (a) TRM was usually inferior to FRP in strengthening the flexural capacity of RC beams based on the parameters studied and (b) when increased the number of TRM layers from one to three, the TRM versus FRP effectiveness ratio was nearly increased. Also, equation proposed by FIB Model Code 2010 for FRP reinforcement was used to predict the mean debonding stress developed in the TRM reinforcement. The experimental results ware in a good agreement with the stresses obtained from the proposed equation.

Almusallam, 2018, [38] investigated the behavior of RC beams strengthened with FRP containing large rectangular web openings in the flexure zone. The parameters such as type of loading, opening size, and strengthening method was studied. Seven RC beams divided into two groups. In the first group, two control beams (one beam with large rectangular web opening in the flexure zone and another beam solid without opening) were tested under four-point bending. In the second group, five beams were studied under center-point loading. One control beam, four beams with large rectangular web opening without strengthening within the maximum-moment region. The other two beams with opening and strengthened by two different FRP schemes. A numerical results were compared with experimental and it was in agreement with experiment results. In other words, it indicated that the finite element was an accurate approach, which may be reliably used in future research on the use of FRP strengthening for RC structural members. The conclusion of the investigation showed that, the ultimate capacity of the RC beams with opening not influenced by the opening in the pure flexural zone if the depth of the top chord was equal or greater than the depth of the concrete stress block.

Ghaedi et al. 2018, [39] Two (RC) beams reinforced with (CFRP) laminate were investigated by FEM adopting the ABAQUS program. They considered the CFRP elements as elastically isotropic and orthotropic materials. To validate this

study, the numerical results were compared with experimental work. The results showed that CFRP with orthotropic or isotropic properties has no important influence on beam responses such as stresses, displacements and damage response under applied loadings.

Zaki and Rasheed, 2020, [40]presented the effect of new flexural anchorage devices on improving the performance of strengthened reinforced concrete beams in flexure. Six reinforced concrete (RC) beams were prepared and tested, three of which having identical T cross-section and the other three with identical rectangular section. The first specimen in each series was tested as a control beam. The second specimen in each series was strengthened using four layers of flexural CFRP in addition to side GFRP bars. The last specimen in each series was strengthened in flexure using identical four layers of CFRP plus GFRP patches installed longitudinally along both sides of the beam. The beams were tested under four-point bending until failure and the results for each series are evaluated. In addition, the outcome is compared with U-wrap anchorage technique that has been examined by others. It was concluded that using CFRP sheets with both anchorage devices significantly increased the flexural capacity beyond that of unanchored and U-wrap anchored specimens. Quantitatively speaking, T beams anchored with GFRP sidebars and GFRP side patches showed 74% and 58% increase in strength over unanchored strengthened specimens respectively.

Bacciocchi et al. 2020, [41]showed that the application of innovative constituents and materials can noticeably affect the mechanical behavior of structures. The research is focused on the long-time behavior of concrete beams reinforced by Carbon Fiber Reinforced Polymer (CFRP) strips applied on their external surfaces. The concrete and the CFRP are both characterized by time-dependent mechanical features according to the theoretical framework provided by the linear viscoelasticity. Their properties are described through the introduction of the proper

creep functions. The reinforcing strips are made of a polymer matrix reinforced by straight long Carbon fibers and randomly oriented Carbon nanotubes (CNTs). The Timoshenko beam theory for laminated beams is employed to describe the mechanical behavior of the structures. A numerical solution is developed to achieve the time dependency of central deflections and the redistribution of stresses along the thickness of the layered structures. The results presented in this paper could be taken into account to improve the structural response of concrete beams in contrasting the creep phenomenon due to the intrinsic nature of the material.

2.3 Strengthening of RC Beam by CFRP for Shear

Lorenzis and Nanni, 2001, [42] presented the NSM technique to reinforce the RC beam by FRP rods for improving the shear strength. Eight RC beams (two control beams and 6 retrofitting beams) were tested. CFRP rods were used for shear strengthening. The variables used in the shear test were spacing of the rods, strengthening pattern, end anchorage of the rods, and presence of steel stirrups. The exploration showed that NSM-FRP rods improved the shear capacity of RC beams. The contribution of the rods by NSM increased the strength capacity in the presence of internal shear reinforcement and provided a larger bond length with anchoring the NSM rods in the beams that will prevent failure mode by debonding. Also, the results of theoretical model were presented and compared with experimental and showed the results was in good agreement.

Ibrahim and Mahmood, 2009, [43] an analyzed model using a finite element were studied. The RC beams reinforced by using (FRP) laminates have been investigated. The finite element models were developed by employing a smeared cracking approach for concrete and 3-dimensional stratified elements for the FRP composites. The results obtained from the FEM using program ANSYS were compared with the experimental tests for six beams. The comparisons were created for load-deflection curves at mid-span, and failure loads. The accuracy of FEM is assessed by comparison with the experimental data. The relationship

between load and deflection curves from the FE analysis agree well with the experimental tests, however, the FE results were stiffer than that from the experimental results. the maximum distinction in ultimate loads for all cases was 7.8%.

Obaidat et al. 2010, [44] nonlinear 3-D numerical model have been developed. ABAQUS finite element program used to predict test the shear behavior of beams retrofitted by CFRP. Two models were used to represent the interface between concrete and CFRP, the first one was a cohesive model and the second one was a perfect bond model. The effectiveness of the model was performed using the results obtained from the experimental work. The results concluded that the cohesive model was best than a perfect model to simulate the composite behavior of RC beams reinforced by CFRP in shear. The model was used to test the influence of orientation and length of CFRP. Change in length of CFRP reinforcement may result in different behaviors of retrofitted beams. The longest CFRP presented a high stiffness and high load.

Abdel Rahman and Osman, 2017, [45] studied RC beams retrofitted for shear with ERB CFRP sheets using finite element method by the ABAQUS program. Three beams were investigated and its results were compared with experimental test results. The first beam is 1.96 m in length with rectangular cross-section of 150 mm width and 300 mm depth. The main tension reinforcement was 2 ϕ 12, the second reinforcement was 2 ϕ 10, and vertical steel stirrups are ϕ 8 at 100 mm spacing. The second beam was molded with the same concrete dimensions but with an increase in main longitudinal steel and a decrease in transverse steel to obtain shear failure. In the third beam CFRP sheets was bonded to the beam on tension face only. The results presented that the CFRP sheets increased the ductility and the maximum shear load by 50% and 23%, respectively compared to the unstrengthened beam. The comparison was performed for strengthened and un-

strengthened beams and the general behaviors showed a good agreement with the experimental results.

Chen et al. 2018, [46] presented an experimental study by using Basalt fiber reinforced polymer (BFRP) of RC beams. BFRP may be a promising material for the application to structure retrofitted with its advantages of low cost, and corrosion resistant. To study the efficacy of the BFRP strengthening beam under three-point bending, six beams including one reference beam and five strengthened beams (namely B150A, B150B, B150C, B150D, and B330B) were used. They found that using U-jackets as an anchor system can change the failure mode from FRP debonding to FRP rupture. For the same amount of materials, it was concluded that the inclined U-jackets (highly recommended) were much more efficient than vertical U-jackets. And also U-jackets anchorage can provide significant anchorage and delaying debonding by increasing the maximum load from 20% to 37.8% with U jackets anchorages.

Benzeguir et al. 2018, [47] presented an experimental work to investigate the effect of beam size on the shear behavior of the RC T-beams section reinforced in shear with externally bonded CFRP sheets. The experimental program involved twelve beams of similar geometrically with different effective depth, d, with and without internal transversal steel reinforcement. Six control beams (un-strengthened) and six beams retrofitted in shear with externally bonded CFRP sheets were studied. The results concluded that an increased in shear strength when increase the size of beams for both control and strengthened beams with and without transverse steel. The size of the beam effected on shear strength with and without CFRP contributions. This was significantly for strengthened specimens without internal transversal steel.

Oller et al. 2019, [48] an experimental program of T-RC beams strengthened for shear by CFRP sheets was achieved. Two longitudinal reinforcement ratios and different externally bonded CFRP shear strengthening with discontinuous and

continuous U-shaped configuration with and without mechanical anchorages. The experimental work consisted of ten RC beams with a T-shaped cross-section. Beams were 5800 mm long with flange and web cross-sections of 600×150 mm and 200 × 400 mm, respectively. The results concluded that the beams strengthened with CFRP will decrease in maximum load when anchorages were low regardless of the CFRP reinforcement ratio. There is a proof of the interaction of all shear strength components, concrete V_c, transversal steel V_s, and CFRP sheets V_f that were obtained from the registered data of the instrumentation. There was an important difference between the total of the V_c, Vs, and V_f components and the sum shear force. The different shear strength components have been obtained for all beams. As observed, the V_f component was much higher for beams with anchorages.

Mostofinejad et al. 2019, [10] examined the structural performance of RC beams reinforced for shear using NSM technique through experimental and numerical study. The variable of the study were concrete compressive strengths and of transversal reinforcements ratio. In the experimental section, four reinforced concrete beams were investigated with and without stirrups to check the effect of the NSM technique as a shear strengthening method. Beams with dimensions 2000× 300×200 mm were examined under four points loading up to failure. The experimental results indicate that the NSM technique increases the shear capability of 69% and 41% for the beams with and without stirrups, respectively. Ductility decreased in beams strengthened CFRP using the NSM technique compared to the un-strengthened beams. The numerical analysis showed that as the compression strength of the concrete increases, the maximum deflection and the load capacity of beams improved. When the compression strength of the concrete increased, the stresses in the adhesive layer also increased. Both numerical and experimental results showed that as the transverse steel reinforcement ratios increase, the

effective strain of CFRP strips decreases. By decreasing the stirrup spacing to 65 mm, the shear failure of the strengthened RC beam changes to a flexural failure.

Al Rjoub et al. 2019, [49] experimentally studied the RC beams strengthened in shear using NSM technique by carbon CFRP. Fourteen beams in dimension (150 × 200 × 1200 mm) were investigated under four-point bending. The effect of side concrete cover depth, NSM-CFRP strip length and NSM-CFRP strip inclination angle on the behavior of RC beams were studied. Six of the beams were investigated with three different concrete cover depths, twenty, thirty and forty millimeters and strengthened in shear by NSM-CFRP with inclination angles of 0° and 45°. Other beams with a side concrete cover depth of thirty millimeters were strengthened in shear by NSM-CFRP with different strip lengths, measured in terms of beam depth (full, 2/3, and 1/3) and inclinations of 0° and 45°. Shear strengthening arrangements using NSM affected the behavior of retrofitted beams in failure modes and maximum load. NSM CFRP reinforcement improved the shear capacity of RC beams by up to 176% and changes the failure mode from shear to flexure in many cases. The results showed that the beams with inclined NSM strips presented higher ultimate shear strengths than those with vertical NSM. Also, it was concluded that the ultimate shear strength for shear increases with increasing the strip length. When decreased side concrete cover depth did not reduce beam ultimate strength.

Kadhim et al. 2019, [50] Three-dimensional finite element (FE) model using ANSYS program was developed for RC beams strengthened with CFRP rods in shear with the NSM technique. The effect of Concrete Compressive Strength, Percentage of Existing Shear Reinforcement, and Distance Between Existing Shear Reinforcement and NSM Rods were studied. The FE models were developed based on existing experiments tests. they showed that with increasing the concrete compression strength (f_c') leads to an increase in the ultimate load by a contribution of NSM CFRP reinforcement. They found that the maximum load increased when percentage of FRP (p_f) is 0.14–0.22%. Also, the maximum load increased by 11%

when (p_f) increased to 0.28%. When increased the percentage of steel stirrups (p_{sw}) from 0.11 to 0.36%, led to increase in the ultimate load from 8% to 15% compared to the unstrengthened beam. When the percentage of steel stirrups (p_{sw}) increased more than 0.36% caused a decrease in the amount of the NSM CFRP technique because of the changing in mode failure. The distance between existing steel stirrups and NSM reinforcement does not effect on the behavior of RC beams reinforced with CFRP.

Al-Rousan, 2020, [51] showed an analytical model to predict the shear strength of reinforced concrete (RC) beams externally strengthened with CFRP composites. The proposed model gives consistently good correlation with test data with an acceptable COV that can be expected for the behavior of RC beams. The results showed that the ACI model has a much wider range of experimental/theoretical failure load ratios of 0.16 to 10.08. The Triantafillou models also give an acceptable range of experimental/theoretical mean values of 0.27 to 2.78. On the contrary, the Colotti model gives a much smaller range of experimental/theoretical mean values of 0.20 to 1.78. Therefore, the proposed model is thus applicable to all externally bonded beams irrespective of whether the bonded reinforcement is made of steel or CFRP.

Mohammed et al. 2020, [52] investigated the influence of important parameters affecting shear transfer strength and deformation of concrete strengthened externally using CFRP laminate. Parameters investigated were the internal steel reinforcement, CFRP layers, existence of preloading, and existence of tension on shear plane. Results showed that there is a relatively high shear strength enhancement of non-reinforced concrete strengthened with CFRP laminate, reaching 91% when two CFRP layers are used for strengthening. Shear enhancement ratio was found to reduce with the increase of the internal steel ratio, of an enhancement between 8% and 29%. Effect of moderate preloading on concrete was found not important on the residual shear strength. There is a good

chance to strengthen concrete subjected to shear and tension for shear enhancement between 22% and 157%. A new proposal was developed for the prediction of direct shear capacity of strengthened concrete, essentially depends on an accurate assessment of FRP laminate contribution to enhance shear.

2.4 Concluding Remarks

1. Most of the previous numerically works represented RC beams strengthened with CFRP on flexural or shear behavior but did not represent both behaviors in the same model. It is very important for any structure is present theoretical contributions to enhance the understanding the beams reinforced with CFRP by work the same model in shear and flexural behavior.

2. Most of the previous numerically and experimental works did not do a parametric study such as the effect of a/d, the shape of CFRP (two sides and U-shaped), the effect of the length ratio of CFRP laminate to clear span and effect of thickness of CFRP in shear and flexural behavior, but in this study have been done, also the results will compare with experimental and ACI.

Chapter Three

Finite Element Method

3.1 Introduction

Finite Element Analysis (FEA) used the Ritz technique of numerical analysis and minimization of variational calculus to get the approximate solutions in vibration systems. Firstly, FEA was limited to pricey mainframe computers usually owned by aeronautics, automotive and defense. By developing the computers and the increase in computing power, FEA has been developed to incredible precision. Nowadays, supercomputers are now able to produce accurate results for all types of parameters [53].

For an engineering system, the property of the material, the boundary, initial and loading conditions are very difficult to solve the governing differential equation using analytical method. In practice, most of the problems are solved using a numerical method like the finite element method (FEM).

The FEM is one of the numerical methods that can be used to solve ordinary and partial differential equations. In FEM, the actual continuous body of matter like solid, liquid or gas is represented as an assemblage of subdivisions called finite elements. These elements are considered to be an interconnected at specified joints which are called nodes or nodal points. The nodes usually lay on the element boundaries where elements are connected. Since the actual variation of the field variable (like stress, displacement, temperature, pressure, or velocity) inside the continuum is not known, it is assumed that the variation of the field variable inside a finite element can be approximated by a simple function.

Finite element analysis uses a complex system of points known as nodes that create a grid known as a mesh. This mesh is programmed to contain the material and structural properties that define however the structure can react to certain loading conditions. Nodes are assigned at an exact density throughout the material depending on the anticipated stress levels of a particular area. Regions that will receive large

amounts of stress should be given more attention than those that experience very little or no stress. Points of interest might consist of: fracture point of previously tested material, fillets, corners, complicated detail, and high-stress areas. The selection of mesh density is a very important step in FE modeling. Adequate range of elements is required to obtain convergence of results. This is often in practice achieved when a rise in the mesh density has a negligible effect on the results[53].

There are typically three types of analyses were utilized: one-dimension, two-dimension modeling, and three-dimension modeling. Two-dimension and one-dimension modeling conserves simplicity and permits the analysis to be run on a conventional computer, it tends to yield less accurate results. Three-dimension modeling, however, produces more accurate results whereas sacrificing the ability to run on almost the fastest computers effectively.

In this chapter, simple three-dimensional finite element models are developed for accurate and efficient prediction of structural behavior of CFRP strengthened RC beams using the commercial FE analysis software ABAQUS. A finite element model FEM is developed first assuming adhesive between FRP and concrete interfaces in external bonded of CFRP sheet or laminate (EBR) and perfect bond for near surface mounted (NSM) [54].

3.2 ABAQUS

There are different finite element analysis tools that can be utilized for numerical simulation and analysis, such as ABAQUS and ANSYS programs.

It is general simulation tool and may use to solve a large range of engineering problems, including structural analysis and heat transfer problems. ABAQUS has an extensive element and material libraries capable of modeling a variety of geometries and material constitutive laws.

program ABAQUS consists of three major products: ABAQUS/Explicit, ABAQUS/Standard and ABAQUS/CAE. ABAQUS/Explicit and ABAQUS/Standard perform analysis, ABAQUS/CAE provides a graphical environment for pre and post-

processing. ABAQUS/Standard and ABAQUS/CAE could be a general-purpose analysis program for solving linear, nonlinear, static and dynamic problems. ABAQUS/Explicit could be a special-purpose analysis program that uses an exact dynamic FE formulation. ABAQUS/CAE are utilized in this thesis for structural analysis.

ABAQUS and ANSYS are both used to simulate structural elements and are also capable of assembling different simple parts to form a more complicated structural element. The ability of ABAQUS to model cohesive elements more accurately makes it the preferred choice for numerical modeling and nonlinear analysis of RC beams reinforced by CFRP in shear and flexure [55].

3.3 Structural Modeling in ABAQUS

Each analytical model in ABAQUS includes ten modules: part, Property, assembly, step, interaction, load, mesh, job, visualization, and sketch. To make a complete analysis model, it is typically necessary to go through most of those modules, as described below:

1. Build up the geometry of the structure under a set of elements. (part module, sketch module, mesh module)
2. Produce element sections (property module)
3. Introduce material information (property module)
4. Assign material properties and section to the members (Property module)
5. Assemble parts to make the complete structure (assembly module, mesh module, and interaction module)
6. Create steps and select analysis method (step module)
7. Introduce boundary conditions and load (load module)
8. Work jobs and submit for analysis (job module)
9. Visualize the result. (visualization module)

3.4 Equilibrium conditions

The equilibrium calculation for a nonlinear structure in static equilibrium is derived using the principle of virtual work. The standard states that if a general structure in equilibrium is subjected to a system of small virtual displacements within a compatible state of deformation, the virtual work due to the external action is equal to the virtual strain energy due to the internal stress [56].

$$\delta W_{int} = \delta W_{ext} \quad \ldots\ldots\ldots\ldots \quad (3.1)$$

W_{int} : inner work (strain energy).

W_{ext} : outside effort (work finished by the implemented pressure)

The virtual inner effort is:

$$W_{int} = \int \{\varepsilon\}^T \{\sigma\} dv \quad \ldots\ldots\ldots\ldots \quad (3.2)$$

$\{\varepsilon\}$: elements of virtual strain vector

$\{\sigma\}$: elements of actual stress vector

dV :infinitesimal volume of the element

Strains may be determined from the corresponding stresses $\{\sigma\}$through by means of the general stress-strain correlation.

$$\{\sigma\} = [D]\{\varepsilon\} \quad \ldots\ldots\ldots\ldots \quad (3.3)$$

[D] : Constitutive matrix

After restitution Equation (3.3) into (3.2), the virtual inner effort can be inscribed as:

$$W_{int} = \int \{\varepsilon\}^T [D] \{\varepsilon\} dv \quad \ldots\ldots\ldots\ldots \quad (3.4)$$

The displacements {U} within the element are associated by means of interpolation to nodal displacements {u} by using:

$$\{U\} = [N] \cdot \{u\} \quad \ldots\ldots\ldots\ldots \quad (3.5)$$

[N] : Matrix of shape function

{u} : Unidentified nodal displacements vector (local displacements)

{U}: body displacements vector (global displacements).

By differentiating Equation (3.5), the strains for an element may be associated to its nodal displacements by using:

$$\{\varepsilon\} = [B]\{u\} \quad \text{(3.6)}$$

[B] : strain-nodal displacement relation matrix, primarily based on the detailed shape features assuming that each result is in the global cartesian system and then combining Equation (3.6) with Equation (3.4) gives:

$$W_{int.} = \{u\}^T \cdot \int [B]^T [D][B]\, dv \cdot \{u\} \quad \text{(3.7)}$$

The external effort, that is resulting from the nodal forces implemented to the element, may be accounted for by using

$$W_{ext.} = \{u\} \cdot \{F\} \quad \text{(3.8)}$$

{F}: nodal forces applied to the section

Eventually, equations (1), (7) and (8) can be mixed to provide:

$$\{u\}^T \int [B]^T [D][B] dv \{u\} = \{u\}^T \{F\} \quad \text{(3.9)}$$

Noticing that $\{u\}^T$ vector is a fixed or arbitrary virtual displacement, the situation required to fulfill equation (3.9) may be reduced to:

$$\{F\} = [K^e] \cdot \{u\} \quad \text{(3.10)}$$

where

$$[K^e] = \int [B]^T [D]\, [B]\, dv \quad \text{(3.11)}$$

$[K^e]$= Stiffness matrix of element

$$dv = dx \cdot dy \cdot dz$$

Equation (3.10) represents the equilibrium equation on a one-element foundation. For all elements, the stiffness matrix of the structure [K] is constructed up by means of including the element stiffness matrices (adding one element at a time), after transforming from the local to the global coordinates, this equation can be written as:

$$\{F^a\} = [K]\{u\} \quad \text{(3.12)}$$

$[K] = \sum_n [k^e]$: Structural stiffness matrix

$\{F^a\}\ and\ \{F\}$: Vector of implemented loads

n : Total number of factors.

3.5 Nonlinear Solution Techniques (FE)

The FE discrimination process yields a set of simultaneous equations:

$$[K]\{U\}=\{F^a\} \quad \text{.....(3.13)}$$

where, $\{U\}$ is the vector of nodal displacements, {K}is the stiffness matrix and $\{F^a\}$ is the vector of loads.

For linear elastic Equation. (3.13) is used to calculated the solution of the unknown displacement $\{U\}$. In the case of nonlinear state, $[K]$ is a function of the unknown displacement. The Equation (3.13) cannot be computed exactly before finding of the unknown displacement $\{U\}$.

There are three techniques for solution the nonlinear Equation (3.13); the basic technique divides into:

(1) Incremental procedure as shown in Fig. (3.1a).

(2) Iterative procedure as shown in Fig. (3.1b).

(3) Incremental- Iterative procedure as shown in Fig. (3.1c).

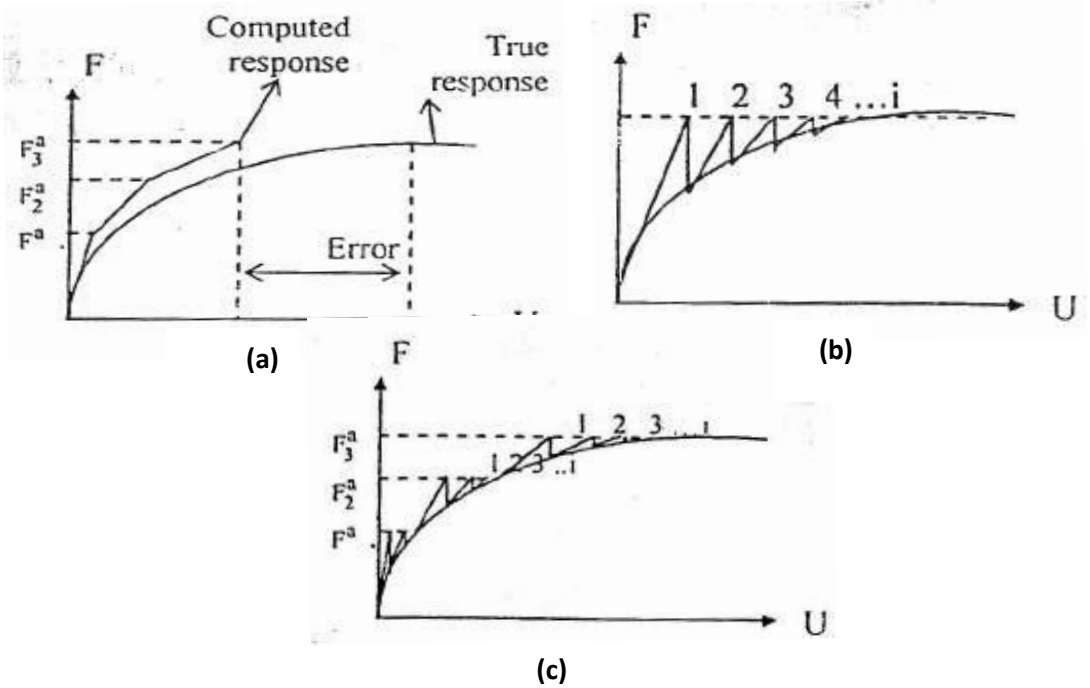

Figure (3.1) Types of technique for solution the nonlinear equation

(a) incremental (b) iterative (c) incremental–iterative [57]

In case the incremental procedure, the load is applied in many small increments, and also the structure is assumed to respond linearly within every increment with its stiffness recomputed depend on the structural geometry and member end actions at the end of the previous load increment. This is often an easy procedure, which requires no iterations, however errors are likely to accumulate after many increments unless very fine increments are used , Fig. (3.1a) [57].

In case the iterative procedure, the load is applied in one increment at the first iteration, the out of balance forces are then computed and used in the next iteration until the final converged solution would be in equilibrium, such that the internal load vector would equal the applied load vector or within some tolerance. This process can be written as:

$$\left[K_i^T\right]\{\Delta U_i\}=\{F^a\}-\{F^{nr}\} \quad \text{.....(3.14)}$$

$$\{U_{i+1}\}=\{U_i\}+\{\Delta U_i\} \quad \text{..... (3.15)}$$

where, $\left[K_i^T\right]$ is the initial stiffness matrix, (i) is the subscript representing the current equilibrium iteration and $\{F^{nr}\}$ is the internal load vector.

This procedure fails to produce information about the intermediate stage of loading. For structural analysis including path-dependent nonlinearities increments are in equilibrium in order to correctly follow the load path. This can be achieved by using the combined incremental-iterative method. In the combined-iterative procedure, a combination of the incremental and iterative scheme is used. The load is applied incrementally, and iterations are performed in order to obtain a converged solution corresponding to the stage of loading under consideration , as shown in Fig. (3.1c) [57].

incremental-iterative solution procedures have been used in this study. The full Newton-Raphson procedure is applied. The stiffness matrix is formed at every iteration. The advantage of this procedure may give a more accurate result. The

disadvantage of this procedure is that a large amount of computational effort may be required to form and decompose the stiffness matrix, as shown in Fig. (3.2) [57].

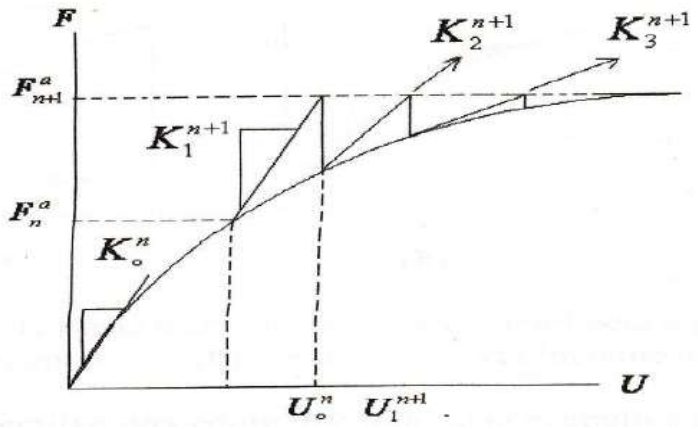

Figure (3.2) Incremental-iterative procedures full newton- raphson procedure [57]

3.6 Convergence criteria

Abaqus/Standard uses Newton's method to solve nonlinear problems. It uses an exact implementation of Newton's method, in the sense that the Jacobian of the system is defined exactly, and quadratic convergence is obtained when the estimate of the solution is within the radius of convergence of the algorithm. The Jacobian is approximated so that the iterative method is not an exact Newton method.

Most nonlinear engineering calculations will be sufficiently accurate if the error in the residuals is less than 0.5%. Therefore, Abaqus/Standard normally uses:

$$\tau_{max}^{\alpha} \leq R_n^{\alpha}\, q^{-\alpha} \quad \text{.....(3.16)}$$

as the residual check, where you can define R_n^{α} (it is 0.005 by default) and $q^{-\alpha} = 0.01$ in this study. If this inequality is satisfied, convergence is accepted if the largest correction to the solution, c_{max}^{α}, is also small compared to the largest incremental change in the corresponding solution variable, ΔU_{max}^{α}.

$$c_{max}^{\alpha} \leq c_n^{\alpha}\, \Delta U_{max}^{\alpha} \quad \text{(3.17)}$$

Where:

$c_n^{\alpha} = 0.01$

3.7 Finite Element Analysis

(FEM) was performed to model the nonlinear behavior of RC beams. The FEM package ABAQUS was used in this study.

3.7.1 Concrete

The plastic damage was performed to model the concrete behavior. This model assumes that the major two failure modes of concrete are tensile cracking and compression failure as shown in Fig. (3.3) [58]. The modulus of elasticity (Ec) and modulus of rupture are calculated theoretically based on experimental values of the compression strength of concrete (f_c^-).

For tension behavior[59]:

$$ft = 0.61\sqrt{f_c^-} \quad \text{(3.16)}$$

$$Ec = 22\,(0.1 \times f_c^-)^{0.3} 1000 \quad \text{(3.17)}$$

$$\varepsilon_{et} = \varepsilon_t = F_t / E_c \quad \text{(3.18)}$$

$$\varepsilon_{t1} = \varepsilon_{et} + 0.0001,\ \varepsilon_{t2} = \varepsilon_{t1} + 0.0001$$

$$\sigma_t = f_t(\varepsilon_{et}/\varepsilon_t)^{0.4} \quad \text{(3.19)}$$

$$\varepsilon_{cst} = \varepsilon_t - (\frac{\sigma}{E_c}) \quad \text{(3.20)}$$

For compressive behavior[59]:

$$k = 1.05 \times E_c(\frac{\varepsilon_{c1}}{f_c^-}) \quad \text{(3.21)}$$

$$\varepsilon_{c1} = 0.0014(2 - e^{0.024 \times f_c^-} - e^{0.14 \times f_c^-}) \quad \text{(3.22)}$$

$$\aleph = \varepsilon_{ii}/\varepsilon_{c1} \quad \text{(3.23)}$$

$$\sigma_c = f_c^- \times (\frac{k \times \aleph - \aleph^2}{1 + (k-2) \times \aleph}) \quad \text{(3.24)}$$

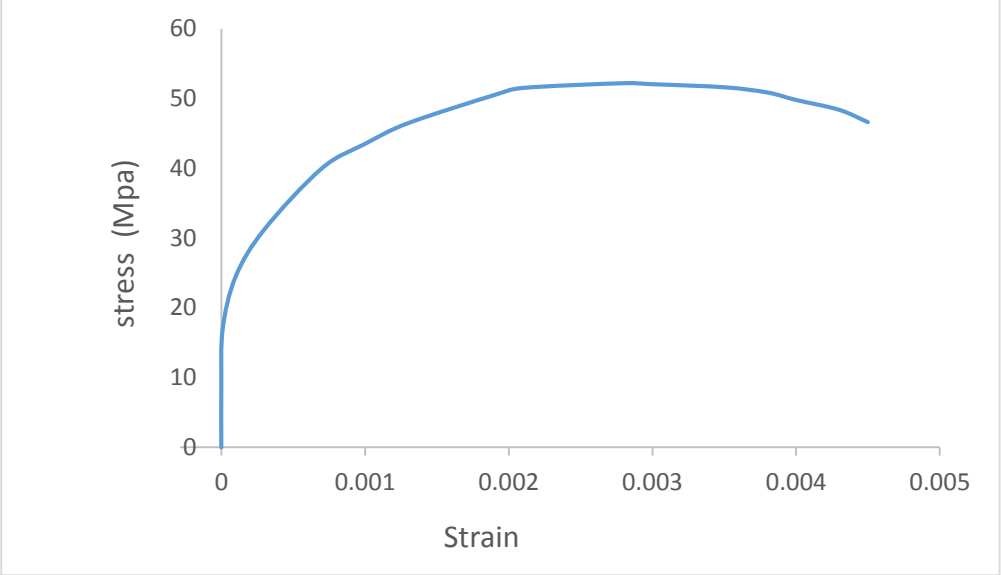

Figure (3.3) Stress-strain curves of concrete compretion

3.7.2 Steel Reinforcement

The steel was assumed to be an elastic–perfectly plastic material and identical in compression and tension as shown in Fig. (3.4). The elastic modulus and the yield stress were obtained from the experimental work conducted by barros et al, 2007 [60]. A Poisson's ratio used in this study equal to 0.3 for the steel reinforcement[44]. The bond between steel reinforcement and concrete was assumed as a perfect bond [44].

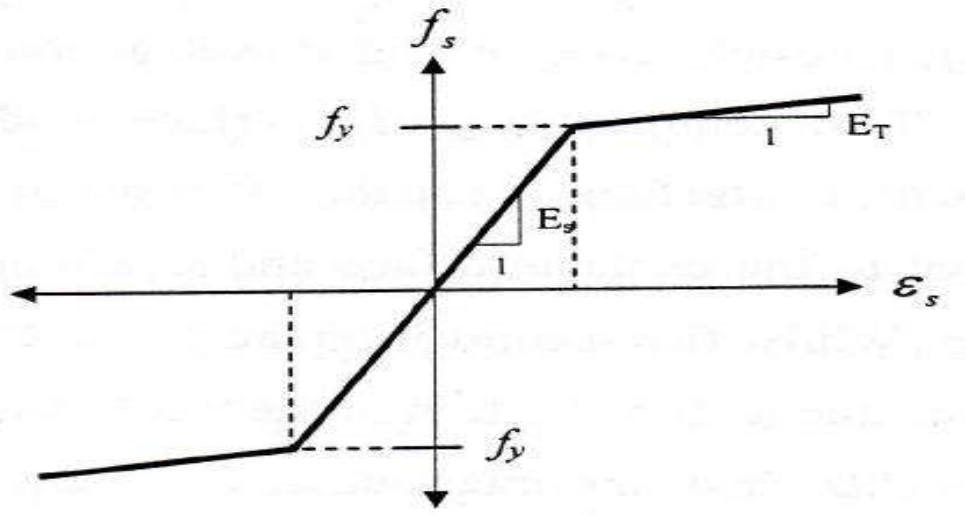

Figure (3.4) Stress-strain relationship steel bar in tension and compression [61]

3.7.3 CFRP

Generally, two different models were used for the CFRP. In the first model, the CFRP material was considered as linear elastic isotropic until failure. In the second model, the CFRP was modeled as a linear elastic orthotropic material. In this study, the first model has been used. The elastic modulus of the CFRP material used in the experimental study by barros et al, 2007 and it is specified by the manufacturer. A Poisson's ratio of 0.3 was used for CFRP[44]. The mode failure was a brittle failure in CFRP as shown in Fig. (3.5).

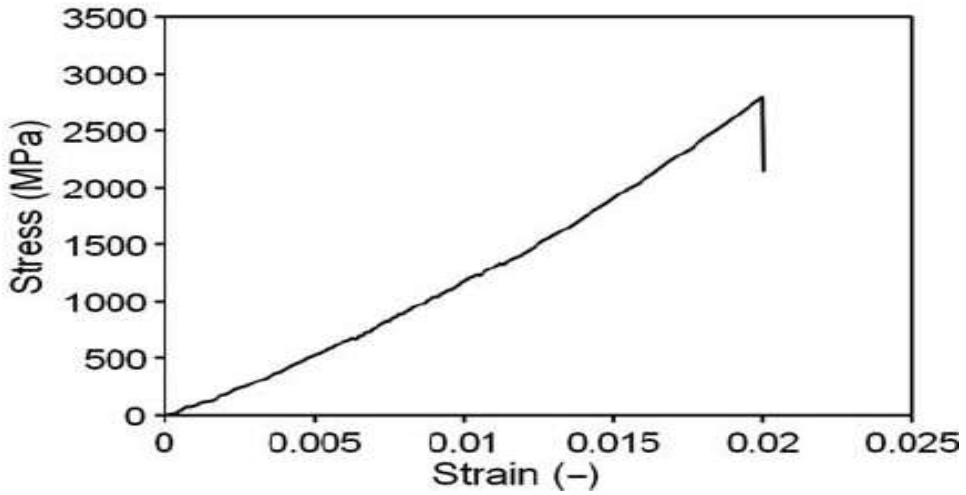

Figure (3.5) Stress-strain curve of CFRP in sheet and laminate [62]

3.7.4 CFRP–Concrete Interface

Two different models are utilized to represent the interface between concrete and CFRP. In the first model, the interface is modeled as a perfect bond while in the second model, the interface is modeled by using a cohesive model (surface to surface contact). Fig. (3.6) shows the relationship between maximum shear stress (τ_{max}) and effective opening displacement(δ) in the interface zone between concrete and CFRP by using simple bilinear traction–separation law. The interface is modeled with a small thickness and the initial stiffness k_0 is defined as [63]:

$$k_0 = \frac{1}{\frac{t_i}{G_i}+\frac{t_c}{G_c}} \quad \text{.....(3.25)}$$

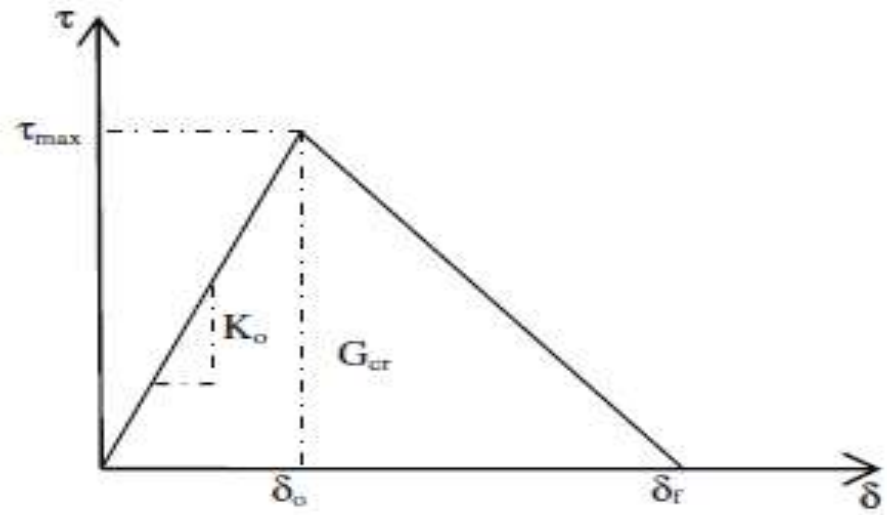

Figure (3.6) Bilinear traction-separation constitutive law

The values used for this study were ti = 0.5 mm, tc = 5 mm, Gi= 0.665 GPa, and Gc = 10.8 GPa.

From Fig. (4.4) it is obvious that the relation between the traction stress and effective opening displacement is defined by the stiffness, K_0, the local strength of the material, τ_{max} , a characteristic opening displacement at fracture (δf) and the energy needed for opening the crack (Gcr) which is equal to the area under the traction-displacement curve. Eq. (3.26), [64], provides an upper limit for the maximum shear stress. (τ_{max}):

$$\tau_{max} = 1.5 \text{ Bw } f_t \quad \text{.....(3.26)}$$

where

$$Bw = \sqrt{\frac{2.25-\frac{bf}{bc}}{1.25+\frac{bf}{bc}}} \quad \text{.....(3.27)}$$

For fracture energy, G_{cr}, previous researches have indicated values from 300 J/m^2 up to 1500 J/m^2[65, 66]. In this study the value of 900 J/m^2, was used.

The initiation of damage was assumed to occur when a quadratic traction function involving the nominal stress ratios reached the value one. This criterion can be represented by [58]:

$$(\sigma_n/\sigma^\circ_n)^2 + (t_s/t^\circ_s)^2 + t_t/t^\circ_t)^{2\square} = 1 \ldots\ldots\ldots\ldots\ldots\ldots\ldots\ldots\ldots\ldots(3.28)$$

The values used for this study were σ°n = ft =4.4 MPa, and t°s = t°t = 1.5 MPa.

3.8 Elements Used in Numerical Modeling

The elements were selected based on their characteristics; these elements had the closest similarity with the experimental behavior of concrete, FRP, and steel in the physical prototype.

Four types of the element were used in numerical modeling of RC retrofitted with CFRP: shell elements, solid elements, and wire. Each of these elements has characteristics which distinguish them from the other types of elements.

For each element, the number of nodes and the order of interpolation, the family type, type of formulation and integration method is normally different from other types of elements, which leads to different properties or characteristics for each element.

The geometry of an element and the related restrictions are determined by the family type of an element. For example, shell elements are appropriate for geometries with negligible thicknesses. This property of shell elements makes them a good choice for modeling the FRP sheet.

The accuracy of the element is calculated by the order of interpolation or the number of nodes in an element. In linear interpolation functions, the nodes are at the corner of the elements, but in higher order elements with quadratic or cubic interpolation functions, there are intermediate nodes between corner nodes. For example, in an 8 node cubic concrete element, the nodes are only assigned at the corners and the shape function is linear, but adding extra nodes can simulate the

concrete behavior more precisely; however, this can be quite time-consuming. Fig. (3.7) shows a linear cubic element and a quadratic cubic element[55].

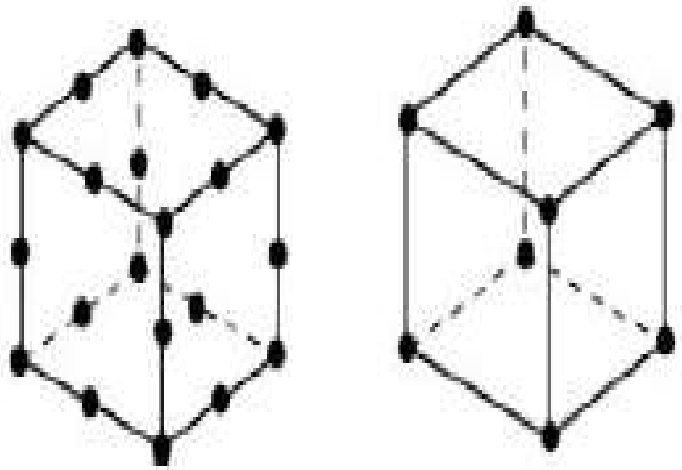

Figure (3.7) Linear element and quadratic element

In this study, the steel reinforcement is represented by wire element while solid element was used to represent the concrete. The shell element was used to model the CFRP sheet and finally the solid element is adopted to represent the CFRP laminate. Table (3.1) shows that types of element used in this study.

Table (3.1) Element types for analytical study model

Material type	ABAQUS element
Concrete	Solid
Steel reinforced	Wire
CFRP sheet	Shell
CFRP laminate	solid
Epoxy	Surface to surface contact

3.8.1 Concrete Representation

The solid 8-node element is used to model the concrete without or with steel bars. This element is capable of plastic deformation, crushing in compression and cracking in tension. For the concrete beam and CFRP laminate, a 3-D eight node element (C3D8R) as shown in Fig. (3.8) with linear approximation of displacement, reduced integration with hourglass control and eight nodes was used. In this element having three degrees of freedom for every node, translations in the nodal x, y, and z directions [67].

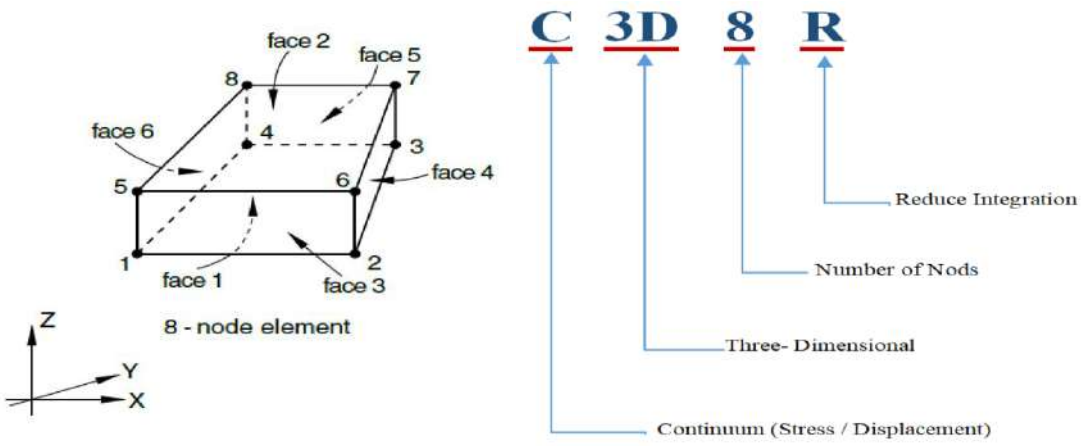

Figure (3.8) solid geometry and node locations [68]

3.8.2 CFRP Sheets Representation

A shell element was used to model the CFRP sheet. This element is suitable for analyzing thin structures. This element (S4R) 4-node doubly curved thin or thick shell, reduced integration, hourglass control, finite membrane strains and 3D element with four nodes and three degrees of freedom each node; the shell element can translate x, y, and z directions in the nodal [67]. The node locations, geometry, and the coordinate system are shown in Fig. (3.9).

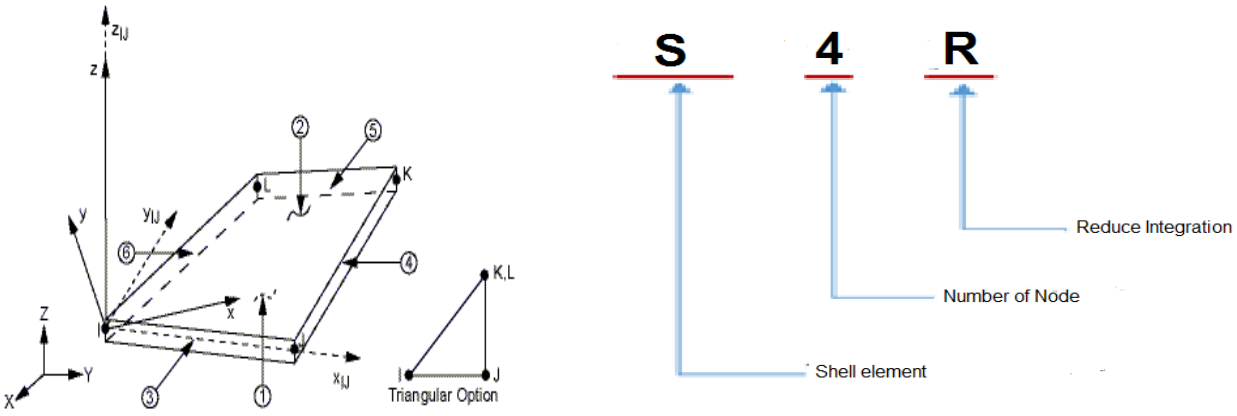

Figure (3.9) shell geometry [68]

3.8.3 Concrete-CFRP interface

Surface to surface contact was used to represent epoxy. The traction-separation modeling procedure is employed for modeling the epoxy. One of the applications of cohesive elements is modeling adhesive materials and bond interface which is a key characteristic. The behavior of cohesive elements depends on several factors, such as their physical properties, their application, and the type of responses simulated [55].

3.8.4 Reinforcement Representation

Steel bars were modeled by using wire elements (T3D2) for both the main and shear reinforcement in vertical and horizontal directions. It is a 1D element having

two nodes with three degrees of freedom which were identical to those for solid and also this element has the capacity of plastic deformation [67] see Fig. (3.10).

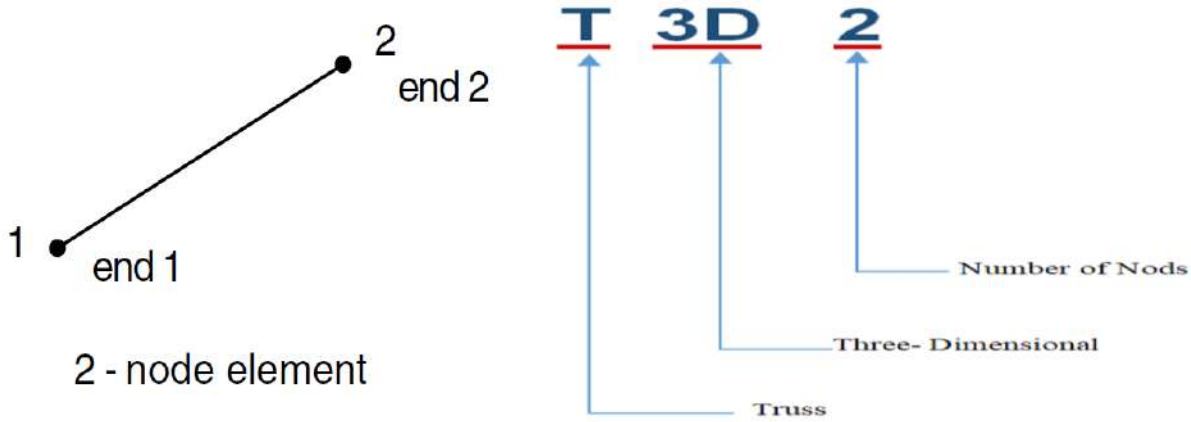

Figure (3.10) wire element [68]

3.9 Model Assembly

Models usually consist of components that are assembled together to form the final shape. These components are known as part instances. For example, the model in this study consisted of CFRP laminates or sheet concrete, steel rods, and epoxy layers. It is more convenient to model each of these elements separately and then assemble them. This method is considerably helpful for forming complex configurations.

Concrete, CFRP sheets, steel rods, and epoxy layers are parts of the numerical model and are used repeatedly in the model and assembled. Each of these components has the same mechanical properties within themselves and are modeled separately. These parts are not analyzed individually but analyzed within a complete model. Mesh can be applied to either individual parts or the whole model. Other properties of the model, based on the kind of the property, can be defined either at the part level or the model level [55].

3.10 Meshing

In any finite element analysis, the first step is the discretization of the domain into smaller subdomains.

The meshing process based on different factors, such as the geometric specifications.

Generally, the meshing process is straightforward. The process consisted of two stages. In the first stage, seeds are assigned to the edge of the components and in the second stage, meshes are assigned to each part. Based on the mesh size is determined and the desired level of accuracy.

The number of elements on the edge of the element is determined After determining the mesh size. Therefore, the numbers of nodes at the edge are defined. Due to the effect of the mesh size and quality on the final results, several factors are considered in devising a better mesh aimed at achieving more reliable results. The location of the nodes, size of the elements and the number of elements are some of the more important factors which affect the mesh quality.

The aspect ratio is very important in calculating the size of the elements, because it calculates the shape of the element. The ratio of the largest dimension of the element to the smallest dimension is called the aspect ratio. The best aspect ratio in modeling procedure is normally one.

Putting nodes depends on the existence of any disruption in the material property, geometry, and load.

As mentioned earlier, the number of elements depends on the desired level of accuracy. In the modeling procedure, the first selected mesh may not provide accurate results; therefore, a more refined mesh is used in the second stage. Note that increasing the number of elements does not necessarily improve the accuracy of the solution indefinitely, because, after a certain point, it merely adds to the time complexity and may result in an increasing number of computational errors[55].

Figure (3.11) shows the mesh for concrete, CFRP laminate, CFRP sheet and assembly reinforced concrete beam.

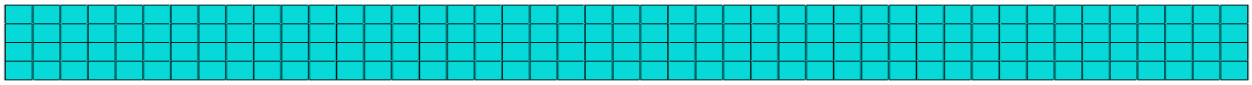

a) CFRP sheet

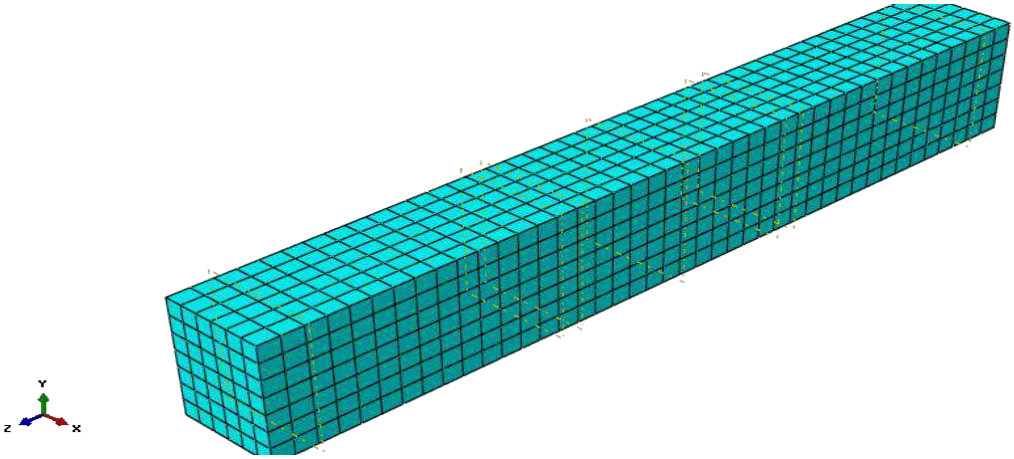

b) Concrete

c) CFRP laminate

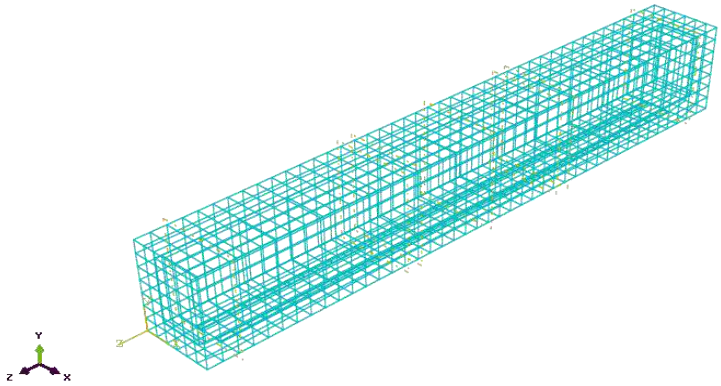

d) Reinforced concrete beam assembly

Figure (3.11) The FE mesh of the a) steel reinforcement, b) concrete, c) CFRP laminate and d) assembly reinforced concrete beams.

Displacement boundary conditions are needed to constrain the model to get a unique solution. To ensure that the model acts the same way as the experimental beam, boundary conditions need to be applied at points of symmetry, and where the supports and loadings exist. Figure (3.12) illustrates applied loading and boundary conditions far at support.

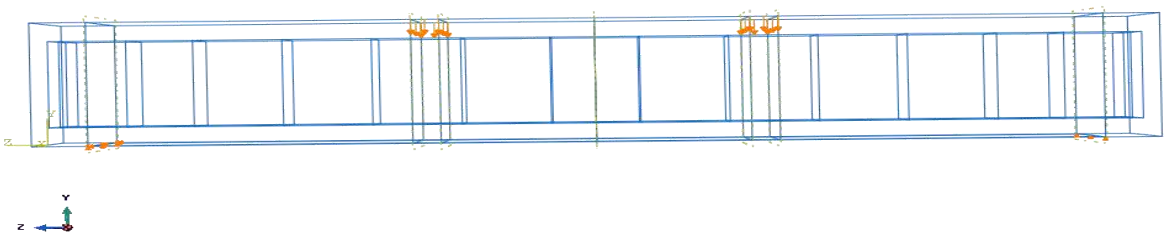

Figure (3.12): Boundary conditions for at support and applied load on the mod

Chapter Four

Results and Discussion

4.1 Introduction

In this study, a nonlinear finite element analysis has been carried out to study the RC beams, which are strengthened by CFRP. The analysis is performed by using the ABAQUS computer program by applying geometrical and material modeling.

In this chapter, verification is done to check the validity and accuracy of the present FE model. The ability of the FE analysis method to simulate the behavior of CFRP-concrete beams is demonstrated through the analysis of RC beams. The results obtained from FEM are compared with the experimental results to check the accuracy and validity of this numerical method.

Also, the effect of several important parameters such as compressive strength of concrete, sheet thickness and length laminate on the flexural behavior and the shear span to depth ratio (a/h ratio), and configuration of CFRP on the shear strength of RC beams are investigated.

4.2 Materials Properties

The same properties of steel reinforcement and concrete that proposed by Barros et al, 2007 [60] have been used in this numerical study.

Table (4.1) shows the properties of the steel bars and concrete used in the numerical proposed from experimental results by Barros et al, 2007.

Two types of CFRP were used in this study: the first type is CFRP-sheets with 80 mm in width used to the flexural strengthening and 25 mm in width used to the shear strengthening. The second type is CFRP- laminates with 1.4×9.6 mm^2 as a cross sectional area in the flexural strengthening and 1.4×10 mm^2 in the shear

strengthening. The properties of the CFRP used in this study are listed in the Table (4.2).

Table (4.1) Properties of the steel bars and concrete [60]

Element type	concrete f_c^-(MPa)	steel		
		$\emptyset_s$(mm)	fy (MPa)	fu (MPa)
Flexural beams	52.2	5	788	890
		6.5	627	765
Shear beams	49.2	6 (stirrups)	540	694
		6 (long.)	622	702
			618	691
	56.2	10	464	581
		12	574	672
			571	673

Table (4.2) Properties of the CFRP materials [60]

CFRP type	Material	Tensile strength (MPa)	Young's modulus (GPa)	Ultimate strain (%)	Thickness (mm)
sheet	primer	12	0.7	3	--------
	epoxy	54	3	2.5	--------
	Flexural strengthening	3700	240	1.5	0.111
	Shear strengthening	3000	390	0.8	0.167
Laminate	Adhesive	16-22	5	-------	-------
	Flexural strengthening	2740	158.8	1.7	1.4
	Shear strengthening	2286	166	1.3	1.4

4.3 Flexural strengthening

Numerical modeling of the structural behavior RC beams strengthened by CFRP under four-point bending was presented depend on the experimental work conducted by Barros et al,2007 [60].

4.3.1 Specimens Details and Loading Condition

the reinforcement arrangements, the geometry of the beams type, the number and position of the CFRP strengthened systems showed in Fig. (4.1). Also, Table (4.3) showed type of strengthening, CFRP type, Number of sheet Layer or laminate strip and thickness of CFRP. FEM was used to model and to study the behavior of RC beams in flexure using the ABAQUS program.

Table (4.3) Beams series for the flexural strengthening

Beam designation	Flexural strengthening systems			
	Type of strengthening	CFRP type	Number of sheet Layer/ laminate strip	thickness of CFRP (mm)
S1-R	-	-	-	-
S2-R	-	-	-	-
S3-R	-	-	-	-
S1-EXT-LAM	external	CFRP laminate	1	1.4
S2-EXT-LAM	external	CFRP laminate	2	1.4
S3-EXT-LAM	external	CFRP laminate	3	1.4
S1-NSM	NSM	CFRP laminate	1	1.4
S2-NSM	NSM	CFRP laminate	2	1.4
S3-NSM	NSM	CFRP laminate	3	1.4
S1-EXT-M	external	CFRP sheet	1	0.111
S2-EXT-M	external	CFRP sheet	2	0.111
S3-EXT-M	external	CFRP sheet	3	0.111

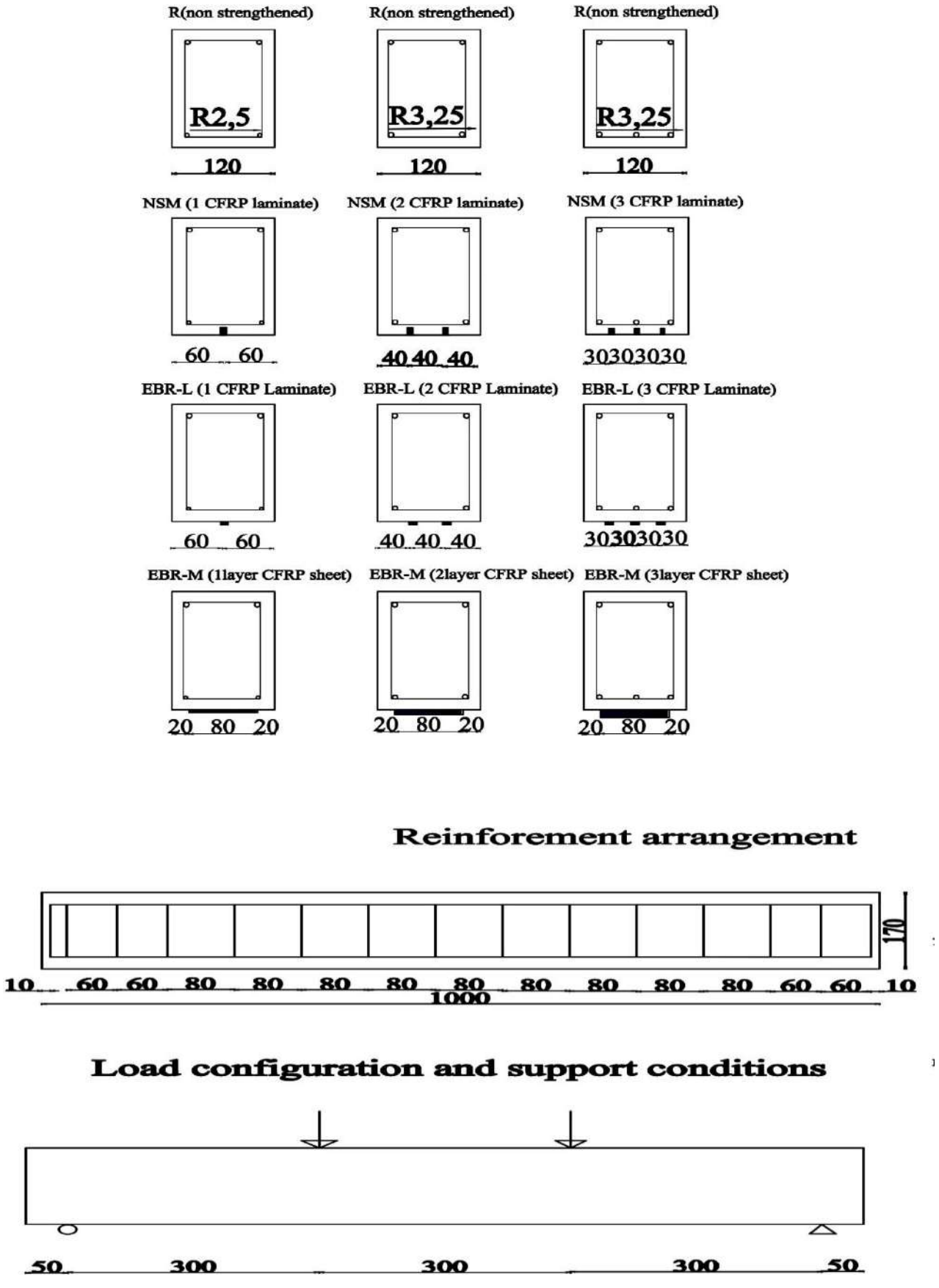

Figure (4.1) Beam series for the flexural strengthening (dimensions in mm)[60].

4.3.2 Flexural Behavior of Beams: Results and Discussion

4.3.2.1 Control Beams (S1-R, S2-R and S3-R)

The control beams S1-R, S2-R, and S3-R failed by yielding of steel reinforcement at loads of 36.9, 47.84 and 67.94 kN respectively.The strain of concrete is 0.0037 mm/mm. The formation of the cracks and the typical crack patterns of flexural members are shown in Fig. (4.2). The first visible crack is observed at the mid span. New cracks started to form when the load was increasing. Also, the crack width increased with increasing the load. The load- deflection curves at midspan for the three unstrengthened beams are shown in Fig. (4.3). It is clear noticed from this figure, It there is good agreement between the results of the experimental and FE using the ABAQUS program for all control beams according to ultimate load and mode of failure. Table (4.4) shows experimental and FE results.

Table (4.4) Finite element and experimental results of control beams.

Beam designation	Experimental (EXP)[60]		Finite element method (FEM)			P_{ult_EXP}/P_{ult_FE}	P_{ser_EXP}/P_{ser_FE}
	P_{ult_EXP} (kN)	P_{ser_EXP} (kN)	P_{ult_FE} (kN)	P_{ser_FE} (kN)	P_{yeild} (kN)		
S1-R	36.6	22.1	36.90	34.33	35.10	0.99	0.64
S2-R	48.5	40.5	47.84	41.68	46.2	1.01	0.97
S3-R	71.8	51.5	67.94	56.2	65.3	1.05	0.91

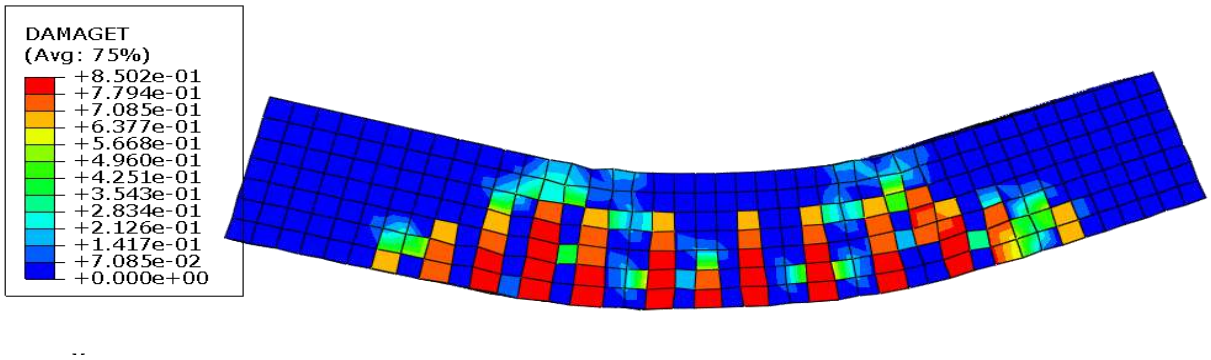

(a) FEM crack of concrete

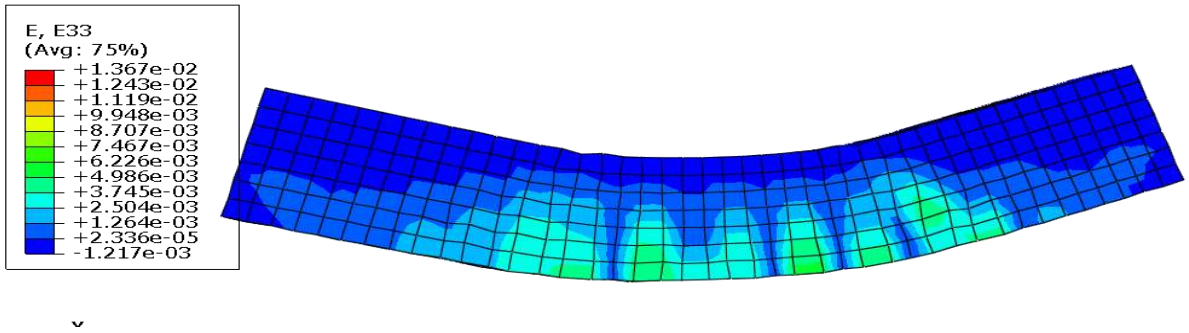

(b) FEM-strain of concrete

(c) experimental failure

Figure (4.2) The typical failure modes of control beams

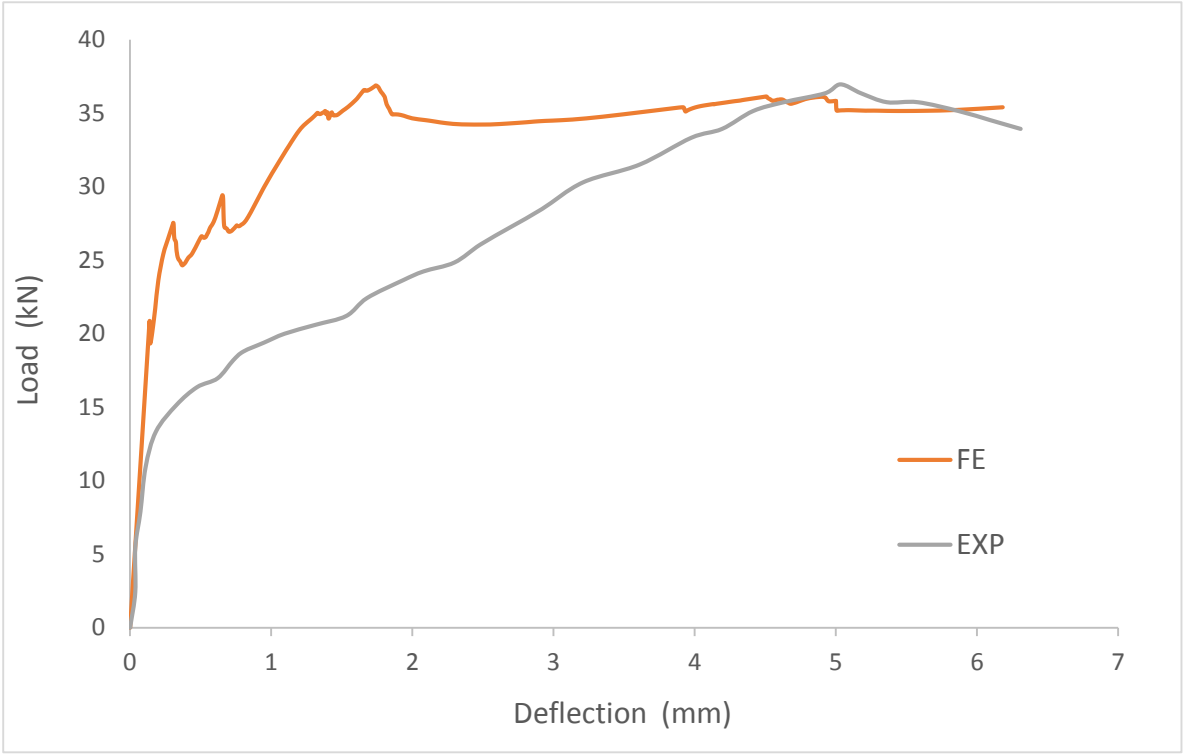

(a) control beam (S1-R)

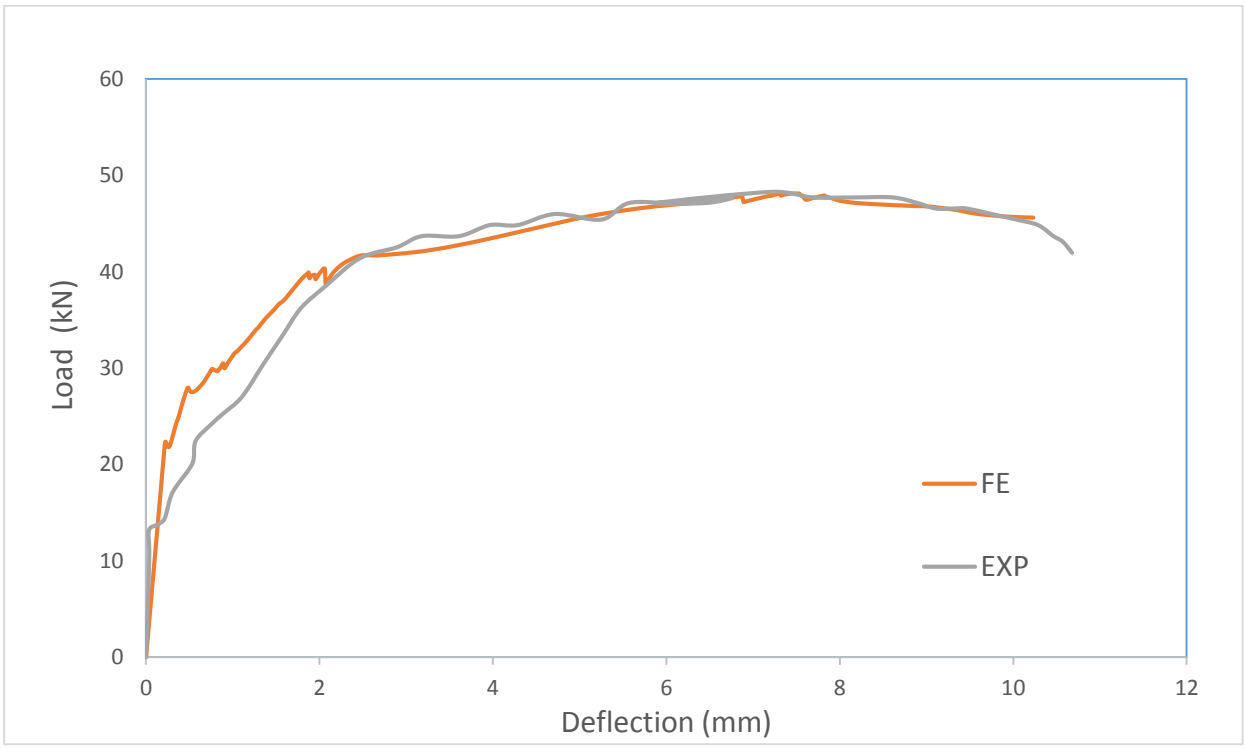

(b)control beam (S2-R)

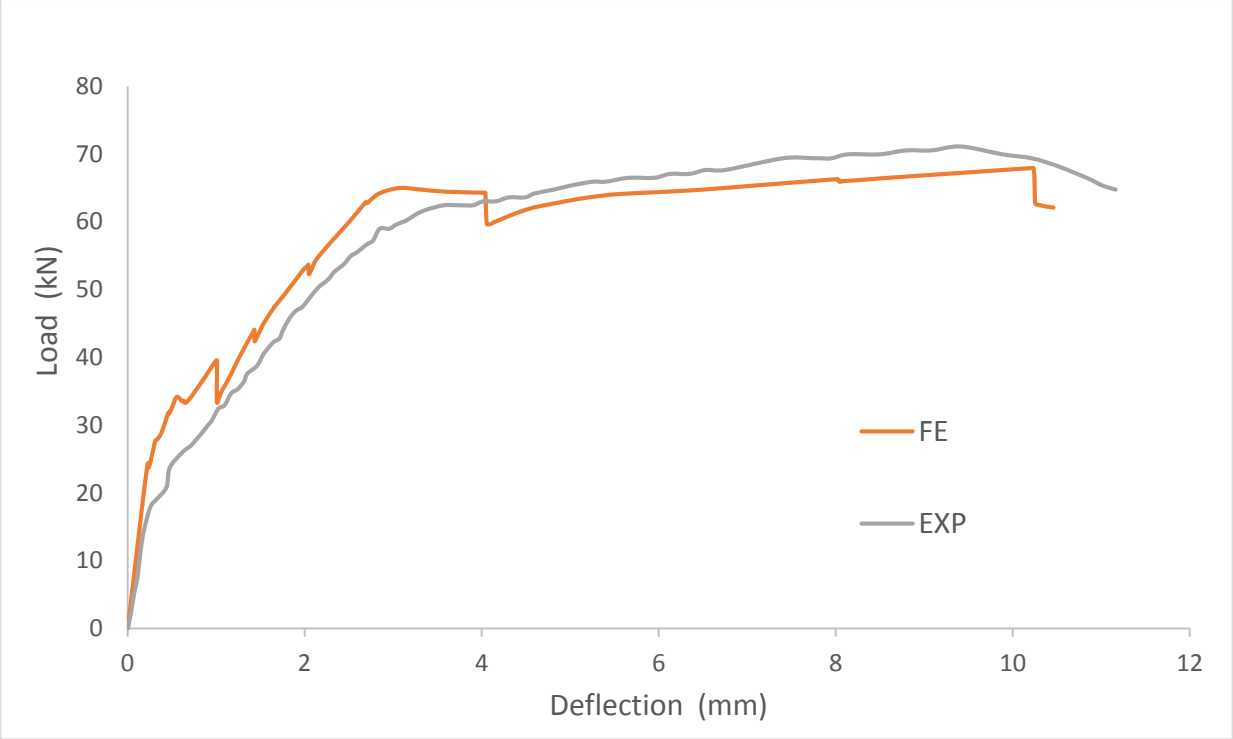

(c) S3-R

Figure (4.3) Load –deflection curves for control beams

4.3.2.2 External Laminate (S1-EXT-LAM)

Beam S1-EXT-LAM strengthened externally by one CFRP strip at the mid of beams. Under loading vertical flexural cracks are observed at the mid-span. The failure occurred at an applied load of 39.34 kN by debonding of CFRP strips at the strip–epoxy interface due to the intermediate crack mechanism typically after yielding of primary steel reinforcement when the flexural cracks widen. The debonding started from end-span as shown in Fig.(4.4). It should be noted that strengthening beam S1-EXT-LAM using one EBR CFRP strips resulted in a 6.6% increase in the maximum load in comparison with the control beam (S1-R). The maximum strain in CFRP is 0.003 mm/mm, which represents about 18% of the ultimate strain of the CFRP. The load–deflection curves at mid span for the S1-EXT-LAM beam are shown in Fig. (4.5).

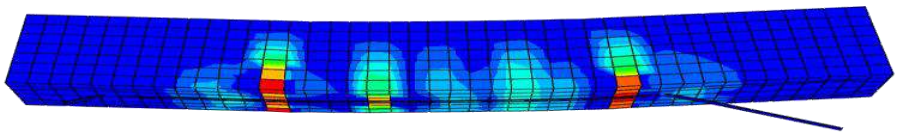

(a) FEM-strain of concrete

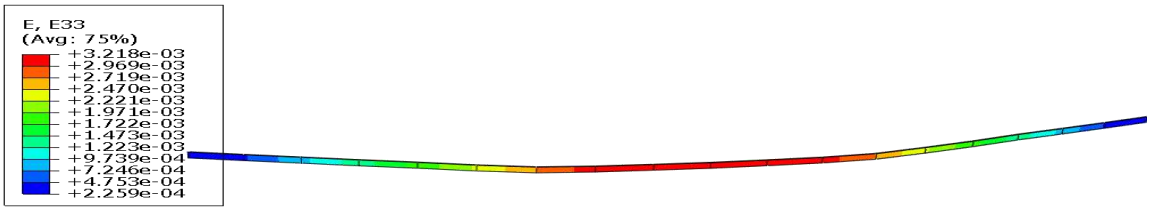

(b) FEM-strain of laminate

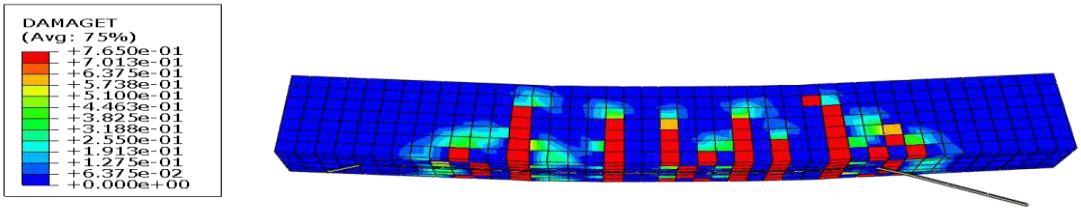

(c) FEM-crack of concrete

(d) experimental failure

Figure (4.4) The typical failure modes of beams strengthened with one CFRP-EBR stripe

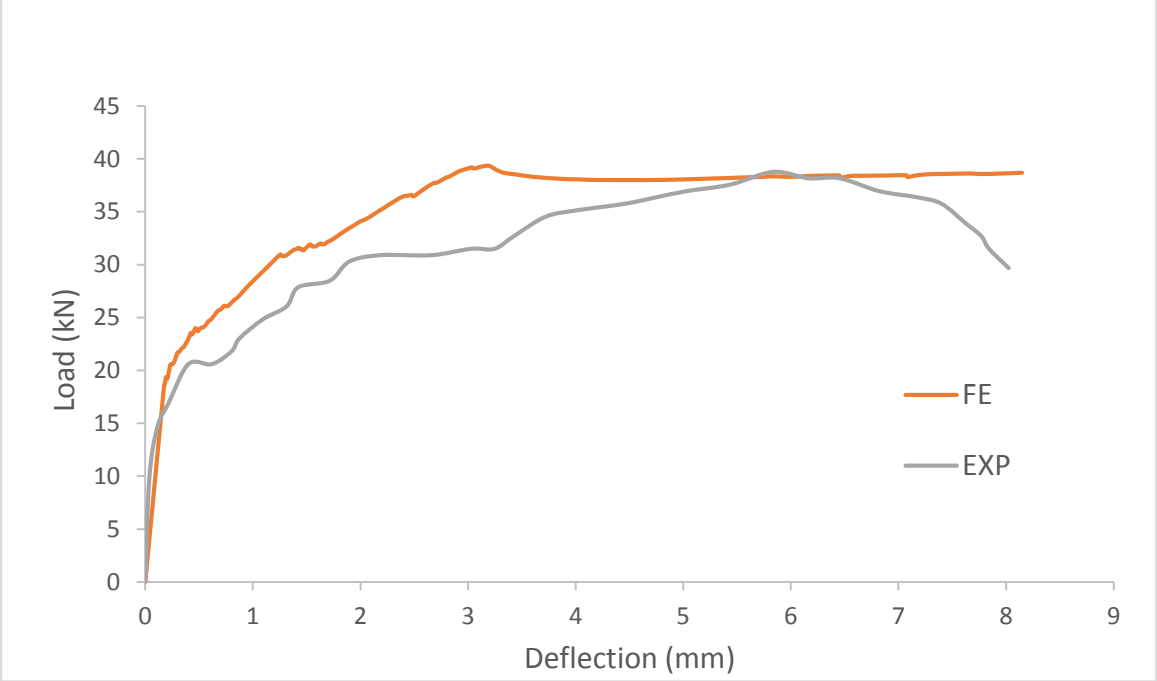

Figure (4.5) Load –deflection curves of RC beam strengthened with one CFRP laminate

4.3.2.3 External Laminate (S2-EXT-LAM)

Beam S2-EXT-LAM strengthened with two EBR CFRP strips. The behavior of this beam is identical to the behavior of the previous beam (S1-EXT-LAM) , in the first stage. The failure occurred at a maximam load of 77.33 kN by debonding of CFRP strips due to the intermediate crack mechanism typically after yielding of primary steel reinforcement when the flexural cracks widen. As author mentioned that in Barron et al the failure mode was as the same in beam S1-EXT-LAM. The debonding started from end-span as shown in Fig. (4.6). It should be noted that strengthening beam S2-EXT-LAM by two EBR CFRP strips resulted in a 61.6% increase in the ultimate load in comparison with that control beam (S2-R) because the CFRP have high tension strength led to increase flexural capacity. The maximum strain of CFRP was 0.003 mm/mm, which represents about 18% of the ultimate strain of the CFRP. The load–deflection curves at mid span for the S2-EXT-LAM beam are shown in Fig. (4.7).

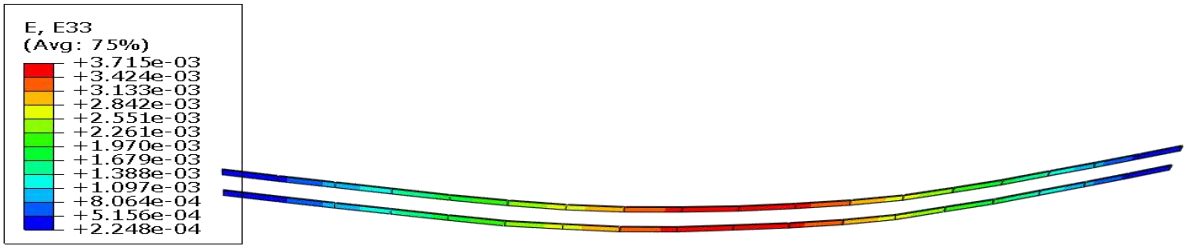

(a) FEM-strain of CFRP laminate

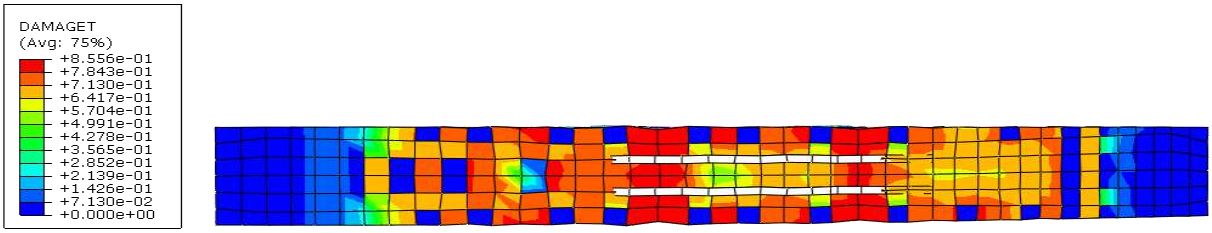

(b) FEM-crack of concrete

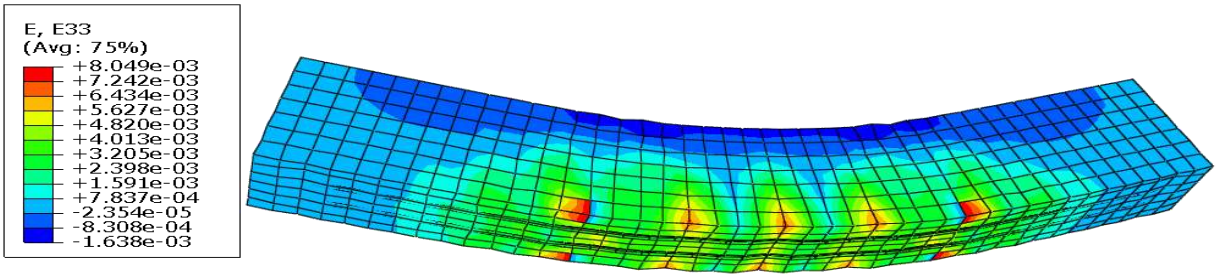

(c) FEM-strain of concrete

Figure (4.6) The typical failure modes of RC beam strengthened with two laminate of CFRP-EBR

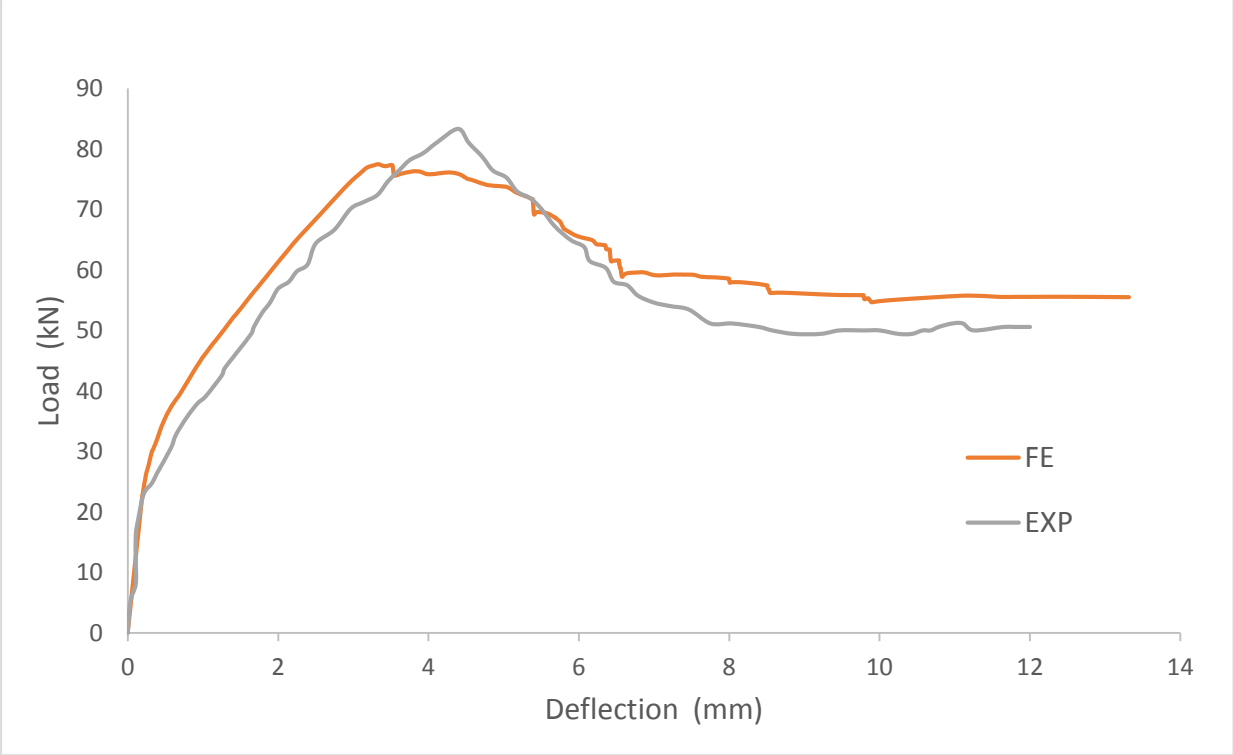

Figure (4.7) Load –deflection curve of RC beam strengthened with two EBR CFRP laminate

4.3.2.4 External Laminate (S3-EXT-LAM)

The beam (S3-EXT-LAM) reinforced with three EBR CFRP strips, The propagation, and formation of cracks are similar to those of beams S1-EXT-LAM and S2-EXT-LAM. The failure occurred due to debonding at the strip at the epoxy–concrete interfaces and it is starting from end-span as shown in Fig. (4.8). The ultimate load of this beam was 80.17 kN. Strengthening beam S3-EXT-LAM with three EBR CFRP strips resulted in an 18% increase in the maximum load in comparison with that of the control beam (S3-R). The maximum recorded CFRP strain is 0.003 mm/mm and represents 18% of the ultimate strain of the CFRP.

Comparing the results of beam S2-EXT-LAM to those of beam S3-EXT-LAM, the amount of CFRP used to strengthen beam S3-EXT-LAM is greater than that used for beam S2-EXT-LAM by 50%. However, only a 3.6% increase in the ultimate load is obtained for S3-EXT-LAM compare with S2-EXT-LAM. This means that increasing at a certain limit may be led to slightly increase in the

ultimate load. The load-deflection curves at mid span for the S3-EXT-LAM beam are shown in Fig.(4.9).

There is good agreement between experimental and FE method using ABAQUS program results for all external laminate beams according to the mode of failure and ultimate load this is clearly from Figs. (4.9, 4.7 and 4.5) and Table (4.5).

Table (4.5) Finite element method and experimental results of beams strengthened with EBR-CFRP stripe for flexure behavior.

Beam designation	Experimental (EXP)[60]		Finite element method (FEM)			$EXP_{p\ ult}/FEM_{p\ ult}$	EXP_{pser}/FEM_{pser}
	P_{ult} (KN)	P_{ser} (KN)	P_{ult} (KN)	P_{ser} (KN)	P_{yeild} (KN)		
S1-EXT-LAM	38.6	31.9	39.34	35.62	38.05	0.98	0.89
S2-EXT-LAM	83.5	57.6	77.33	64.90	74.30	1.07	0.88
S3-EXT-LAM	86.5	74.1	80.17	70.12	78.66	1.07	1.05

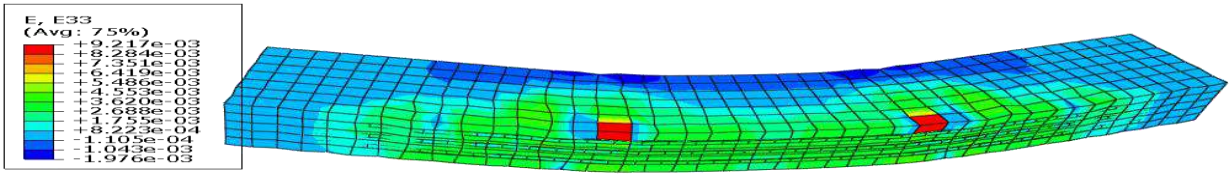

(a) FEM-strain of concrete

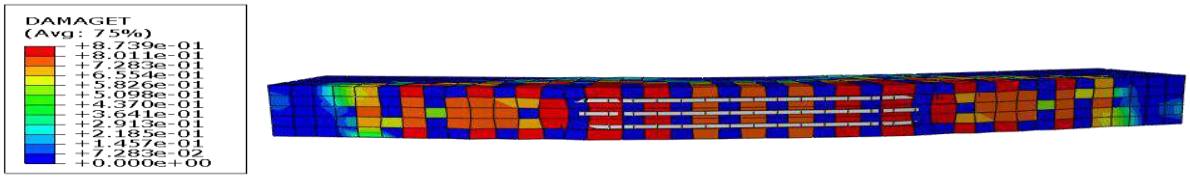

(b) FEM-crack of concrete

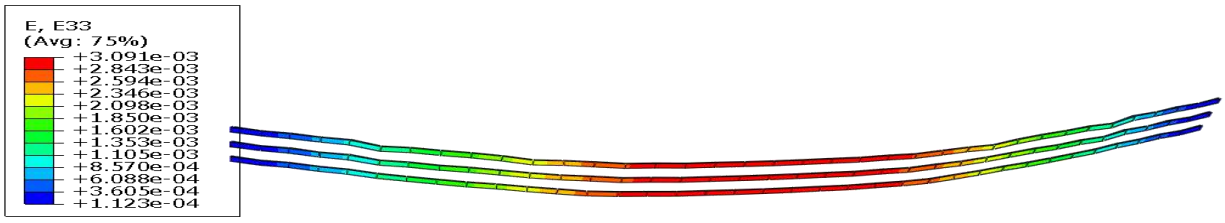

(c) FEM-strain of CFRP laminate

Figure (4.8) The typical failure modes of RC beam strengthened by three EBR-CFRP laminate

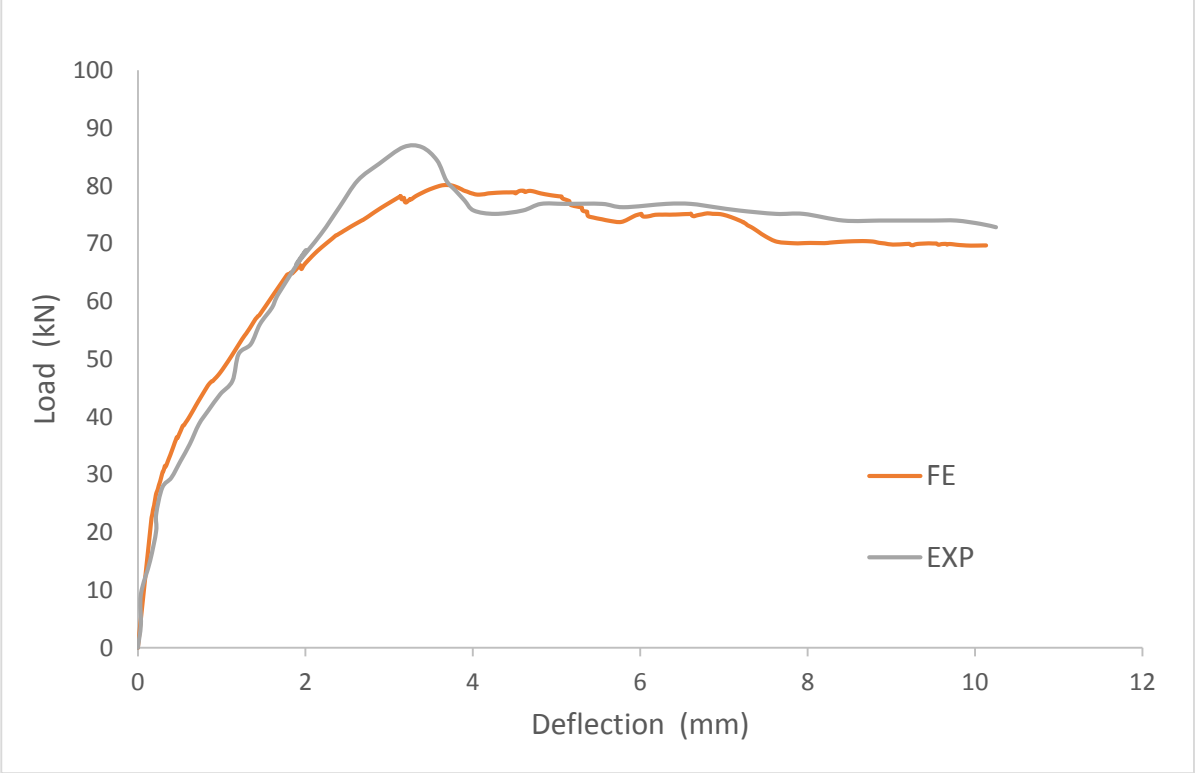

Figure (4.9) Load –deflection curve of RC beam strengthened with three laminates-EBR

4.3.2.5 Near Surface Mounted (S1-NSM)

Beam S1-NSM strengthened with one CFRP strip in one groove, the ultimate applied load was 77.05 kN, which is 108.8% and 18% higher than that of the control beam, S1-R and the beam strengthened with the same amount of CFRP in the form of one EBR CFRP strips respectively. This is mean that the NSM strengthening technique using one CFRP strips is more effective than the

externally bonded strengthening. Fig. (4.10) shows that the failure occurred after the yielding of steel reinforcement and CFRP strips rupture .This failure mode usually takes place in lightly reinforced and lightly strengthened section. The maximum strain in CFRP and stress failure is 0.017 mm/mm and 2740 MPa, respectively, These which represents 100% of the maximum strain and stress of CFRP. This is may be attributed to concentrate of high stresses in concrete cover. The load - deflection curves at mid span for the (S1-NSM) beam are shown in Fig. (4.11).

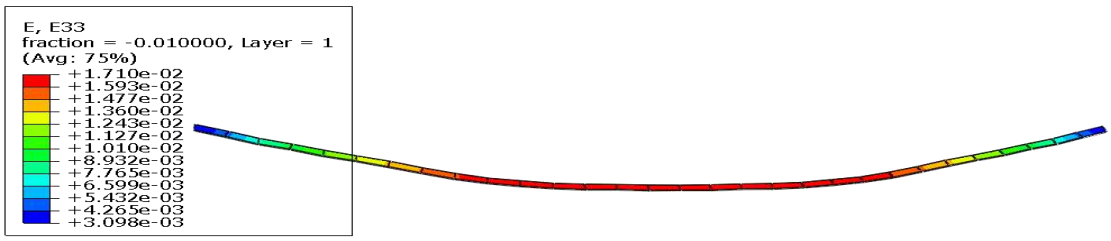

(a) FEM-strain of CFRP laminate

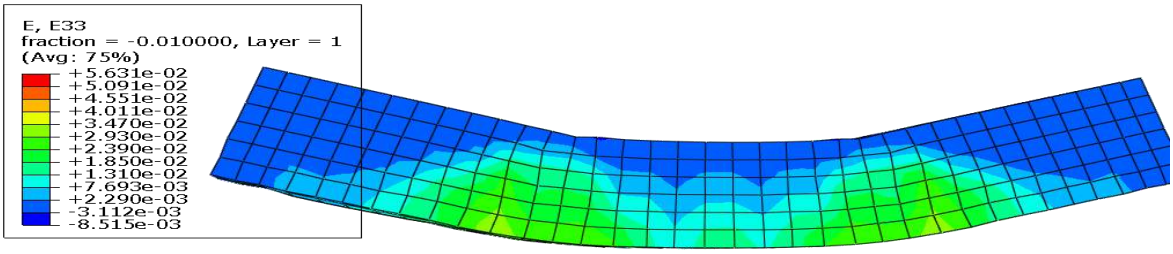

(b) FEM-strain of concrete

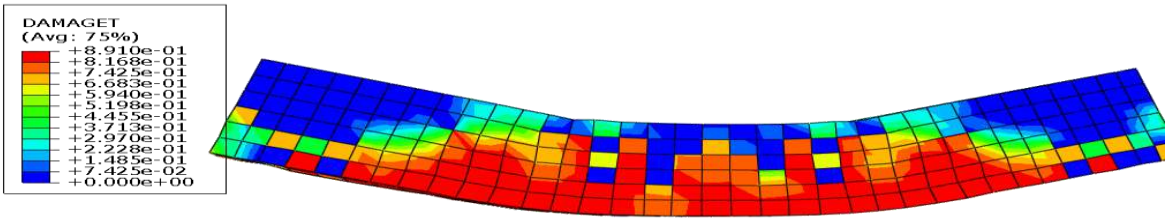

(c) FEM-crack of concrete

(d) experimental failure

Figure (4.10) The typical failure modes of RC beam strengthened one strip-NSM

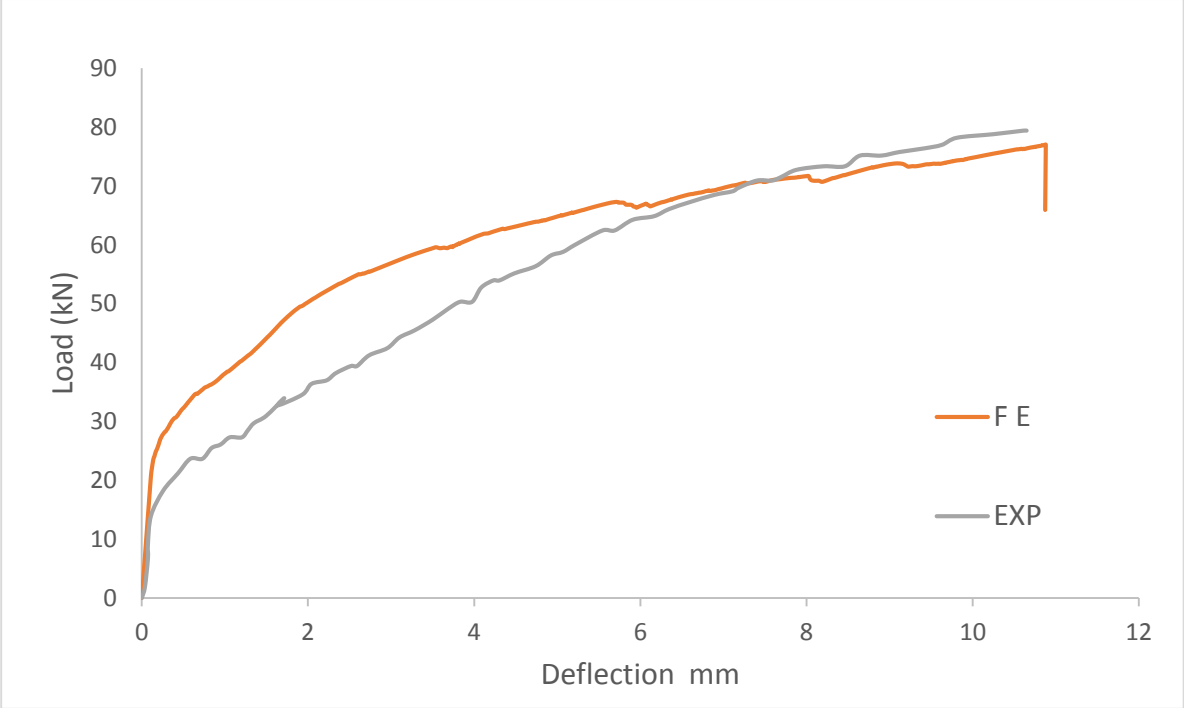

Figure (4.11) Load-deflection curve of RC beam strengthened one strip-NSM

4.3.2.6 Near Surface Mounted (S2-NSM)

In case of beam S2-NSM strengthened with two NSM CFRP strips installed in two grooves. Failure mode starts at the FRP curtailment because of stress concentration at the plate or sheet.The maximum strain in CFRP is 0.009 mm/mm which represents 47% of the maximum strain of the CFRP shown in Fig. (4.12). The ultimate load was 86.12 kN, which is 79.96% higher than that of the control

beam (S2-R) because the CFRP have high tension strength led to increase flexural capacity. The load versus midspan deflection curves for the (S2-NSM) beam are shown in Fig (4.13).

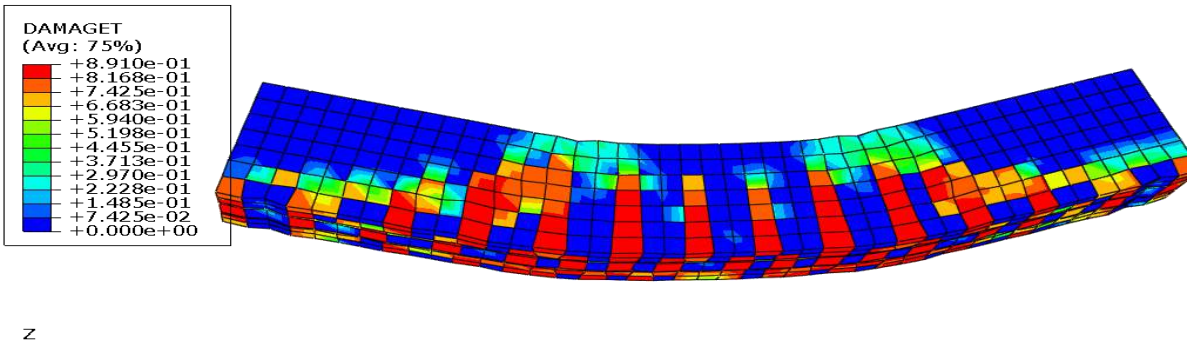

(a) FEM-crack of concrete

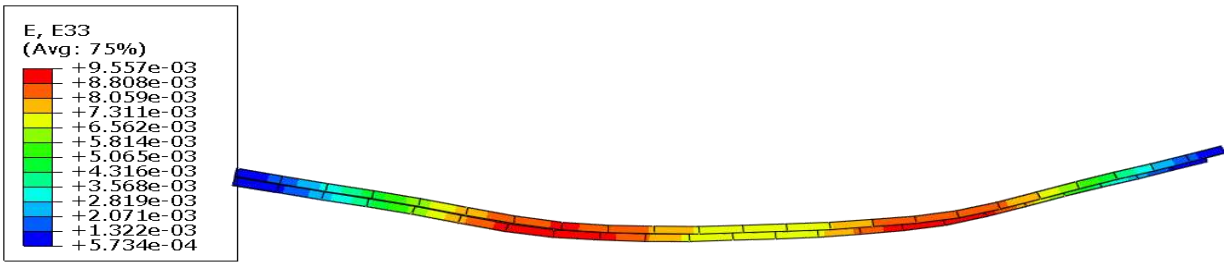

(b) FEM-strain of CFRP laminate

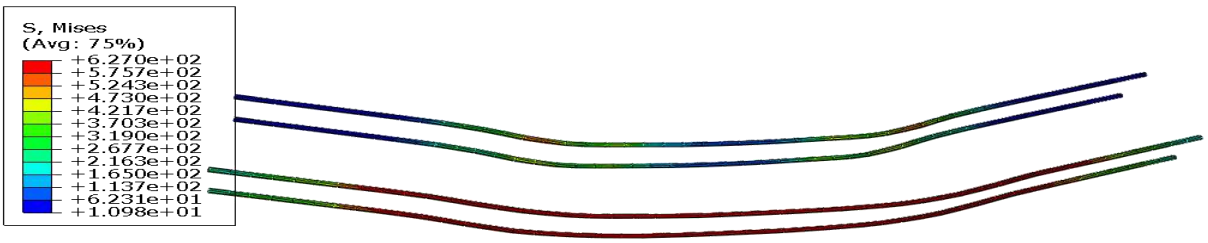

(c) FEM- stress of steel

(d) experimental failure

Figure (4.12) The typical failure modes of RC beam strengthened with two CFRP-NSM laminate

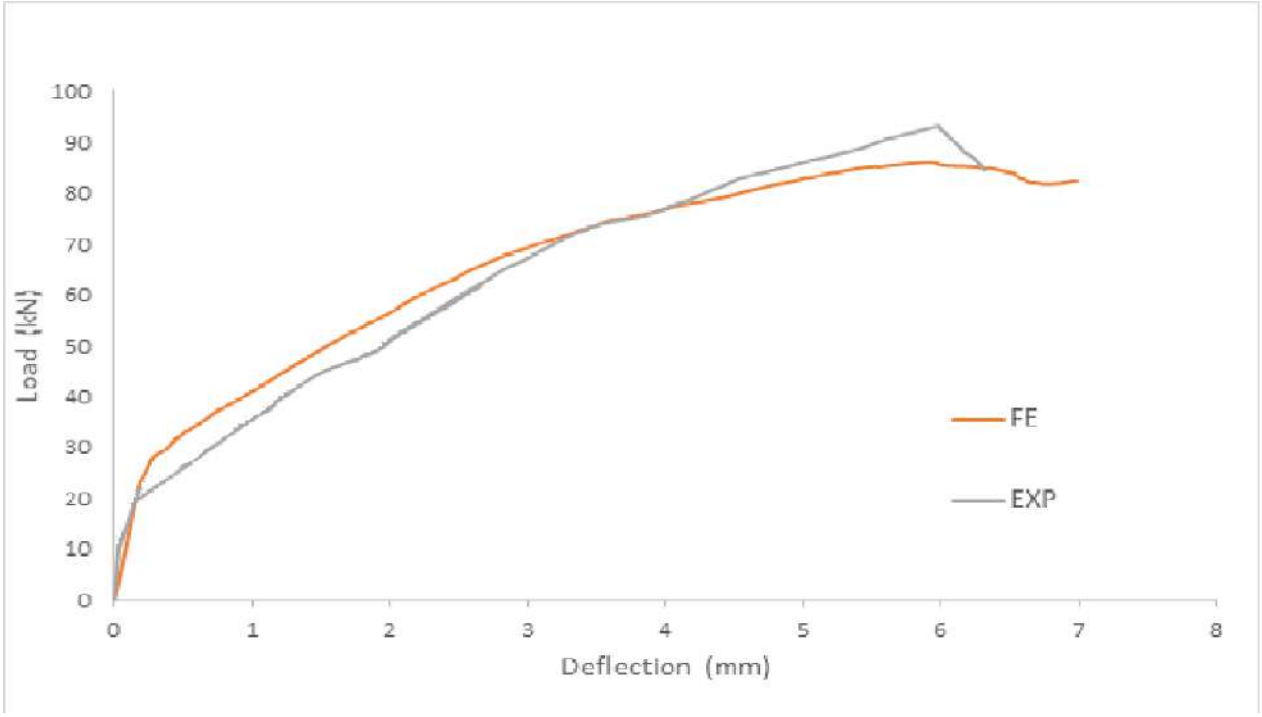

Figure (4.13) Load-deflection curve of RC beam strengthened with two CFRP-NSM laminate

4.3.2.7 Near Surface Mounted (S3-NSM)

The beam S3-NSM strengthened with three NSM CFRP strips installed in three grooves (i.e., one strip in each groove), failure occurred similar to NSM2 by yielding of the longitudinal steel and then separation of the concrete cover as shown in Fig. (4.14). As author mentioned that in Barron et al the failure mode was as the same in beam S2-NSM. The maximum strain in CFRP is 0.005 mm/mm, which represents 30%

of the ultimate strain of the CFRP. The ultimate load was 85.6 kN, which is 26% higher than that of the control beam (S3-R). The load-deflection curves at mid span for the beam S3-NSM beam are shown in Fig. (4.15).

It can be seen from Figs. (4.13, 4.11 and 4.9) and Table (4.6) that there is good agreement between experimental and FEM using program ABAQUS results for all near surface mount beams according to maximum load, deflection, crack and modes of failure. However, the failure mode of S1-NSM by FEM is different from experimental failure. Numerically the beam failed by rupture of CFRP laminate while experimentally the beam failed by yielding of the longitudinal steel reinforcement and then separation of the concrete cover because the difference in the failure mode may be attributed to the assumption of numerically model such as properties of the meterial as well as using identical boundary condition.

Table (4.6) Finite element method and experimental results of flexural NSM beams

Beam designation	Experimental (EXP)[60]		Finite element method (FEM)			$EXP_{p\ ult}/FEM_{p\ ult}$	EXP_{pser}/FEM_{pser}
	P_{ult} (kN)	P_{ser} (kN)	P_{ult} (kN)	P_{ser} (kN)	P_{yeild} (kN)		
S1-NSM	79.9	37.5	77.05	52.42	49.62	1.03	0.71
S2-NSM	93.3	56.3	86.12	60.73	72.50	1.03	0.92
S3-NSM	96.6	71.5	86.31	66.53	83.49	1.12	1.07

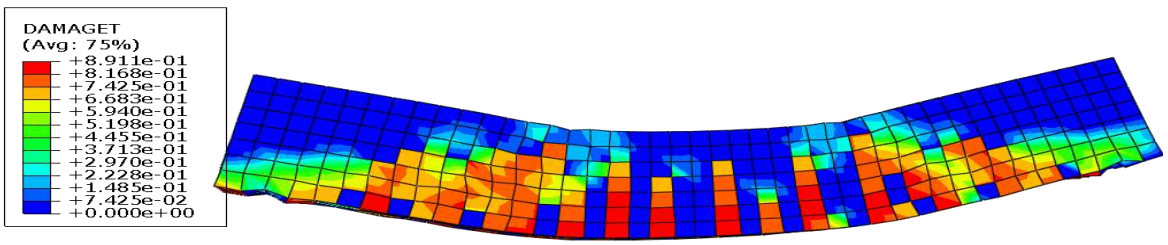

(a) FEM-crack of concrete

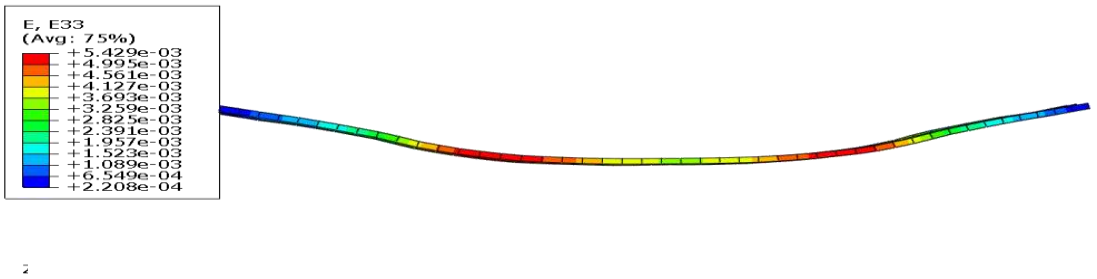

(b) FEM-strain of CFRP laminate

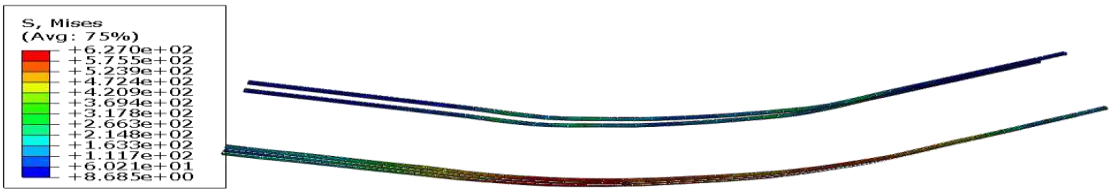

(c) FEM- stress of steel

Figure (4.14) The typical failure modes of RC beam strengthened with three CFRP-NSM laminate

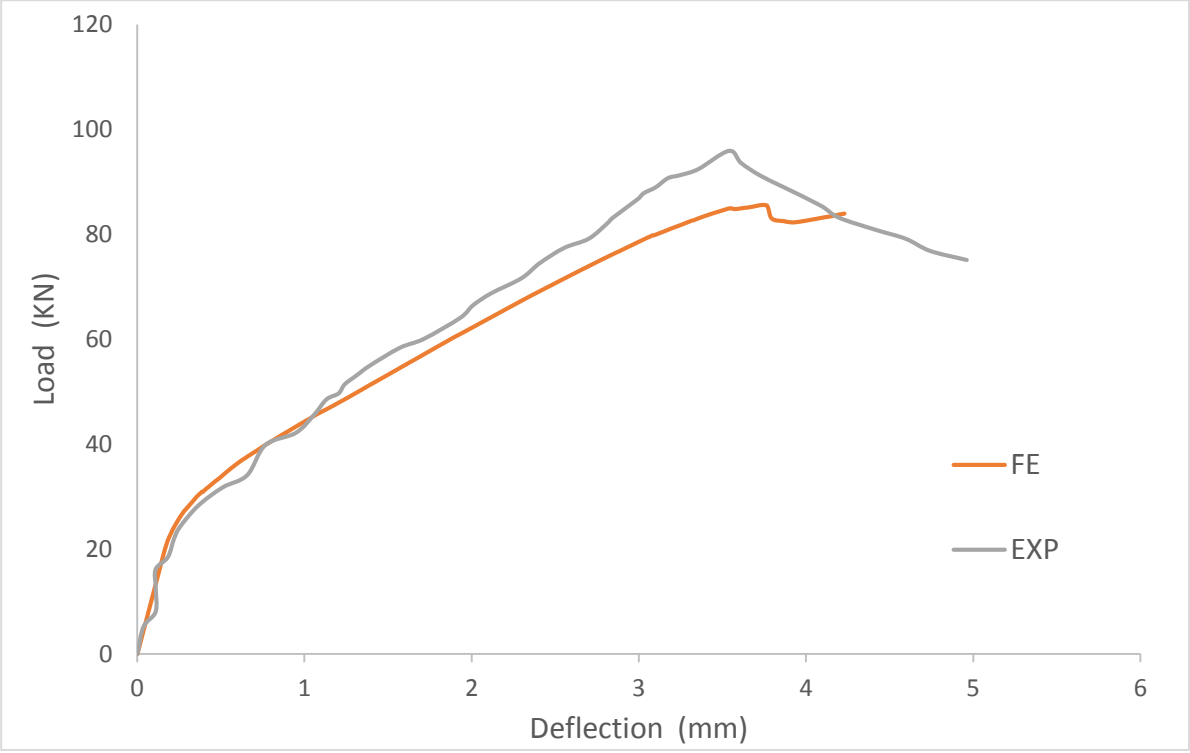

Figure (4.15) Load-deflection curve of RC beam strengthened with three CFRP-NSM laminate

4.3.2.8 External Sheet (S1-EXT-M)

Beam S1-EXT-M strengthened with one layer CFRP sheet with cross section (0.111×0.8) placed at the bottom beam. The maximum load of this beam was 43.72 kN and failure occurred due to fracture of CFRP sheet in two pieces as shown in Fig. (4.16).This failure mode occurred due to lightly reinforced and lightly strengthened section. Due to CFRP rupture, the flexural capacity of the beam dropped gradually and the beam carried a higher load than that of the unstrengthened beam, S1-R by about 18.4% but this beam did not reach the ductility of the unstrengthened beam S1-R because the behavior of CFRP is brittle linear elastic. The maximum strain in CFRP was 0.015 mm/mm, which represents 100% of the ultimate strain of the CFRP sheet. The load - deflection curves at midspan for the S1-EXT-M beam are shown in Fig.(4.17).

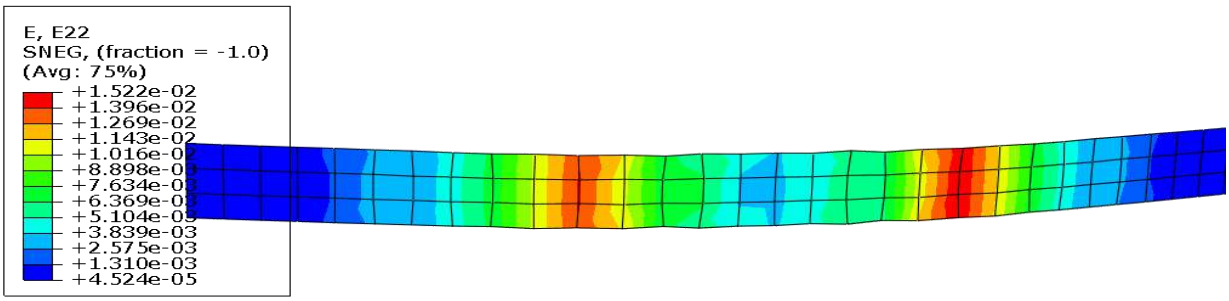

(a) FEM-strain of CFRP sheet

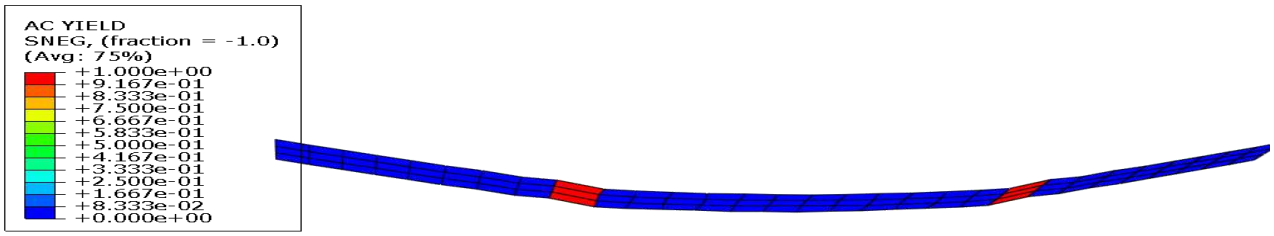

(b) FEM-yielding in CFRP sheet

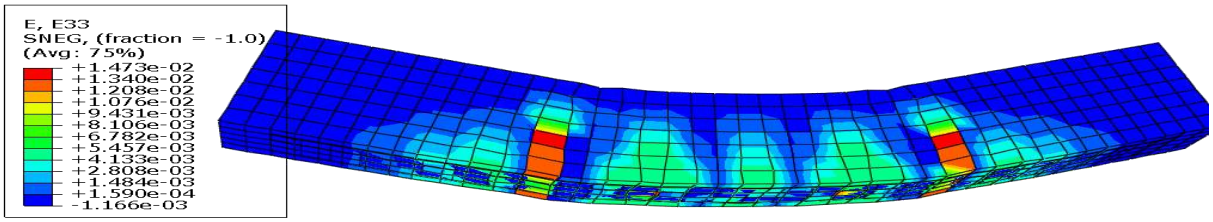

(c) FEM-strain of concrete

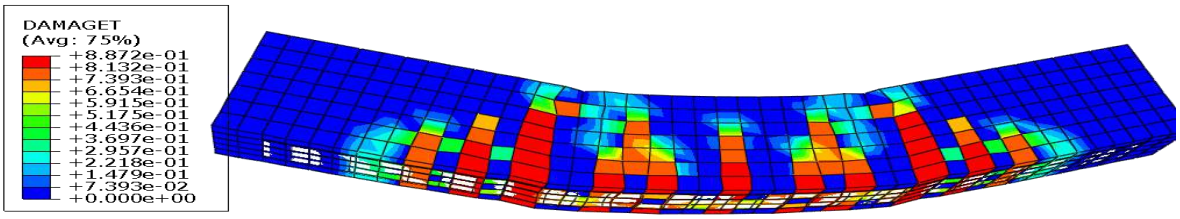

(d) FEM-crack of concrete

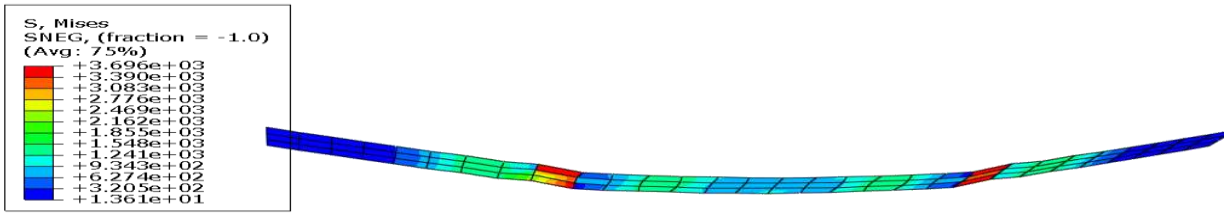

(e) FEM-stress of CFRP sheet

(f) experimental failure

Figure (4.16) The typical failure modes of RC beam strengthened with one layer of CFRP sheet

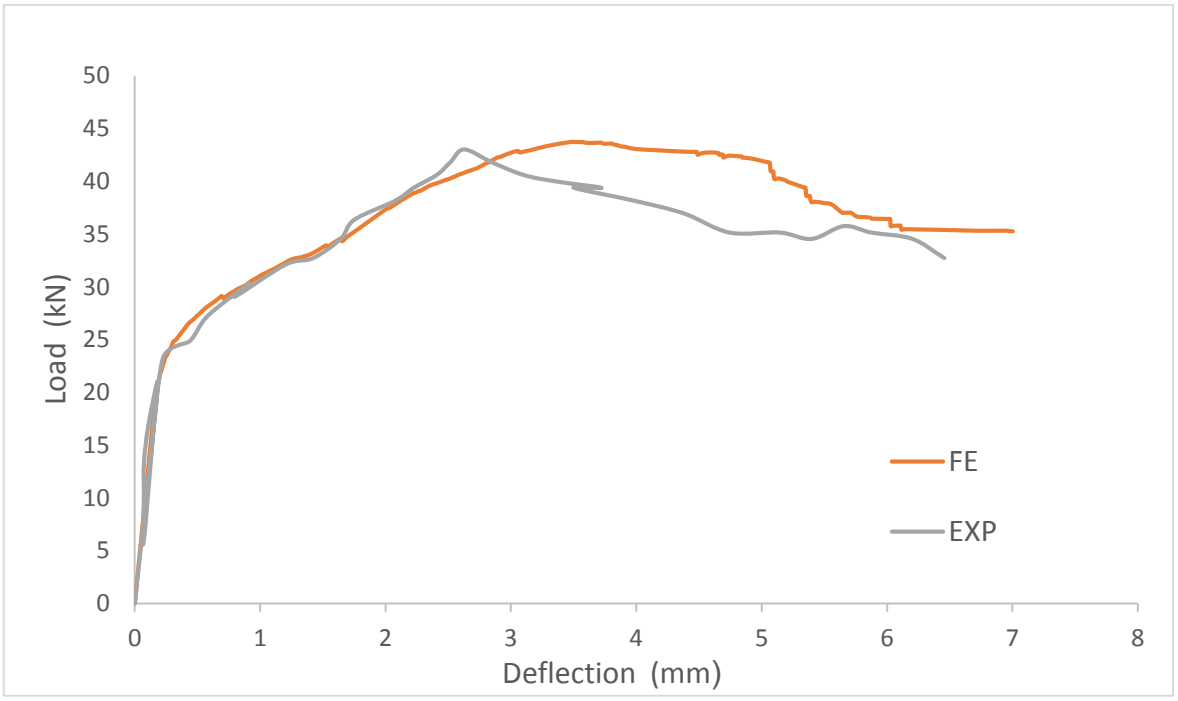

Figure (4.17) Load-deflection curve of RC beam strengthened with one layer of CFRP sheet

4.3.2.9 External Sheet (S2-EXT-M)

Beam S2-EXT-M strengthened with two layers of the CFRP sheet. This beam failed by cover separation at the end of CFRP due to high stresses in cover concrete as shown in Fig. (4.18). In FEM failure started with inclined cracks in the concrete cover and extended along the tensile reinforcing bars. The maximum applied load is 84.38 kN, which is 76.3% higher than that of the control beam

(S2-R) due to increase the tension strength by CFRP sheet. The maximum strain in CFRP is 0.0095 mm/mm, which represents 68% of the ultimate strain of the CFRP sheet. The load-deflection curves at mid span for the S2-EXT-M beam are shown in Fig. (4.19).

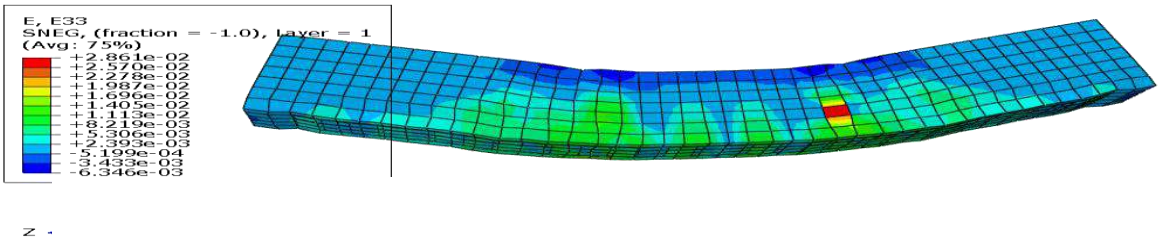

(a) FEM-strain of concrete

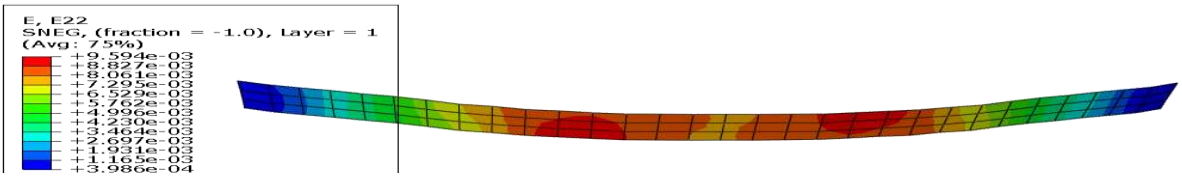

(b) FEM-strain of CFRP sheet

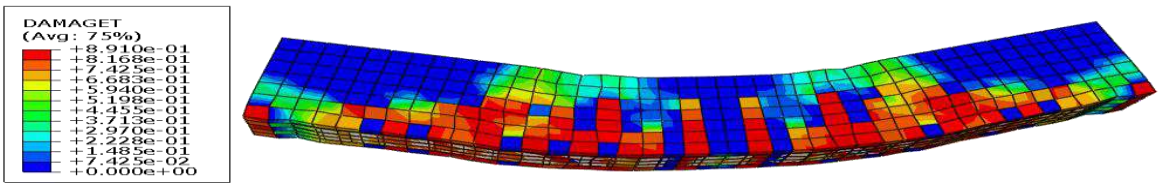

(c) FEM-crack of concrete

(d) experimental failure

Figure (4.18) The typical failure modes of RC beam strengthened with two layers CFRP sheet

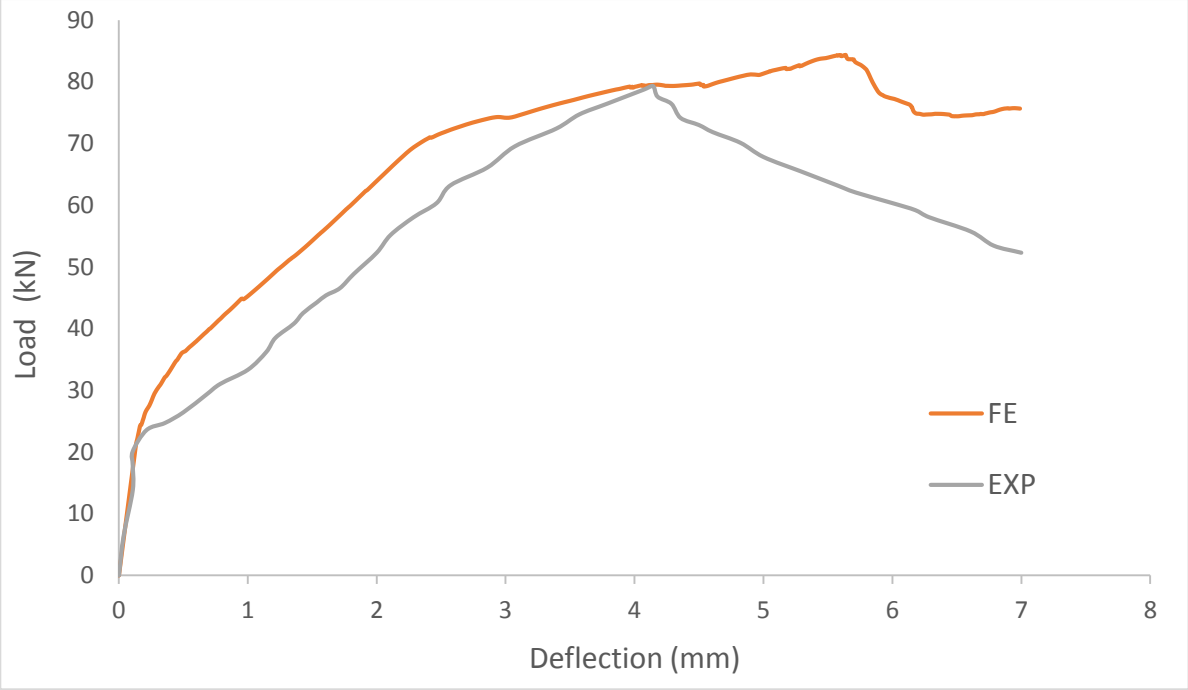

Figure (4.19) Load-deflection curve of RC beam strengthened with two layers CFRP sheet

4.3.2.10 External Sheet (S3-EXT-M)

Beam S3-EXT-M strengthened with three layers of the CFRP sheet. The ultimate load in this specimen is 89.76 KN, which is 32.1% higher than that of the control beam (S3-R). The failure occurred by yielding of the longitudinal steel and separation of the concrete cover similar to specimen S2-EXT-M as shown in Fig. (4.20). The maximum strain in CFRP was 0.0044 mm/mm, which represents 30% of the ultimate strain of the CFRP sheet. The load - deflection curves at mid span for the (S3-EXT-M) beam are shown in Fig (4.21).

Figure (4.21, 4.19 and 4.17) and Table (4.7) shows that there is good agreement between experimental and FEM results for all beams retrofitted with external CFRP.

The mode failure of beam S2-EXT-M by FEM is different from the experimental. Numerically the beam (S2-EXT-M) failed by cover separation at the end of FRP while experimentally the beam failed by rupture of the CFRP sheet because the difference in the failure mode may be attributed to the assumption of numerically model such as

properties of the meterial as well as using identical boundary condition. . When increasing the number of CFRP sheet from one layer to two layer the maximum load increase from 43.72 to 84.38 kN. Also, we noted that when increase the layers from two to three no significant increase has been accaured. Figure (4.22) shows the effect of number layers on maximum load of RC beams. Table (4.8) shows the percentage increase in the capacity of the strength of RC beams strengthened with CFRP compare with refrenced beams for flexural.

Table (4.7) Finite element method and experimental results of flexural external sheet beam

Beam designation	Experimental (EXP)[60]		Finite element method (FEM)			$EXP_{p\ ult}$/ $FEM_{p\ ult}$	EXP_{pser}/ FEM_{pser}
	P_{ult} (KN)	P_{ser} (KN)	P_{ult} (KN)	P_{ser} (KN)	P_{yeild} (KN)		
S1-EXT-M	43	40.3	43.72	39.02	42.83	0.98	1.03
S2-EXT-M	79.5	59.5	84.38	68.96	78.10	0.94	0.86
S3-EXT-M	87.3	73.4	89.76	74.85	87.41	0.97	0.98

Table (4.8) Increase ratio of RC beams strengthened with CFRP for flexural

series beam	control Max Load (KN)	NSM Max load (KN)	Percentage NSM %	EXT-LAM Max load (KN)	Percentage EXT-LAM %	EXT-M Max load (KN)	Percentage EXT-M %
S1	36.90	77.05	108.8	39.34	6.6	43.72	18.4

S2	47.84	86.12	79.96	77.33	61.6	84.38	76.3
S3	67.94	86.13	26	80.17	18	89.76	32.1

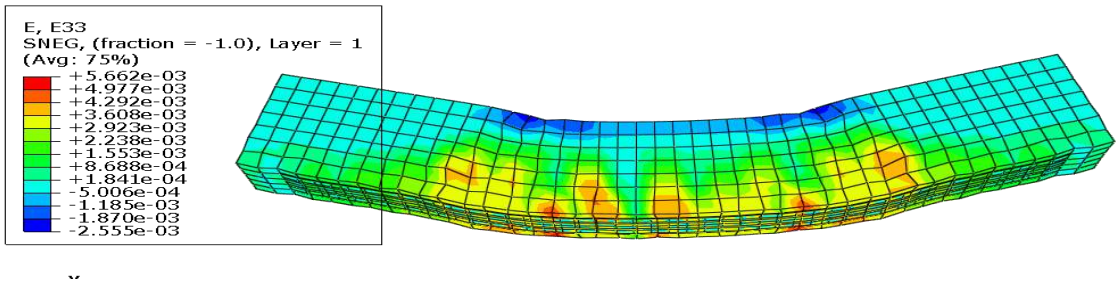

(a) FEM-strain of concrete

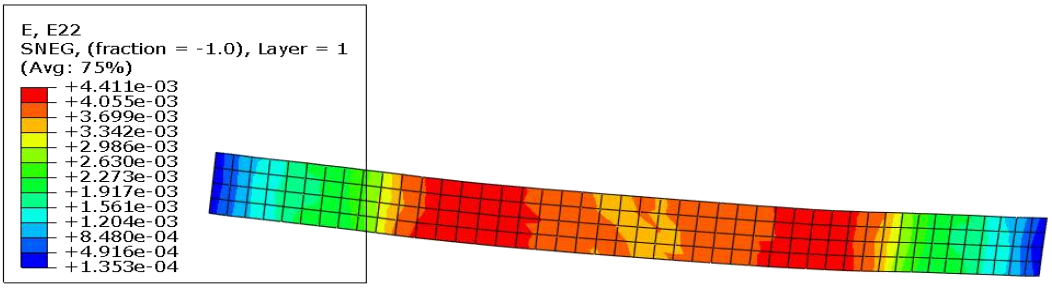

(b) FEM-strain of CFRP sheet

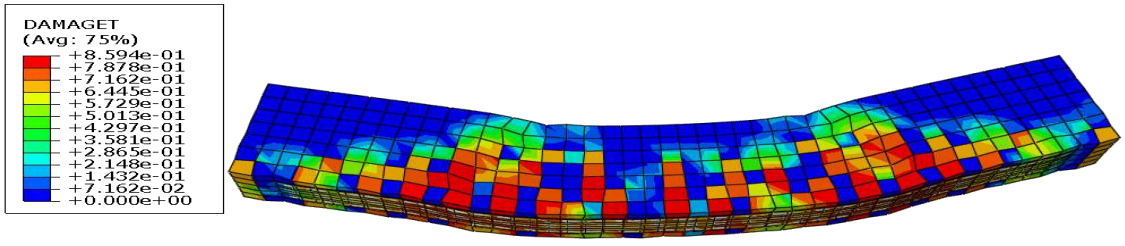

(c) FEM-crack of concrete

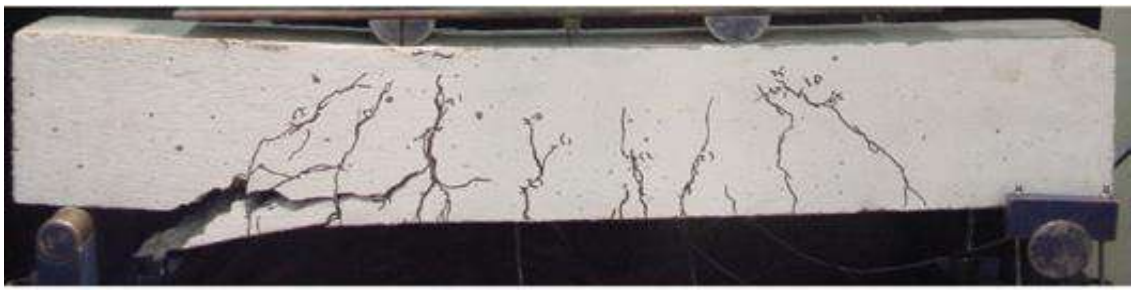

(d) experimental failure

Figure (4.20) The typical failure modes of RC beam strengthened with three CFRP layers

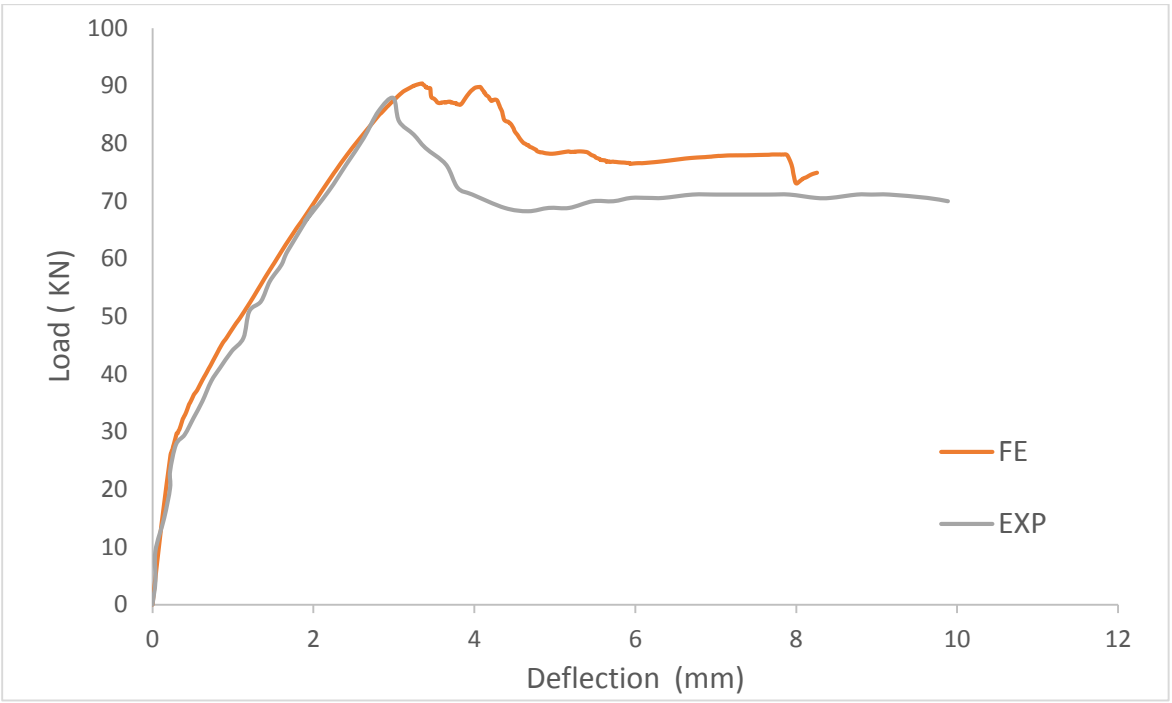

Figure (4.21) Load-deflection curve of RC beam strengthened with three CFRP layers

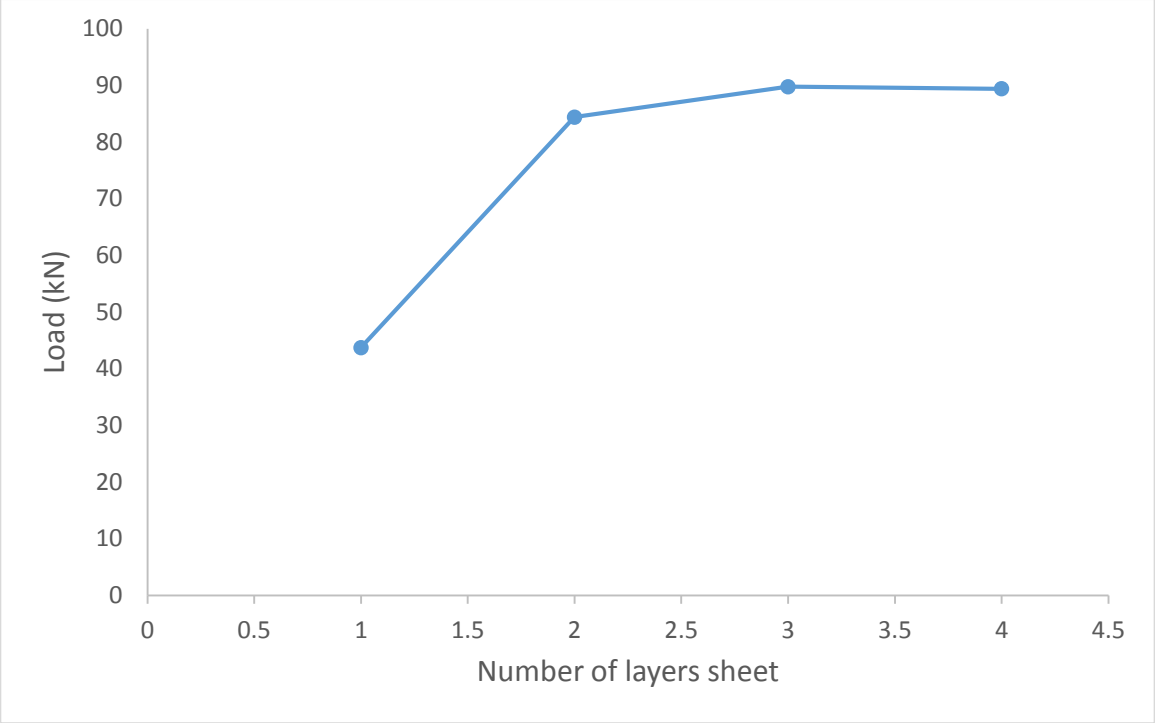

Figure (4.22) Relationship between max load and number of CFRP sheet layers

4.3.3 Parametric Study in Flexure

4.3.3.1 Effect of Concrete Compressive Strength

The concrete compressive strength is an important parameter in the behavior of RC beams. Five different concrete compressive strengths (30, 40, 52.2, 60, and 70 MPa) are considered to investigate its effect of this study. Fig. (4.23) show the effect of the concrete compression strength on the behavior of EBR and NSM reinforced concrete. It seems that ultimate load increased with increased compressive strength due to increase bending moment. Fig. (4.24) explain the relation between compressive strength and maximum load. Mode failure change from rupture CFRP stirp to delamination of the concrete cover in near surface mount techniques when f_c' =30 MPa only , other beam do not change in mode failure.

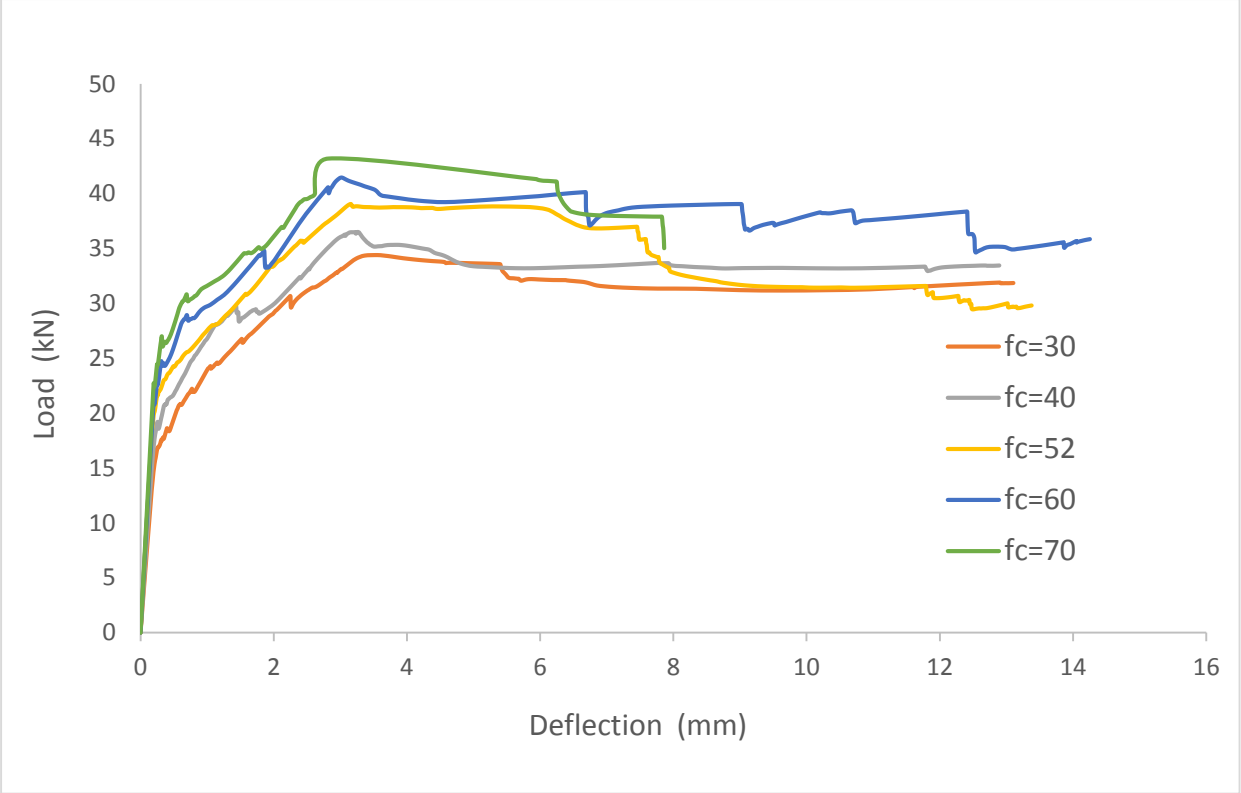

(a) Load-deflection curve with different compressive strength of concrete of (S1-R) beam

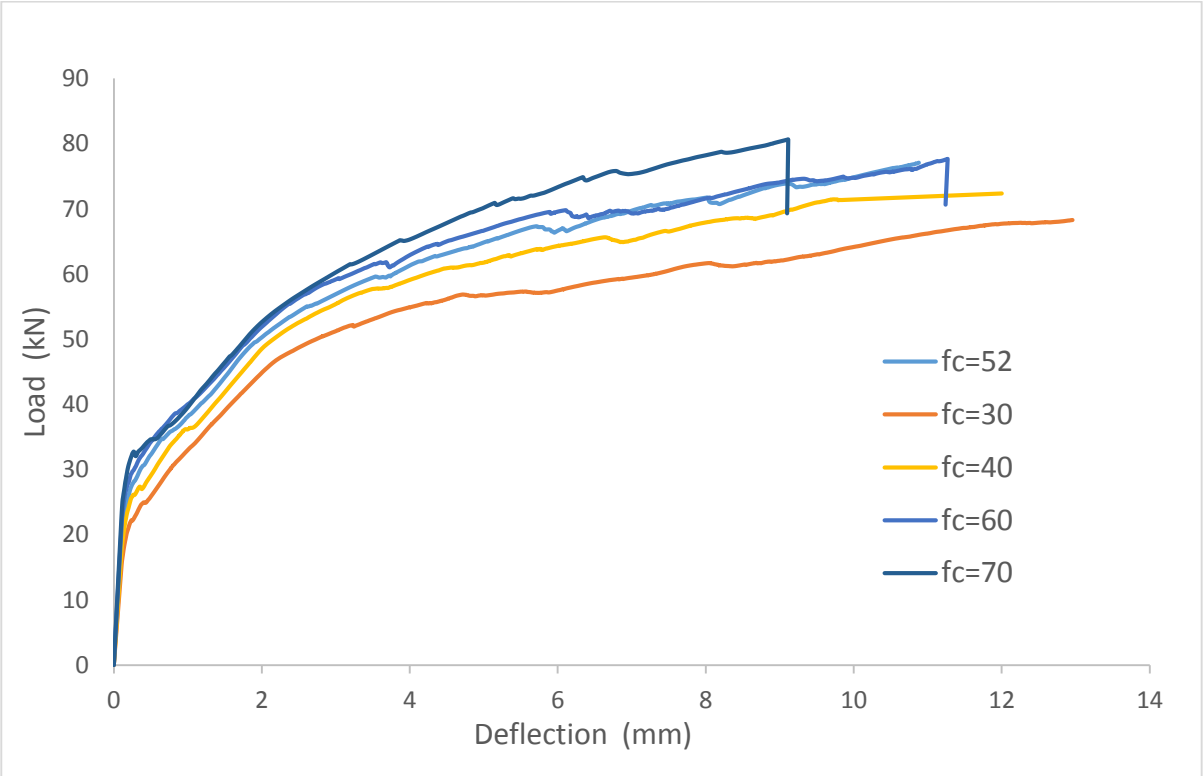

(b) Load-deflection curve with different compressive strength of concrete of NSM-beam

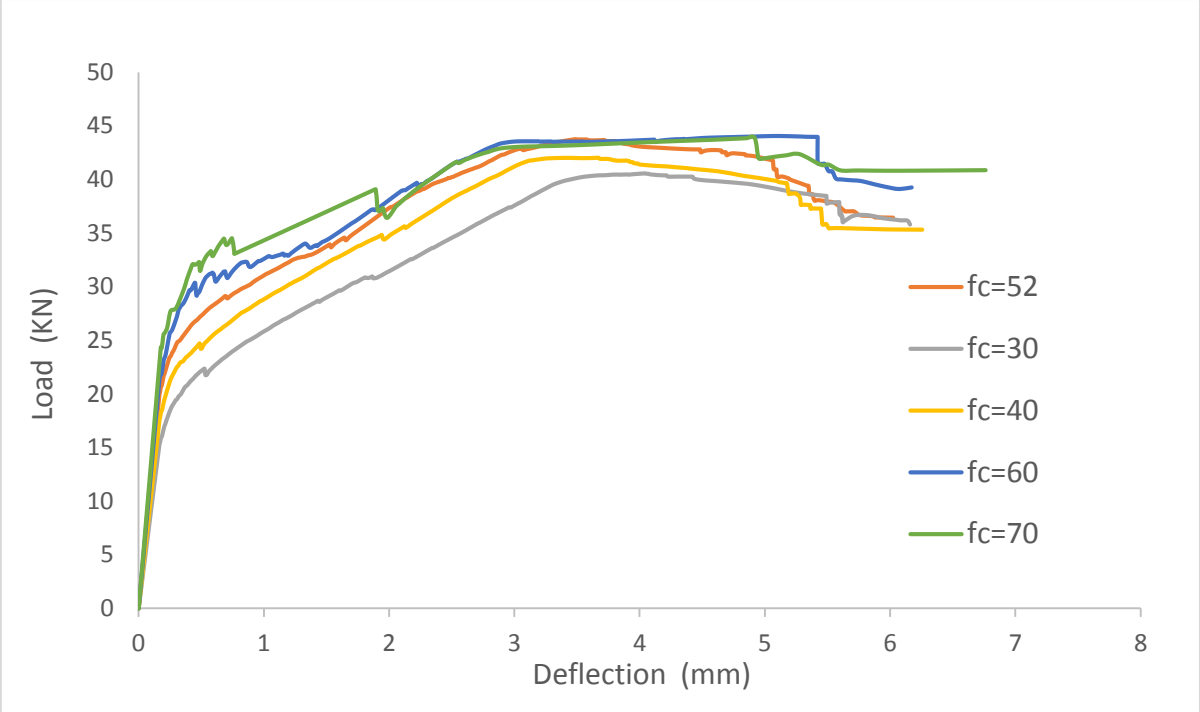

(c) Load-deflection curve with different compressive strength of concrete of S1-EXT-M beam

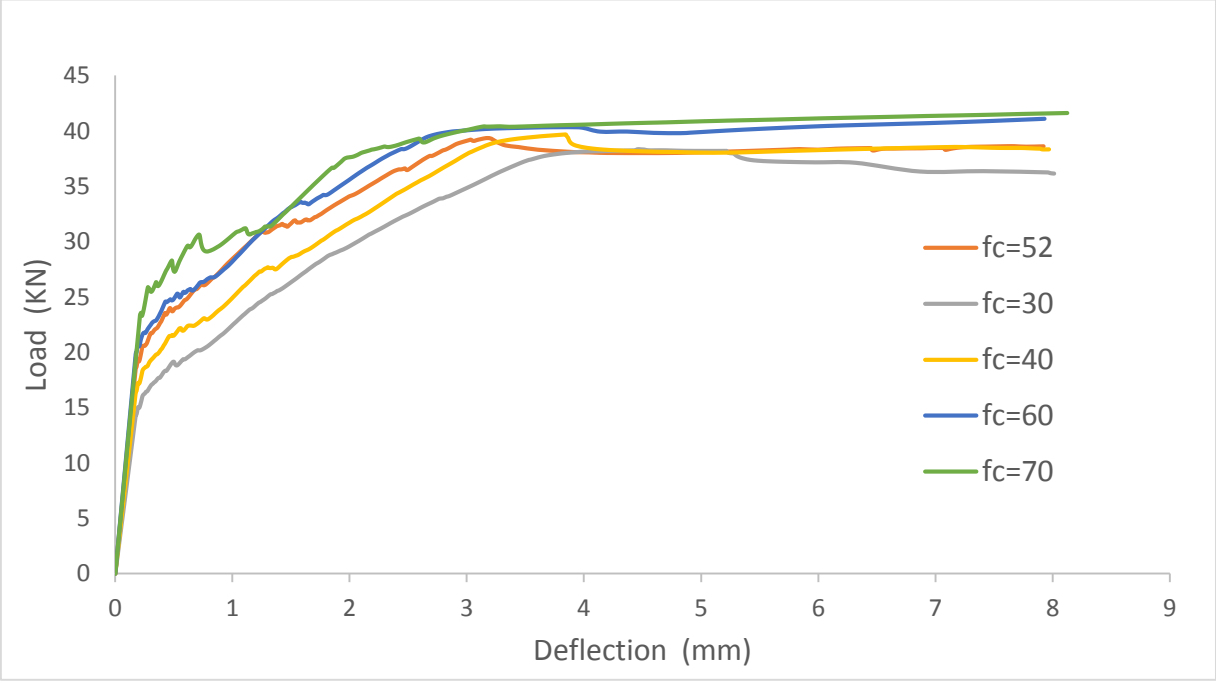

(d) Load-deflection curve with different compressive strength of concrete of S1-EXT-LAM beam

Figure (4.23) Load-deflection curve with different compressive strength of concrete

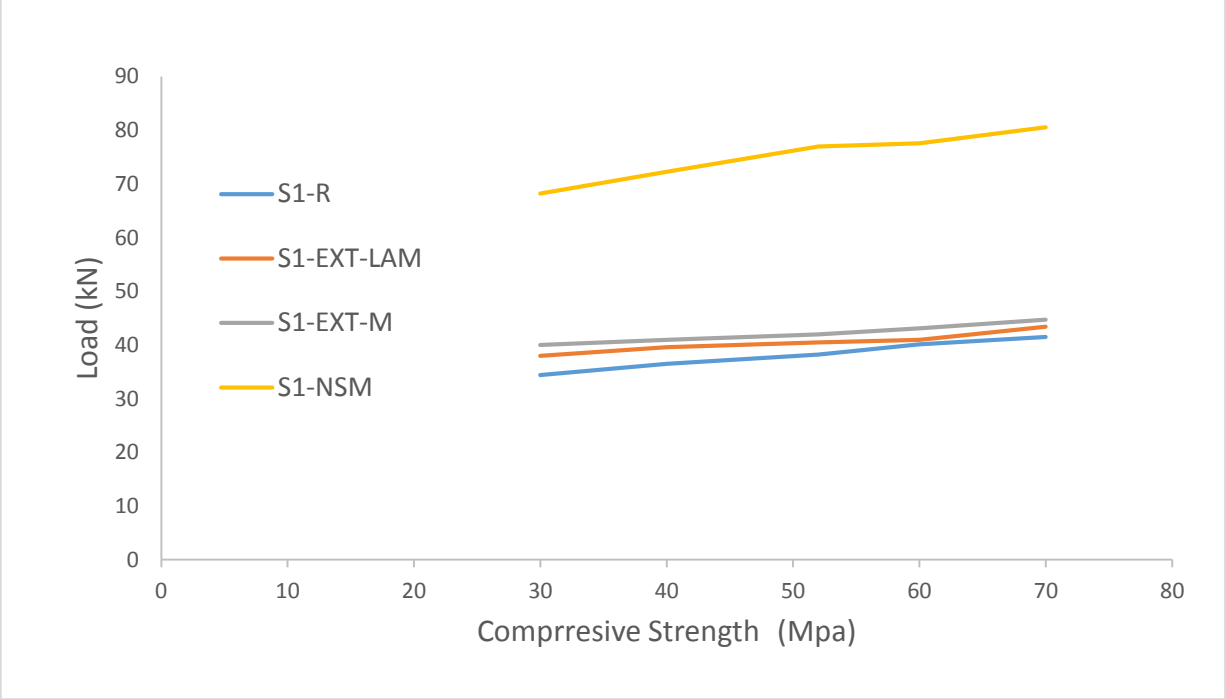

Figure (4.24) Effect of compressive strength on the maximum load

4.3.3.2 Effect of Length of CFRP Laminate

The efficiency of the strengthening RC beam by CFRP in flexure depends on the length of the CFRP laminate. Three different ratio of length of CFRP laminate (L) to length of clear span (S) (L/S=1 L/S=0.83, and L/S=0.66) have been used to study the effect of the length ratio on the behavior of the RC beams strengthened with CFRP. Fig. (4.25) shows that the stiffness of all beams at a load equal to 20 kN is almost the same. After that load, the beam strengthened with L/S equal to 1 is more stiffness than the beam with L/S equal to 0.66. This may be attributed to beam strengthened with L/S equal to 1 have a full anchorage length outside the maximum moment region and it is more efficient in the cracking zone. The debonding failure has been occurred in all beams due to high shear stress occurring at CFRP laminate end. However, the properties of the epoxy are important in relation to debonding failure. Also from this figure can be seen that the maximum load of beam strengthened with L/S equal to 1 higher than loads of beam with L/S equal to 0.66 and 0.83 as

shown in Fig. (4.26). Finally, it can be concluded that the length ratio of CFRP to clear span has an effect on the stiffness as well as on the strength of RC beams.

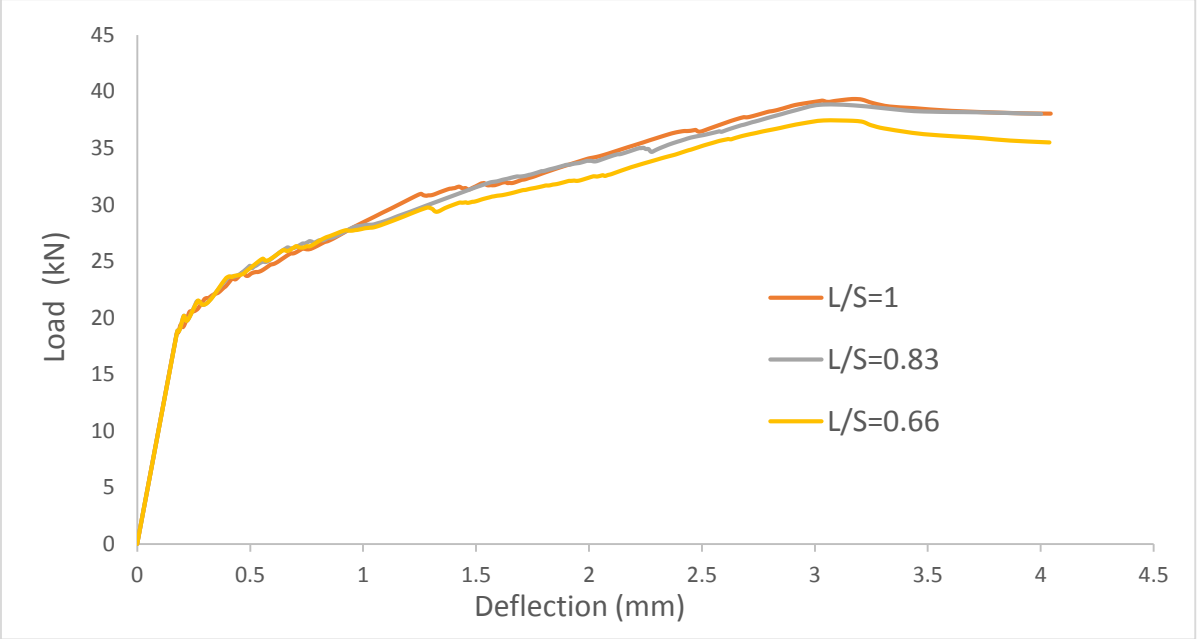

(a) Load-deflection curve for beam S1-EXT-LAM strengthened by different length of CFRP laminate

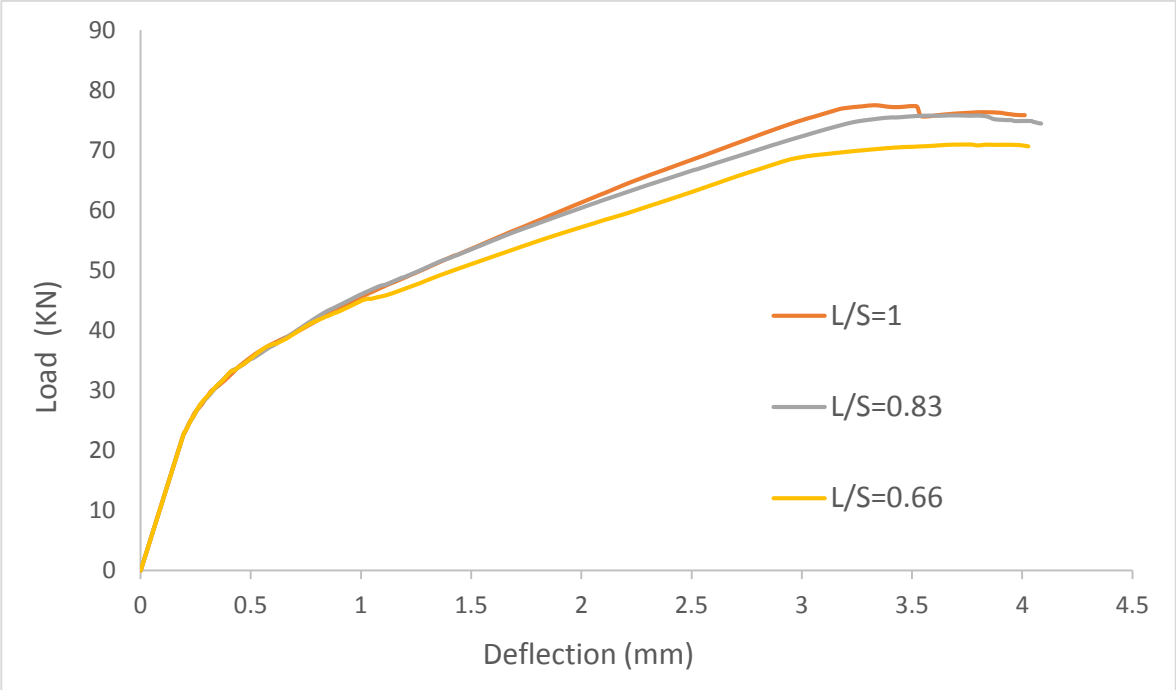

(b) Load-deflection curve for beam S2-EXT-LAM strengthened by different length of CFRP laminate

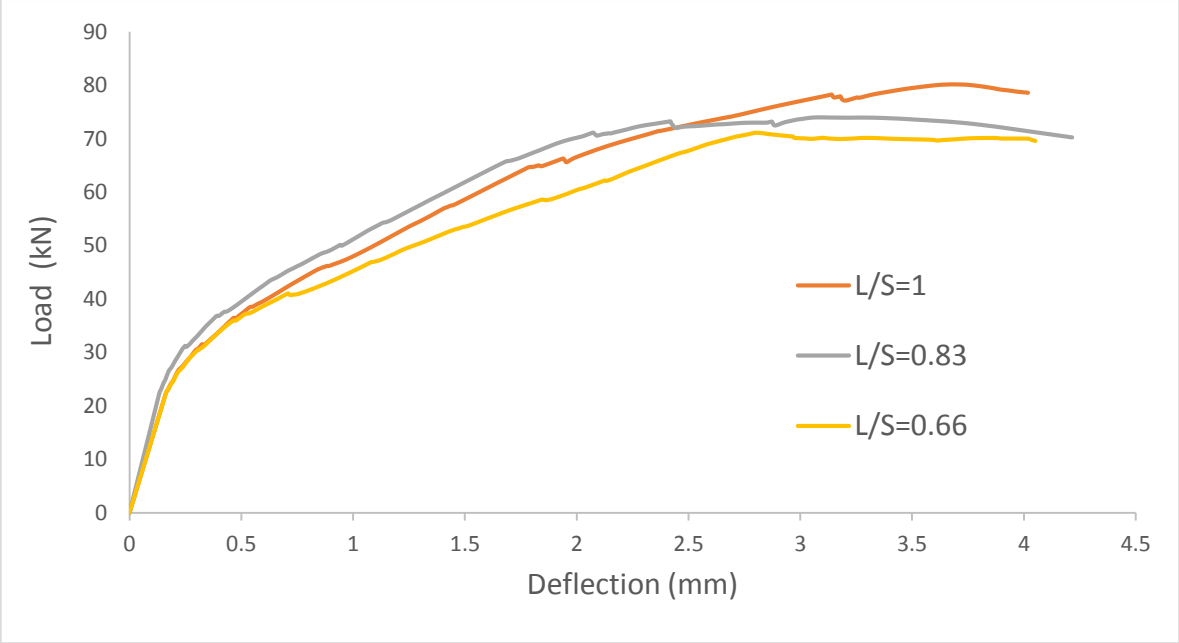

(c) Load-deflection curve for beam S3-EXT-LAM strengthened by different length of CFRP laminate

Figure (4.25) Load-deflection curve of strengthened beams with different length of CFRP

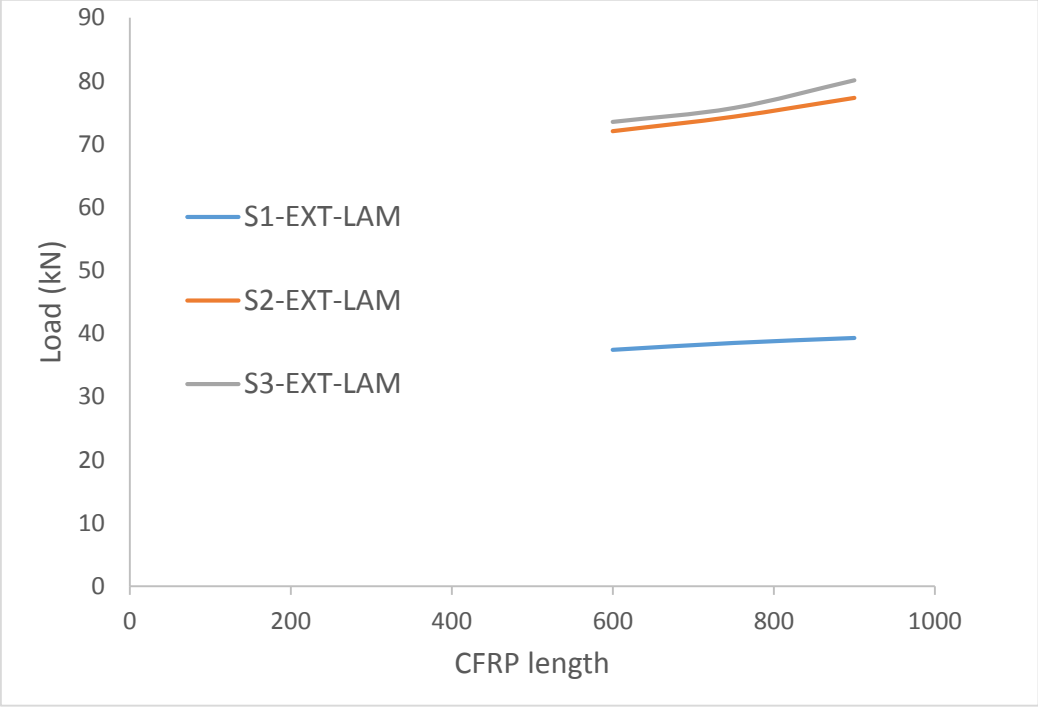

Figure (4.26) Effect length of CFRP on the maximum load

4.3.3.3 Effect of thickness of CFRP sheet

Three beams (S1-EXT-M, S2-EXT-M, and S3-EXT-M) have been used as a case study to investigate the effect of CFRP sheet thickness on the behavior of strengthened RC beams. Two values of thickness are used (0.5, 0.25 and 0.111 mm) in this study. Fig. (4.27) shows that increasing the thickness of the CFRP sheet leads to an increase in the ultimate load of the beams due to increase the cross section of CFRP sheet. Also, Fig. (4.28) shows the relationship between the max load and the thickness of the CFRP sheet.

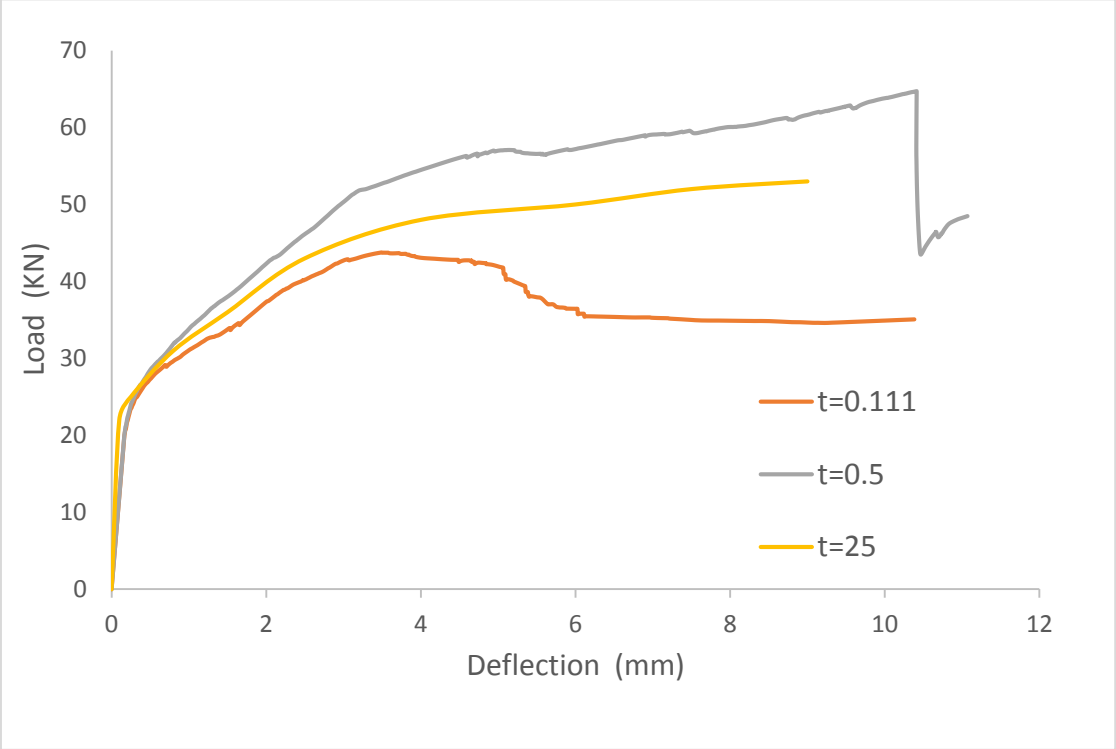

(a) load-deflection curves of S1-EXT-M beams strengthened with different thickness of CFRP

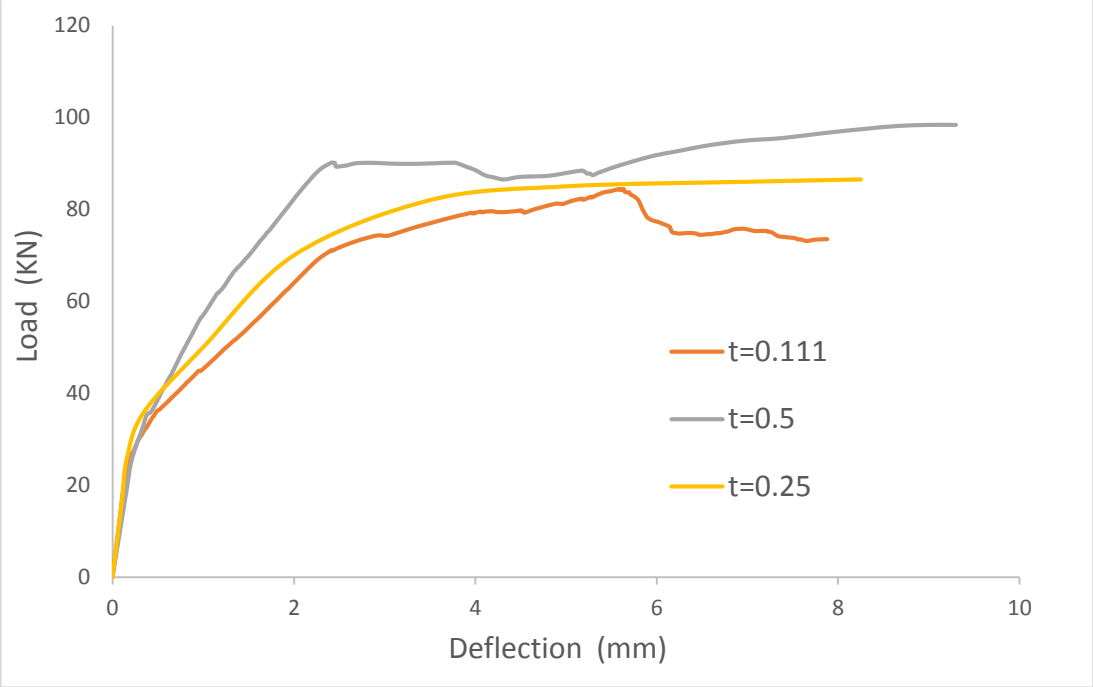

(b) load-deflection curves of S2-EXT-M beams strengthened with different thickness of CFRP

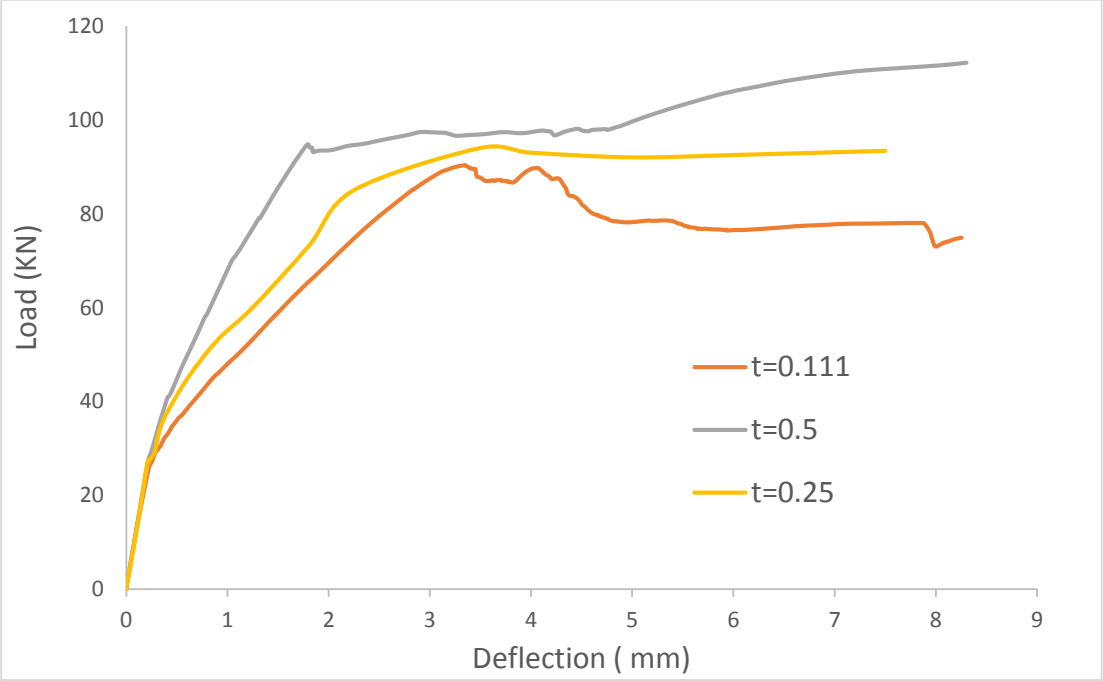

(c) load-deflection curves of S3-EXT-M beams strengthened with different thickness of CFRP

Figure (4.27) load-deflection curves of RC beams strengthened with different thickness of CFRP

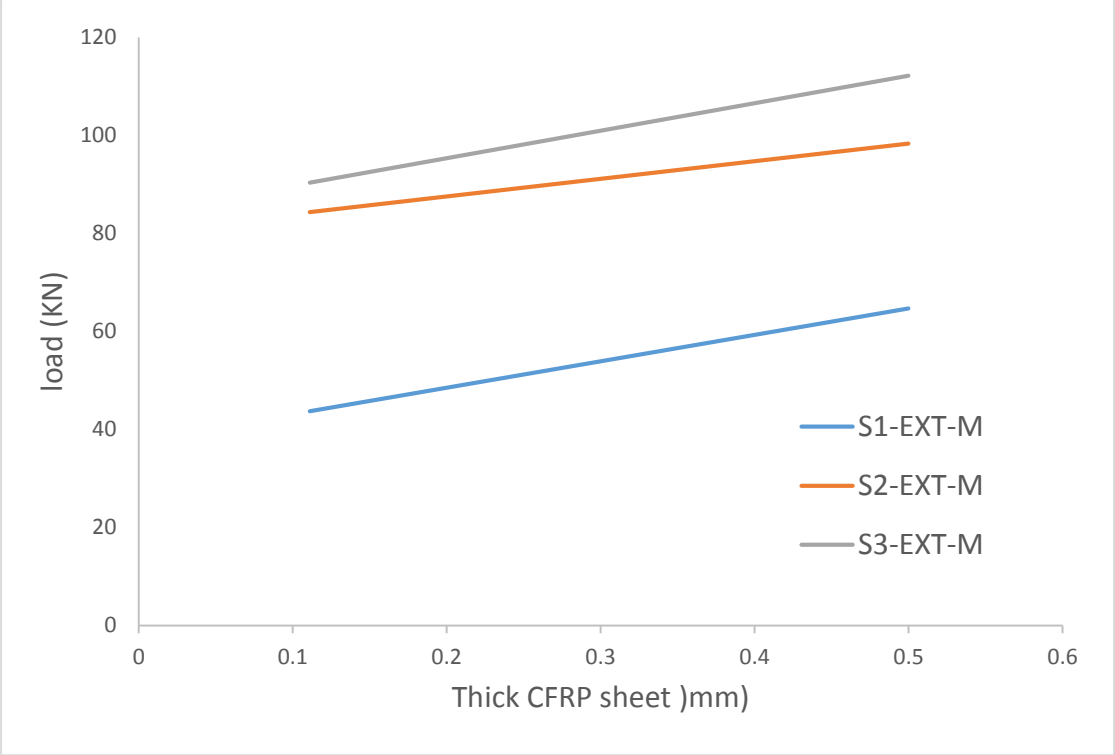

Figure (4.28) Relationship between maximum load and thickness of CFRP sheet

4.3.3.4 The effect of CFRP on steel bar stresses

In this study, four beams (S2-EXT-M, S2-NSM, S2-EXT-LAM, and S2-R) have been used to investigate the effect of the presence of CFRP on steel bar stresses. Fig. (4.29) shows that the load at yield point of steel reinforcement in S2-R, S2-NSM, S2-EXT-LAM, and S2-EXT-M beams is 46.2, 72.5, 74.3 and 78.1 kN, respectively. This indicated that the presence of CFRP has a significant effect on the applied load at the yielding of steel regardless of the type of strengthening. This means that the CFRP has a contribution to carrying the applied load.

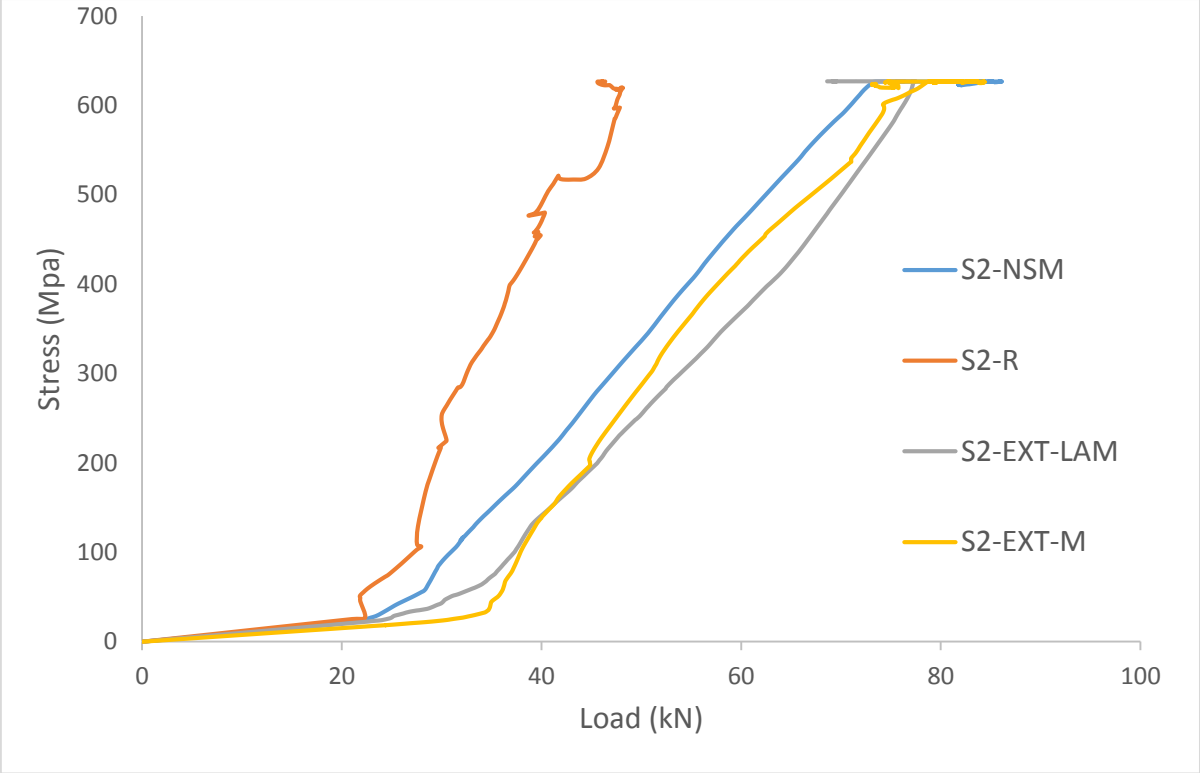

Figure (4.29) Relationship between stresses in steel bar and maximum load in beam

4.3.3.5 Compression the strains through depth control and strengthened beams

In this study, FE models with an effective depth of 300 mm are developed for beams (S2-R, S2-NSM, S2-EXT-LAM, and S2-EXT-M) to show the strain distribution through the depth of the beam when load equal to 40 kN. Fig. (4.30) shows the strain distribution for beams (S2-R, S2-NSM, S2-EXT-LAM, and S2-EXT-M) through the depth. It is clear that the beam strengthened with CFRP sheet or laminate more strain in compression and tension zone than control beam (S2-R).

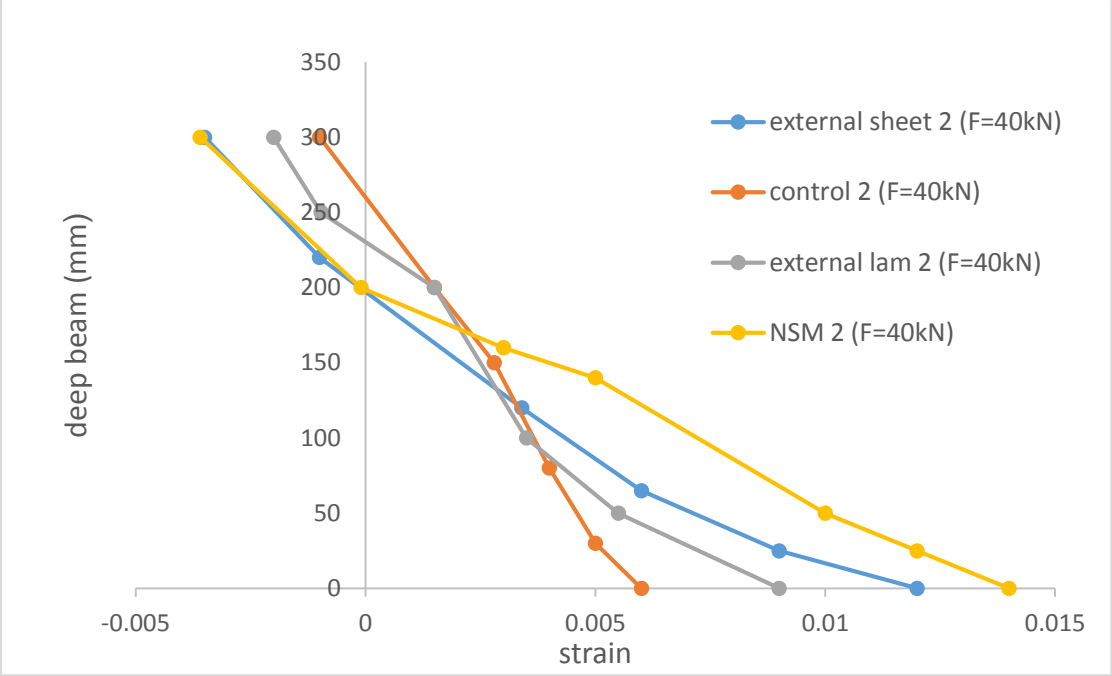

Figure (4.30) Strain distrubution of concrete through the depth of beams

4.3.4 Appraisal of the ACI-440

The strength design approach requires that the design flexural strength of a member exceed its required factored moment as indicated by Equ. (4.1). The design flexural strength ϕM_n refers to the nominal strength of the member multiplied by a strength reduction factor, and the factored moment M_u refers to the moment calculated from factored loads.

$$\phi M_n \geq M_u \quad \text{.....(4.1)}$$

To prevent such an intermediate crack-induced debonding failure mode, the effective strain in FRP reinforcement should be limited to the strain level which debonding may occur, ε_{fd}, as defined in Equ. (4.2).

$$\varepsilon_{fd} = 0.083 \times \sqrt{\frac{f_c^-}{nE_f\ t_f}} \leq 0.9 \times \varepsilon_{fu} \quad \text{.....(4.2)}$$

The following assumptions are made in calculating the flexural resistance of a section strengthened with an externally applied FRP system.

• Design calculations are based on the dimensions, internal reinforcing steel arrangement, and material properties of the existing member being strengthened.

• The strains in the steel reinforcement and concrete are directly proportional to the distance from the neutral axis. That is, a plane section before loading remains plane after loading.

• There is no relative slip between external FRP reinforcement and the concrete.

• The shear deformation within the adhesive layer is neglected because the adhesive layer is very thin with slight variations in its thickness.

• The maximum usable compressive strain in the concrete is 0.003.

• The tensile strength of concrete is neglected.

• The FRP reinforcement has a linear elastic stress-strain relationship to failure.

The effective strain level in the FRP reinforcement at the ultimate limit state can be found from Equ. (4.3).

$$\varepsilon_{fu} = \varepsilon_{cu}\left(\frac{d_{f-c}}{c}\right) - \varepsilon_{bi} \leq \varepsilon_{fd} \ldots\ldots\ldots\ldots\ldots\ldots\ldots\ldots\ldots\ldots\ldots\ldots\ldots\ldots (4.3)$$

The effective stress level in the FRP reinforcement is the maximum level of stress that can be developed in the FRP reinforcement before flexural failure of the section. This effective stress level can be found from the strain level in the FRP, assuming perfectly elastic behavior.

$$f_{fe} = E_f\ \varepsilon_{fe} \quad \ldots\ldots\ldots\ldots\ldots\ldots\ldots\ldots\ldots\ldots\ldots\ldots\ldots\ldots\ldots\ldots\ldots\ldots\ldots (4.4)$$

Based on the strain level in the FRP reinforcement, the strain level in the steel reinforcement can be found from Equ. (4.5) using strain compatibility as shown in Fig. (4.31).

$$\varepsilon_s = (\varepsilon_{fe} + \varepsilon_{bi})\left(\frac{d-c}{d_f-c}\right) \ldots\ldots\ldots\ldots\ldots\ldots\ldots\ldots\ldots\ldots\ldots\ldots\ldots\ldots (4.5)$$

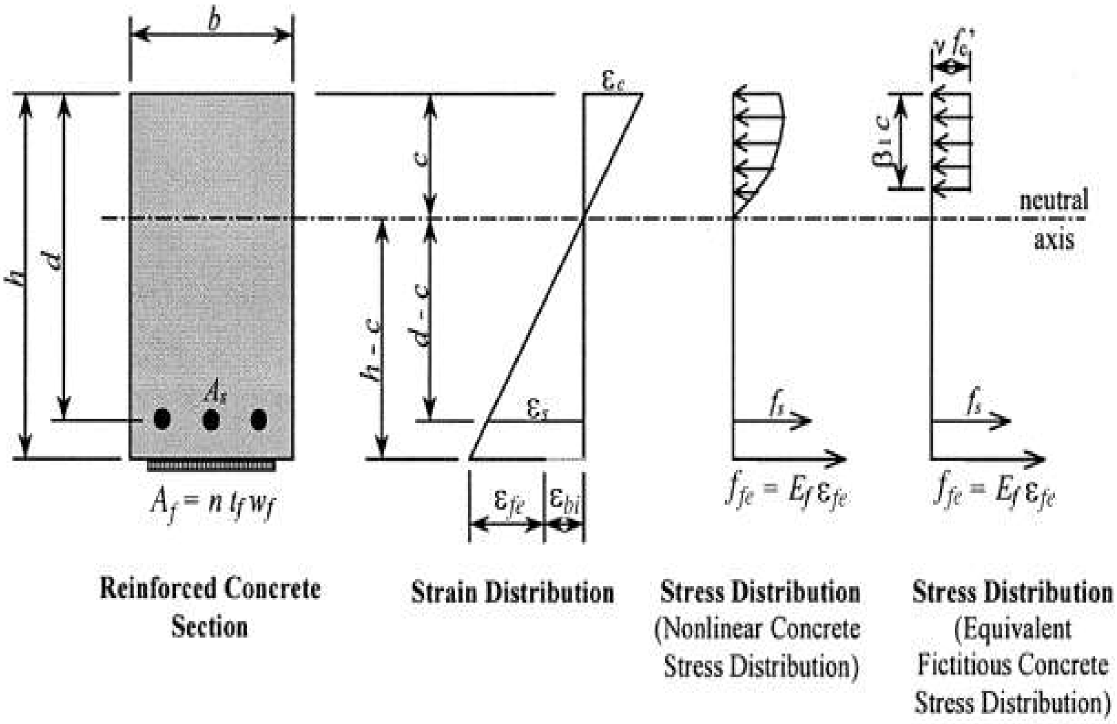

Figure (4.31) Internal strain and stress distribution for a rectangular section under flexure at ultimate limit state.

The stress in the steel is determined from the strain level in the steel using its stress-strain curve.

$$f_s = E_s\, \varepsilon_s \le f_y \ldots\ldots\ldots\ldots\ldots\ldots\ldots\ldots\ldots\ldots\ldots\ldots\ldots\ldots\ldots\ldots\ldots (4.6)$$

With the strain and stress level in the FRP and steel reinforcement determined for the assumed neutral axis depth, internal force equilibrium may be checked using Equ. (4.7).

$$c = \frac{A_s f_s + A_f f_{fe}}{\alpha_1 f_c^{-} \beta_1 b} \quad \ldots\ldots\ldots\ldots\ldots\ldots\ldots\ldots\ldots\ldots\ldots\ldots\ldots\ldots\ldots\ldots\ldots\ldots (4.7)$$

The terms α_1 and β_1 in Eq. (10-12) are parameters defining a rectangular stress block in the concrete equivalent to the nonlinear distribution of stress. If concrete crushing is the controlling mode of failure (before or after steel yielding), α_1 and β_1 can be taken as the values associated with the Whitney stress block (α_1 = 0.85 and β_1 from Section 10.2.7.3 of ACI 318-05).

The ultimate load of externally bonded reinforcment (EBR) strengthened RC beams can be estimated from the design resisting of cross-section of beams to bending moment . ACI-440 propose the following equations [17]:

$$M_n = A_s \times f_s \left(d \frac{\beta_1 c}{2} \right) + \varphi_f A_f f_{fe} \left(h \frac{\beta_1 c}{2} \right) \quad \ldots\ldots\ldots\ldots\ldots\ldots (4.8)$$

The difference between the finite element method and ACI results is 13%, 10%, 23%, 22%, 13%, 37%, 28%, 16%, 37% in beam S1-EXT-LAM, S2-EXT-LAM, S3-EXT-LAM, S1-NSM, S2-NSM, S3-NSM, S1-EXT-M, S2-EXT-M and S3-EXT-M respectivlty because the ACI-440 uses factor of safty for the most equation and There is no relative slip between external FRP reinforcement and the concrete.

Table (4.9) showes the results of finite element method and ACI equation for RC beams in flexure behavior, from this table it can be calculated the ACI equation is under estimate.

Table (4.9) Results of finite element method (FEM) and ACI equation

Beam designation	FEM	ACI	FE/ACI
	Maximum load (kN)	Maximum load (kN)	
S1-EXT-LAM	39.34	45.3	0.87
S2-EXT-LAM	77.33	70.4	1.10
S3-EXT-LAM	80.17	103.8	0.77
S1-NSM	77.05	62.8	1.22
S2-NSM	86.09	99.2	0.87
S3-NSM	85.6	136.7	0.63
S1-EXT-M	43.72	60.8	0.72
S2-EXT-M	84.38	100.5	0.84
S3-EXT-M	89.76	143.5	0.63

4.4 Shear behavior of CFRP-beams

Numerical modeling of the behavior of beam strengthened with CFRP for shear under four-point loading using ABAQUS program based on the experimental work conducted by Barros et al,2007 [60].

4.4.1 Specimens Details and Loading Condition

The numerical study has been developed based on the experimental study of four series of tested beams presented by barros et al,2007 [60]. Fig. (4.32) and Table (4.10) show the reinforcement arrangement, support conditions and geometry of the beams of these series. Each series is consisted of a beam without shear reinforced (R) and the beams retrofitted with shear reinforcing: strips of CFRP sheet (M), steel stirrups (S), strips of CFRP at 45^0_ with the beam

longitudinal axis (IL) and laminate strips of CFRP at 90^0_ with the beam longitudinal axis laminate (VL).

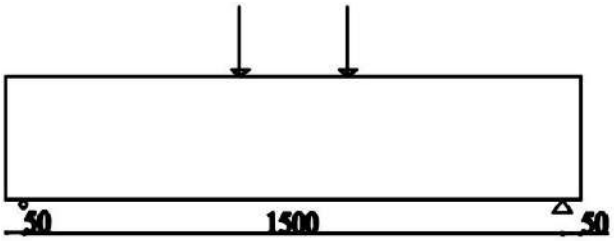

A10-R

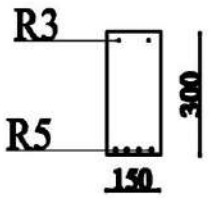

Cross section

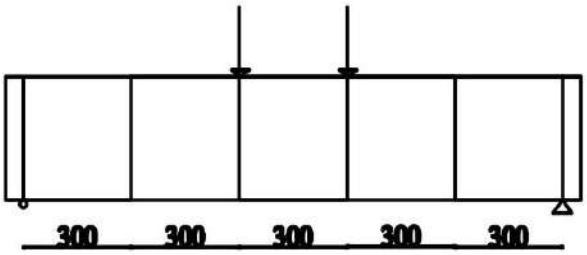

A10-S

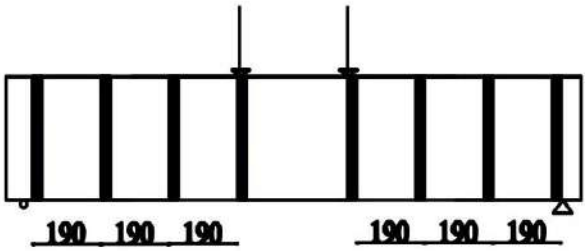

A10-M

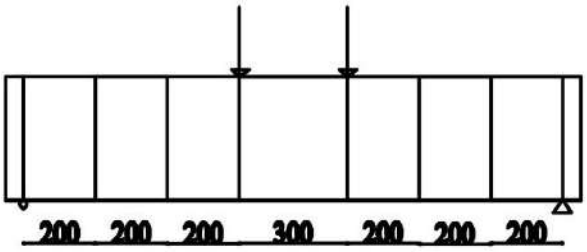

A10-VL

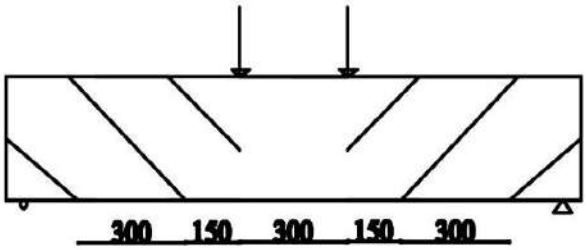

A10-IL

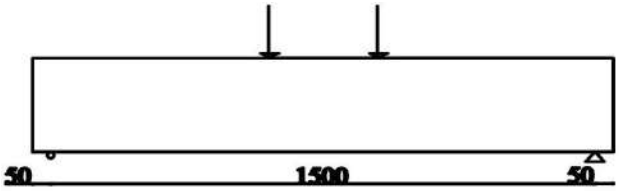

A12-R

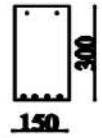

Cross section

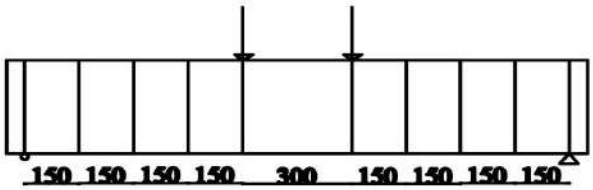

A12-S

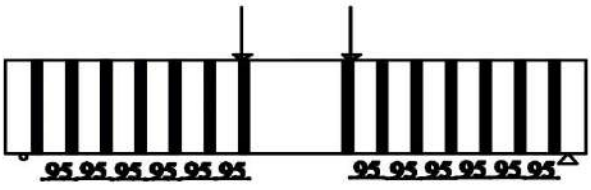

A12-M

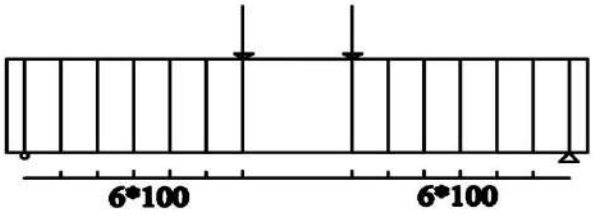

A12-VL

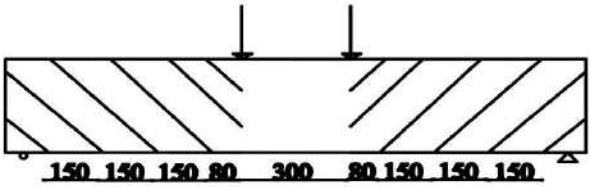

A12-IL

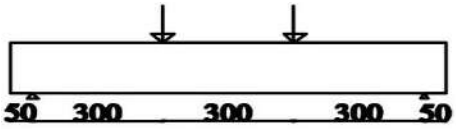

B10-R

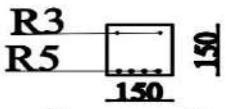

Cross section

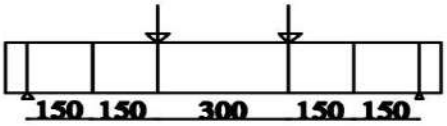

B10-S

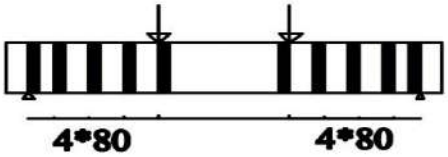

B10-M

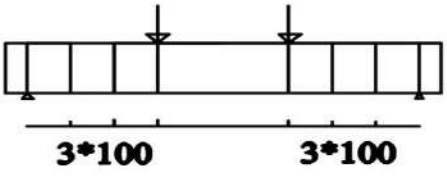

B10-VL

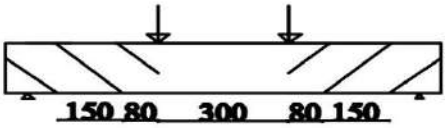

B10-IL

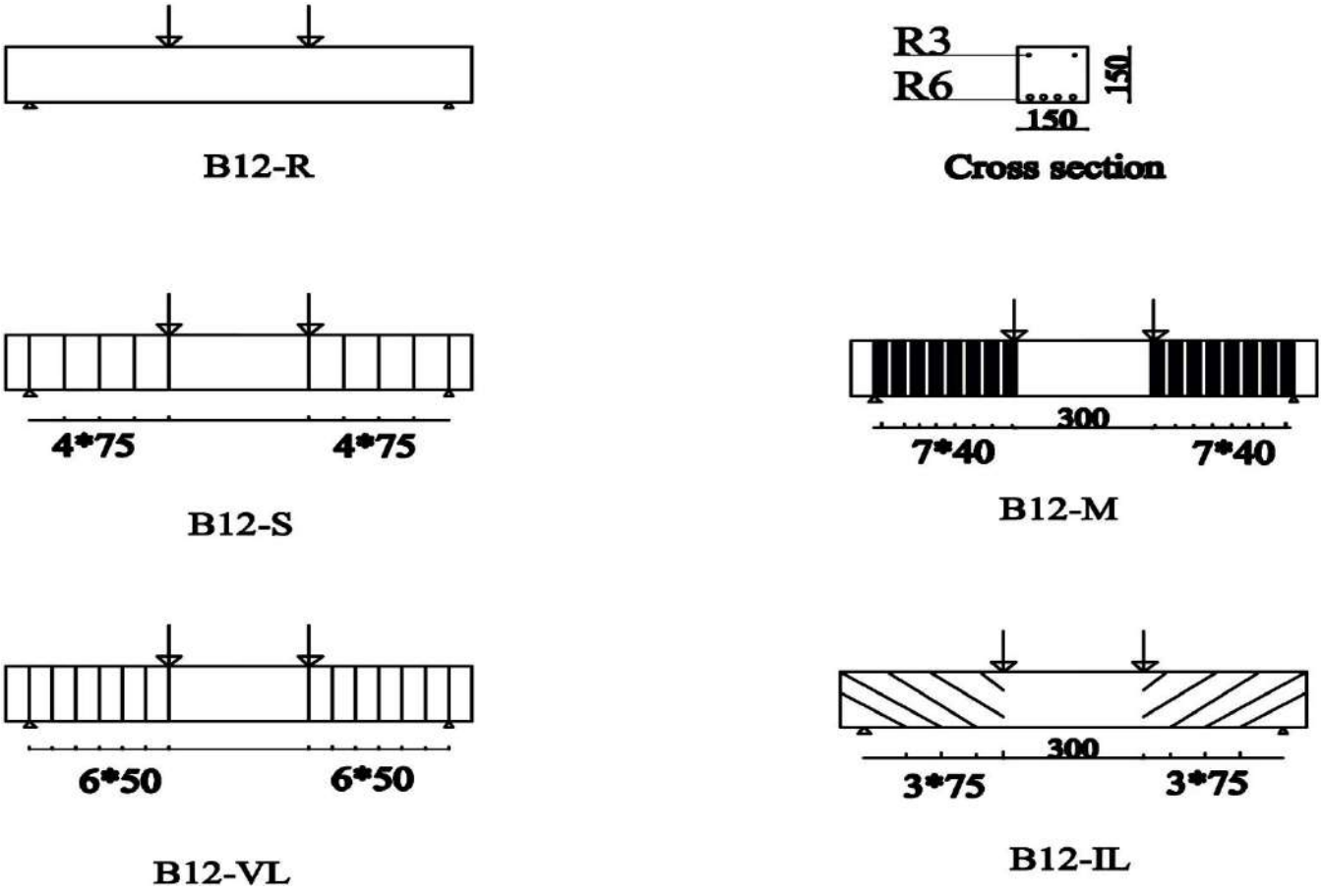

Figure (4.32) Series beams strengthened for the shear (dimensions in mm)[60]

Table (4.10) Series beams strengthened for the shear [60]

Beam designation			Shear strengthening systems			
			Material	Quantity	Spacing (mm)	Angle (°)
A series	A10 seies	A10-R	-----	-----	------	------
		A10-S	Steel stirrups	6Ø6 of two branches	300	90
		A10-M	CFRP sheet	8×2 layers of 25 mm (U shape)	190	90
		A10-VL	CFRP laminate	16 CFRP laminates	200	90
		A10-IL	CFRP laminate	12 CFRP laminates	300	45
		A12-R	-----	-----	------	------
		A12-S	Steel stirrups	10Ø6 of two branches	150	90

	A12 series	A12-M	CFRP sheet	14×2 layers of 25 mm (U shape)	95	90
		A12-VL	CFRP laminate	28 CFRP laminates	100	90
		A12-IL	CFRP laminate	24 CFRP laminates	150	45
B series	B10 seies	B10-R	-----	-----	------	------
		B10-S	Steel stirrups	6Ø6 of two branches	150	90
		B10-M	CFRP sheet	10×2 layers of 25 mm (U shape)	80	90
		B10-VL	CFRP laminate	16 CFRP laminates	100	90
		B10-IL	CFRP laminate	12 CFRP laminates	150	45
	B12 series	B12-R	-----	-----	------	------
		B12-S	Steel stirrups	10Ø6 of two branches	75	90
		B12-M	CFRP sheet	16×2 layers of 25 mm (U shape)	40	90
		B12-VL	CFRP laminate	28 CFRP laminates	50	90
		B12-IL	CFRP laminate	24 CFRP laminates	75	45

4.4.2 Shear Behavior: Results and Discussion

4.4.2.1 Control Beams A10-R, A12-R, B10-R and B12-R

Control beams for all seires (beams without shear reinforcement) have failed by the formation of shear failure cracks without yielding of the longitudinal tensile reinforcement as shown in Figs. (4.33, 4.34, 4.35 and 4.36). The control beams A10-R, A12-R, B10-R and B12-R failed at a ultimate load of 96.2, 119, 73.39 and 73.36 kN, respectively. The relationship between the applied load and the deflection at mid span of the beam for FEM and experimental results is depicted in Fig. (4.37). There is good agreement between experimental and FEM using program ABAQUS results for all unstrengthened beams. Also,it can be seen that from Table (4.11).

Table (4.11) Finite element method and experimental results.

Beam designation	Experimental (EXP) ultimate load (kN)	Finite element method (FE) ultimate load (kN)	EXP/FE
A10-R	100.4	96.2	1.04
A12-R	116.5	119	0.98
B10-R	74.02	73.39	1.01
B12-R	75.7	73.36	1.03

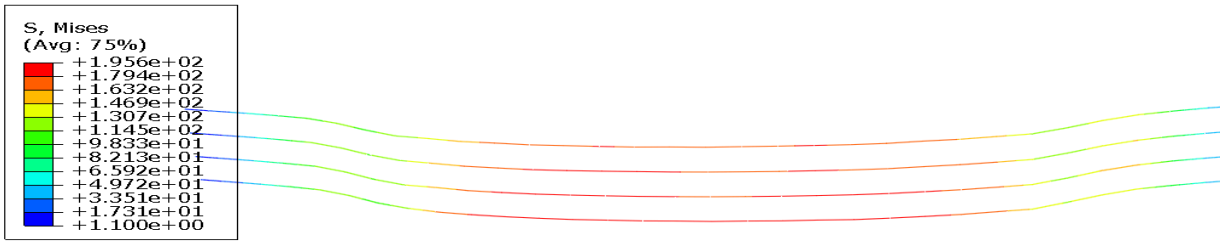

(a) stresses in steel bar

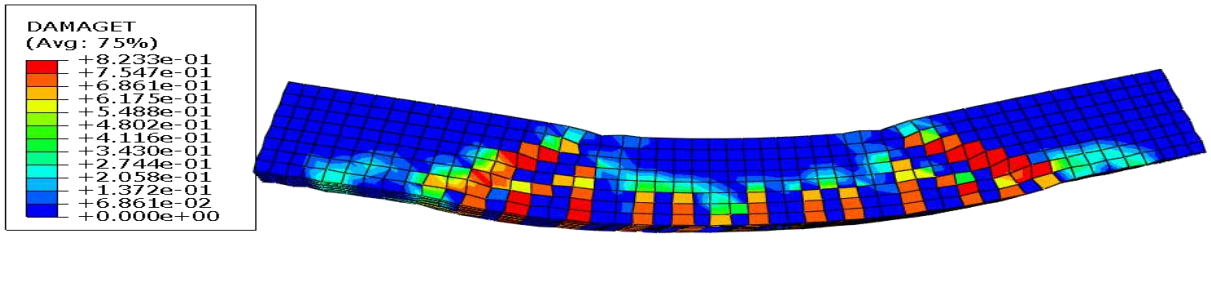

(b) crack in concrete

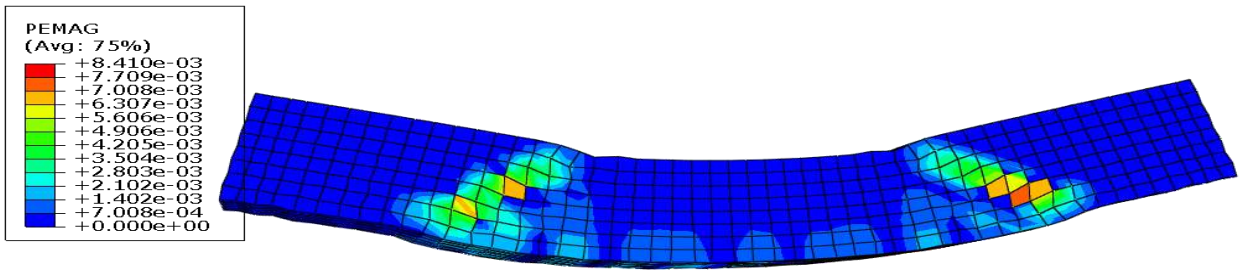

(c) strain in concrete

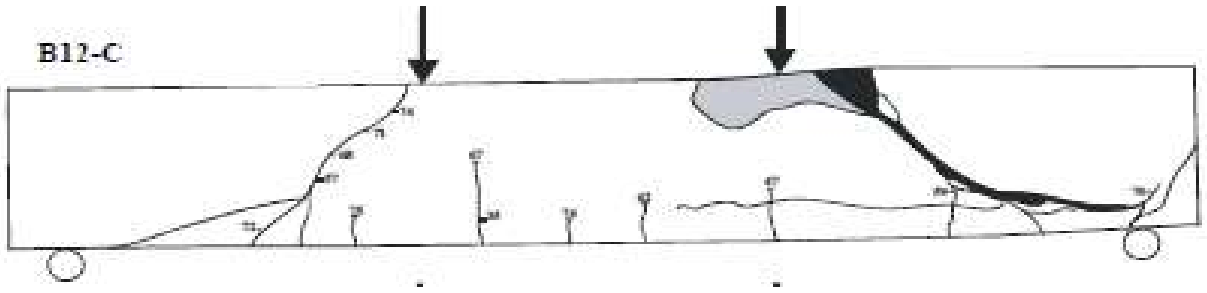

(d) experimental failure

Figure (4.33) Mode of failure of control beam (B12-R)

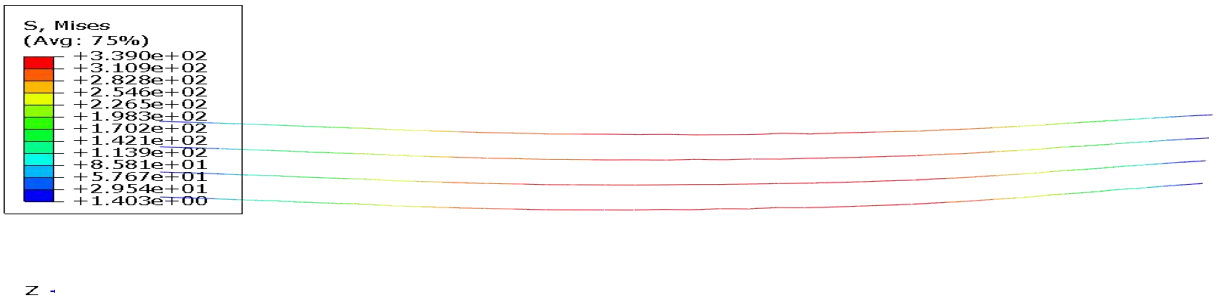

(a) stresses in steel bar

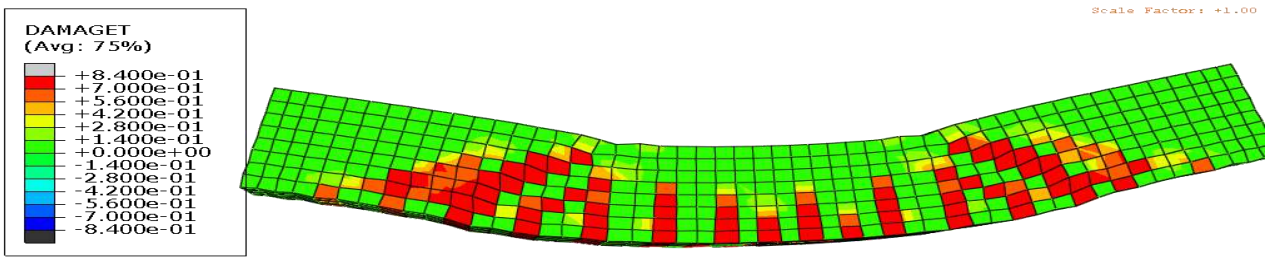

(b) crack in concrete

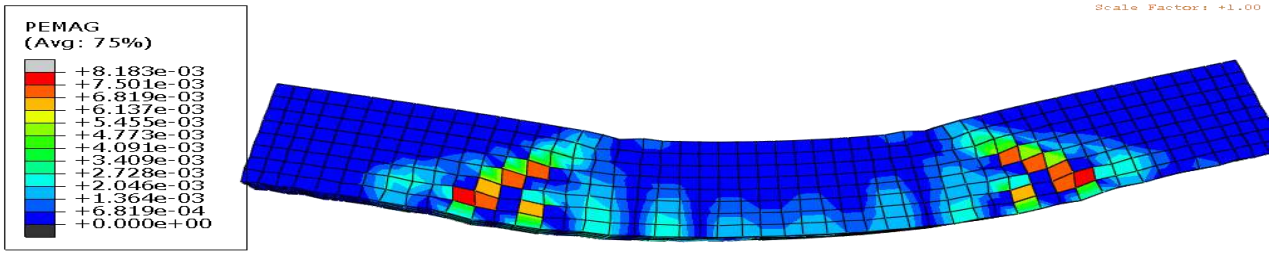

(c) strain in concrete

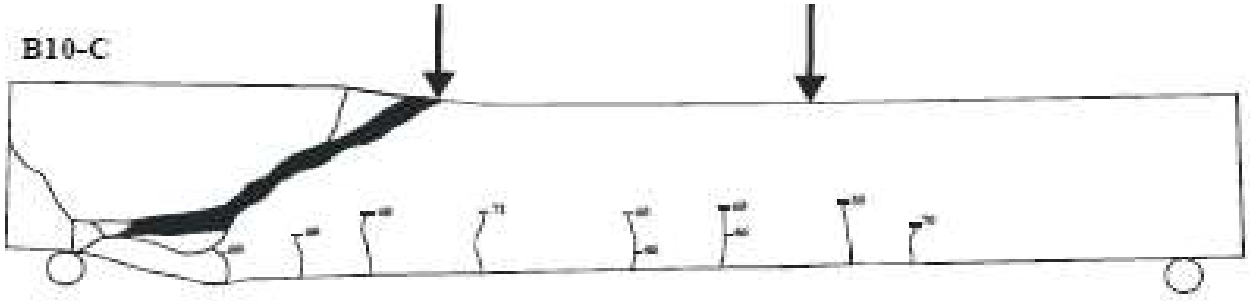

(d) experimental failure

Figure (4.34) Mode of failure of control beam (B10-R)

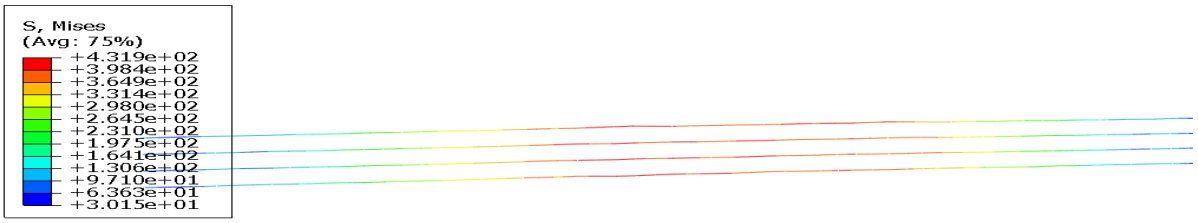

(a) stresses in steel bar

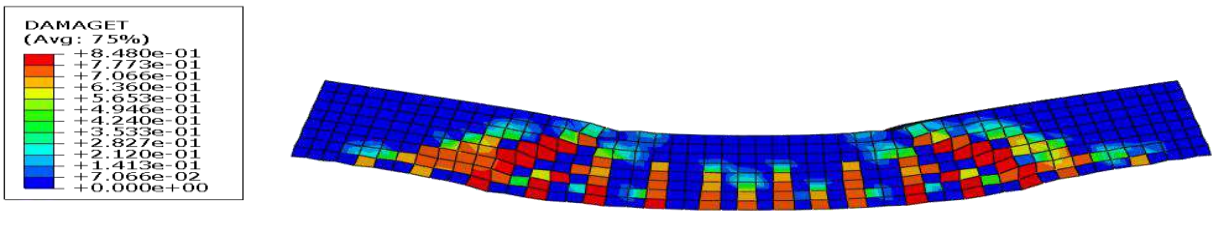

(b) crack in concrete

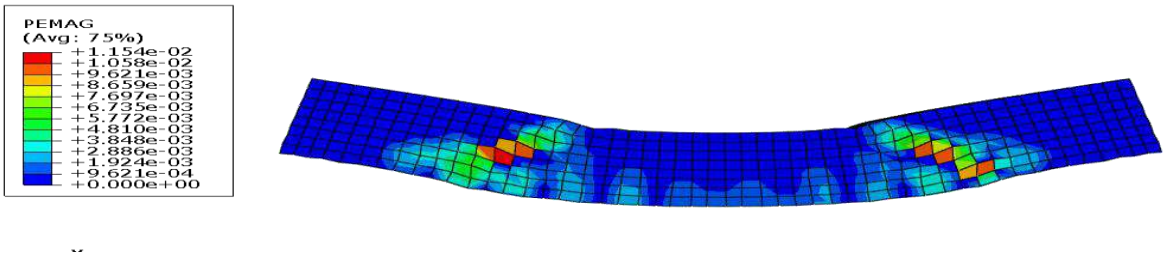

(c) strain in concrete

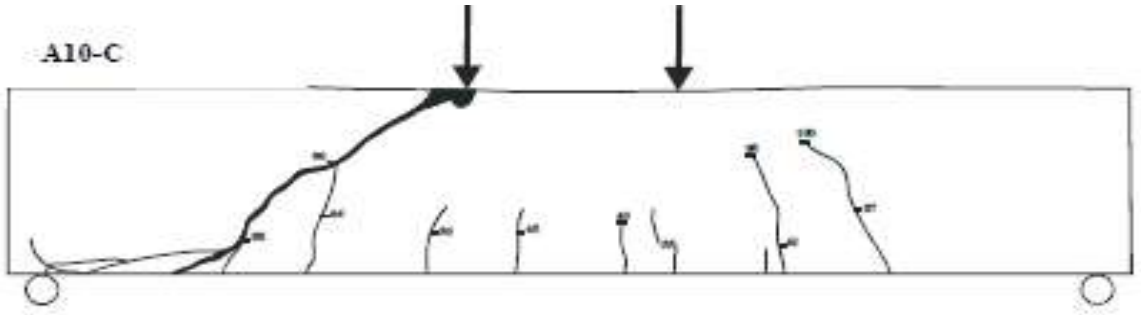

(d) experimental failure

Figure (4.35) Mode of failure of control beam (A10-R)

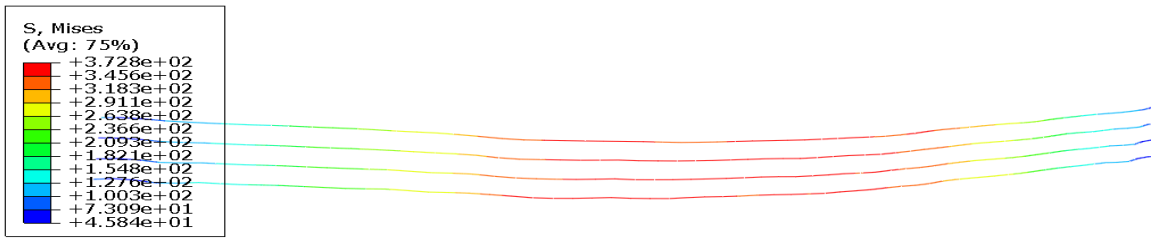

(a) stresses in steel bar

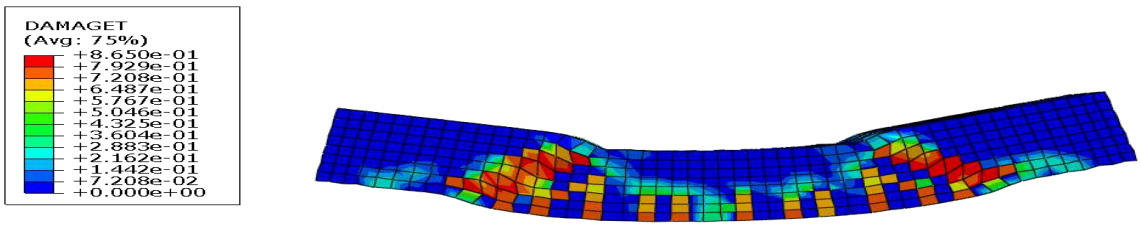

(b) crack in concrete

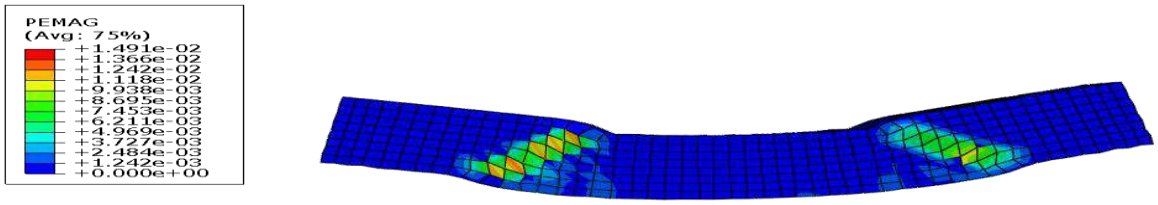

(c) strain in concrete

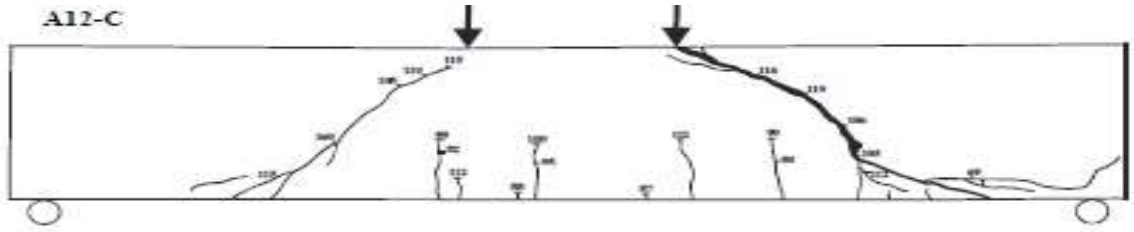

(d) experimental failure

Figure (4.36) Mode of failure of control beam (A12-R)

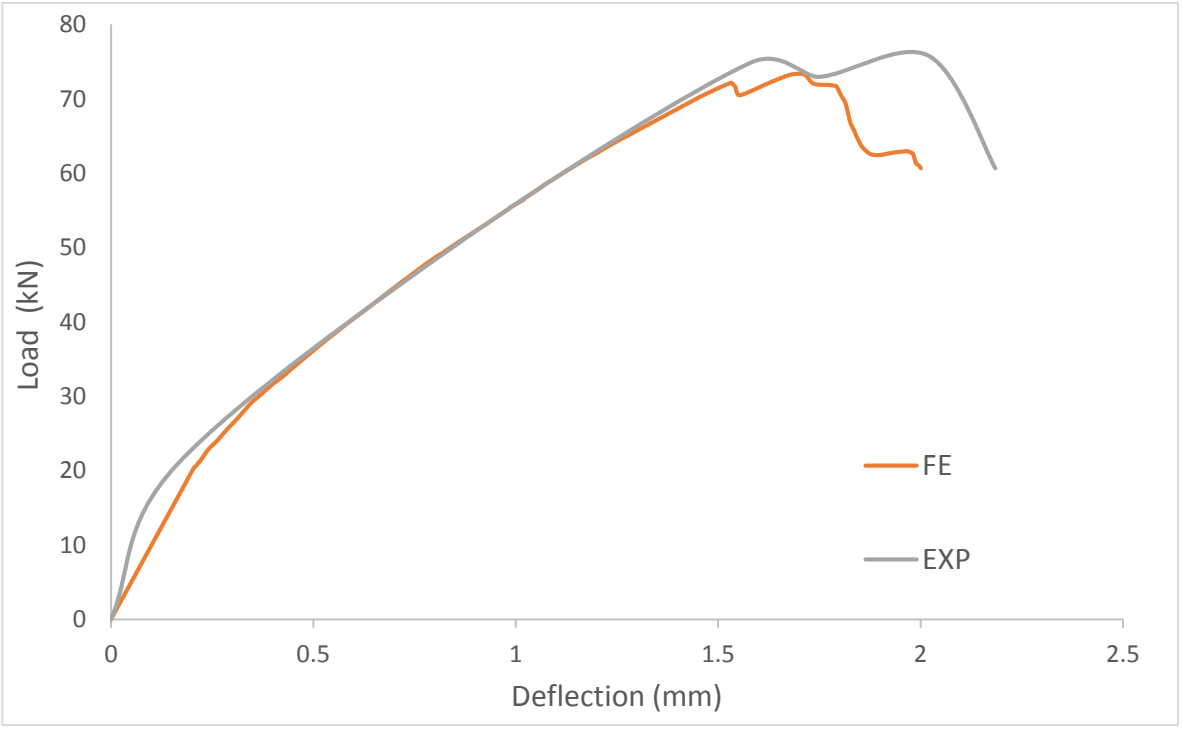

(a) Load-deflection curve of control beams (B12-R)

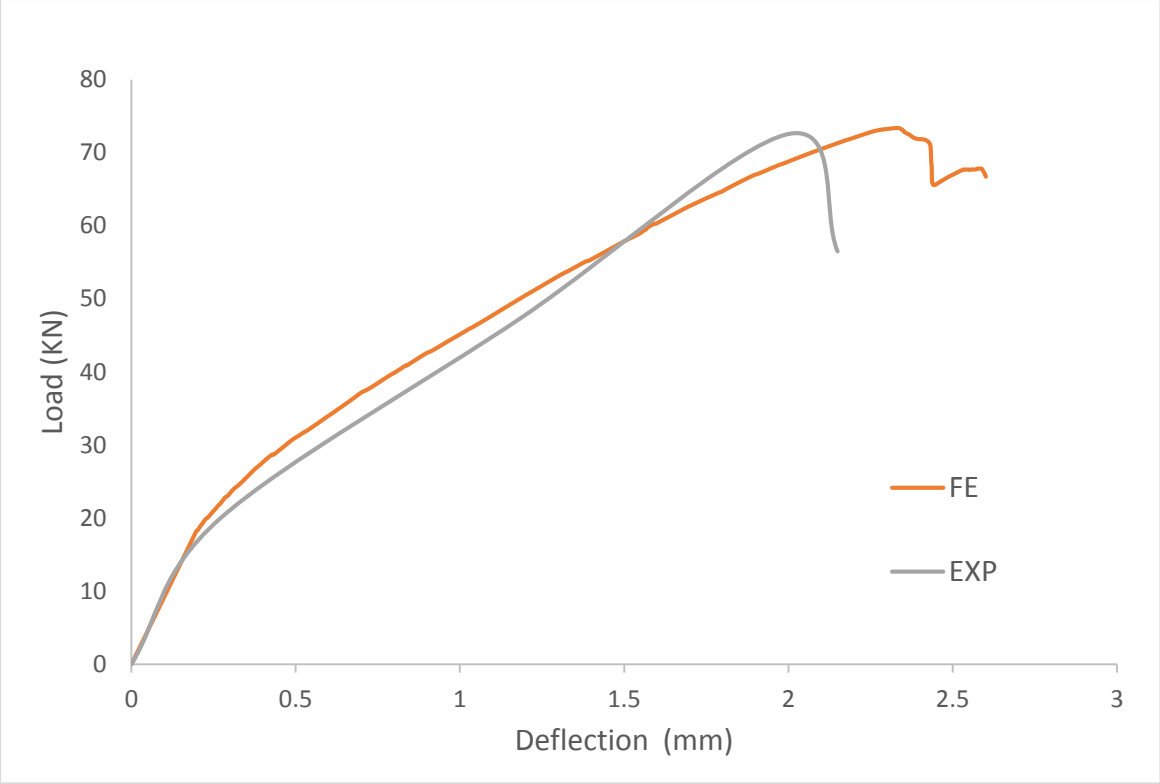

(b) Load-deflection curve of control beams (B10-R)

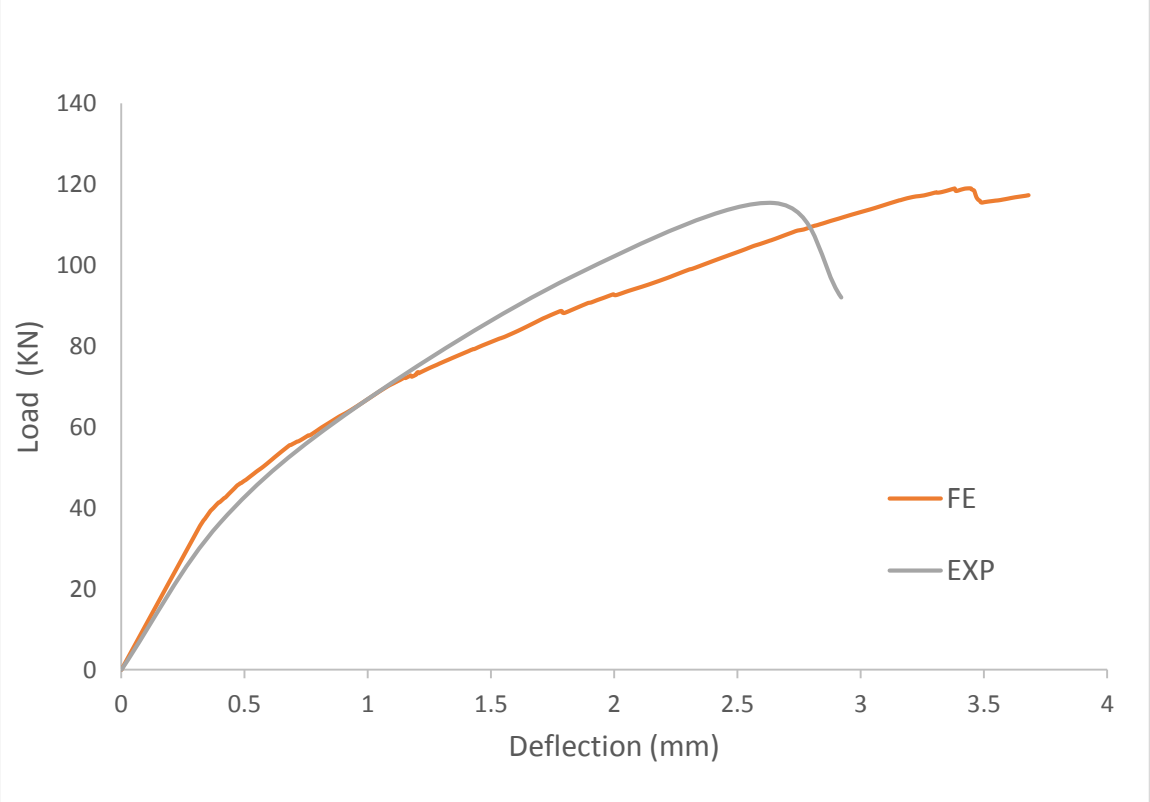

(c) Load-deflection curve of control beams (A12-R)

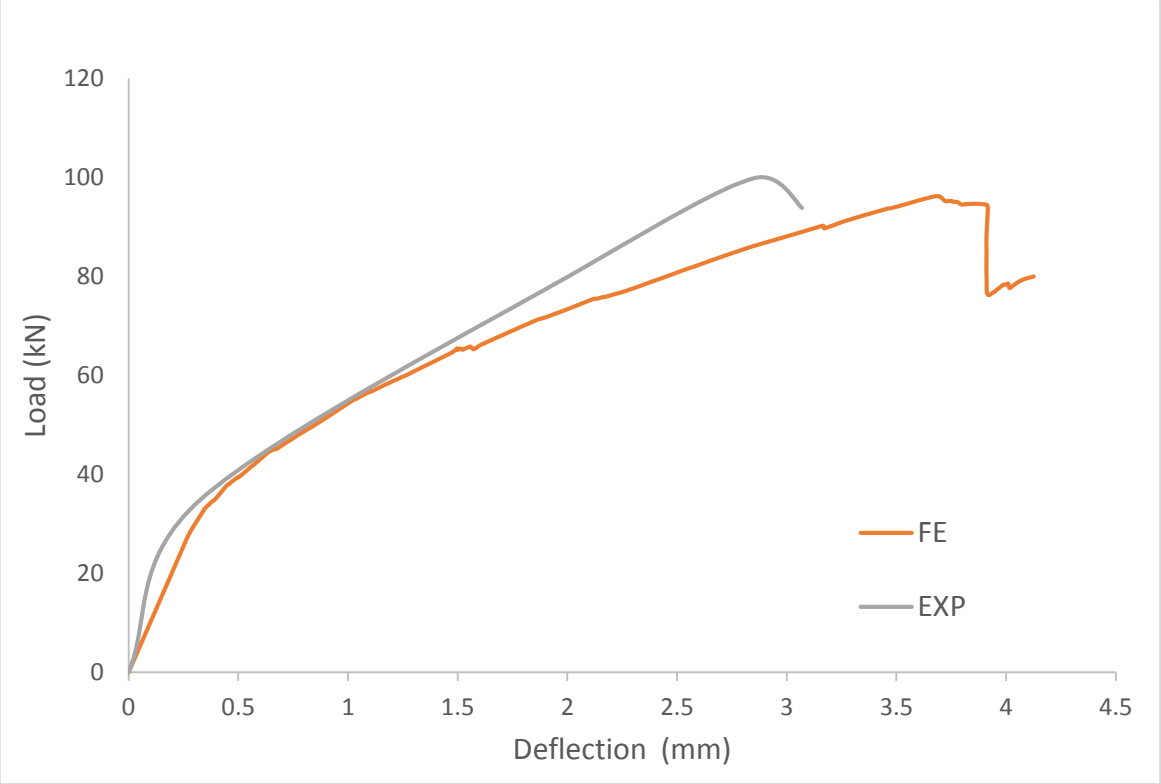

(d) Load-deflection curve of control beams (A10-R)

Figure (4.37) Load-deflection curve of control beams

4.4.2.2 Beams with Steel Stirrups A10-S, A12-S, B10-S and B12-S

Beam with traditional stirrups has been investigated numerically using program ABAQUS. The maximum load of beams A10-S, A12-S, B10-S, and B12-S were 183.12, 205.5, 107.69 and 154.3 kN, respectively. It can be noted that A10-S, A12-S, B10-S, and B12-S with steel stirrups resulted in 90.3%, 71.3%, 46.7%, and 110.3% respectively increase in the maximum load in comparison with control beam without stirrups because the steel stirrups inside the beam resistance the inclined crack see Table (4.11). In beams, A10_S and A12_S shear failure crack occurred after the yielding of the longitudinal steel reinforcement. Beams (B10-S and B12-S) were failed by the formation of a shear crack before the yielding of the longitudinal steel reinforcement. Due to the combined crack opening and crack sliding of the shear failure crack, a stress gradient occurred in the cross section of the steel stirrup crossing the shear failure

crack, leading to its rupture. Figs. 4.38, 4.39, 4.40, 4.41, and 4.42 show the mode failure of these beams.

Table (4.12) show the a good agreement numerical analysis and the experimental results between for all beams.

Table (4.12) Finite element method and experimental results.

Beam designation	Experimental (EXP)	Finite element method (FE)	EXP/FE
	Max load (kN)	Max load (kN)	
A10-S	169.35	183.12	0.92
A12-S	215.04	205.5	1.04
B10-S	120.64	107.69	1.12
B12-S	159.10	154.3	1.03

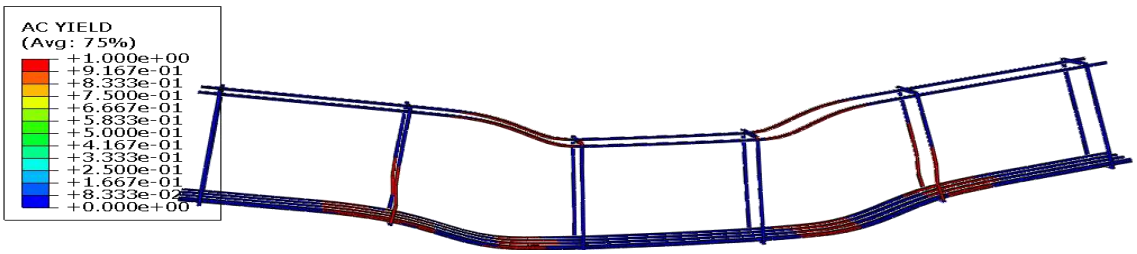

(a) yield of steel stirrups

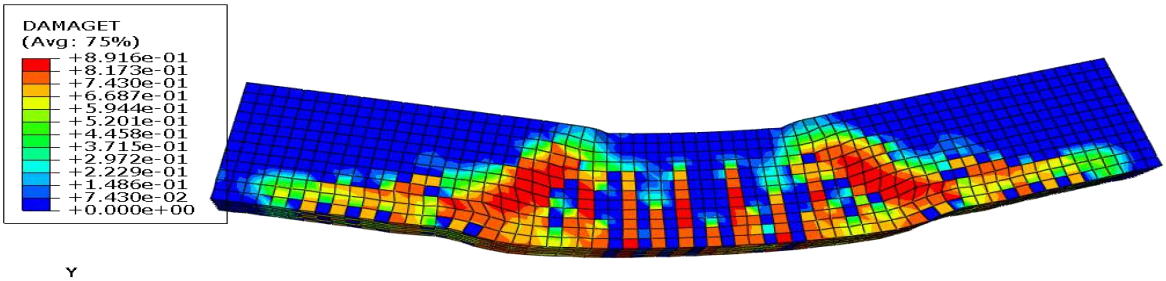

(b) crack in concrete

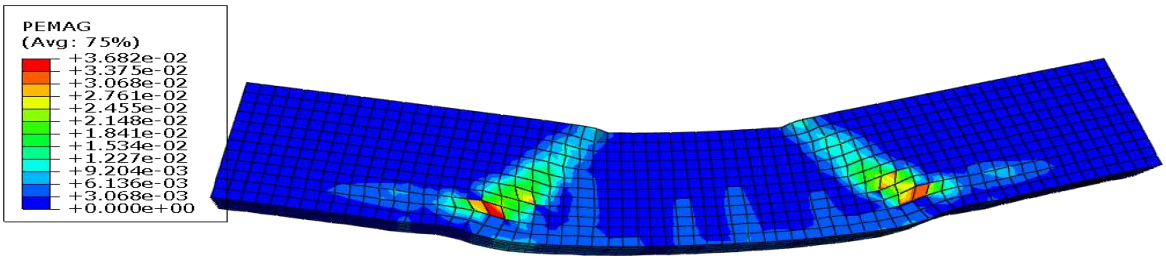

(c) strain in concrete

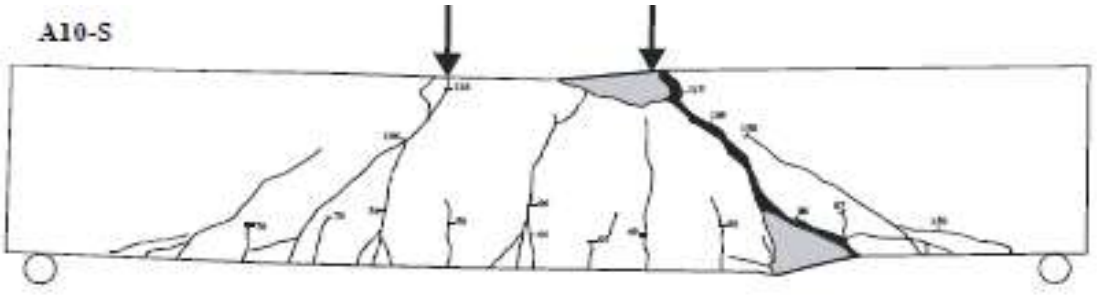

(d) experimental failure

Figure (4.38) Mode of failure of beam with steel stirrups (A10-S)

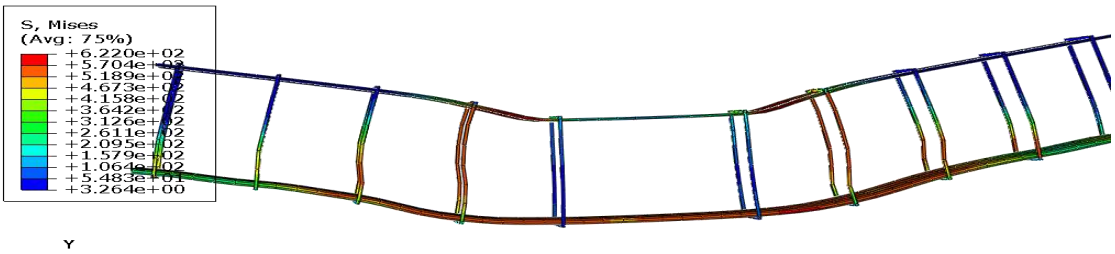

(a) yield of steel stirrups

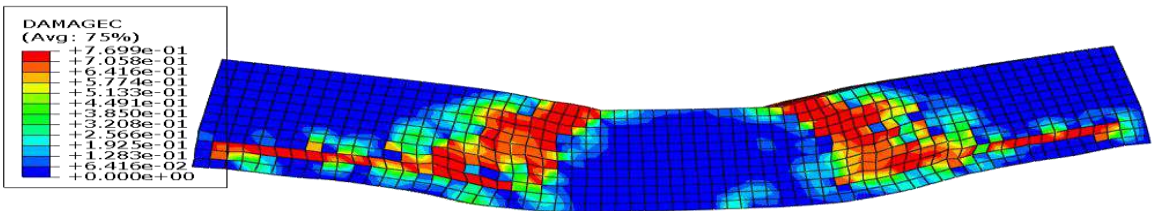

(b) crack in concrete

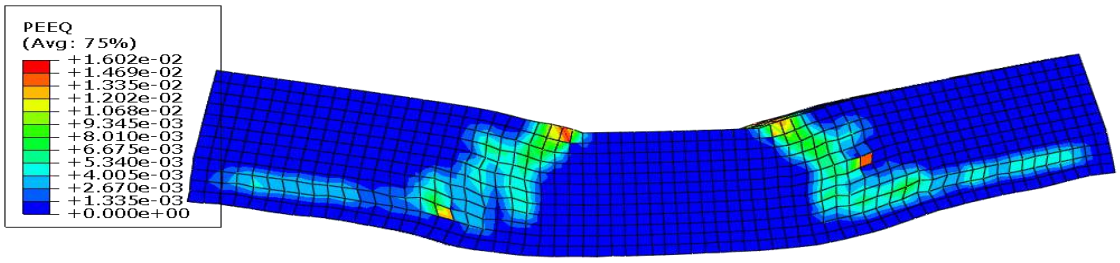

(c) strain in concrete

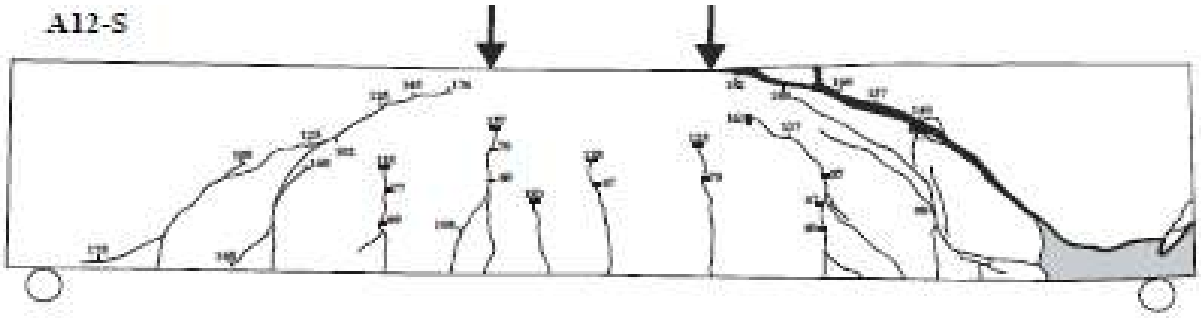

(d) experimental failure

Figure (4.39) Mode of failure of beam with steel stirrups (A12-S)

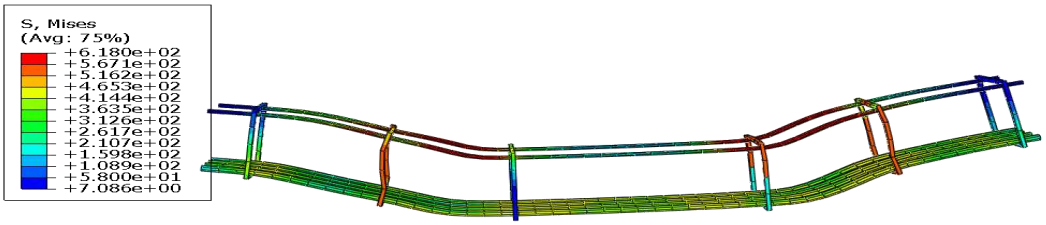

(a) yield of steel stirrups

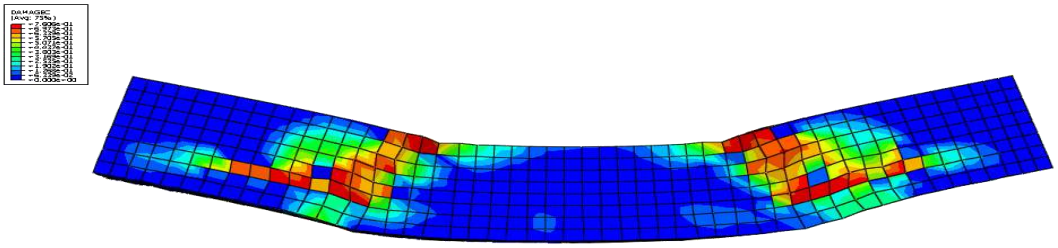

(b) crack in concrete

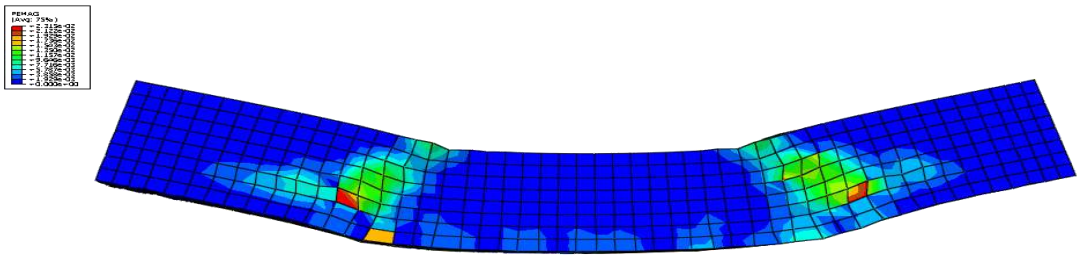

(c) strain in concrete

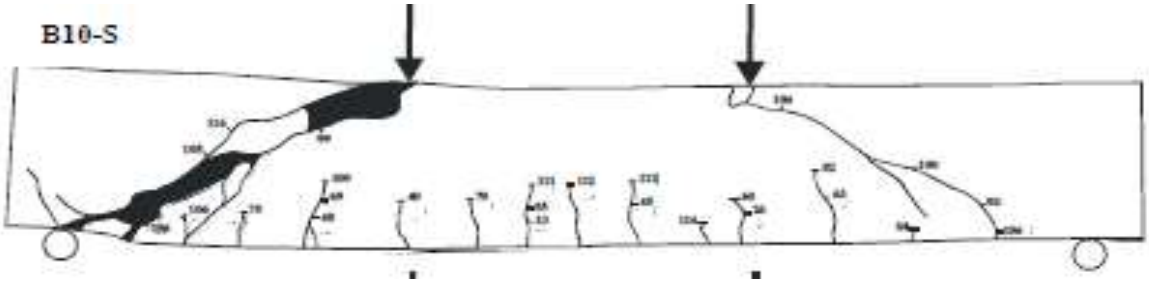

(d) experimental failure

Figure (4.40) Mode of failure of beam with steel stirrups (B10-S)

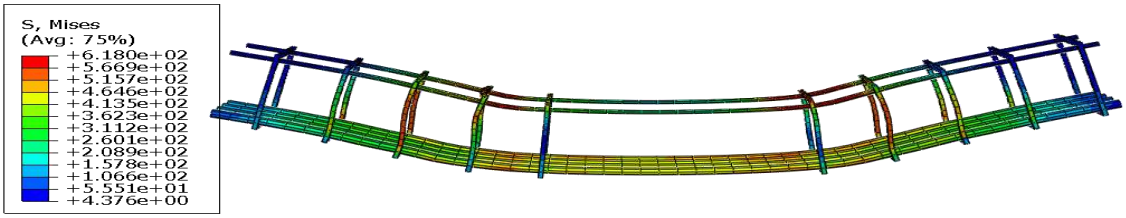

(a) yield of steel stirrups

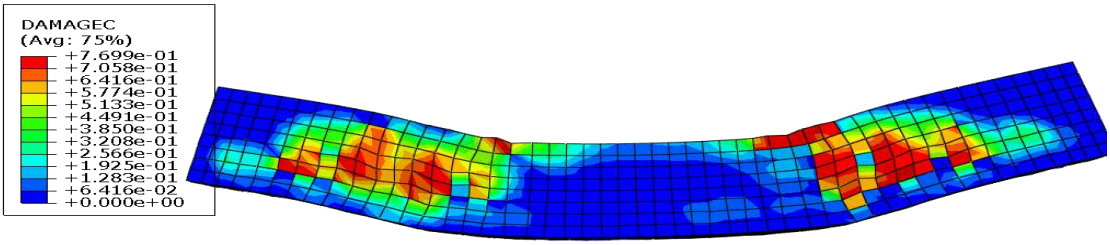

(b) crack in concrete

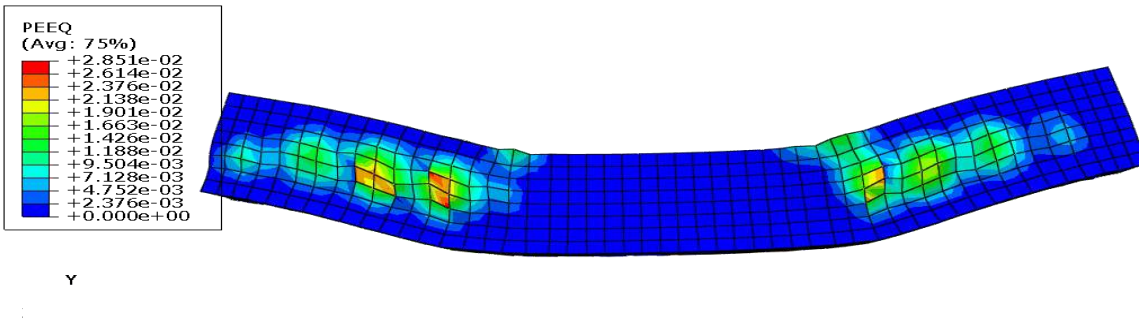

(c) strain in concrete

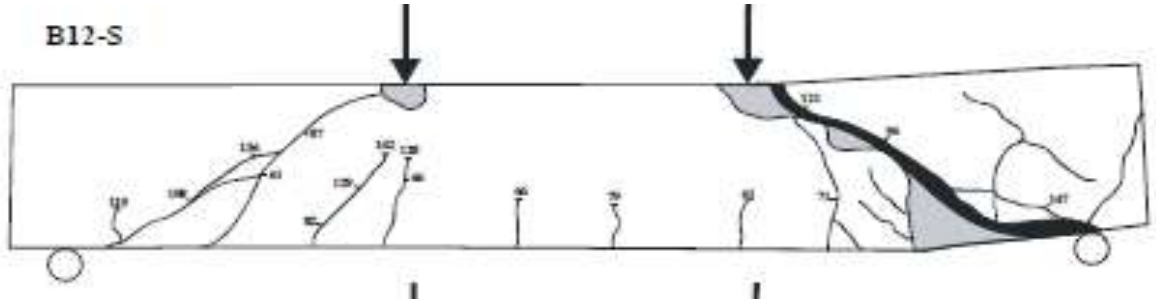

(d) experimental failure

Figure (4.41) Mode of failure of beam with steel stirrups (B12-S)

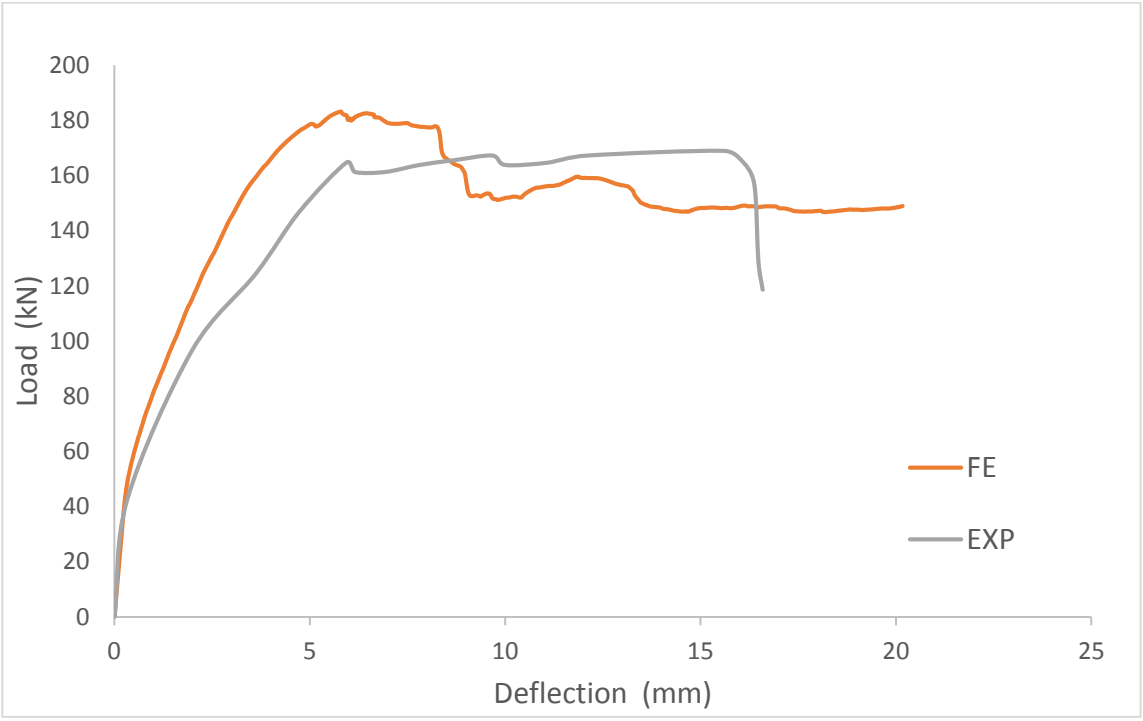

(a) Load-deflection curves of beam with steel stirrups (A10-S)

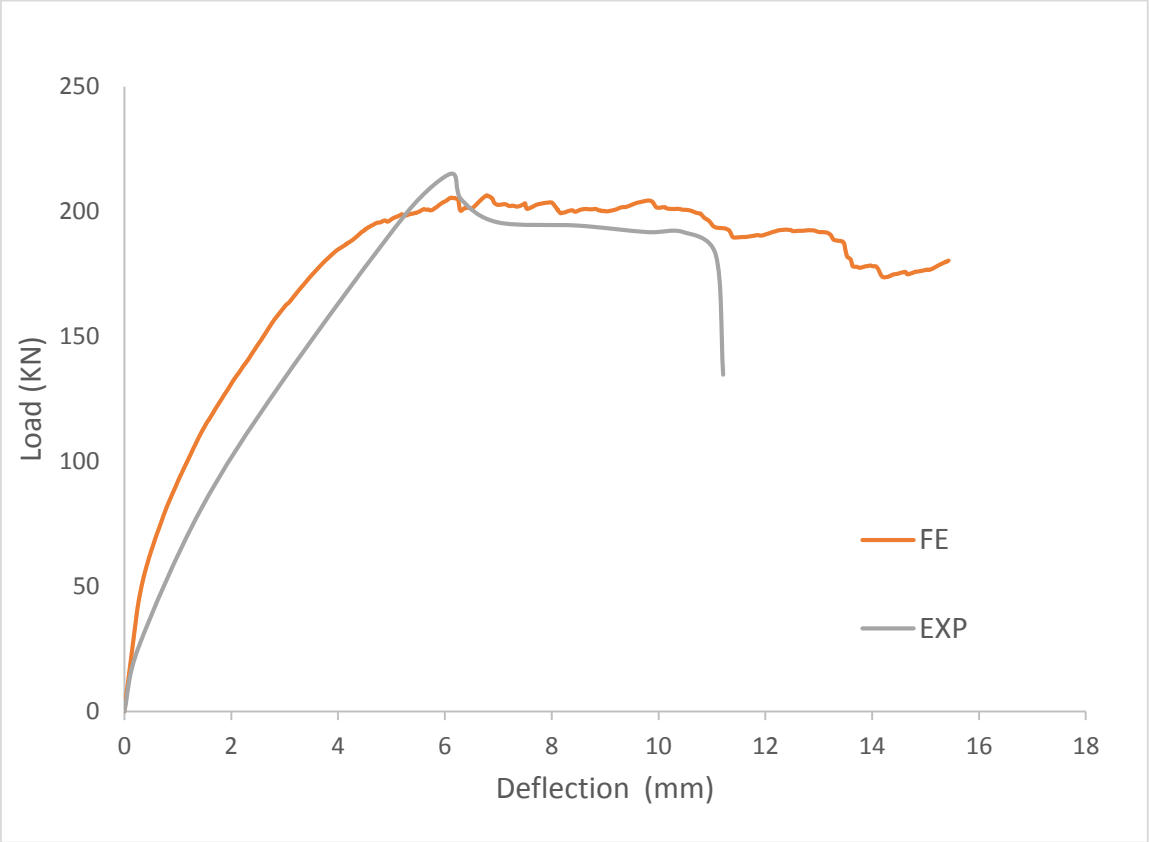

(b) Load-deflection curves of beam with steel stirrups (A12-S)

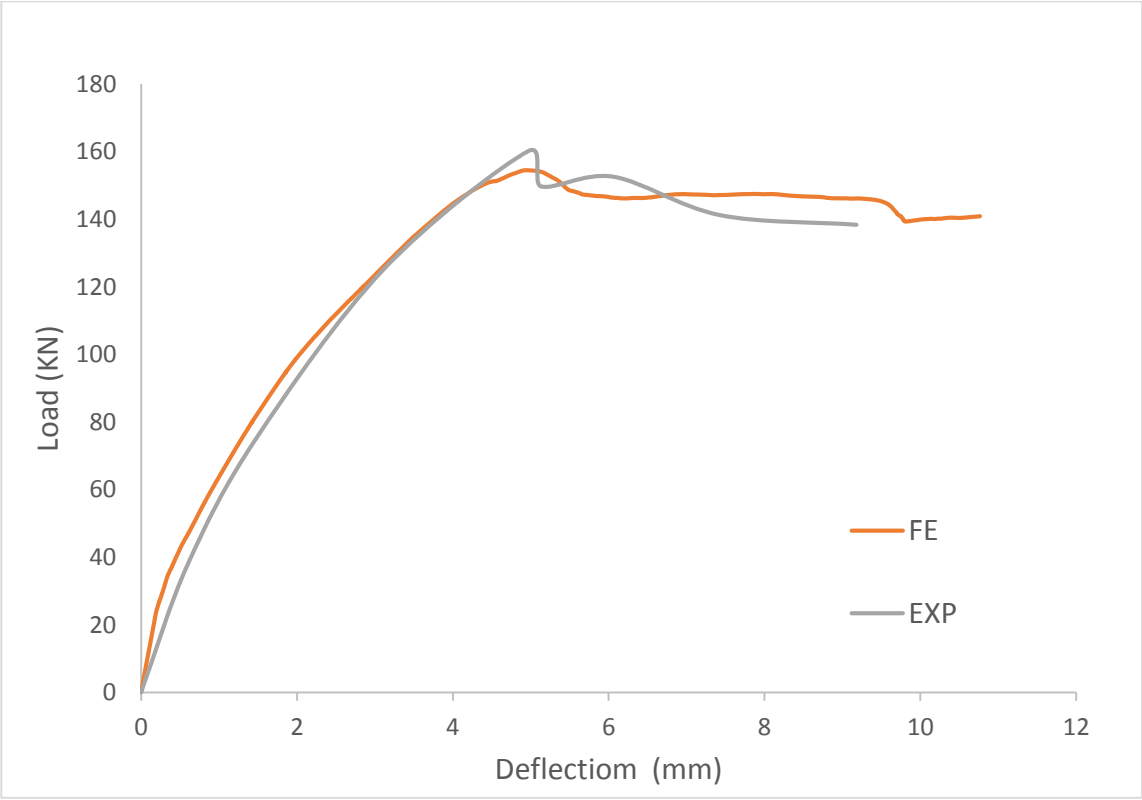

(c) Load-deflection curves of beam with steel stirrups (B12-S)

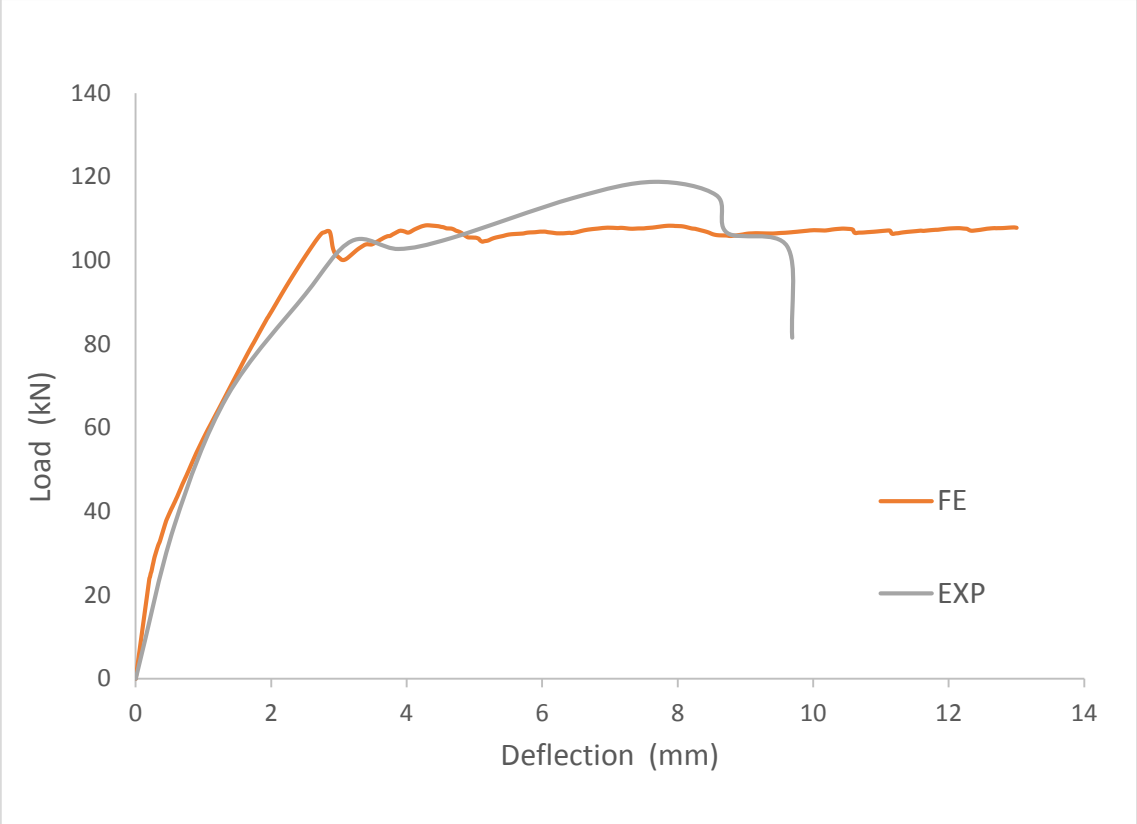

(d) Load-deflection curves of beam with steel stirrups (B10-S)

Figure (4.42) Load-deflection curves of beams with steel stirrups

4.4.2.3 Beams Strengthened with CFRP Sheet A10-M, A12-M, B10-M and B12-M

All beams strengthened by the CFRP sheet using externally bond techniques. The maximum loads of beams A10-M, A12-M, B10-M, and B12-M were 121.7, 166.48, 105.55 and 134.35 kN, respectively. It can be noted from the results of these beams A10-M, A12-M, B10-M and B12-M increase in the maximum load 26.5%, 39%, 43.8%, and 83.1% respectively comparison with that of the un-strengthened beams because of increasing the strength capacity of shear span by CFRP sheet. All beams failed by the formation of a shear crack without yielding of tensile reinforcement. Figs. 4.43, 4.44, 4.45 and 4.46 show the mode of failure of the beams. The crack of shear is started from compression zone to tension zone due to the U configuration of the CFRP sheet. The stresses in the CFRP sheet by FEM different from the experimental

results. Numerically the CFRP sheet did not rupture while it is rupture as shown in experimental results because the difference in the failure mode may be attributed to the assumption of numerically model such as properties of the meterial as well as using identical boundary condition. Table (4.13) and Fig. (4.47) showed that there is a convergence between experimental and numerical results.

Table (4.13) Finite element method and experimental results

Beam designation	Experimental (EXP)	Finite element method (FE)	EXP/FE
	ultimate load (KN)	ultimate load (KN)	
A10-M	122.06	121.7	1.002
A12-M	179.54	166.48	1.07
B10-M	111.14	105.55	1.05
B12-M	143	134.35	1.06

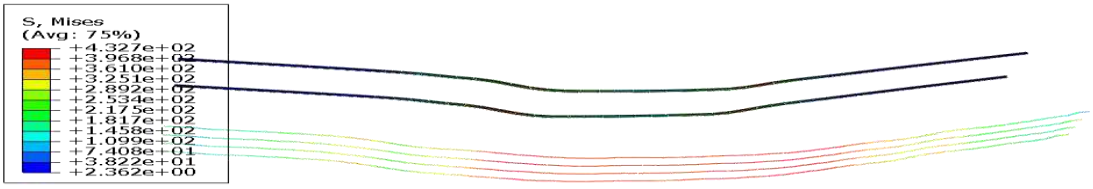

(a) yield of steel bar

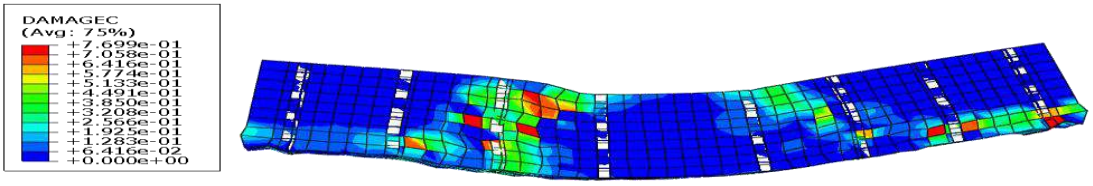

(b) crack in concrete

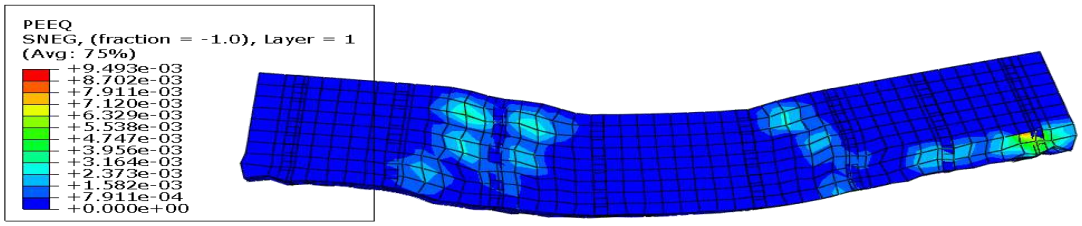

(c) strain in concrete

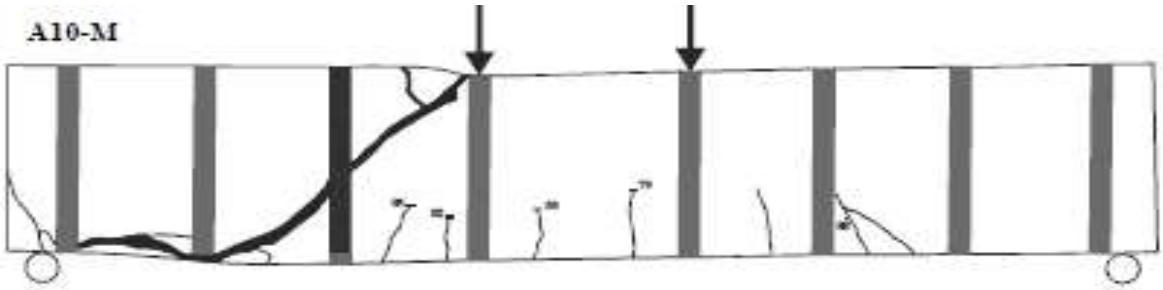

(d) experimental failure.

Figure (4.43) Mode of failure of beams strengthened with CFRP sheet (A10-M)

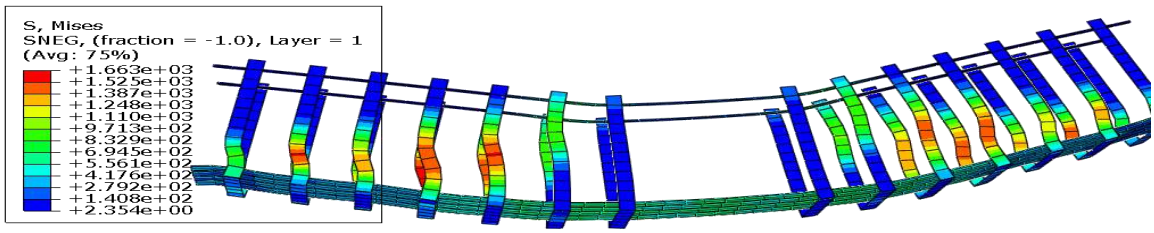

(a) stresses in steel bar and CFRP sheet

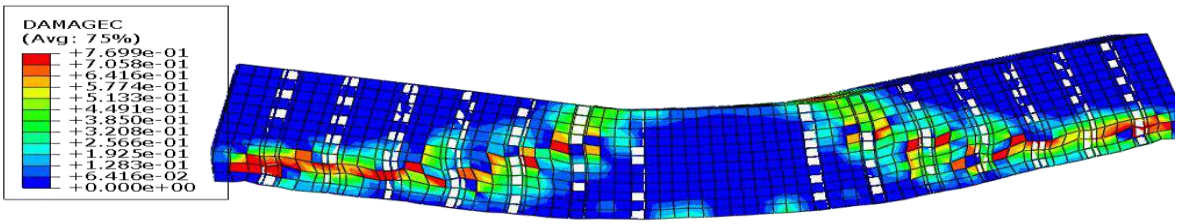

(b) crack in concrete

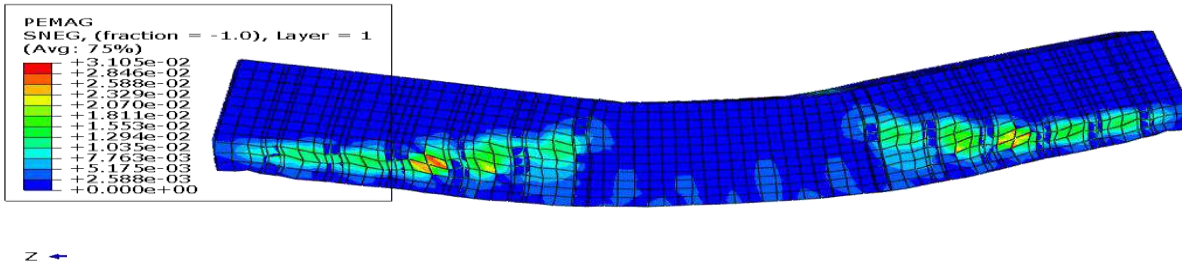

(c) strain in concrete and

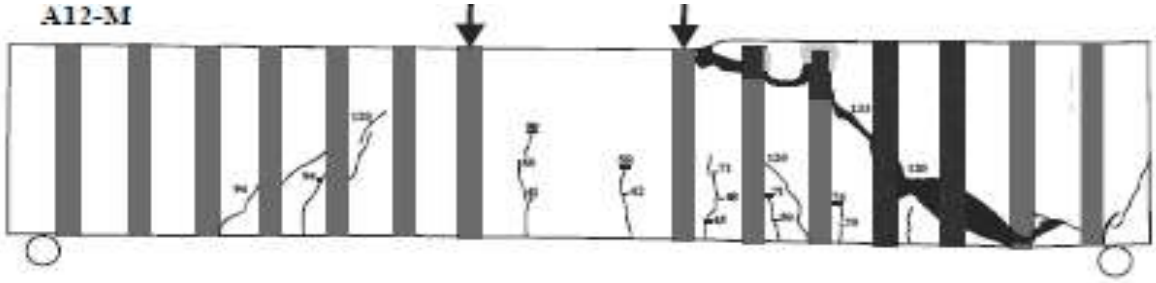

(d) experimental failure

Figure (4.44) Mode of failure of beams strengthened with CFRP sheet (A10-M)

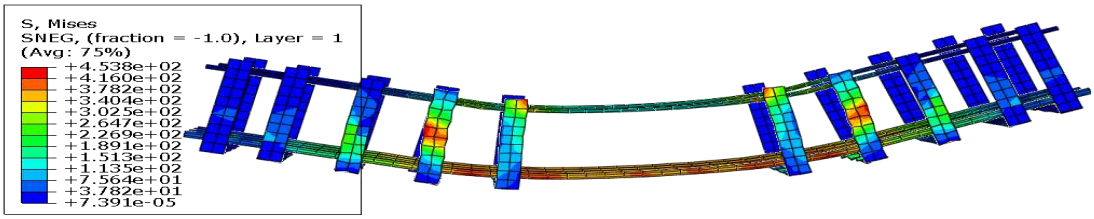

(a) stresses in steel bar and CFRP sheet

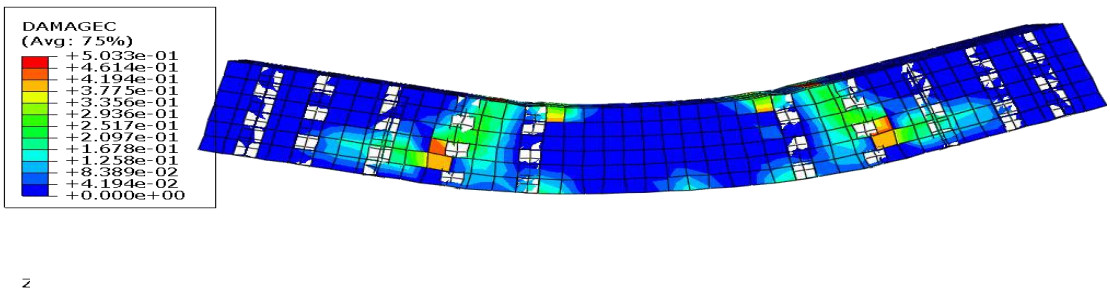

(b) crack in concrete

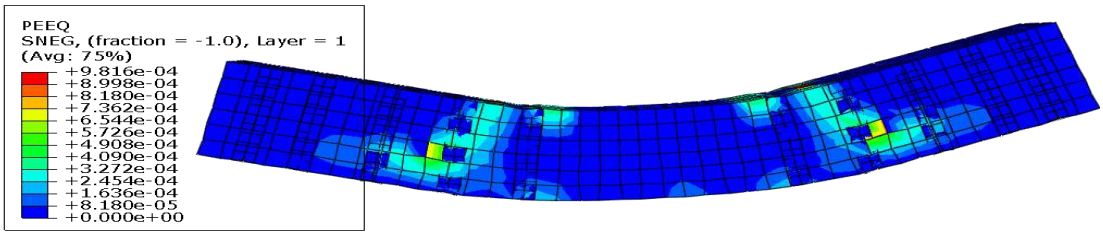

(c) strain in concrete

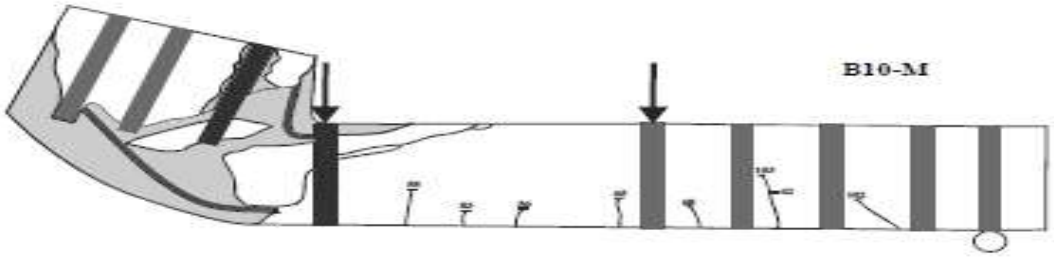

(d) experimental failure

Figure (4.45) Mode of failure of beams strengthened with CFRP sheet (B10-M)

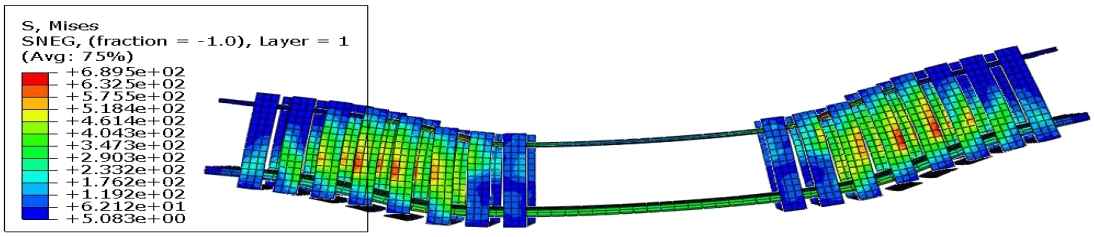

(a) stresses in steel bar and CFRP sheet

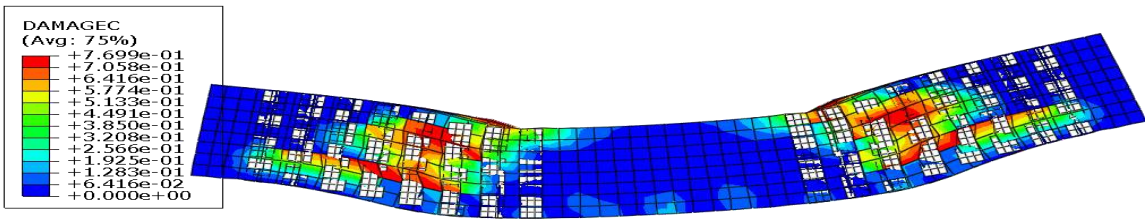

(b) crack in concrete

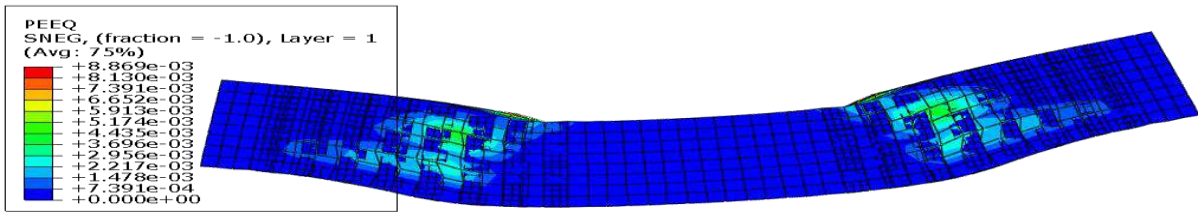

(c) strain in concrete

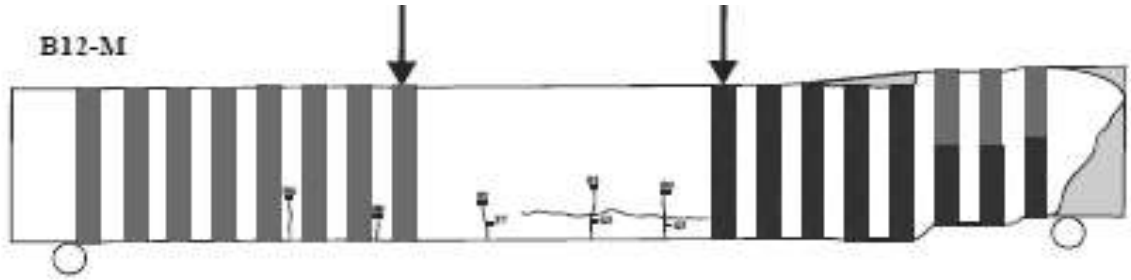

(d) experimental failure

Figure (4.46) Mode of failure of beams strengthened with CFRP sheet (B12-M)

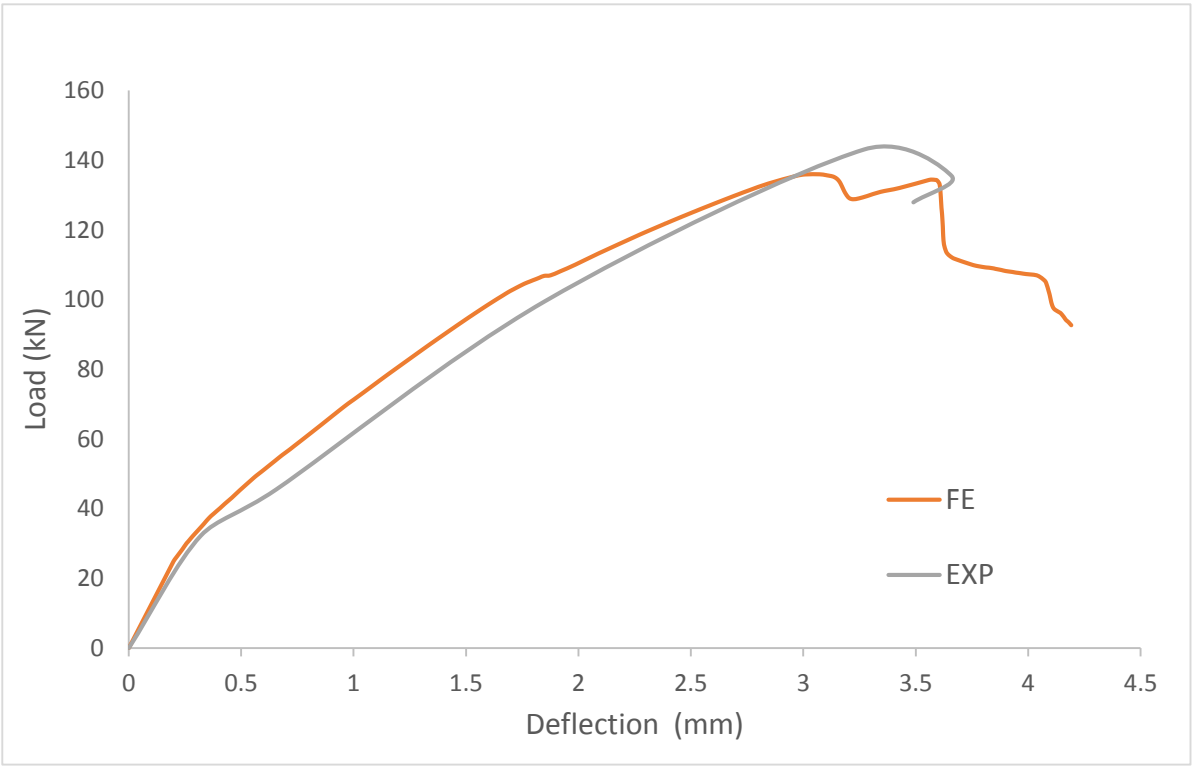

(a) Load-deflection curves of beams strengthened with CFRP sheet (B12-M)

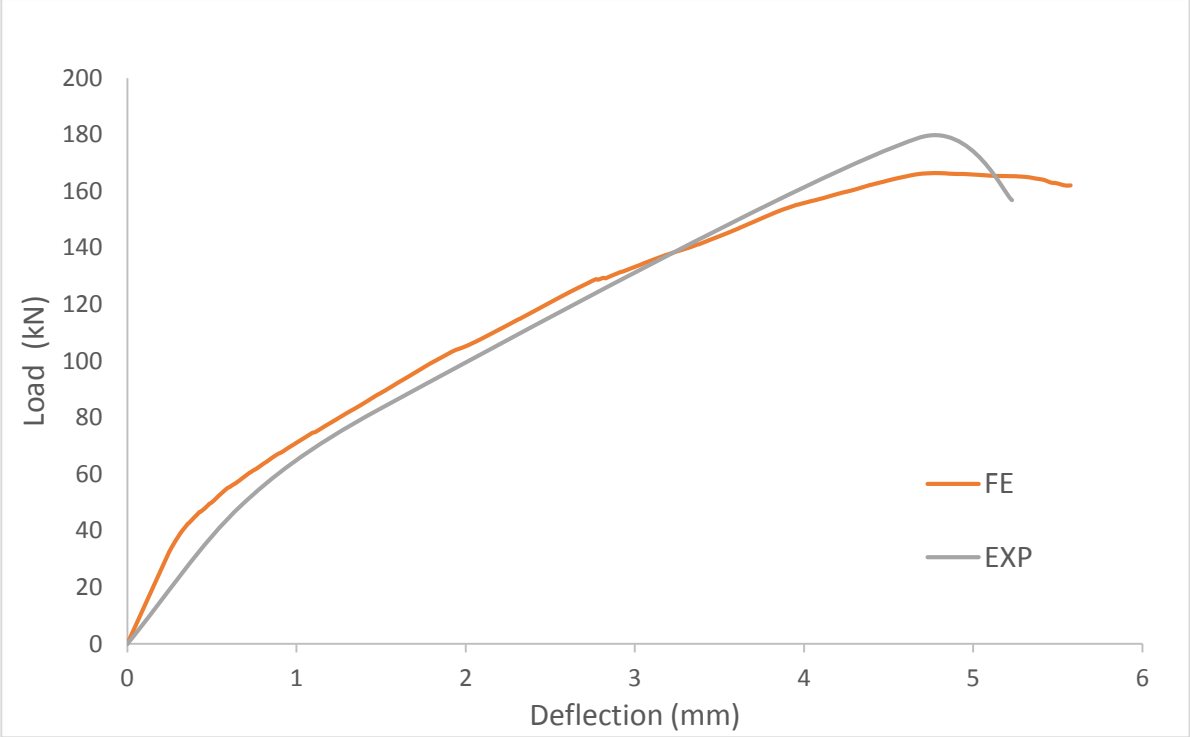

(b) Load-deflection curves of beams strengthened with CFRP sheet (A12-M)

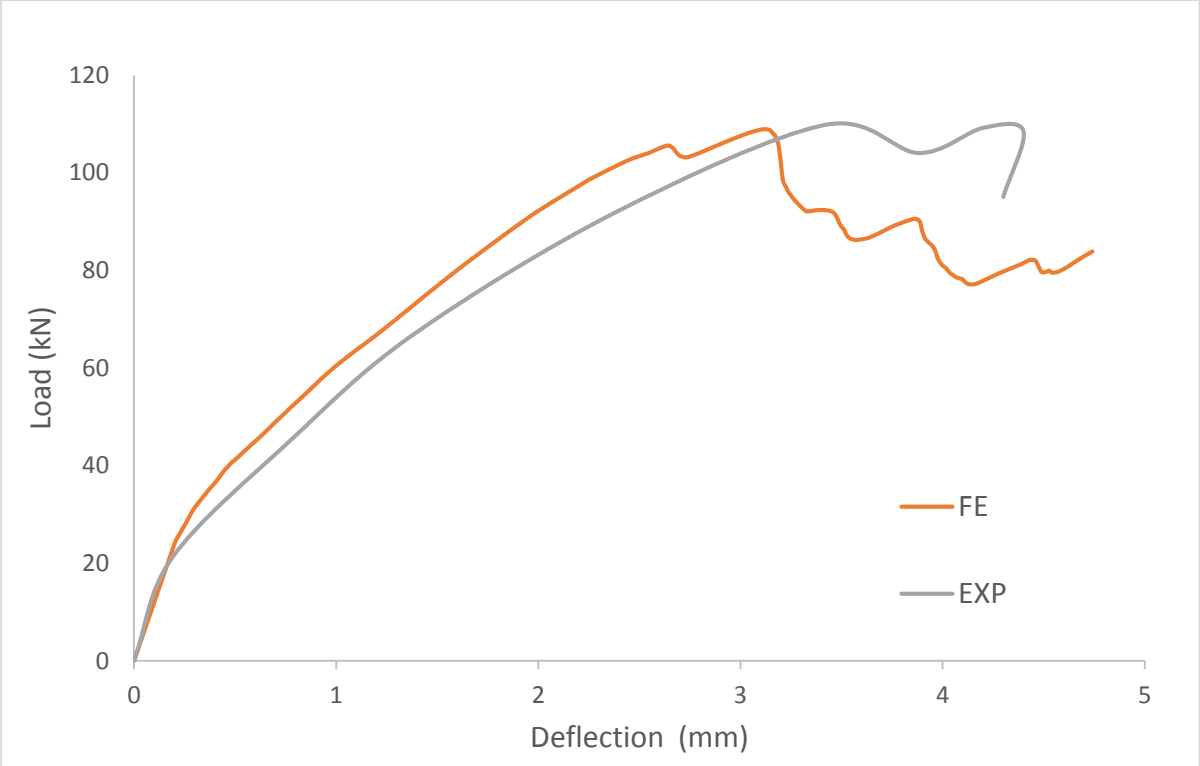

(c) Load-deflection curves of beams strengthened with CFRP sheet (B10-M)

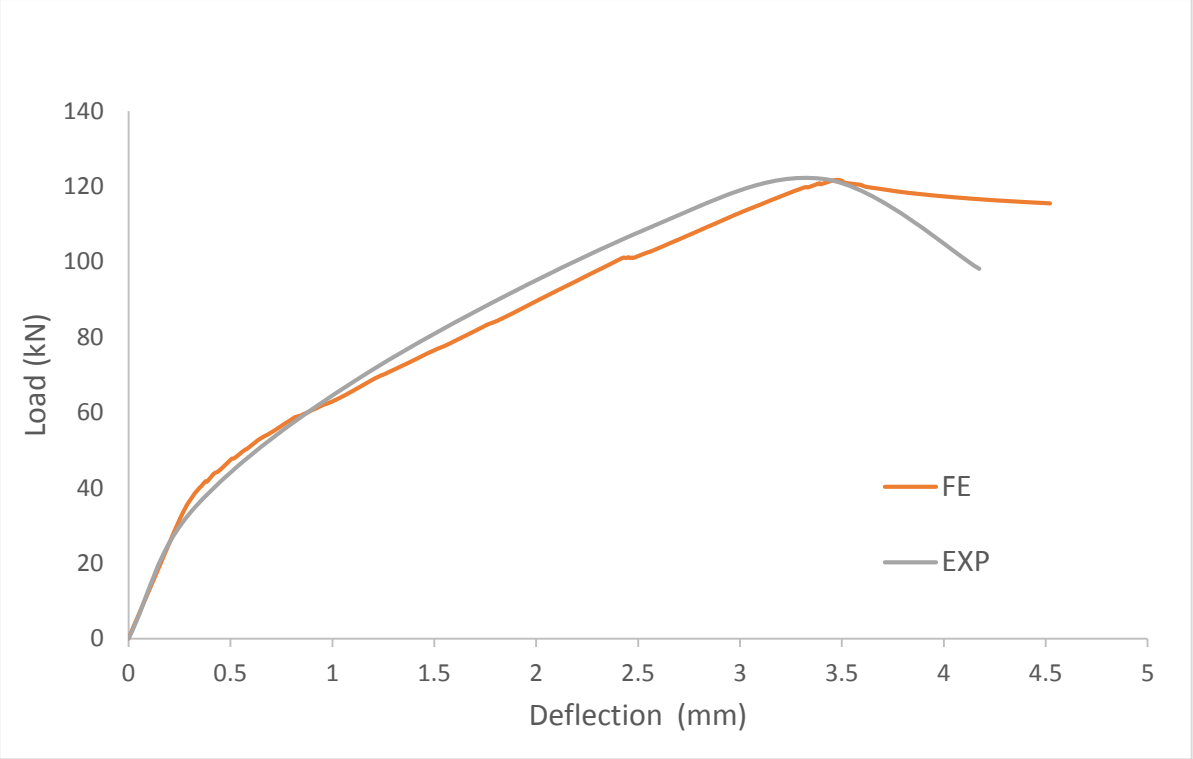

(d) Load-deflection curves of beams strengthened with CFRP sheet (A10-M)

Figure (4.47) Load-deflection curves of beams strengthened with CFRP sheet

4.4.2.4 Beams Strengthened with CFRP Laminate A10-VL, A12-VL, B10-VL and B12-VL

All beams strengthened by CFRP Laminate using near surface mounted (NSM) technique. The maximum loads of A10-VL, A12-VL, B10-VL and B12-VL are 156.4, 225.02, 119.36 and 130.65 KN respectively. It should be noted that the beams A10-VL, A12-VL, B10-VL and B12-VL increase in the maximum load a 62.5%, 87.93%, 62.6% and 78% respectively in comparison with that of the un-strengthened control beam because the applied stress in the shear span resistant by CFRP laminate . In beam A10_VL, the longitudinal tensile reinforcement has yielded and then a shear failure crack has been formed. Beam A12_VL failed in shear crack without yielding of longitudinal tensile reinforcement. The CFRP laminate crossing this crack debonded by its shorter bond length. Mode of failure in beams B10_VL and B12_VL is forming shear crack from load to support without yielding of longitudinal

tensile reinforcement as shown in Figs. (4.48, 4.49, 4.50 and 4.51). The ultimate load beams (A10-S, A12-S, B10-S and B12-S) at failure is higher than beams (A10-M, A12-M, B10-M and B12-M) due to the premature FRP debonding which took place before reaching failure. Table (4.14) and Fig (4.52) show that there is a good agreement between exprimental and numerical results according to maximum load , deflection and mode of failure.

Table (4.14) Finite element method and experimental results

Beam designation	Experimental (EXP)	Finite element method (FE)	EXP/FE
	ultimate load (kN)	ultimate load (kN)	
A10-VL	158.64	156.4	1.01
A12-VL	235.11	225.02	1.04
B10-VL	131.22	119.36	1.10
B12-VL	139.20	130.65	1.06

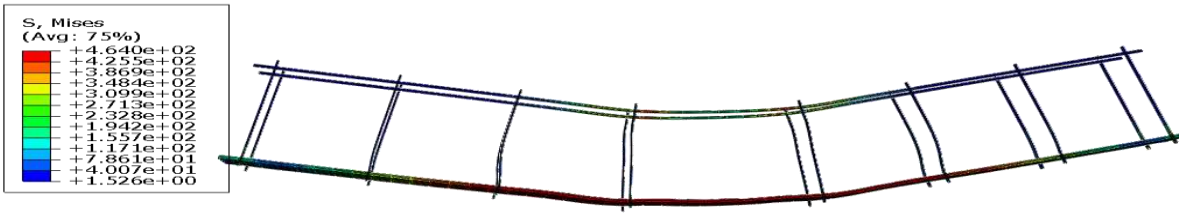

(a) stresses in steel bar and CFRP laminate

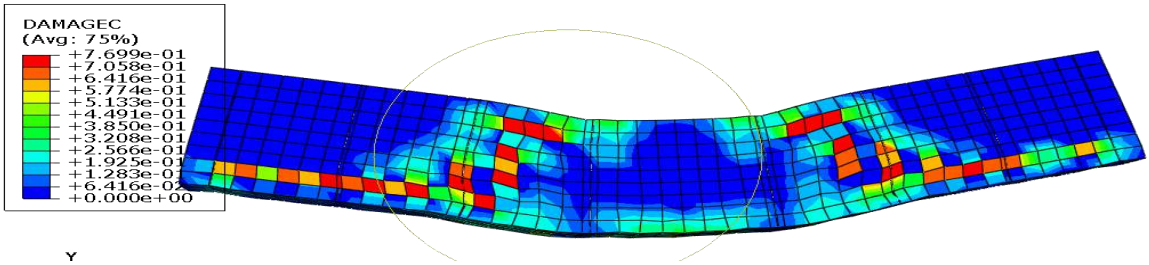

(b) crack in concrete

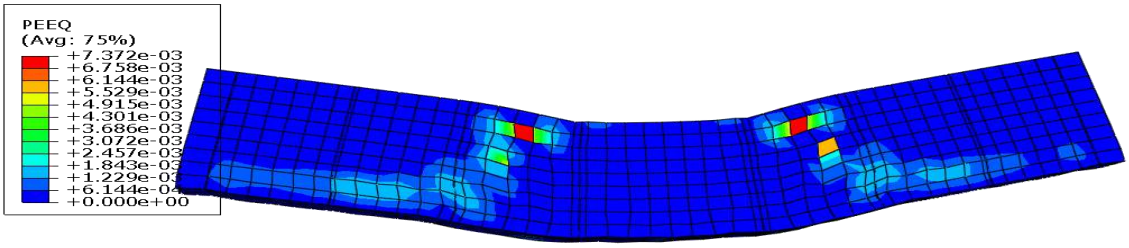

(c) strain in concrete

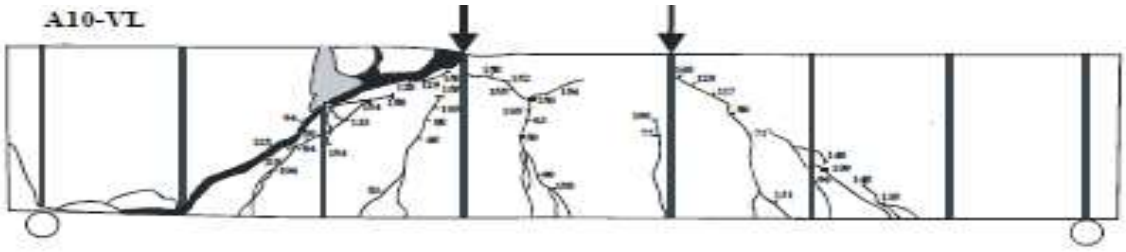

(d) experimental failure

Figure (4.48) Mode of failure of beam strengthened with CFRP vertical laminate (A10-VL)

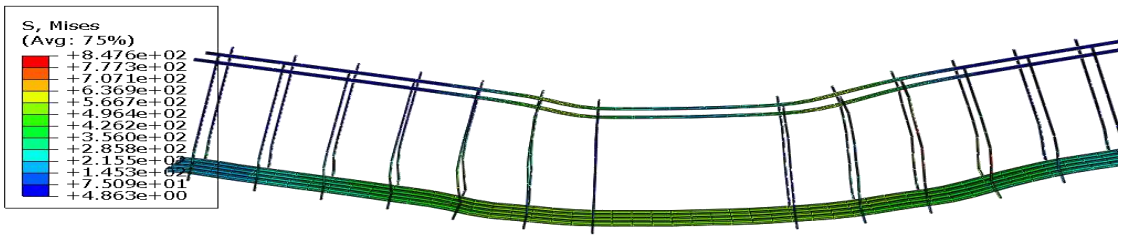

(a) stresses in steel bar and CFRP laminate

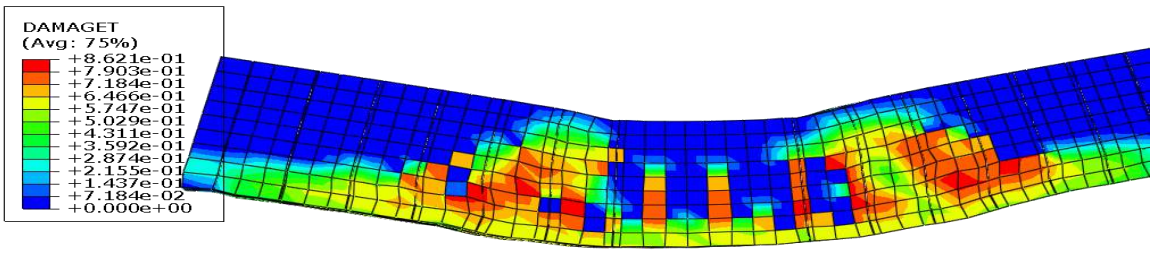

(b) crack in concrete

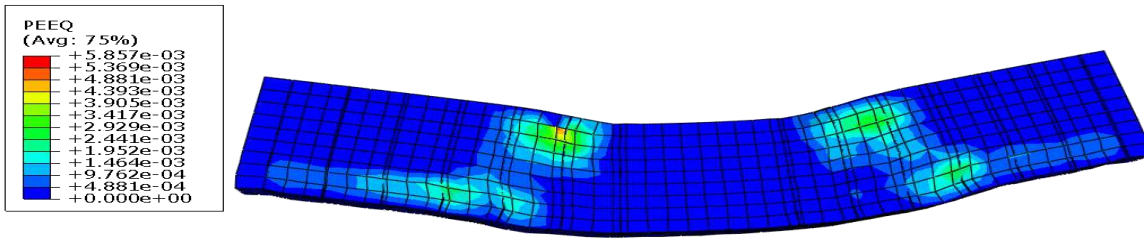

(c) strain in concrete

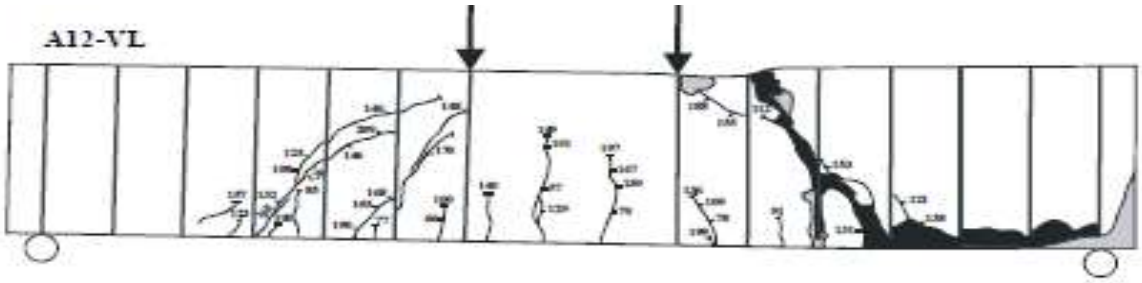

(d) experimental failure

Figure (4.49) Mode of failure of beam strengthened with CFRP vertical laminate (A12-VL)

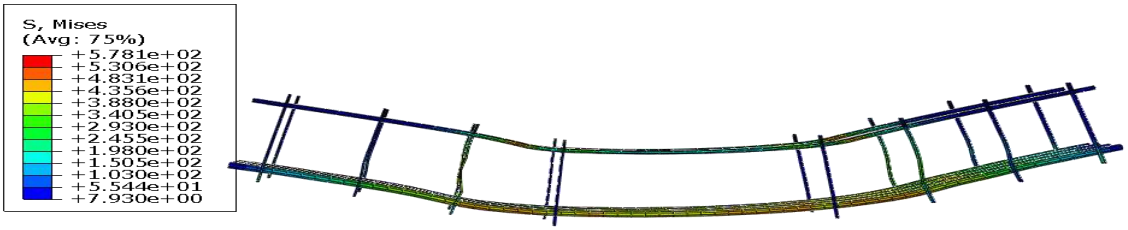

(a) stresses in steel bar and CFRP laminate

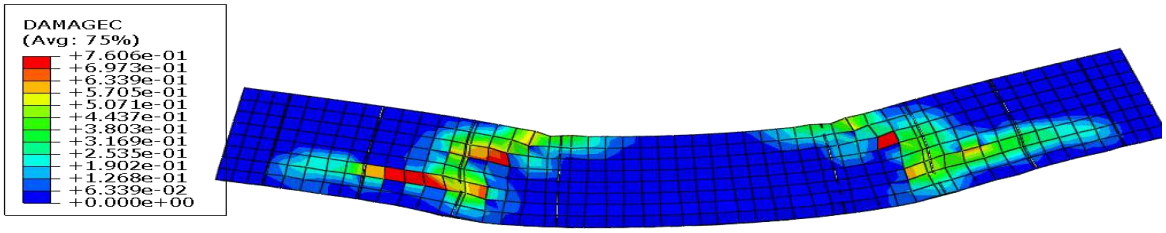

(b) crack in concrete

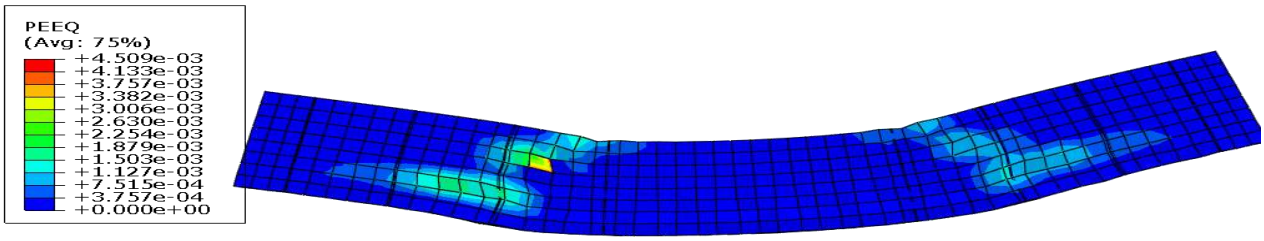

(c) strain in concrete

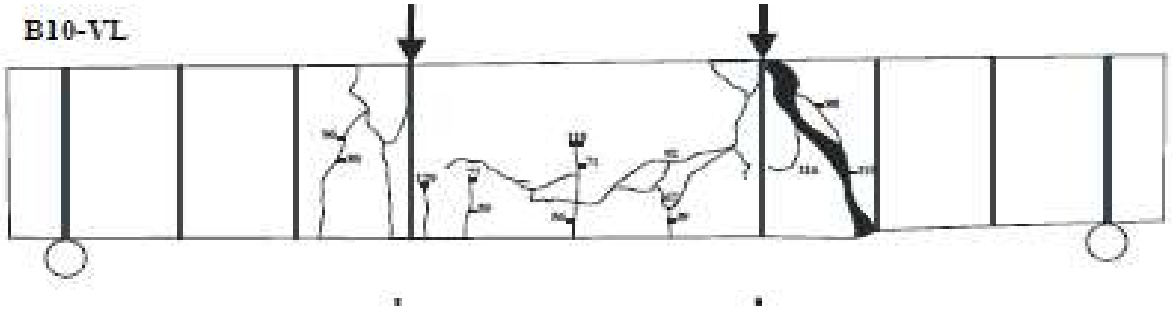

(d) experimental failure

Figure (4.50) Mode of failure of beam strengthened with CFRP vertical laminate (B10-VL)

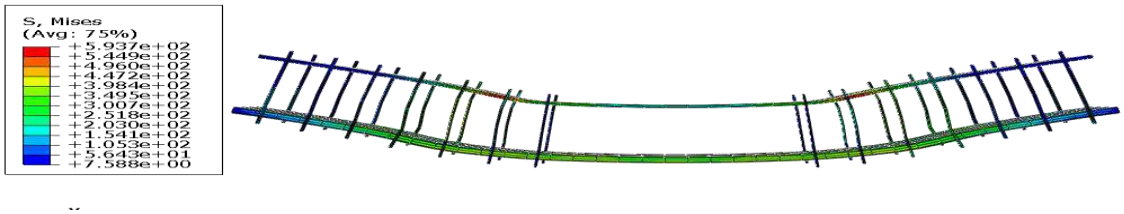

(a) stresses in steel bar and CFRP laminate

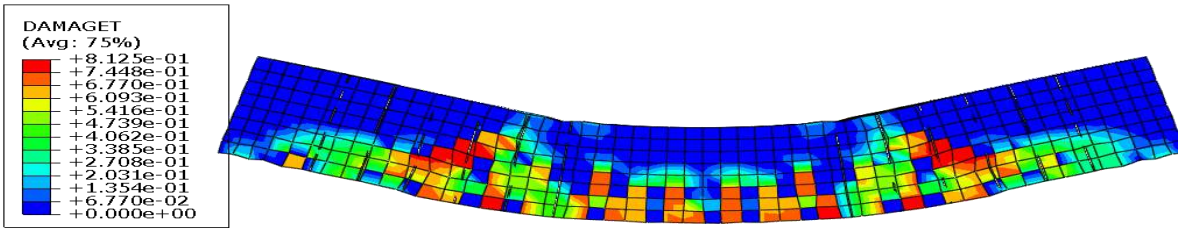

(b) crack in concrete

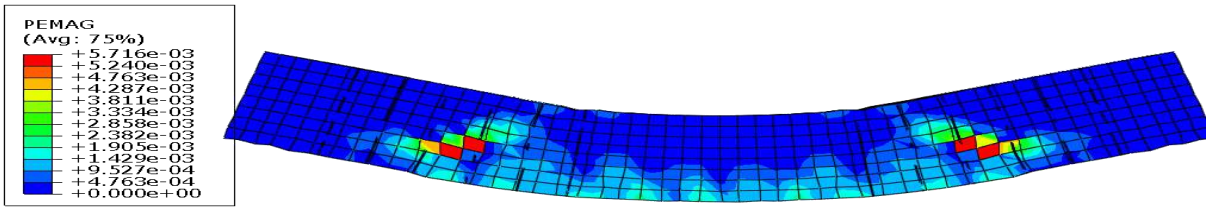

(c) strain in concrete

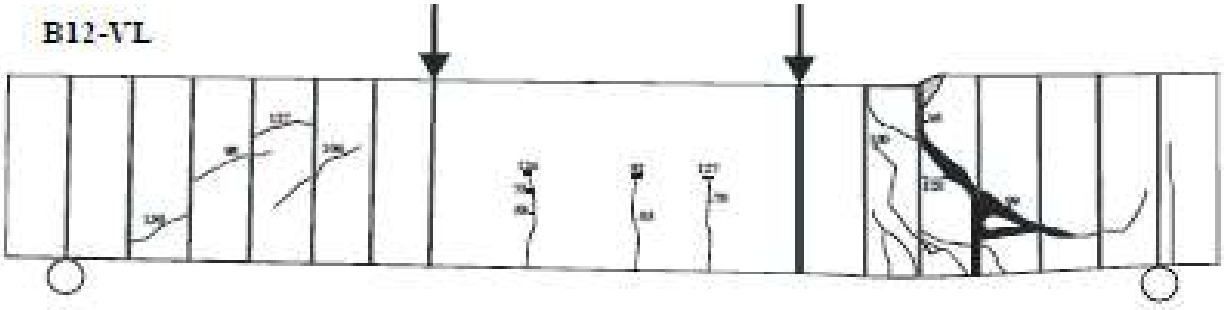

(d) experimental failure

Figure (4.51) Mode of failure of beam strengthened with CFRP vertical laminate (B12-VL)

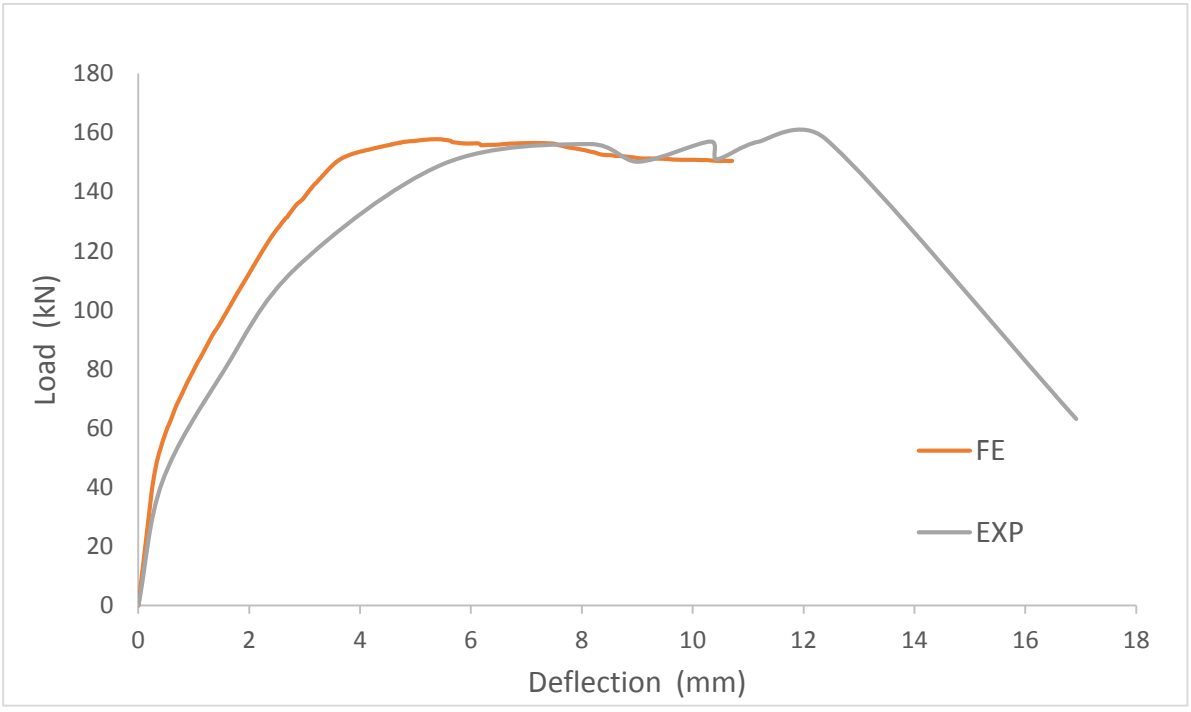

(a) load-deflection curves of beam strengthened with CFRP vertical laminate (A10-VL)

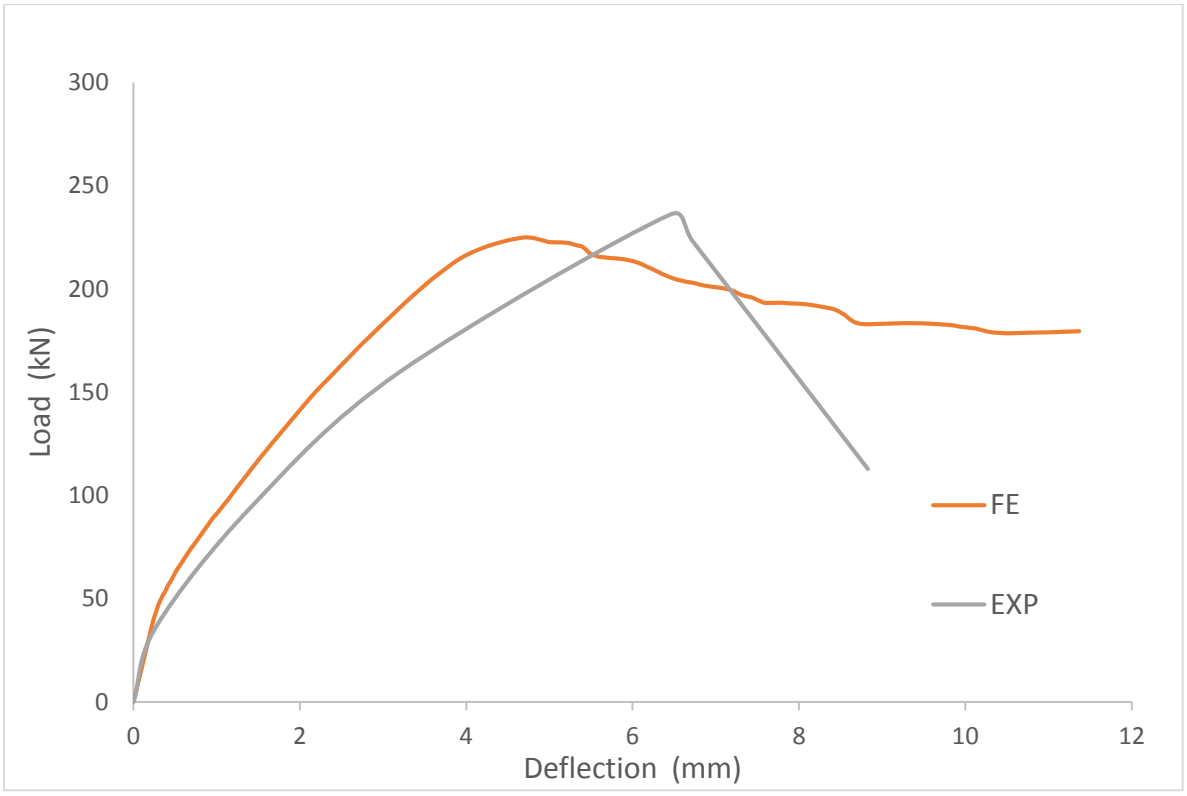

(b) load-deflection curves of beam strengthened with CFRP vertical laminate (A12-VL)

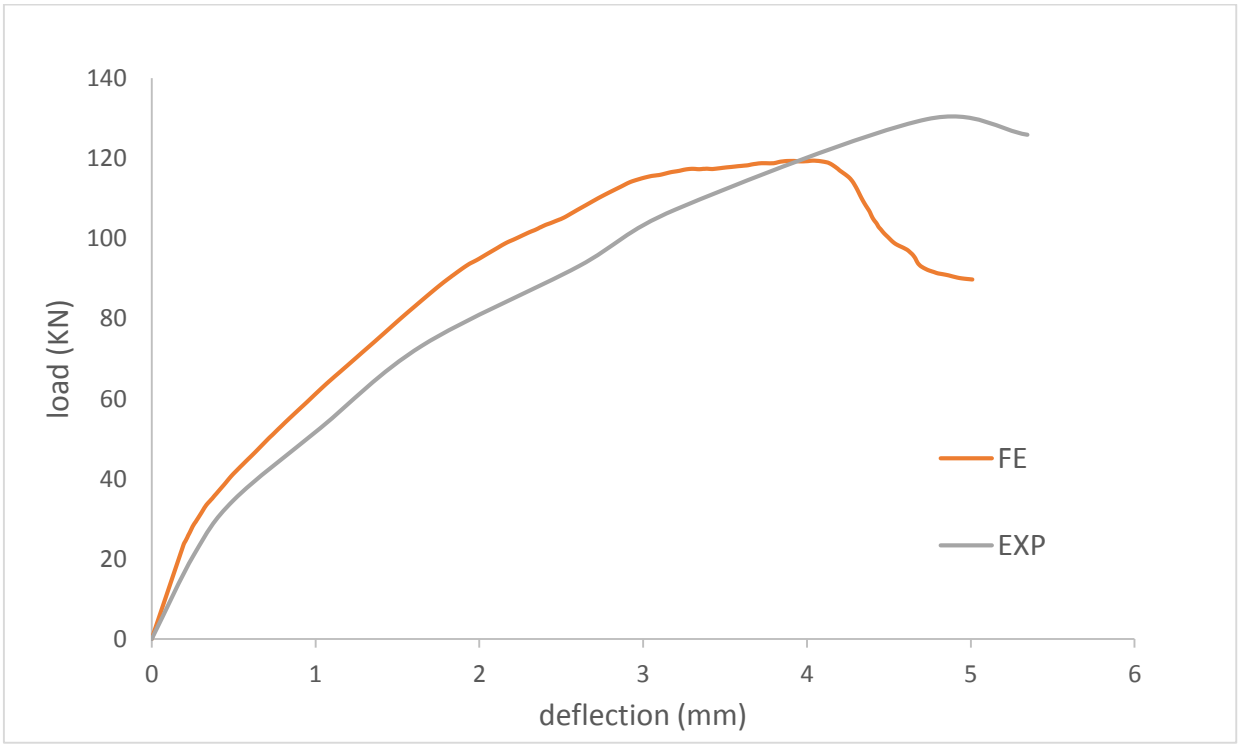

(c) load-deflection curves of beam strengthened with CFRP vertical laminate (B10-VL)

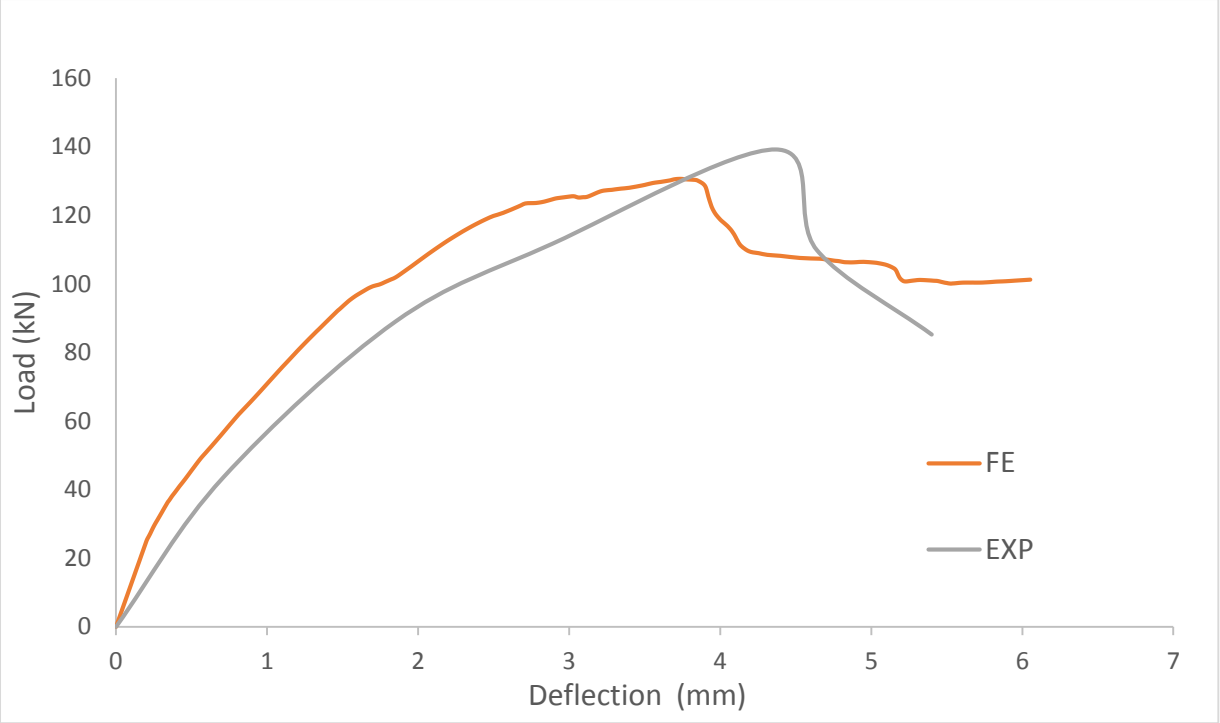

(d) load-deflection curves of beam strengthened with CFRP vertical laminate (B12-VL)

Figure (4.52) Load-deflection curves of beams strengthened with CFRP vertical laminate

4.4.2.5 Beams Strengthened with CFRP Inclined Laminate A10-IL, A12-IL, B10-IL and B12-IL

The maximum load of beams strengthened by an inclined laminate of CFRP using near surface mounted technique (A10-IL, A12-IL, B10-IL, and B12-IL) are 165.39, 237.60, 128.85 and 155.32 kN respectively. The strengthened beams (A10-VL, A12-VL, B10-VL, and B12-VL) increase in the maximum load a 72%, 98.4%, 75.5%, and 111.7% respectively comparison with control beam. Beams (A10_IL and A12_IL) failed by the formation of a flexural failure cracks as showing in Figs. (4.53 and 4.54). The midspan deflection drops gradually after longitudinal tensile reinforcement yielded. Mode of failure of B10_IL, B12_IL beams is forming shear cracks from load to support as shown in Figs. (4.55 and 4.56) without yielding of the longitudinal tensile reinforcement. The ultimate load beams (A10-IL, A12-IL, B10-IL and B12-IL) at failure is higher

than beams (A10-VL, A12-VL, B10-VL and B12-VL). It can be concluded from the Table (4.15) and Fig. (4.57) that there is good agreement between experimental and numerical results.

Table (4.16) shows the percentage increase in the capacity of the strength of RC beams strengthened with CFRP compare with refrenced beams for shear.

Table (4.15) Finite element method and experimental results

Beam designation	Experimental (EXP)	Finite element method (FE)	EXP/FE
	ultimate load (kN)	ultimate load (kN)	
A10-IL	157.90	165.39	0.95
A12-IL	262.38	237.60	1.10
B10-IL	120.44	128.85	0.93
B12-IL	148.50	155.32	0.95

Table (4.16) Increase ratio of RC beams strengthened with CFRP for shear

series beam	control Max Load (KN)	NSM-VL Max load (KN)	Ratio NSM -VL %	NSM-IL Max load (KN)	Ratio NSM -IL %	EXT-M Max load (KN)	Ratio EXT -M %	Stirrups (S) Max Load (KN)	Ratio S %
A10	96.2	156.4	62.5	165.39	72	121.7	26.5	183.12	90.3
A12	119	225.02	87.93	237.6	98.4	166.48	39	205.50	71.3
B10	73.39	11936	62.6	128.85	75.5	105.55	43.8	107.69	46.7
B12	73.36	130.65	78	155.32	111.7	134.35	83.1	154.30	110.3

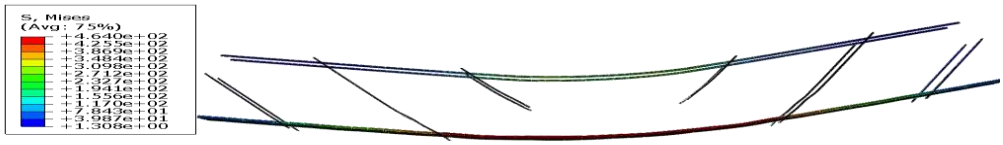

(a) stresses in steel bar and CFRP laminate

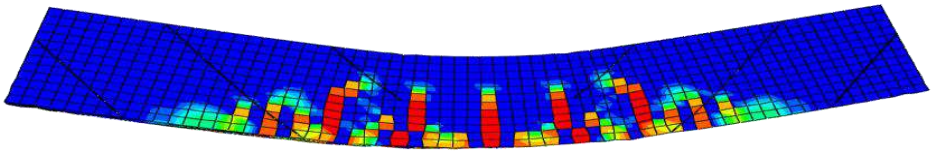

(b) crack in concrete

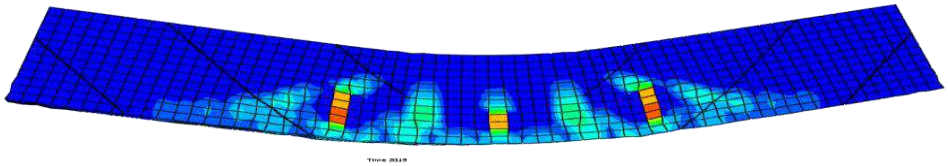

(c) strain in concrete

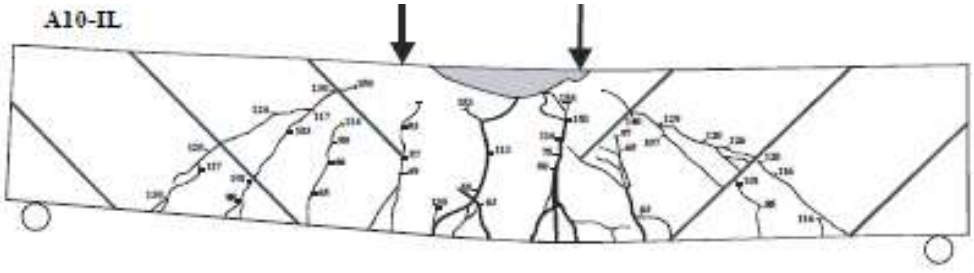

(d) experimental failure

Figure (4.53) Mode of failure of beam strengthened with CFRP inclined laminate (A12-IL)

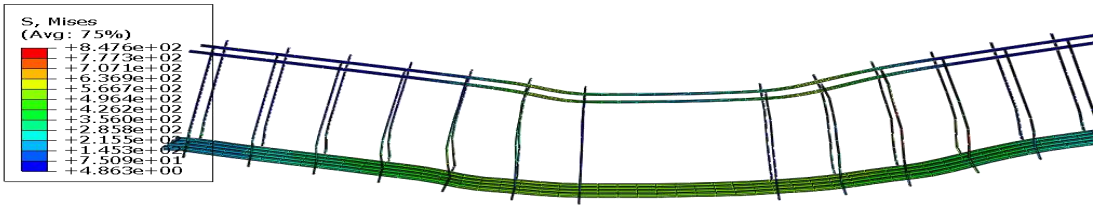

(a) stresses in steel bar and CFRP laminate

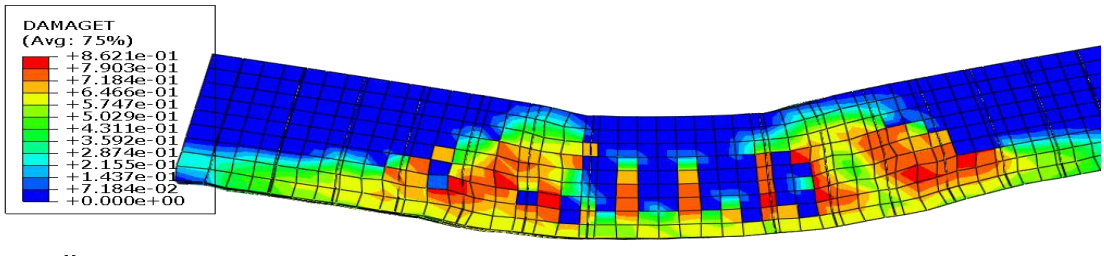

(b) crack in concrete

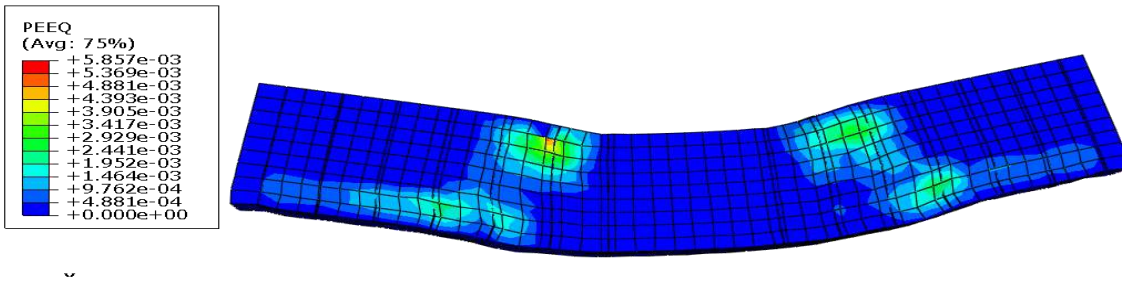

(c) strain in concrete

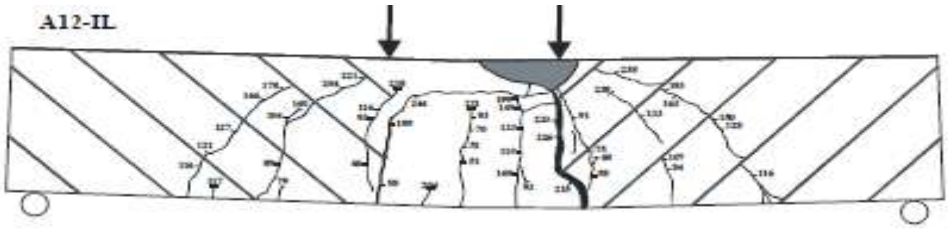

(d) experimental failure

Figure (4.54) Mode of failure of beam strengthened with CFRP inclined laminate (A12-IL)

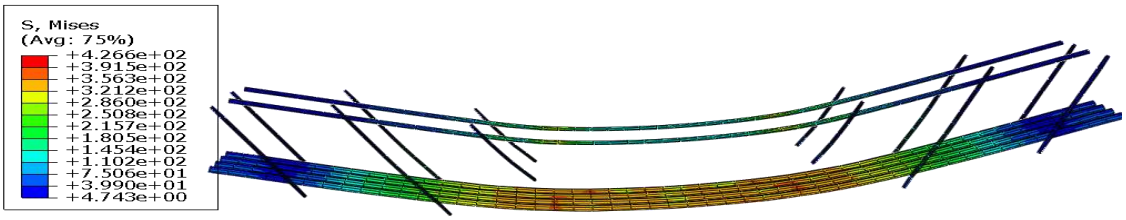

(a) stresses in steel bar and CFRP laminate

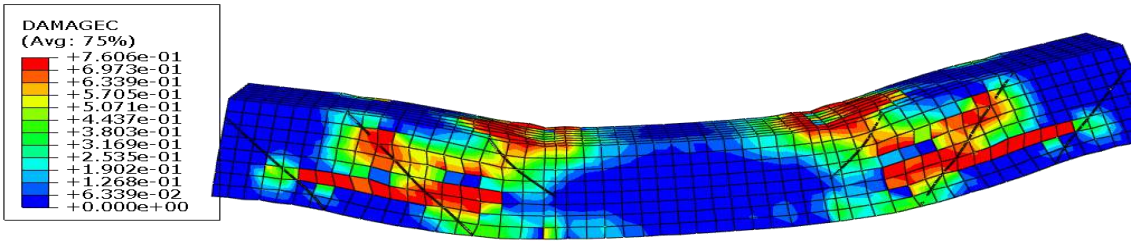

(b) crack in concrete

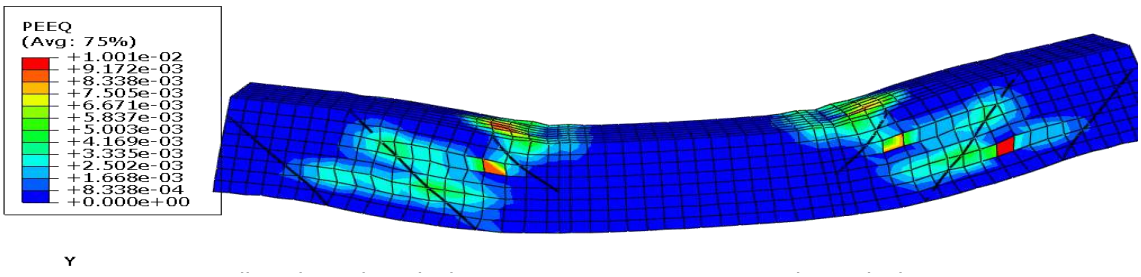

(c) strain in concrete

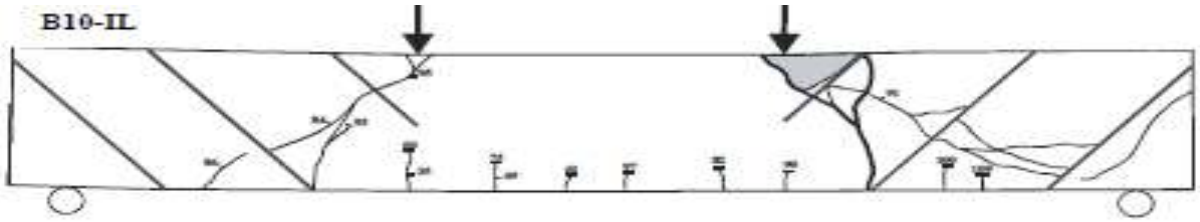

(d) experimental failure

Figure (4.55) Mode of failure of beam strengthened with CFRP inclined laminate (B10-IL) .

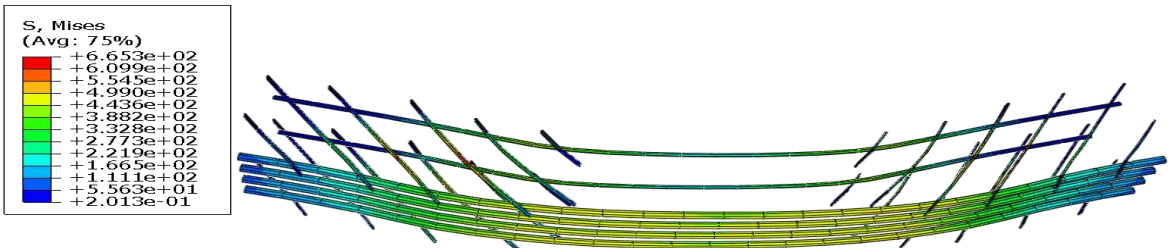

(a) stresses in steel bar and CFRP laminate

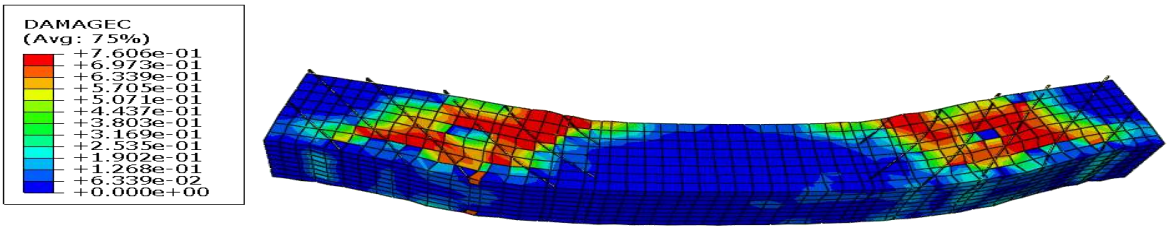

(b) crack in concrete

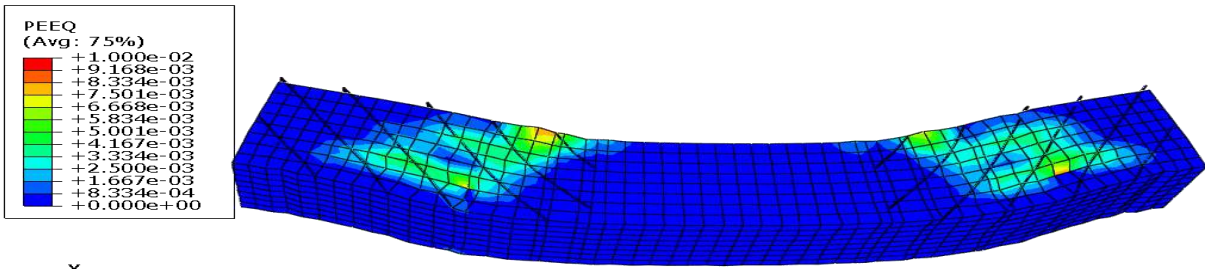

(c) strain in concrete

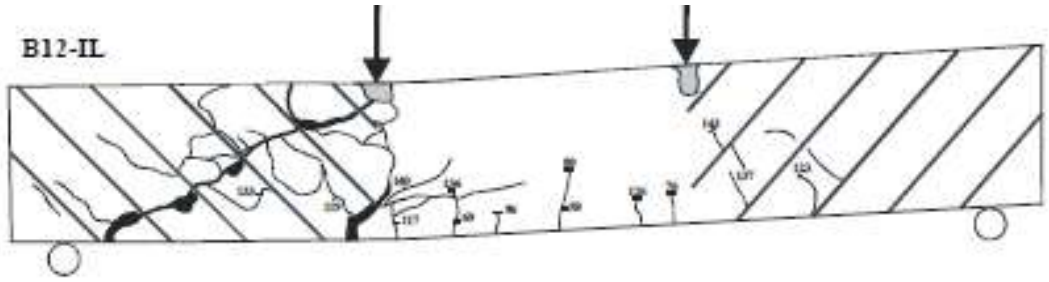

(d) experimental failure

Figure (4.56) Mode of failure of beam strengthened with CFRP inclined laminate (B12-IL)

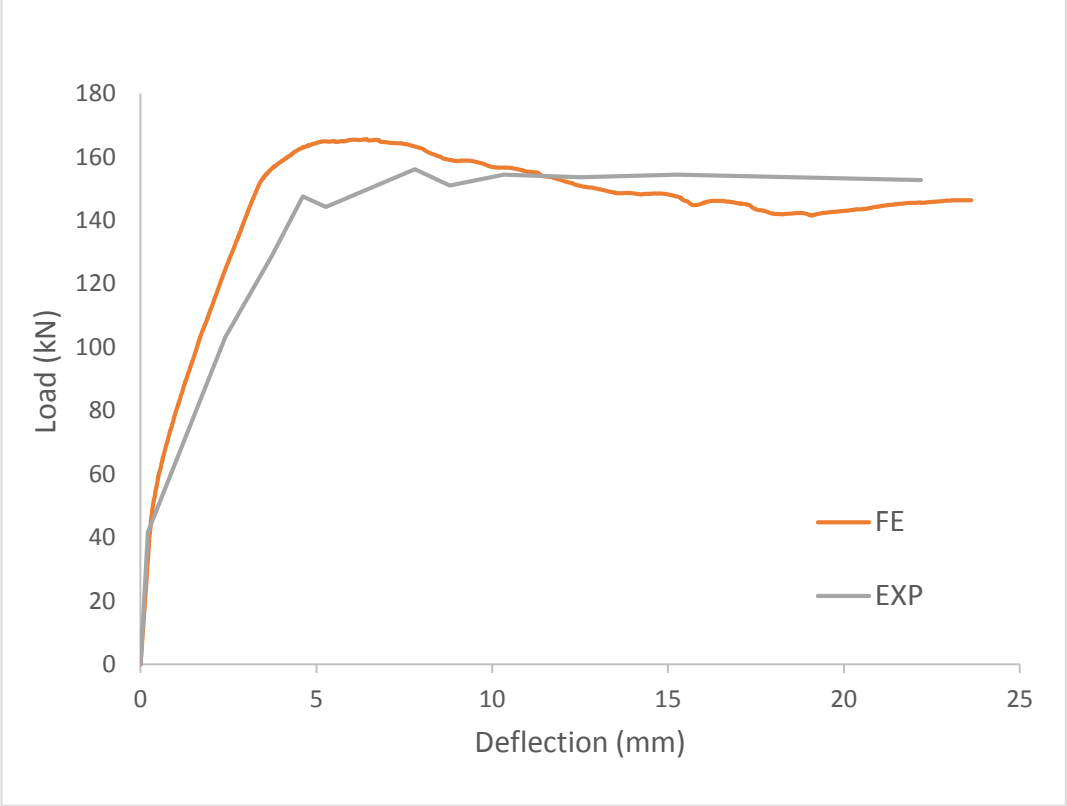

(a) Load-deflection curve of beam strengthened with CFRP inclined laminate (A10-VL)

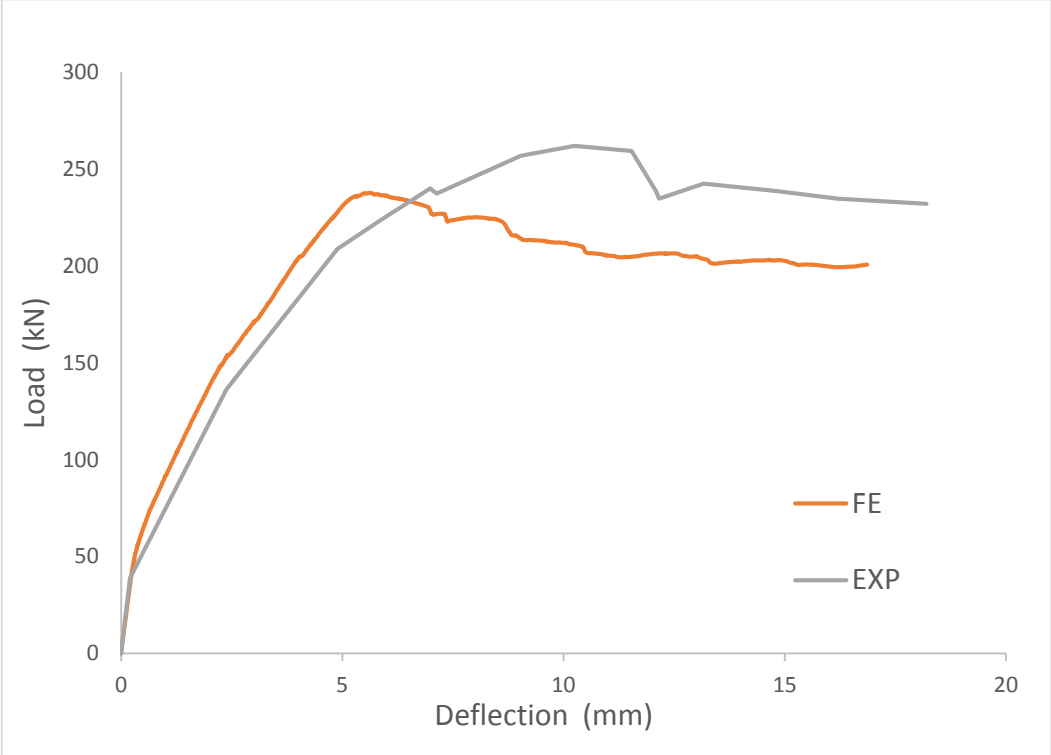

(b) Load-deflection curve of beam strengthened with CFRP inclined laminate (A12-VL)

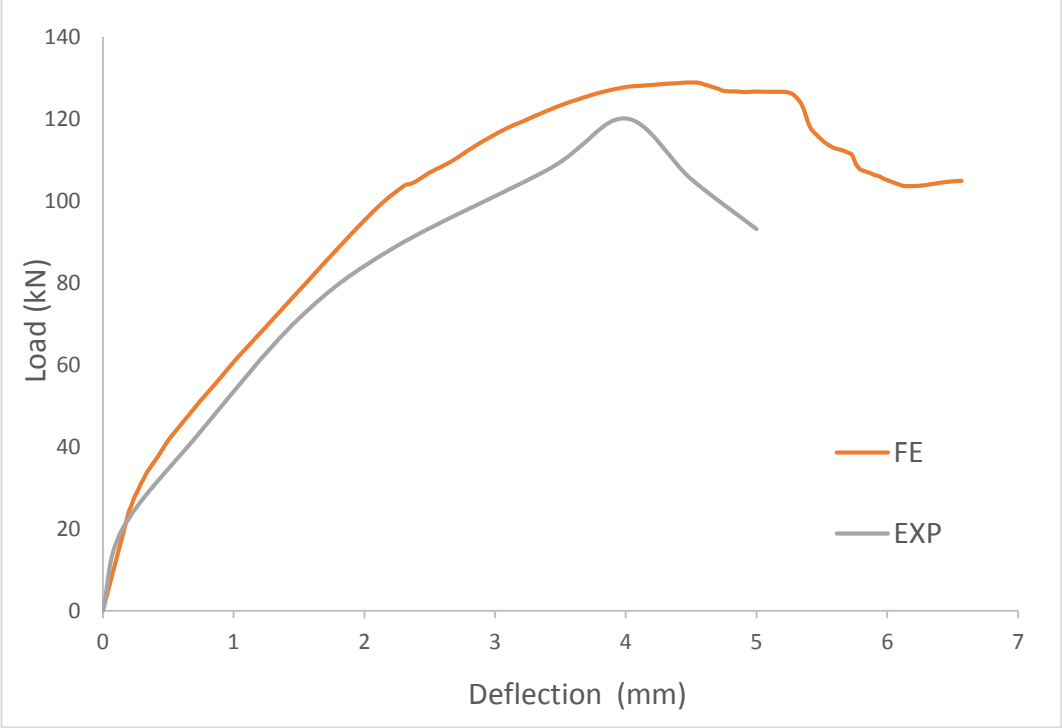

(c) Load-deflection curve of beam strengthened with CFRP inclined laminate (B10-VL)

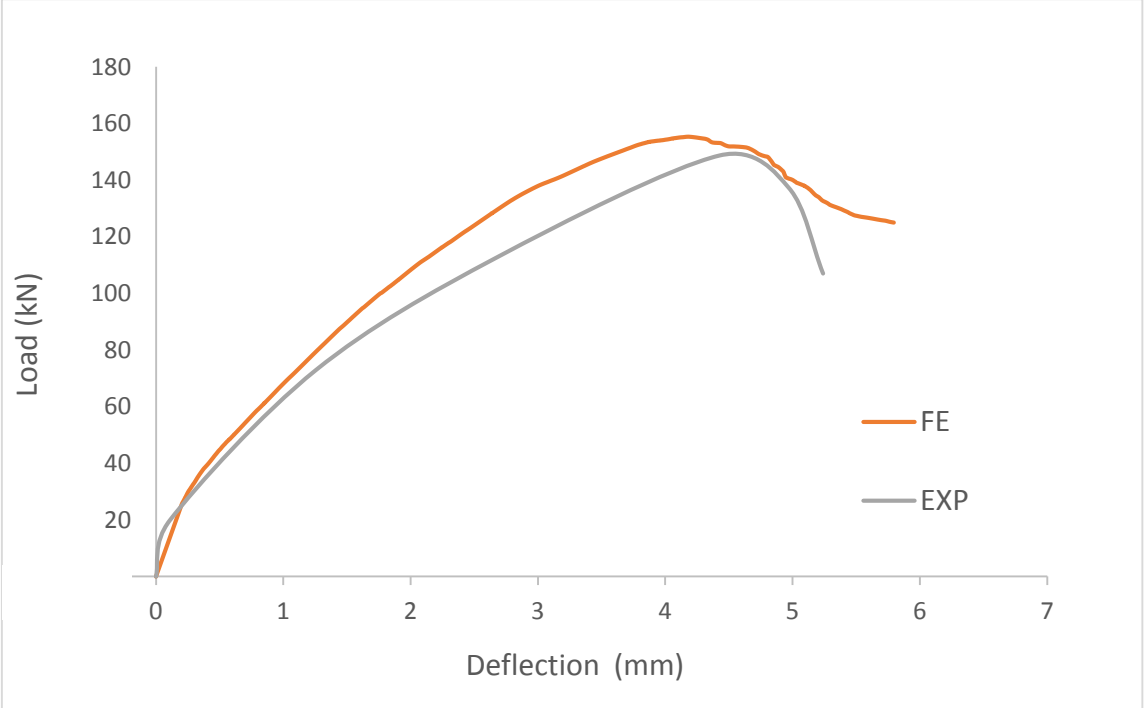

(d) Load-deflection curve of beam strengthened with CFRP inclined laminate (B12-VL)

Figure (4.57) Load-deflection curve of beam strengthened with CFRP inclined laminate

4.4.3 Parametric Study in Shear

4.4.3.1 Effect of Compressive Strength of Concrete

A parametric study is carried out to evaluate the effects of compressive strength of concrete on the shear capacity strengthened RC beams. Twelve beams are analyzed numerically by considering three different values of compressive strength of concrete which are 40, 56, and 65 MPa to investigate this parameter in this study. Figs. 4.58(a) to 4.58(d) show the effect of the concrete strength on load-deflection curves for control and strengthened beams with CFRP. All figures indicated that the ultimate load increased whenever increased compressive strength for concrete due to increase the strength of concrete for shear (V_c). Fig. (4.59) show the relationship between ultimate load and compression strength of concrete. Also, It is observed from FE analysis that as the compressive strength of concrete increased the stresses in CFRP sheet or laminite have been increased. Beams B10-S failed by yielding longitudinal tensile reinforcement when f_c' equal to 65 MPa while the B10-S beam did not yield when f_c' equal to 40 and 56.2 MPa. Beam B10-M failed by ruptured of CFRP sheet when compressive strength equal to 65 MPa while it failed by forming shear crack without rupturing of CFRP when f_c' equal to 40 and 56.2 MPa.

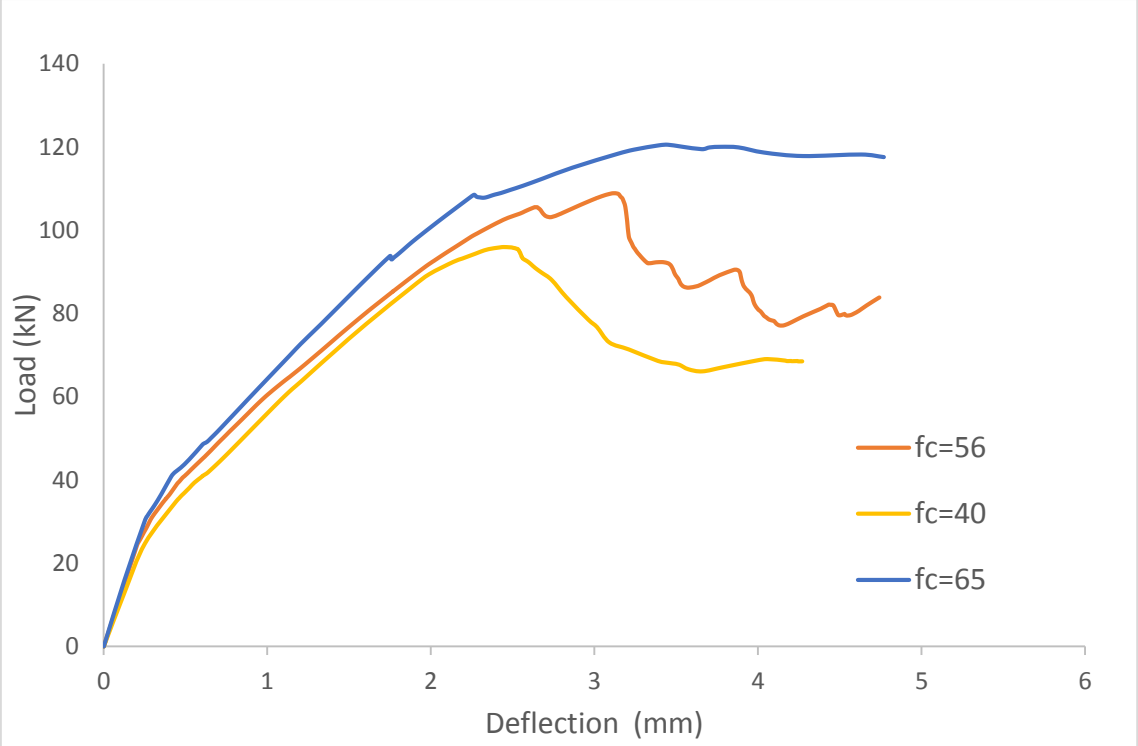

(a)Load-deflection curve for different compression strength of concrete of beam(B10-M)

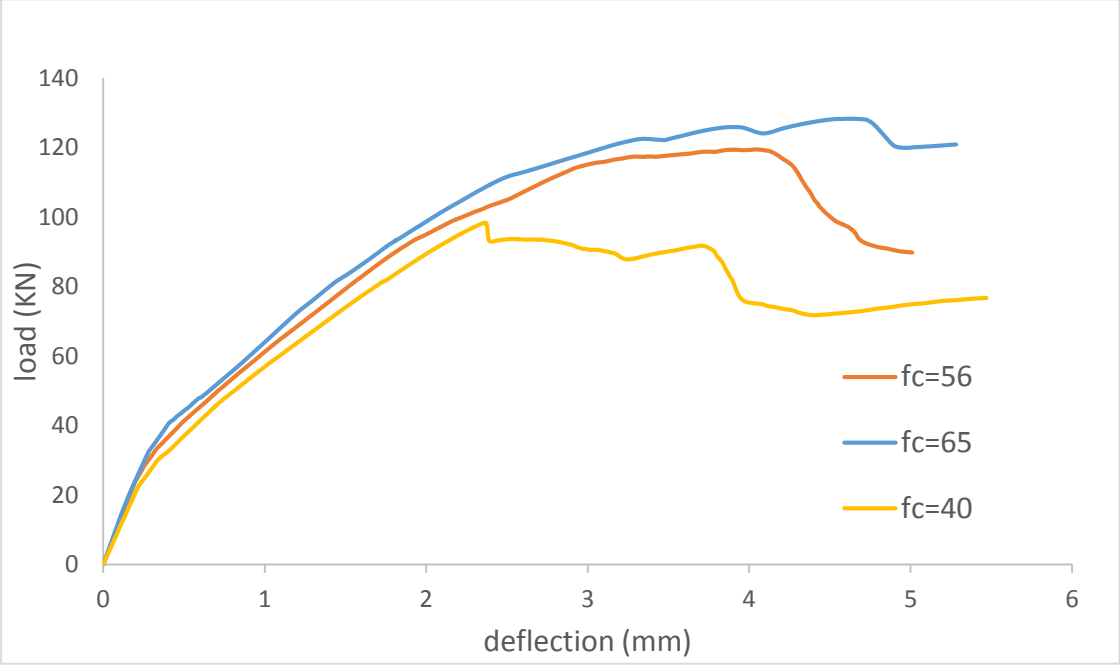

(b) Load-deflection curve for different compression strength of concrete of beam(B10-VL)

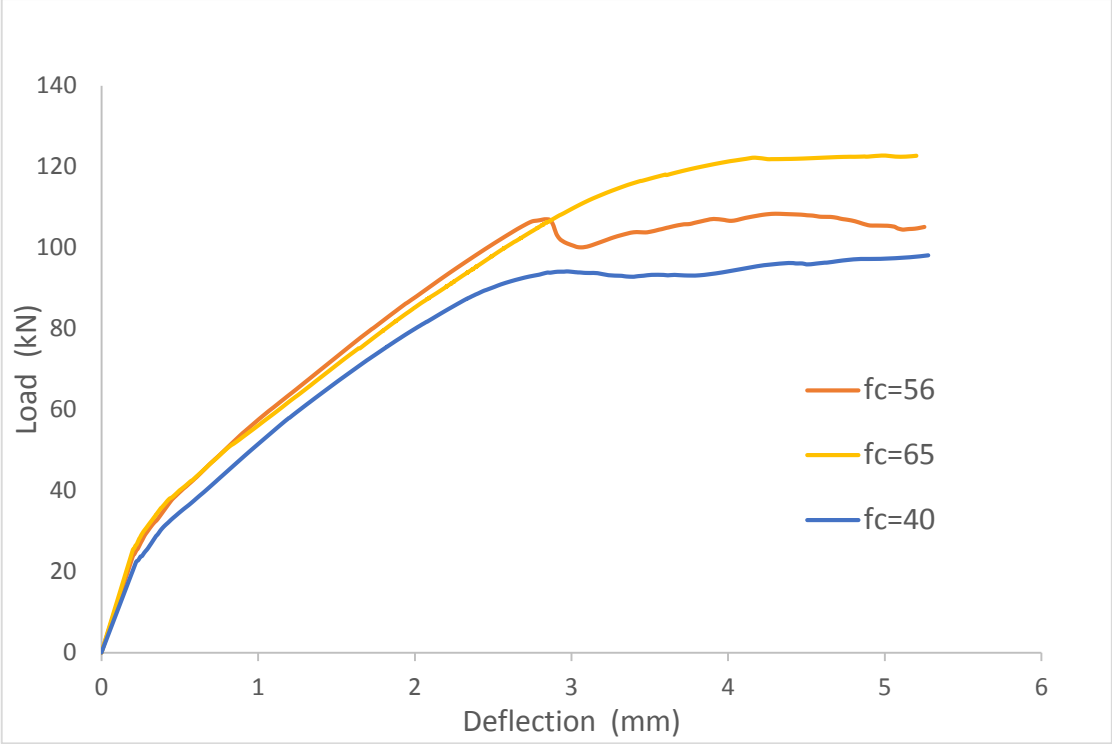

(c) Load-deflection curve for different compression strength of concrete of beam(B10-S)

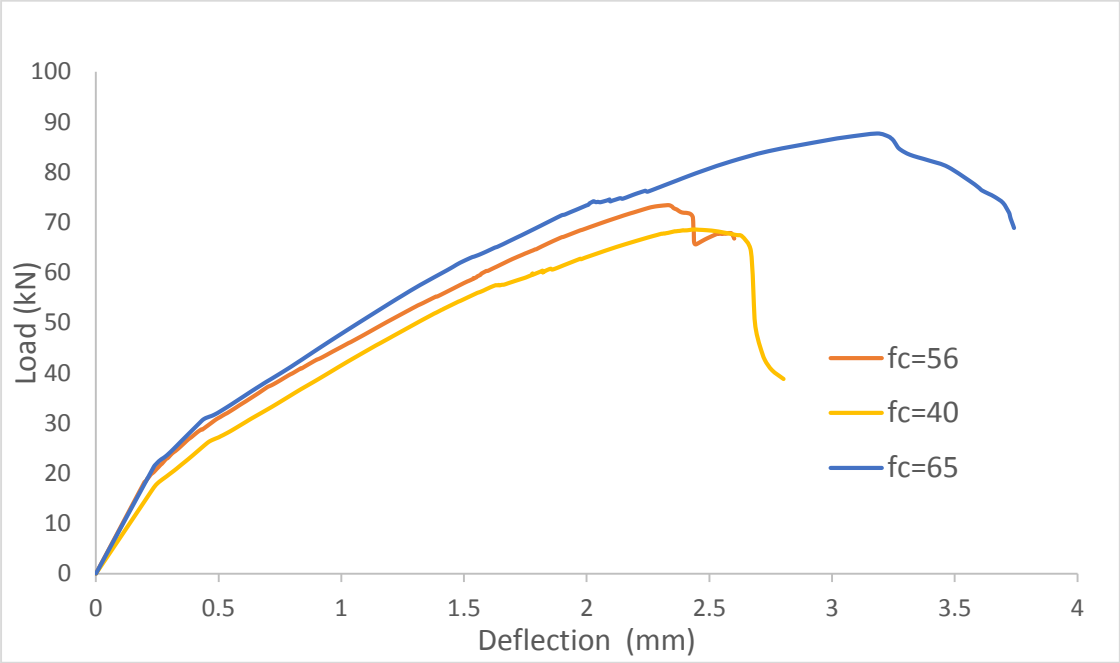

(d) Load-deflection curve for different compression strength of concrete of beam(B10-R)

Figure (4.58) Load-deflection curve for different compression strength of concrete

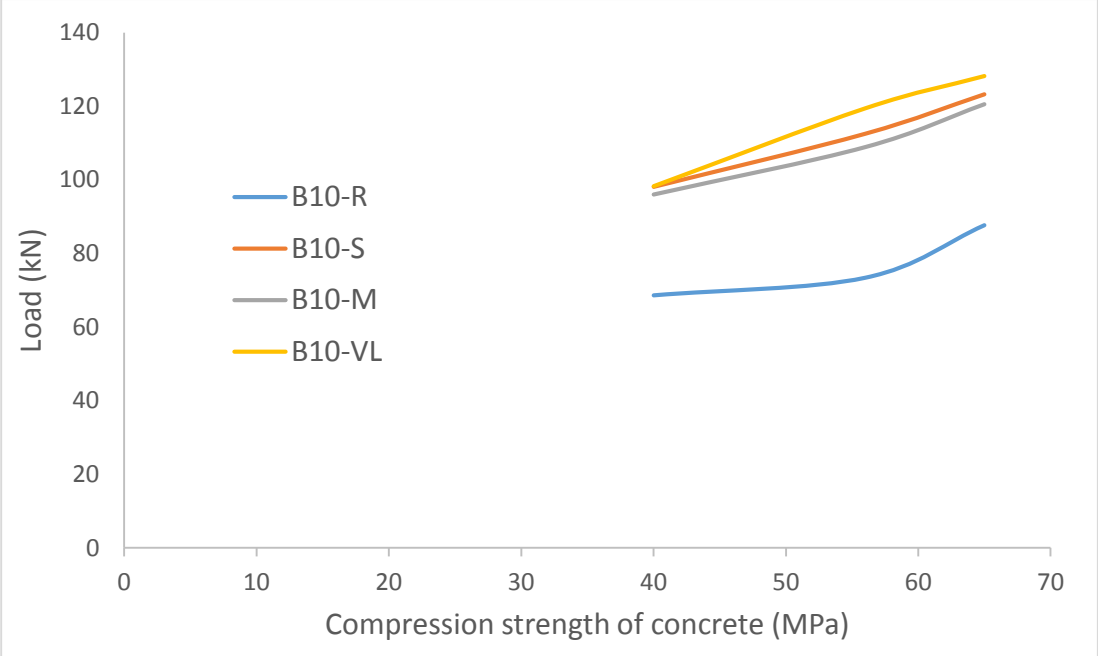

Figure (4.59) Relationship between load and compression strength of concrete

4.4.3.2 Effect of Shear Span to Depth Ratio (a/h)

The inclined cracking of RC beams are strongly affected by the relative magnitudes of the shearing stress . This effect may be conveniently considered as a function of a/h ratio. The influence of a/h ratio is investigated in this study by developing FE models. Three values of a/h ratios in the range from 1.66, 2 and 2.3 were considered. Figs. (4.60) and (4.61) show that increasing the a/h ratio has a negative effect on the predicted shear strength due to increase the shear stresses on shear span led to decrease the strength shear capacity of RC beams . Shear strength decreased by about (20 to 30)% when increased the ratio (a/h) from 1.66 to 2.33.

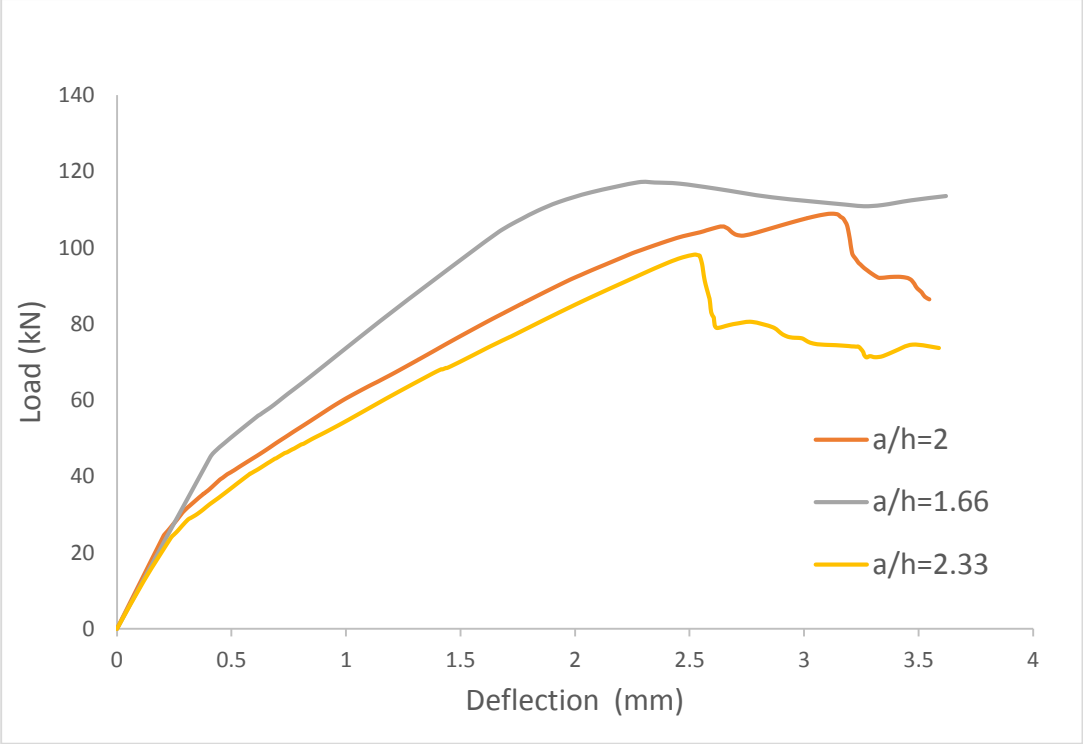

(a) Relationship between load and deflection for different depth ratio (a/h) of beam(B10-M)

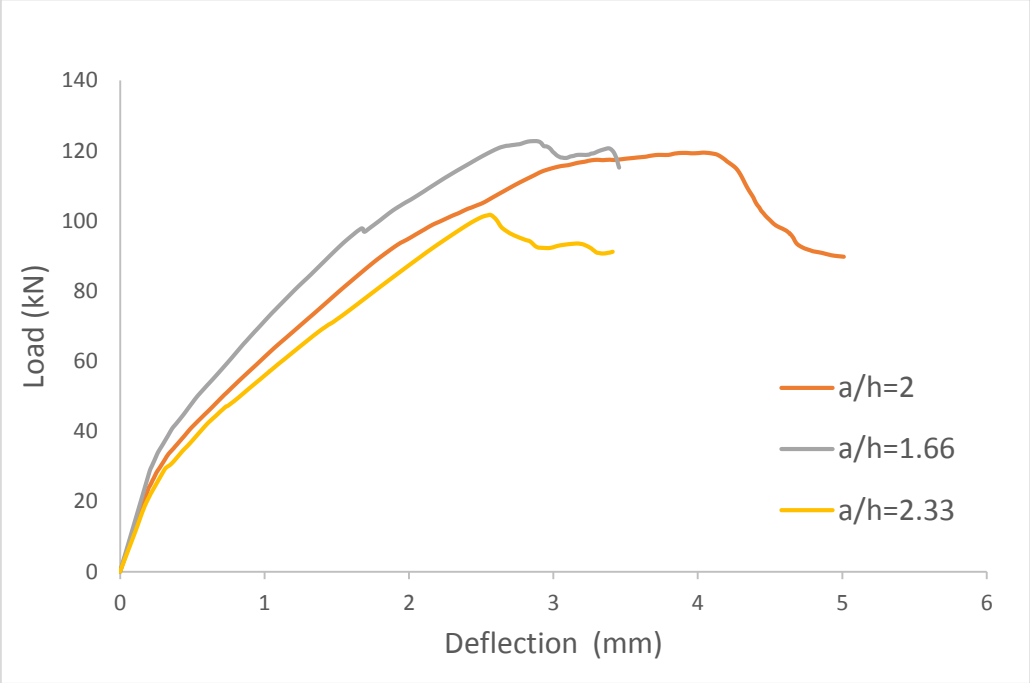

(d) Relationship between load and deflection for different depth ratio (a/h) of beam(B10-VL)

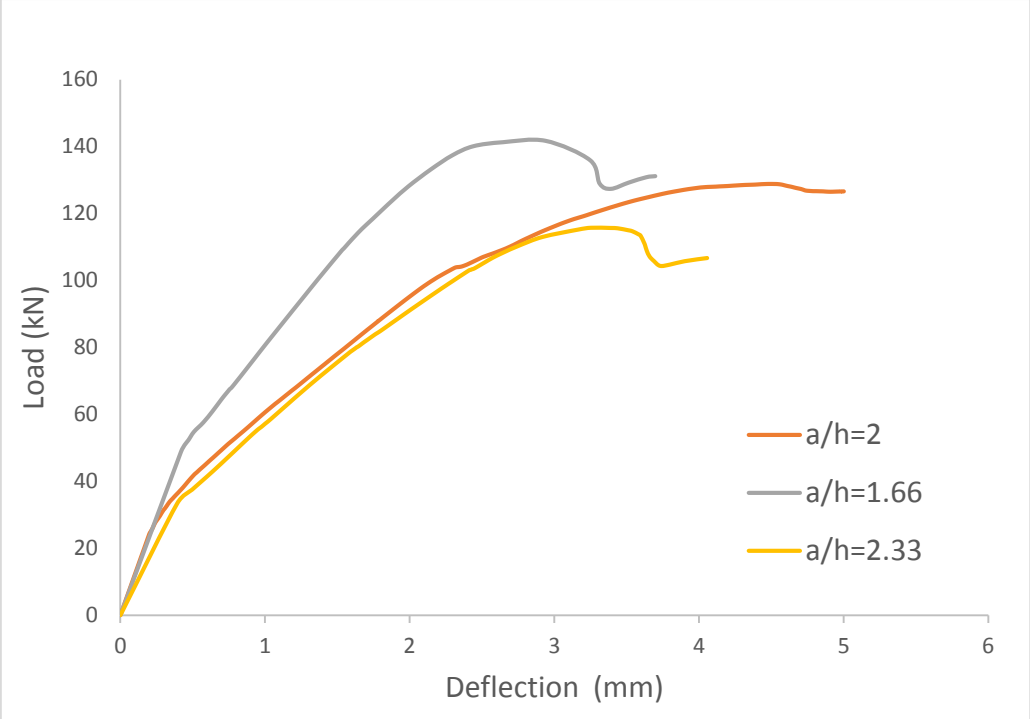

(e) Relationship between load and deflection for different depth ratio (a/h) of beam(B10-IL)

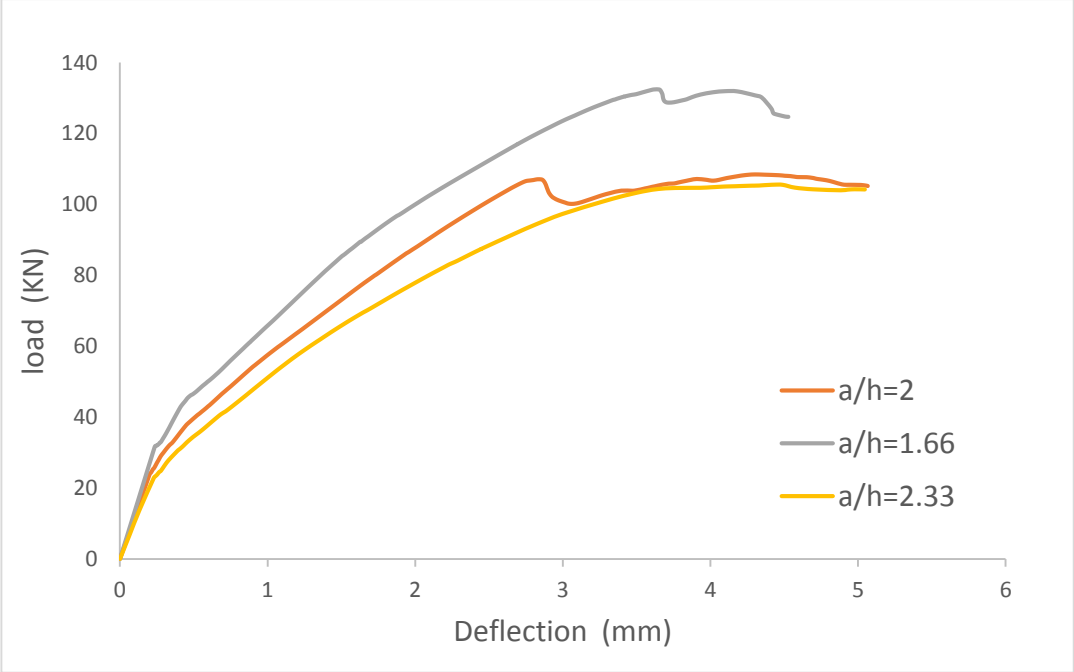

(f) Relationship between load and deflection for different depth ratio (a/h) of beam(B10-S)

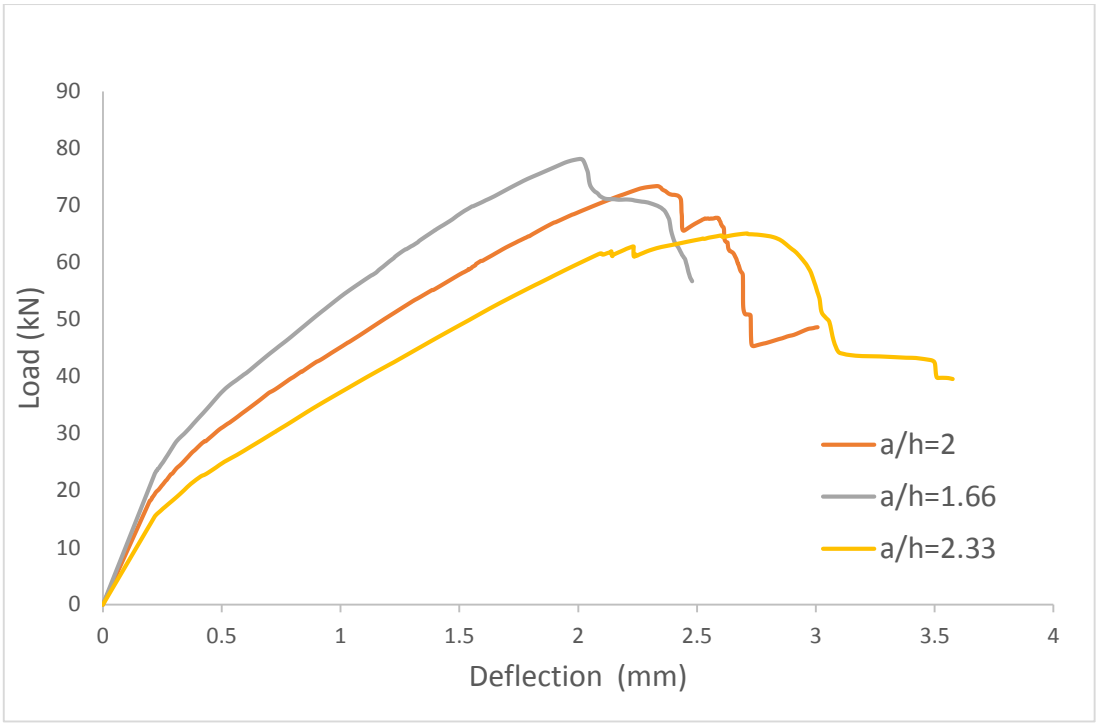

(g) Relationship between load and deflection for different depth ratio (a/h) of beam(B10-M)

Figure (4.60) Relationship between load and deflection for different depth ratio (a/h)

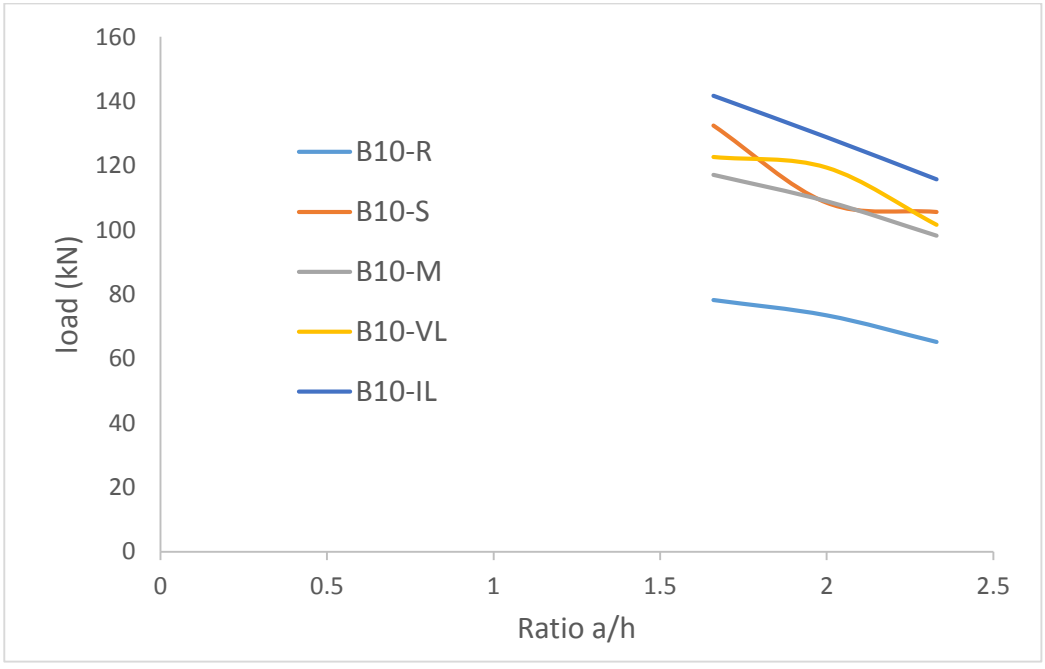

Figure (4.61) Relationship between max load to effect-depth ratio (a/h)

4.4.3.3 Effect of Shape of CFRP on Shear Strength

Generally, three types of CFRP wrapping schemes had been used to improve the shear strength of RC members such as beams and column which one (completely wrapping, U-wrap shape and two side abond shape). Completely wrapping the FRP system around the section on all four sides is the most efficient wrapping scheme and is most commonly used in column applications. In beam applications, the shear strength can be improved by wrapping the FRP system about three sides of the beam (U-wrap) or bonding to the 2 sides of the member. In this study, two types of strengthening: U shape and two side bond shapes are used. Fig. (4.62) shows that the retrofitting with U shape is slightly improves the strength more than two sides bonding. The ultimate load in A10-M, A12-M, B10-M, and B12-M beams strengthened with U shape CFRP increased by 6.2%, 5.9%, 11.5%, and 9.5% respectively compared with beams retrofitted with two side shape due to increased the length ancharage.

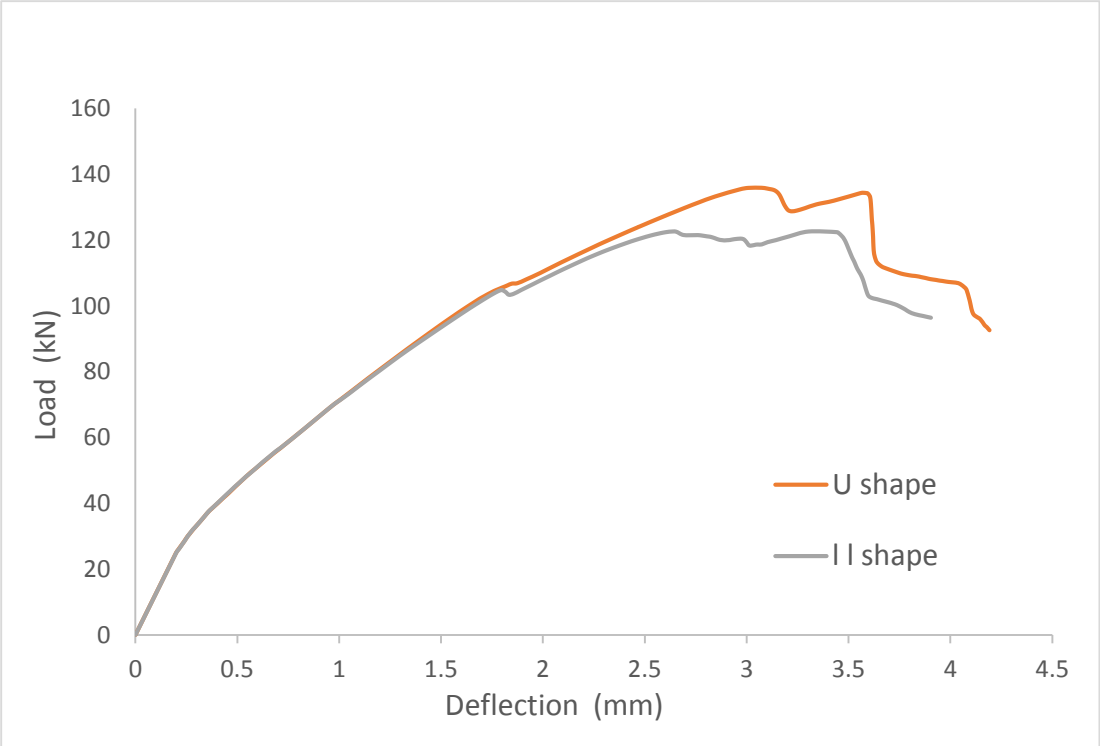

(a) Beams strengthened with CFRP U shape and 2 side bond shape (B12-M)

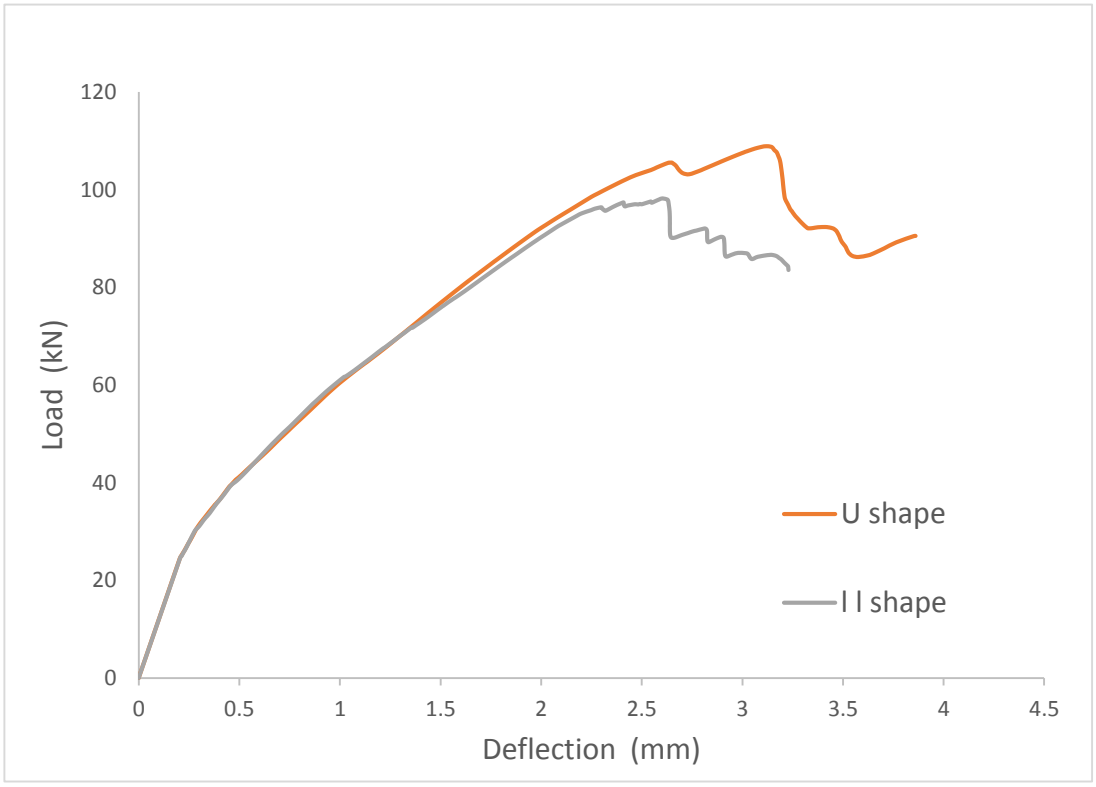

(b) Beams strengthened with CFRP U shape and 2 side bond shape (B10-M)

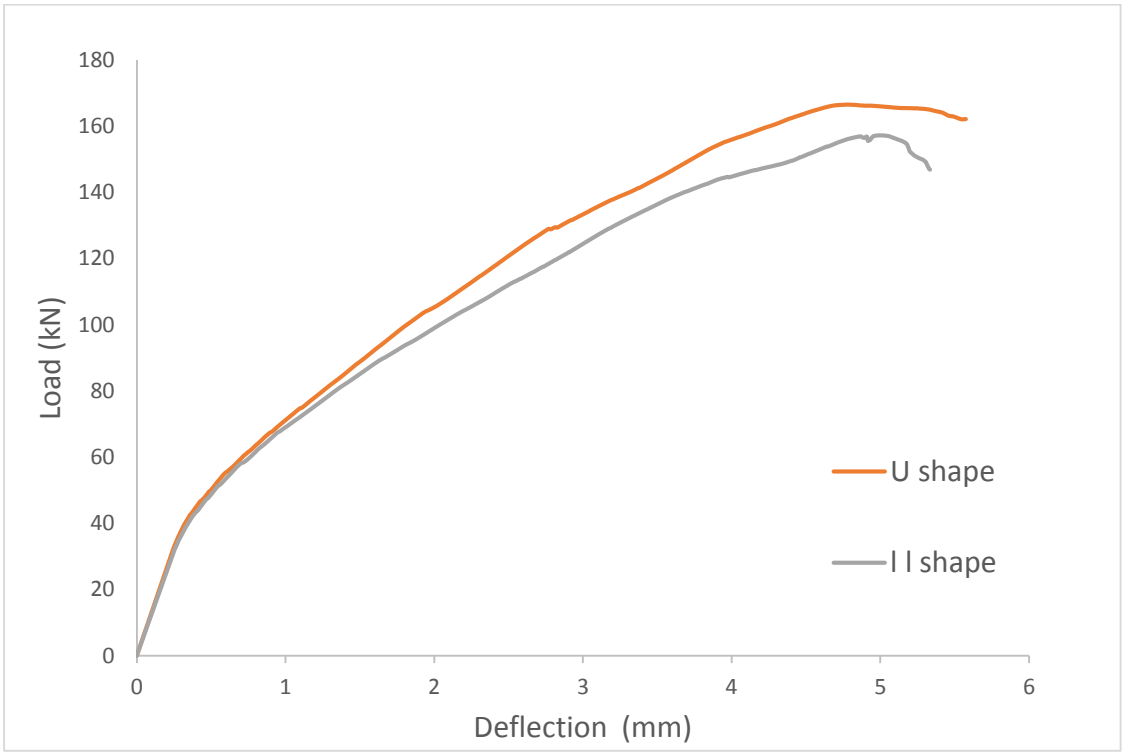

(c) Beams strengthened with CFRP U shape and 2 side bond shape (A12-M)

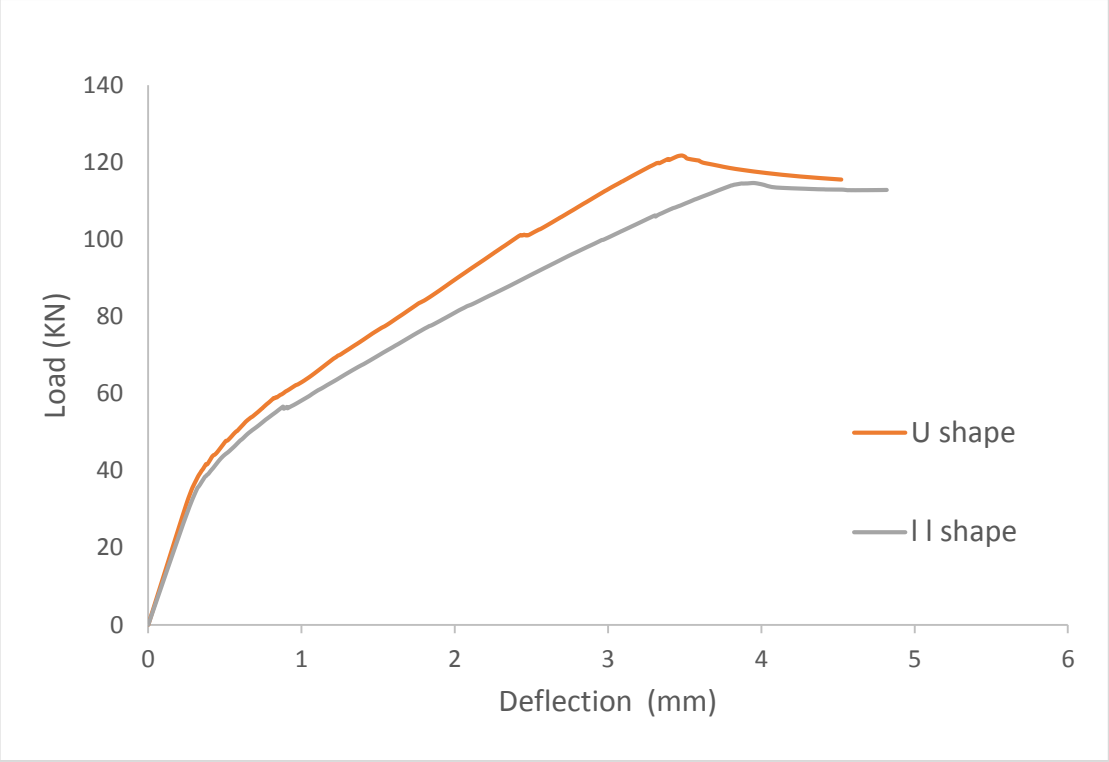

(d) Beams strengthened with CFRP U shape and 2 side bond shape (A10-M)

Figure (4.62) Beams strengthened with CFRP U shape and 2 side bond shape

4.4.4 Appraisal of the ACI-440

According to ACI, the nominal shear strength for the beam strengthened with CFRP is calculated from the following equation [17]:

$$V_n = V_s + V_c + V_{ff} \quad \text{.....(4.9)}$$

$$V_s = A_v f_y \frac{d}{s} \quad \text{.....(4.10)}$$

$$V_c = \frac{1}{6} \times \sqrt[2]{f_c^-}\, b\, d \quad \text{.....(4.11)}$$

the design value for shear strength of the CFRP is given by:

$$V_{fd} = \emptyset\, \psi_f \left(\frac{A_{fv} f_{fe} d_f}{s_f}\right) \quad \text{.....(4.12)}$$

for concrete material, Φ has a value of 0.85, ψ f has a value for the U-wraps shape equal to 0.85 and for completely wrapped members equal to 0.95.

$$A_{fv} = 2n\ t_f\ w_f \quad \text{.....(4.13)}$$

The effective stress in the FRP f fe, is obtained by multiplying the effective strain by the Young's modulus of the FRP (Ef),

$$\varepsilon_{fe} = k_v \times \epsilon_{fu} \leq 0.004 \quad \text{.....(4.14)}$$

Where;

$$k_v = \frac{k_1 k_2 L_e}{11900\varepsilon_{fu}} \leq 0.75 \quad \text{.....(4.15)}$$

where:

$$L_e = (23300)/(nt_f\ E_f)^{0.58} \quad \text{.....(4.16)}$$

$$k_1 = (\frac{f_c^-}{27})^{2/3} \quad \text{.....(4.17)}$$

$$k_2 = \frac{d_f - L_e}{d_f} \quad \text{.....(4.18)}$$

In Eqs. (4.18) and Eqs.. (4.12) df is the effective depth of beam. fc' is the concrete compression strength. The force and the length unities of the variables in Eqs. (4.15) to equ .(4.18) are Newton and millimeter respectively. The difference between the finite element method and ACI results is 24%, 53%, 109%, 110%, 49%, 23%, 47%, 34%, 5%, 8%, 43%, 21% in beam A10-R, A12-R, B10-R, B12-R, A10-S, A12-S, B10-S, B12-S, A10-M, A12-M, B10-M and B12-M respectivlty because the ACI-440 uses factor of safty for the most equation and There is no relative slip between external FRP reinforcement and the concrete.

Table (4.17) shows the results for finite element method and ACI of RC beams in shear behavior and compared between them.

Table (4.17) Finite element method (FEM) and ACI results

Beam designation	FEM ultimate load (kN)	ACI ultimate load (kN)	FE/ACI
A10-R	96.2	77.5	1.24
A12-R	119	77.28	1.53
B10-R	73.39	35.04	2.09
B12-R	73.36	34.82	2.1
A10-S	183.12	122.46	1.49
A12-S	205.5	166.86	1.23
B10-S	107.69	73.08	1.47
B12-S	154.3	110.22	1.34
A10-M	121.7	115.82	1.05
A12-M	166.48	153.66	1.08
B10-M	105.55	73.46	1.43
B12-M	134.35	111.04	1.21

Chapter Five

Conclusions and Recommendations

5.1 Conclusions

The current study includes modeling and analysis of RC beams strengthened with CFRP materials against flexure and shear using FEM using the ABAQUS program and compared with experimental results from the study, the following conclusions are stated.

5.1.1 Conclusions for Flexural

1. The general behavior of RC beams strengthened with CFRP sheet or laminate using ABAQUS application represented by load- midspan deflection indicate a good agreement with the available experimental results. The ultimate load difference between the analytical and experimental results is 12% in beam strengthened with three NSM CFRP strips installed in three grooves.
2. In this study, the strengthening by the CFRP system improves the ultimate load of the RC beams up to 108.8% in beam strengthened with one NSM CFRP strips installed in one grooves and serviceability load up to 80% in beam strengthened externally by two CFRP strips.
3. Increasing the compressive strength of concrete tends to increase the ultimate load of strengthened RC beams. Increasing compressive strength from 30 MPa to 70 MPa makes an increase in the load to reach 25.6% in beam strengthened with one NSM CFRP strips installed in one grooves.
4. Increasing the number of strips or number layers of sheet tends to increase the strength capacity of the RC beam. However, two layers of the sheet is the best choice to increase the ultimate load.
5. Increasing the length ratio of CFRP laminate to clear span from 0.66 to 1 leads to an increase in the ultimate load by 12.7% in beam strengthened externally by two CFRP strips.

6. Increasing thickness of the CFRP sheet from 0.11 mm to 0.5 mm increase the ultimate load by 47.9% in beam strengthened externally by one CFRP strips.

5.1.2 Conclusions for Shear

1. The good agreement between FEM using program ABAQUS and experimental results for the RC beams strengthened with CFRP laminate or sheet. The maximum difference between the experimental and analytical results is 12% in beam with traditional stirrups (B10-S).
2. In this study, strengthening RC beams for shear using CFRP sheet or laminate improves the load-carrying capacity of the RC beams up to 111.7% in beam strengthened by an inclined laminate of CFRP using NSM (B12-IL).
3. Strengthening RC beams using either U shape wrapped or 2 side bond shape is very important to increase the shear strength. The U shape wrapped beam is more efficient in increasing the ultimate load and stiffness than the 2 side bond shape. The maximum load of beams strengthened with U shape of increased by 5.9% to 11.5% for beams strengthened with CFRP sheet using externally bond techniques A12-M and B10-M respectively when compared with the same beams strengthened with two sides bond shape of CFRP.
4. The difference between FEM results and experimental results is 12%, while the difference between FEM and ACI 440.1R-17 approach reached 109% because the ACI-440 approach uses factor of safty for the most equation and There is no relative slip between external FRP reinforcement and the concrete. So the finite element method (FEM) is a very good tool to predicate the structural and it could be used efficiently in predicting the ultimate load of concrete beams reinforced with CFRP.

5. The crack patterns obtained from the finite element models, in general, are similar to the crack patterns observed from the experimental work for both flexure and shear behavior.
6. The decrease of shear span to depth ratio (a/h) from 1.66 to 2.33 leads to increasing the load-carrying capacity by 23% in beams strengthened with CFRP sheet using externally bond techniques (B10-M).
7. As mentioned in flexure strengthening, the NSM was the most efficient of the CFRP systems than EBR in shear also. This efficacy was not only in terms of the beam load carrying capacity but also in terms of deformation capacity at beam failure.

5.2 Recommendations for Future Works

The following recommendations are suggested for further studies:

1. The repair of RC beams by strengthening with CFRP using program ABAQUS may be studied.
2. The finite element method uses to represent RC beams strengthened by CFRP should be a mode with different types of load (uniformly distributed load, three-point load) and different boundary conditions.
3. Investigate the structural behavior of RC beams strengthened with CFRP by using program ABAQUS under cyclic and dynamic loading conditions.
4. The structural behavior of RC beams strengthened with CFRP sheets subjected to large changes in temperatures is other areas for future work by using FEM.
5. Studying the torsion strength of RC beams strengthened with CFRP sheets by using FEM.
6. Using FEM to represent RC beams strengthened with glass fiber reinforced polymer (GFRP) in flexural and shear behavior.
7. Using FEM for predicting and studying the flexural and shear behavior of concrete T-sections reinforced with CFRP.

References

1. Obaidat, Y.T., Structural retrofitting of reinforced concrete beams using carbon fibre reinforced polymer. 2011, Department of Construction Sciences, Structural Mechanics.
2. Hull, D. and T.W. Clyne, An introduction to composite materials. 1996: Cambridge university press.DOI.
3. AL-Tai, S.L.H., Nonlinear Behavior of Reinforced Concrete T-Beams Strengthened with CFRP Subjected to Shear. 2010, University of Technology.
4. Nacer, R., Évaluation des propriétés physiques et mécaniques de laminés en matériaux composites fabriqués par enroulement filamentair. 2006, Sherbrooke University.
5. Carolin, A., Carbon fibre reinforced polymers for strengthening of structural elements. 2003, Luleå tekniska universitet.
6. Manual, I.D., Reinforcing Concrete Structures with Fibre Reinforced Polymers (FRPs). ISIS Canada, 2007.DOI.
7. Jain, R. and L. Lee, Fiber reinforced polymer (FRP) composites for infrastructure applications: focusing on innovation, technology implementation andsustainability.2012:Springer.DOI:https://link.springer.com/content/pdf/10.1007/978-94-007-2357-3.pdf.
8. Guide for the Design and Construction of Concrete Reinforced with FRP Bars: ACI 440.1 R-03. 2003. American Concrete Institute.DOI.
9. report on fiber reinforced plastic (FRP) reinforcement for concrete structures. 1996. American Concrete Institute.DOI.
10. Mostofinejad, D., M.R. Esfahani, and A. Shomali, Experimental and numerical study of the RC beams shear-strengthened with NSM technique. Journal of CompositeMaterials,2019:p.0021998319830777.DOI:https://doi.org/10.1177%2F0021998319830777.

11. Masuelli, M.A., Introduction of fibre-reinforced polymers− Polymers and composites: Concepts, properties and processes, in Fiber Reinforced Polymers-The Technology Applied for Concrete Repair. 2013, IntechOpen.DOI.
12. Feeser, W., Guide Examples for the Design of Concrete Reinforced with Fiber Reinforced Polymer Bars. 2005, Widener University.
13. Bakis, C.E., et al., Fiber-reinforced polymer composites for construction—State-of-the-art review. Journal of composites for construction, 2002. 6(2): p. 73-87.DOI.
14. Russell, J.S. and A.S.o.C. Engineers, Perspectives in Civil Engineering: Commemorating the 150th Anniversary of the American Society of Civil Engineers. 2003: American Society of Civil Engineers.DOI.
15. Ali, A.A., experimental and theoretical investigation for behavior of concrete deep beams reinforced with CFRP bar falling in shear. 2011, Basra university.
16. ACI Committee 440. 2006.DOI.
17. 440.2R-02, Guide for the Design and Construction of Externally Bonded FRP Systems for Strengthening Concrete Structures.
18. Michaluk, C.R., et al., Flexural behavior of one-way concrete slabs reinforced by fiber reinforced plastic reinforcements. ACI structural Journal, 1998. 95: p. 353-365.DOI.
19. Shehata, E., R. Morphy, and S. Rizkalla, Fibre reinforced polymer shear reinforcement for concrete members: behaviour and design guidelines. Canadian Journal of Civil Engineering, 2000. 27(5): p..872-859 DOI.
20. Bank, L. and M. Ozel, Shear failure of concrete beams reinforced with 3-D fiber reinforced plastic grids. Special Publication, 1999. 188: p. 145-156.DOI.
21. Razaqpur, A. and D. Mostofinejad, Experimental study of shear behavior of continuous beams reinforced with carbon fiber reinforced polymer. Special Publication, 1999. 188: p. 169-178.DOI.
22. Arduini, M., A. Di Tommaso, and A. Nanni, Brittle failure in FRP plate and sheet bonded beams. ACI Structural Journal, 1997. 94(4): p. 363-370.DOI.

23. Saadatmanesh, H. and M.R. Ehsani, RC beams strengthened with GFRP plates. I: Experimental study. Journal of structural engineering, 1991. 117(11): p. 3417-3433.DOI.
24. Fanning, P.J. and O. Kelly, Ultimate response of RC beams strengthened with CFRP plates. Journal of Composites for Construction, 2001. 5(2): p. 122-127.DOI.
25. Rasheed, H.A., et al., Ductile strengthening using externally bonded and near surface mounted composite systems. Composite Structures, 2010. 92(10): p. 2379-2390.DOI.
26. Cosenza, E., G. Manfredi, and R. Realfonzo, Behavior and modeling of bond of FRP rebars to concrete. Journal of composites for construction, 1997. 1(2): p. 40-51.DOI.
27. De Lorenzis, L., A. Nanni, and A. La Tegola. Strengthening of reinforced concrete structures with near surface mounted FRP rods. in International Meeting on Composite Materials, PLAST 2000, Proceedings, Advancing with Composites.2000.DOI:https://www.academia.edu/download/48497838/Strengthening_of_Reinforced_Concrete_Str20160901-6048-n42m5.pdf.
28. Barros, J.A. and A. Fortes, Flexural strengthening of concrete beams with CFRP laminates bonded into slits. Cement and Concrete Composites, 2005. 27(4): p. 471-480.DOI.
29. Obaidat, Y.T., S. Heyden, and O. Dahlblom, The effect of CFRP and CFRP/concrete interface models when modelling retrofitted RC beams with FEM. Composite Structures, 2010. 92(6): p. 1391-1398.DOI.
30. Obaidat, Y.T., et al., Retrofitting of reinforced concrete beams using composite laminates. Construction and Building Materials, 2011. 25(2): p. 591-597.DOI: https://doi.org/10.1016/j.conbuildmat.2010.06.082.
31. Attari, N., S. Amziane, and M. Chemrouk, Flexural strengthening of concrete beams using CFRP, GFRP and hybrid FRP sheets. Construction and Building Materials,2012. DOI: https://doi.org/10.1016/j.conbuildmat.2012.07.052.

32. Pecce, M., G. Manfredi, and E. Cosenza, Experimental response and code Modelsof GFRP RC beams in bending. Journal of Composites for Construction, 2000. 4(4): p. 182-190.DOI.
33. Bilotta, A., et al., Efficiency of CFRP NSM strips and EBR plates for flexural strengthening of RC beams and loading pattern influence. Composite Structures, 2015. 124: p. 163-175.DOI.
34. Zhang, D., Q. Wang, and J. Dong, Simulation study on CFRP strengthened reinforced concrete beam under four-point bending. Vol. 17. 2016. 407-421.DOI: 10.12989/cac.2016.17.3.407.
35. Khalifa, A.M., Flexural performance of RC beams strengthened with near surface mounted CFRP strips. Alexandria Engineering Journal, 2016. 55(:(2p. 1497-1505.DOI: https://doi.org/10.1016/j.aej.2016.01.033.
36. Garyfalia G. Triantafyllou1, T.C.R., and Athanasios I. Karabinis, Experimental and numerical response of CFRP strengthened concrete beams with low or medium steel corrosion. 2017.DOI.
37. Raoof, S.M., L.N. Koutas, and D.A. Bournas, Textile-reinforced mortar (TRM) versus fibre-reinforced polymers (FRP) in flexural strengthening of RC beams. Construction and Building Materials, 2017. 151: p. 279-291.DOI.
38. Almusallam, T., et al., Behavior of FRP-Strengthened RC Beams with Large Rectangular Web Openings in Flexure Zones: Experimental and Numerical Study. International Journal of Concrete Structures and Materials, 2018. 12(1): p. 47.DOI.
39. Ghaedi1, K., et al., finite element analysis of astrengthened beam deliberrating elastically isotropic and orthotropic CFRP material Journal of Civil Engineering, Science and Technology, 2018.DOI: http://publisher.unimas.my/ojs/index.php/JCEST/article/view/991/651.
40. Zaki, M.A. and H.A. Rasheed, Behavior of reinforced concrete beams strengthened using CFRP sheets with innovative anchorage devices. Engineering Structures, 2020. 215: p. 110689.DOI.

41. Bacciocchi, M. and A.M. Tarantino, Modeling and numerical investigation of the viscoelastic behavior of laminated concrete beams strengthened by CFRP strips and carbon nanotubes. Construction and Building Materials, 2020. 233: p. 117311.DOI.
42. De Lorenzis, L. and A. Nanni, Shear strengthening of reinforced concrete beams with near-surface mounted fiber-reinforced polymer rods. Structural Journal, 2001. 98(1): p. 60-68.DOI.
43. Ibrahim, A.M. and M.S. Mahmood, Finite element modeling of reinforced concrete beams strengthened with FRP laminates. European Journal of Scientific Research, 2009. 30(4): p. 526.541-DOI: https://www.researchgate.net/profile/Mohammed_Mahmood2/publication/242163873_Finite_Element_Modeling_of_Reinforced_Concrete_Beams_Strengthened_with_FRP_Laminates/links/54ac15a60cf2bce6aa1df984/Finite-Element-Modeling-of-Reinforced-Concrete-Beams-Strengthened-with-FRP-Laminates.pdf.
44. Obaidat, Y.T., O. Dahlblom, and S. Heyden, Nonlinear FE modelling of shear behaviour in RC beam retrofitted with CFRP. 2010: p. 47.DOI: https://www.researchgate.net/profile/Fatimah_Naser/post/How_we_can_apply_FRP_in_Concrete_beam_with_Abaqus/attachment/5ae88996b53d2f63c3c92b68/AS%3A621501925576707%401525189014697/download/Abaqua.pdf#page=57.
45. Ramadan, A.G.M.a.O.M., finite element modeling of RC beams shear strengthened with side bond CFRP sheet. 2017.DOI.
46. Chen, W., et al., Experimental study of flexural behaviour of RC beams strengthened by longitudinal and U-shaped basalt FRP sheet. Composites Part B:Engineering,2018.134:p.114126.DOI:https://doi.org/10.1016/j.compositesb.2017.09.053.

47. Benzeguir, Z., G. El-Saikaly, and O. Chaallal, influenceE of size on the behavior of RC T-beams strengthened in shear with externally bonded CFRP. 2018.DOI.
48. Oller, E., M. Pujol, and A. Marí, Contribution of externally bonded FRP shear reinforcement to the shear strength of RC beams. Composites Part B: Engineering, 2019. 164: p. 235-248.DOI.
49. Al Rjoub, Y.S., et al., Shear strengthening of RC beams using near-surface mounted carbon fibre-reinforced polymers. Australian Journal of Structural Engineering, 2019.2.DOI: https://doi.org/10.1080/13287982.2019.1565617.
50. Kadhim, M.M., A.H. Adheem, and A.R. Jawdhari, Nonlinear Finite Element Modelling and Parametric Analysis of Shear Strengthening RC T-Beams with NSM CFRP Technique. International Journal of Civil Engineering, 2019: p. 1-12.DOI: https://link.springer.com/article/10.1007/s40999-018-0387-8.
51. Al-Rousan, R., Predicting the Optimum Shear Capacity of Reinforced Concrete Beams Externally Strengthened With CFRP Composites. Procedia Manufacturing, 2020. 44: p. 631-638.DOI.
52. Mohammed, A.A. and O.A.H. Fattah, Investigation of parameters affecting direct shear behavior of concrete strengthened with CFRP laminate. Journal of Building Engineering, 2020: p. 101480.DOI.
53. Adams, V. and A. Askenazi, Building better products with finite element analysis. 1999: Cengage Learning.DOI.
54. Pathak, P., Nonlinear Finite Element Analysis of FRP Strengthened RC Beams under Static and Cyclic Loads. 2016, University of New South Wales Canberra, Australia.
55. Minouei, M.B., Finite element analysis of bond characteristics at the FRP-concrete interface. 2014, McGill University Libraries.
56. Huebner, K.H., et al., The finite element method for engineers. 2001: John Wiley & Sons.DOI.

57. Chan, S.-L. and P.-T. Chui, Non-linear static and cyclic analysis of steel frames with semi-rigid connections. 2000: Elsevier.DOI.
58. Hibbitt, K., Sorensen, Inc. ABAQUS theory manual. 2000, Pawtucket, USA: Hibbitt, Karlsson & Sorensen, Inc.
59. Design of concrete structures - Part 1-1: General rules and rules for buildings. 2004.
60. Barros, J.A., S.J. Dias, and J.L. Lima, Efficacy of CFRP-based techniques for the flexural and shear strengthening of concrete beams. Cement and Concrete Composite.2006 DOI: https://doi.org/10.1016/j.cemconcomp.2006.09.001.
61. Design of steel structures-Part 1-1: General rules and rules for buildings. Brussels: CEN, 2005.DOI.
62. Szpieg, M., M. Wysocki, and L. Asp, Mechanical performance and modelling of a fully recycled modified CF/PP composite. Journal of composite materials, 2012. 46(12): p. 1503-1517.DOI.
63. Guo, Z., et al. Experimental study on bond stress-slip behaviour between FRP sheets and concrete. in FRP in construction, proceedings of the international symposium on bond behaviour of FRP in structures. 2005.DOI: https://www.researchgate.net/profile/Serge_Shilko/post/how_to_study_slip_and_interface_effects_of_steel_confined_composite_beams_under_flexure/attachment/59d6280779197b807798662a/AS14552947096@328343963619331:/60download/Experimental+Study+on+Bond+StressSlip+Behaviour+between+FRP+Sheets+and+Concrete.pdf.
64. Lu, X., et al., Bond–slip models for FRP sheets/plates bonded to concrete. Engineeringstructures,2005.DOI:https://doi.org/10.1016/j.engstruct.2005.01.014.
65. JCI., Technical report on retrofit technology for concrete structures, in Technical committee on retrofitting technology for concrete structures. 2003. p. p. 79–97.

66. JCI., Technical report on retrofit technology for concrete structures., in Technical committee on retrofitting technology for concrete structures. 1998. . p. 24-116.
67. Sarsam, K.F., N.A. Al-Bayati, and A.S. Mohammed, finite element anaylisis of porcelanite lightweight aggregate reinforced concrete deep beams strengthened by externally bonded carbon fiber stripe. Journal of Engineering and Sustainable Development, 2017. 21(1): p. 124-138.DOI.
68. Karlsson, B.I.a.S., E.P, ABAQUS: Analysis user's guide volume IV: Elements, Pawtucket, Rhode Island, Hibbitt Publication, 2006.DOI.

Mesh sensitivity analysis

The mesh was refined to check the acceptance of the element size. Three different mesh sizes were considered. As mentioned earlier, initially a 40 mm finite element mesh was used for modeling concrete and steel, but then the model was changed to a 30 mm mesh. Subsequently, 25 mm finite element mesh size was used for the model.

Figure (1) compares the effect of using the different mesh sizes on the load-displacement diagram for control beam.

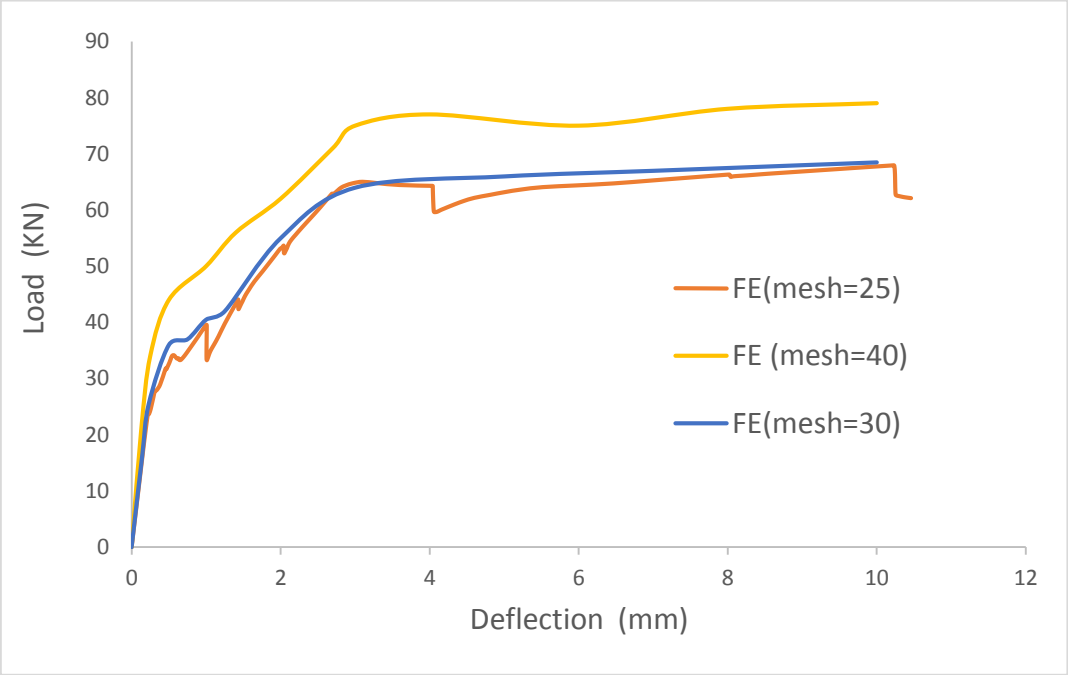

Figure (1) Load -displacement diagram for different mesh sizes

It was found that a slight variance occurred in the deflection and load of control beam for mesh from 30 to 25 mm. Therefore, the element size of 25 mm has been accepted.

1. Introduction to Abaqus/CAE

Abaqus/CAE is the Complete Abaqus Environment that provides a simple, consistent interface for creating Abaqus models, interactively submitting and monitoring Abaqus jobs, and evaluating results from Abaqus simulations. Abaqus/CAE is divided into modules, where each module defines a logical aspect of the modeling process; for example, defining the geometry, defining material properties, and generating a mesh. As you move from module to module, you build up the model. When the model is complete, Abaqus/CAE generates an input file that you submit to the Abaqus analysis product. Abaqus/Standard or Abaqus/Explicit reads the input file generated by Abaqus/CAE, performs the analysis, sends information to Abaqus/CAE to allow you to monitor the progress of the job, and generates an output database. Finally, you use the Visualization module to read the output database and view the results of your analysis.

2. Components of the main window

You interact with Abaqus/CAE through the main window. Fig. (1) shows the components that appear in the main window. The components are:

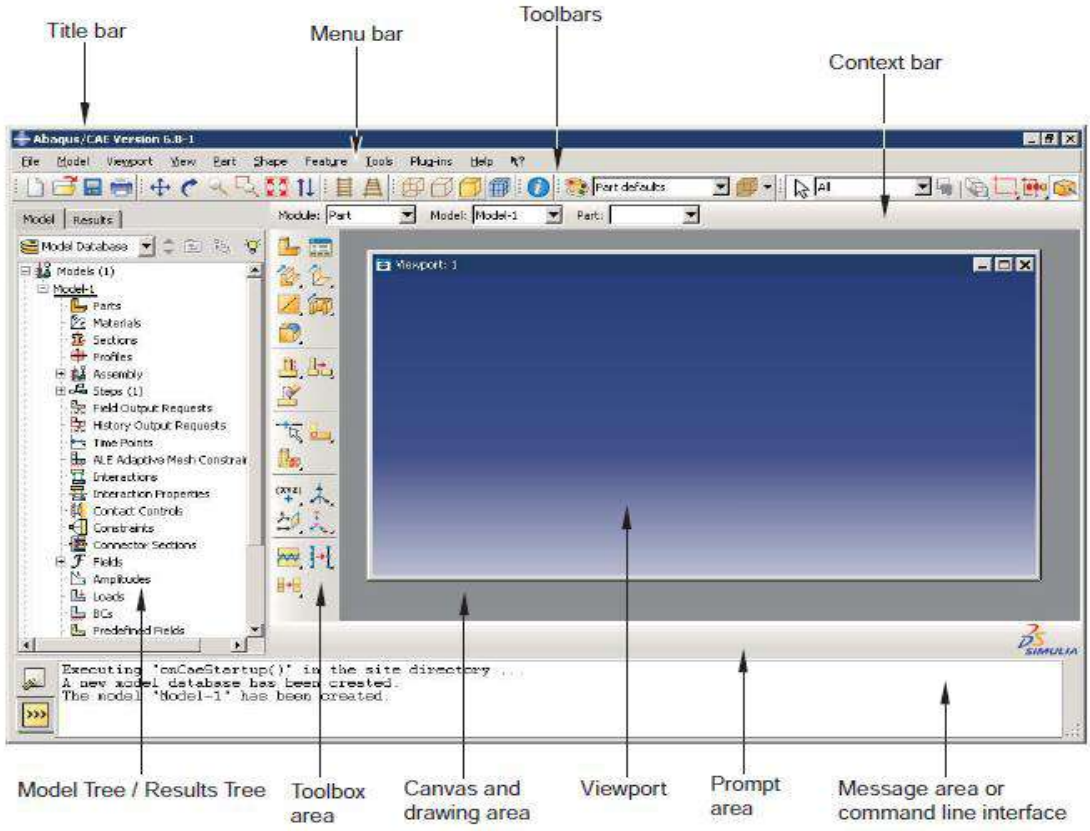

Figure (1) Components of the main window

3.What is a module?

As mentioned earlier, Abaqus /CAE is divided into functional units called modules. Each module contains only those tools that are relevant to a specific portion of the modeling task. For example, the Mesh module contains only the tools needed to create finite element meshes, while the Job module contains only the tools used to create, edit, submit, and monitor analysis jobs.

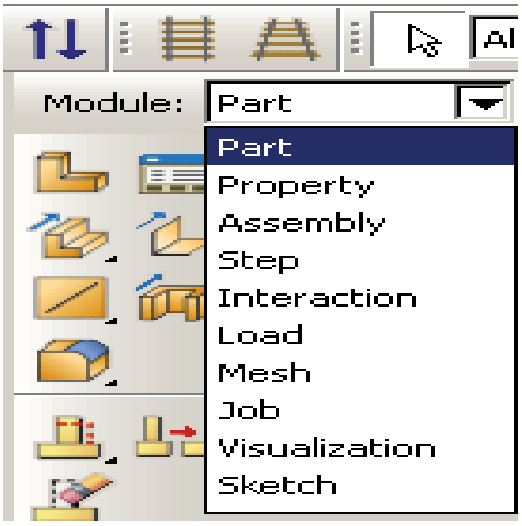

Fig.(2) Selecting a module.

You select a module from the **Module** list in the context bar, as shown in Fig. (2). The order of the modules in the menu corresponds to a logical sequence you may follow to create a model. In many circumstances you must follow this natural progression to complete a modeling task; for example, you must create parts before you create an assembly. Although the order of the modules follows a logical sequence, Abaqus/CAE allows you to select any module at any time, regardless of the state of your model. However, certain obvious restrictions apply; for example, you cannot assign section properties, such as cross-sectional dimensions of an I-beam, to geometry that has not yet been created.

A completed model contains everything that Abaqus needs to start the analysis. Abaqus/CAE uses a model database to store your models. When you start Abaqus/CAE, the **Start Session** dialog box allows you to create a new, empty model database in memory. After you start Abaqus/CAE, you can save your model database to a disk by

selecting **File→Save** from the main menu bar; to retrieve a model database from a disk, select **File→Open**.

The following list of themodules available within Abaqus/CAE briefly describes the modeling tasks you can perform in each module. The order of the modules in the list corresponds to the order of the modules in the context bar's **Module** list (see Fig. (2))

Part

The Part module allows you to create individual parts by sketching their geometry directly in Abaqus/CAE such as solid, shell, and wire as shown in Fig.(3) or by importing their geometry from other geometric modeling programs.

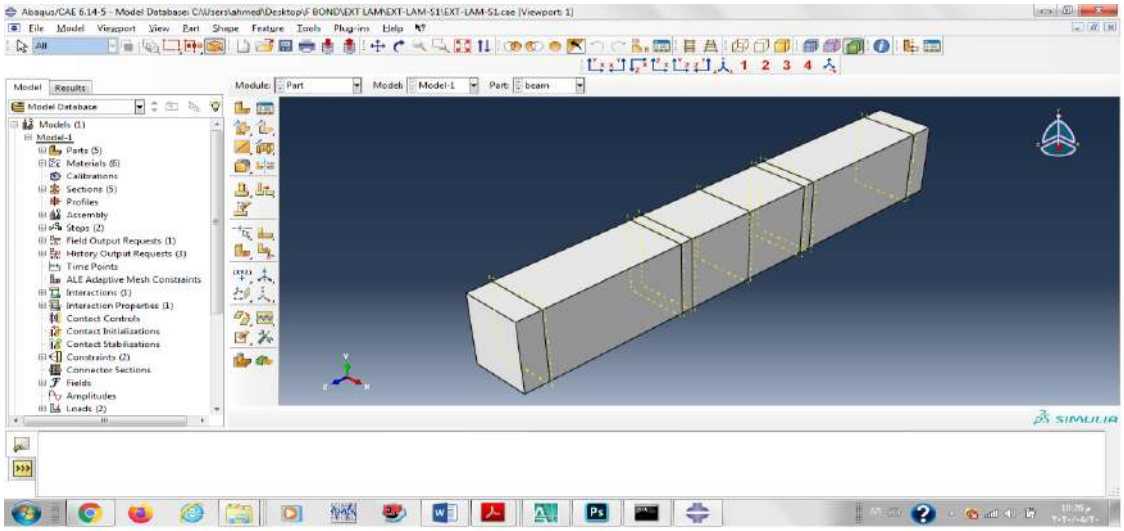

Solid part

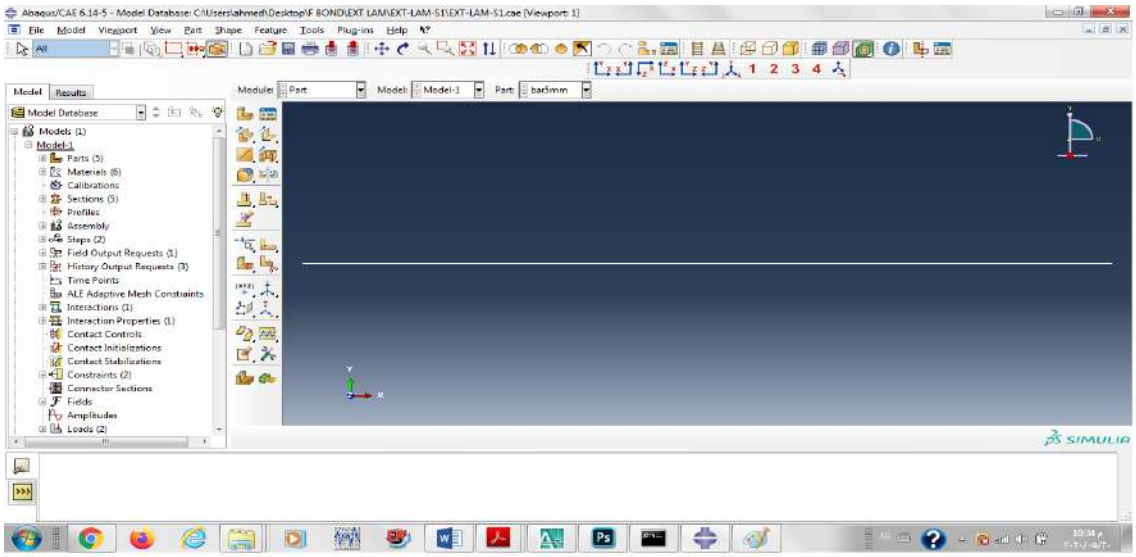

wire part

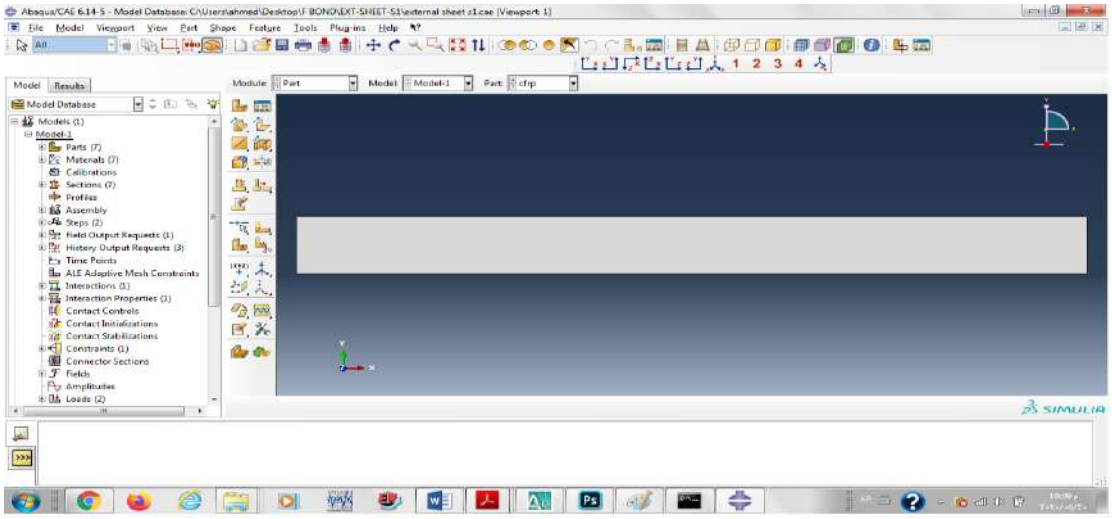

Shell part

Figure (3) part element

Property

A section definition contains information about the properties of a part or a region of a part, such as a region's associated material definition and cross-sectional geometry. In the Property module you create section and material definitions and assign them to regions of parts as shown Fig. (4).

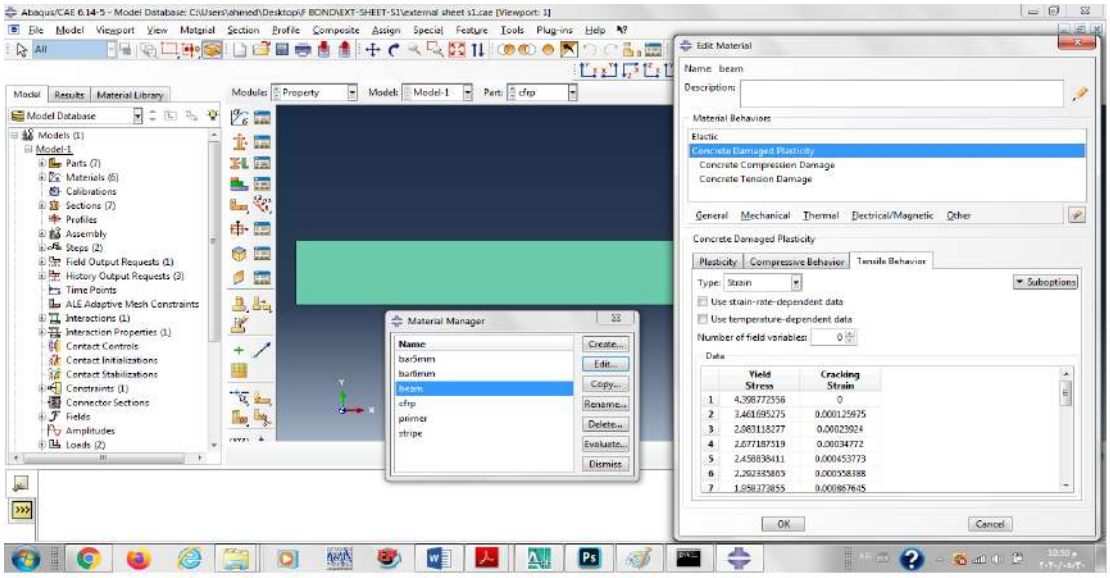

Figure(4) the properties of a part

Assembly

When you create a part, it exists in its own coordinate system, independent of other parts in the model. You use the Assembly module to create instances of your parts and to position the instances relative to each other in a global coordinate system, thus creating an assembly. An Abaqus model contains only one assembly as shown in Fig. (5).

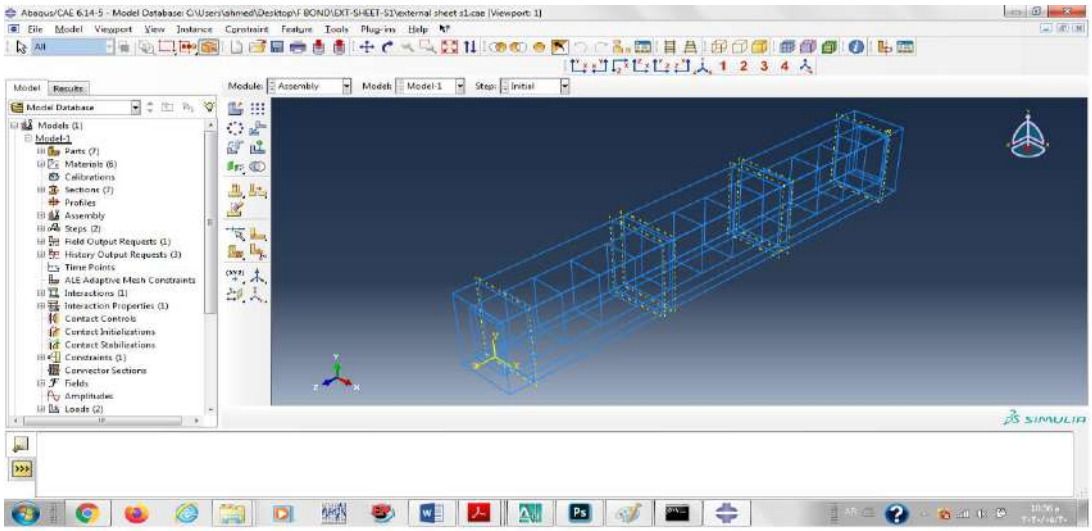

Figure (5) assembly of part

Step

You use the Step module to create and configure analysis steps and associated output requests. The step sequence provides a convenient way to capture changes in a model (such as loading and boundary condition changes); output requests can vary as necessary between steps as shown in Fig. (6).

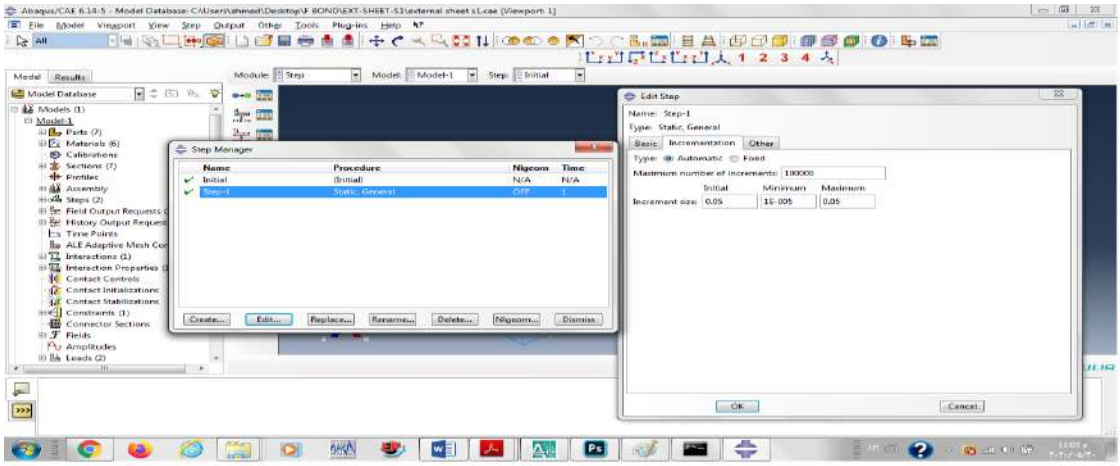

Figure (6) Step of module

Interaction

In the Interaction module you specify mechanical and thermal interactions between regions of a model or between a region of a model and its surroundings. An example of an interaction is contact between two surfaces see Fig. (7).

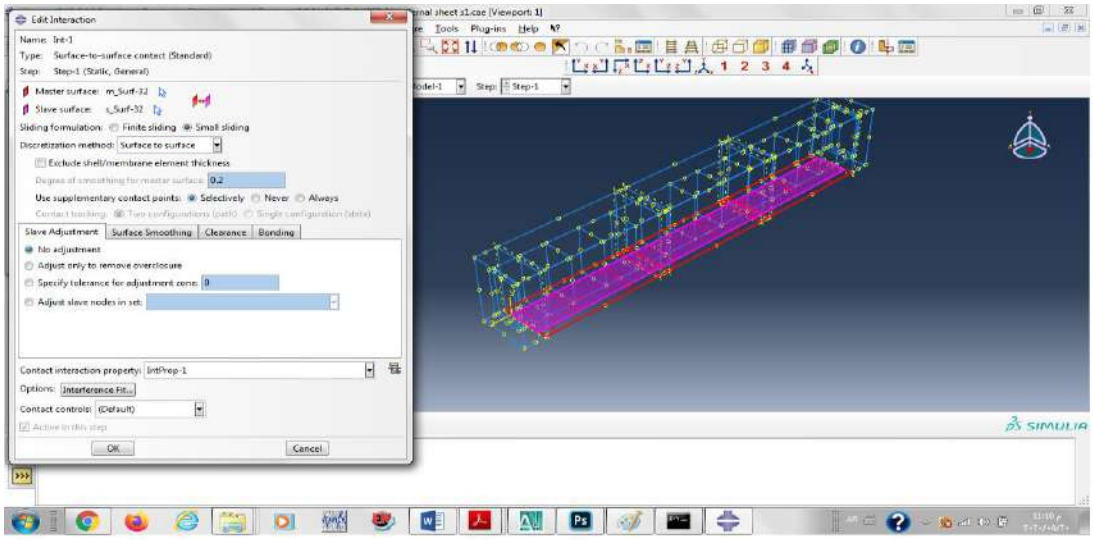

Figure (7) Interaction between two surfaces

Load

The Load module allows you to specify loads, boundary conditions, and predefined fields as shown in Fig. (8). Loads and boundary conditions are step-dependent objects, which means that you must specify the analysis steps in which they are active; some predefined fields are step-dependent, while others are applied only at the beginning of the analysis.

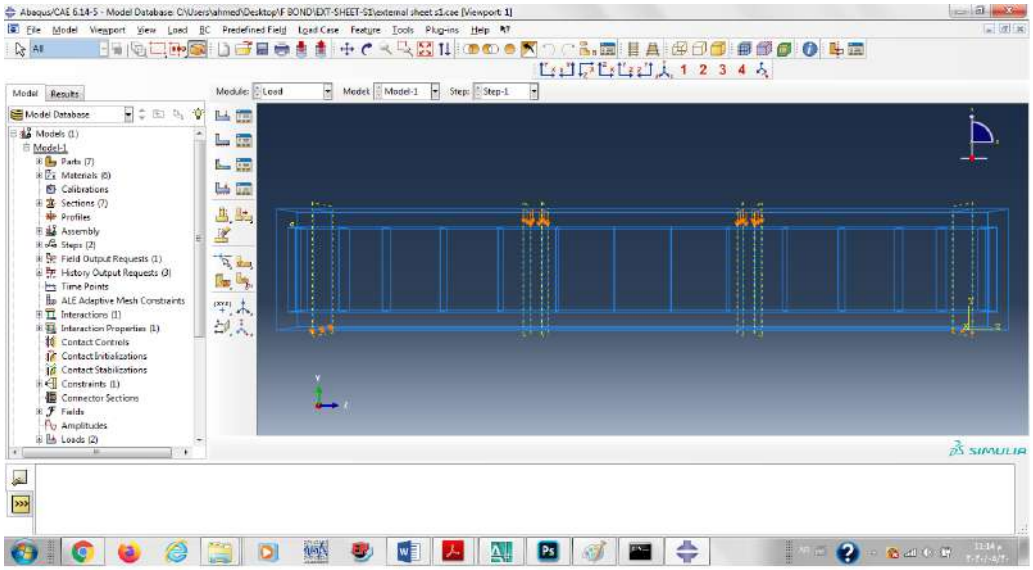

Figure (8) Loads and boundary conditions

Mesh

The Mesh module contains tools that allow you to generate a finite element mesh on an assembly created within Abaqus/CAE. Various levels of automation and control are available so that you can create a mesh that meets the needs of your analysis as shown in Fig (9).

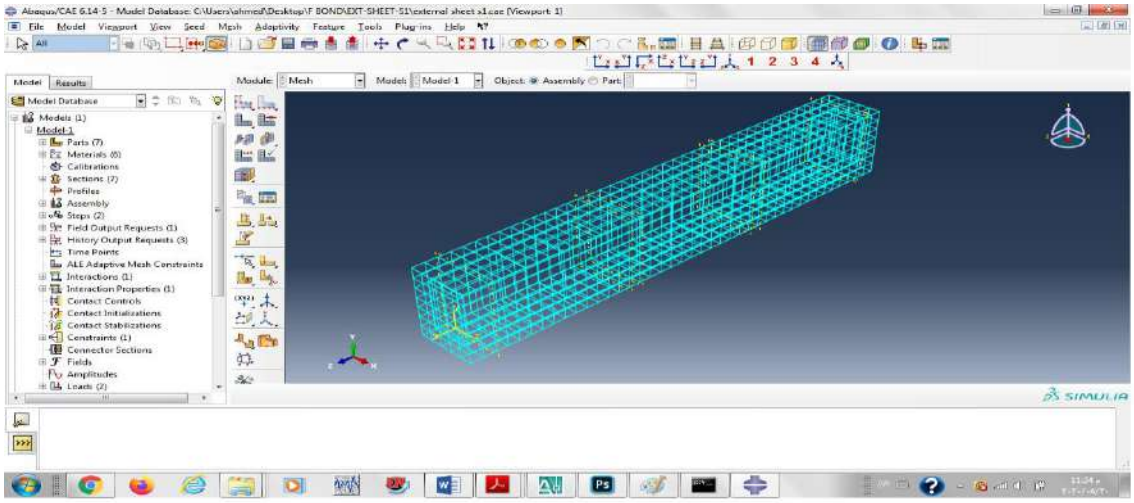

Figure (9) Mesh of assembly of part

Job

Once you have finished all of the tasks involved in defining a model, you use the Job module to analyze your model. The Job module allows you to interactively submit a job for analysis and monitor its progress.

Visualization

The Visualization module provides graphical display of finite element models and results. It obtains model and result information from the output database; you can control what information is written to the output database by modifying output requests in the Step module.

الملخص

هنالك طريقتين لتقوية المنشات الخرسانية المسلحة بالبوليمر المسلح بالياف الكاربون. الأول تقويه داخليه بالقرب من سطح الكونكريت (NSM) والثاني تقويه خارجية (EBR). في هذه الدراسة تم توظيف طريقة نماذج العناصر المحدده لتمثيل تصرف العتبات الخرسانيه المسلحه المقواة بالبوليمر المسلح بالياف الكاربون باستخدام برنامج ABAQUS ومقارنة النتائج النظرية مع النتائج العملية للتحقق من صحة ودقة طريقة العناصر المحددة.

عنصر ثلاثي الابعاد يحتوي ثمانية عقد(C3D8R) استخدم لتمثيل الخرسانة،عنصر احادي الابعاد(T3D2) استخدم لتمثيل الحديد، وعنصر ثلاثي الابعاد(S4R) استخدم لتمثيل الياف الكاربون المسلح وكذلك استخدم ربط سطح الى سطح لتمثيل لربط بين الخرسانة والياف الكاربون المسلح.

تم دراسة العلاقه بين الحمل والانحراف، مسار التشقق، انفعالات الخرسانة مع العمق وانماط الفشل للعتبات الخرسانيه المسلحه التي سبق وان تم اجراء اختبارات عملية من قبل باحثين اخرين لها. بعد التحقق من كفاءة النماذج تم تقديم دراسة لتقييم تاثير مقاومة الانضغاط للكونكريت ، وترتيب البوليمر المسلح بالياف الكاربون بالإضافة الى مقارنة التقوية للعتبات على شكل حرف U مع التقويه من جانبين وأخيرا نسبة (a/h) هذا لمقاومة العتبات الخرسانية للقص .اما لمقاومة الانحناء فقد تم دراسة تاثير مقاومة انضغاط الخرسانةوكذلك سمك صفائح البوليمر المسلح بالياف الكاربون وخيرا طول قطع البوليمر المسلح بالياف الكاربون .

النتائج لمقاومة الانحناء في هذه الدراسة بينت بان سعة المقاومه للعتبات الخرسانية المسلحه التي تم تقويتها بالبوليمر المسلح بالياف الكاربون يزداد من 6.6% الى 108.8% مقارنة مع العتبات الغير مقواة. وكذلك وجد بان زيادة مقاومة الانضغاط للخرسانة من 30 ميكا باسكال الى 70 ميكا باسكال يزداد الحمل الأقصى 25.6%. زيادة طول البوليمر المسلح بالياف الكاربون من 600 ملم الى 900 ملم يزيد الحمل الأقصى 12.7%.واخيرا زيادة سمك صفائح البوليمر المسلح بالياف الكاربون من 0.11 ملم الى 0.5 ملم سوف يزيد الصلادة وكذلك الحمل ب 47.9%.

أظهرت نتائج تصرف القص بان سعة المقاومه القصوى للعتبة الخرسانيه المسلحة المقواة بالبوليمر المسلح بالياف الكاربون تزداد ب 111.7% مقارنة مع العتبة الغير مقواة. وكذلك وجد بان زيادة مقاومة الانضغاط للخرسانة من 40 الى 65 ميكا باسكال سعة التحميل تزداد بنسبة 28% والصلادة تزداد أيضا بينما تقليل نسبة العمق الى طول فضاء القص (a/h) من 1.66 الى 2.33 يقود لزيادة الحمل بنسبة 23%.الحمل

الأقصى للعتبات الخرسانية المقواة على شكل حرف U بنسبة تتراوح من 5.9% الى 11.5% للعتبات المقواة بالبوليمر المسلح بالياف الكاربون (A12-M) و(B10-M) على التوالي عندما تقارن مع نفس العتبات الخرسانية المقواة من جانبين، هنالك كسب للمقاومة بنسب تتراوح من 8.7% الى 22.7% للعتبات المقواة بالبوليمر المسلح بالياف الكاربون بوجود حديد التسليح للقص مقارنة مع العتبات الغير مقواة (بوجود حديد تسليح القص).

تقوية العتبات الخرسانية المسلحة بواسطة البوليمر المسلح بالياف الكاربون باستخدام التسليح الداخلي القريب من السطح (NSM) اكثر كفاءة من طريقة الربط الخارجي (EBR).

النتائج التي تم الحصول عليها من طريقة العناصر المحددة تكون متقاربة اذا ما تم مقارنتها مع النتائج العملية . وكذلك تم مقارنة هذه النتائج مع المواصفة الامريكية (ACI) واظهرت النتائج عدم وجود تطابق بين النتائج النظرية ونتائج (ACI) بسبب استخدام معامل الأمان لاغلب معادلات (ACI) وكذلك اهمال الانزلاق بين الياف الكاربون المسلح والخرسانة.

جمهورية العراق
وزارة التعليم العالي والبحث العلمي
جامعة ميسان-كلية الهندسة
قسم الهندسة المدنية

التحليل العددي للعتبات الخرسانية المسلحة المقوى بالياف الكاربون المسلح

رسالة

مقدمة إلى كلية الهندسة في جامعة ميسان كجزء من متطلبات نيل شهادة

الماجستير في علوم الهندسة المدنية

(إنشاءات)

من قبل

احمد كاظم صكبان

(بكالوريوس، هندسة مدني)

بإشراف

الأستاذ الدكتور محمد عويش مشري